Effective realistic interactions for low momentum Hilbert spaces

Effektive realistische Wechselwirkungen für Niedrigimpuls-Hilberträume
Zur Erlangung des Grades eines Doktors der Naturwissenschaften (Dr. rer. nat.)
genehmigte Dissertation von Dennis Weber, M.Sc. aus Darmstadt
2012 — Darmstadt — D 17

TECHNISCHE
UNIVERSITÄT
DARMSTADT

Fachbereich Physik
GSI Theorie

Effective realistic interactions for low momentum Hilbert spaces
Effektive realistische Wechselwirkungen für Niedrigimpuls-Hilberträume

Genehmigte Dissertation von Dennis Weber, M.Sc. aus Darmstadt

1. Gutachten: Prof. Dr. Hans Feldmeier
2. Gutachten: Prof. Dr. Robert Roth

Tag der Einreichung: 08.10.2012
Tag der Prüfung: 12.11.2012

Darmstadt — D 17

Bitte zitieren Sie dieses Dokument als:
URN: urn:nbn:de:tuda-tuprints-
URL: http://tuprints.ulb.tu-darmstadt.de/

Erklärung zur Dissertation

Hiermit versichere ich, die vorliegende Dissertation ohne Hilfe Dritter nur mit den angegebenen Quellen und Hilfsmitteln angefertigt zu haben. Alle Stellen, die aus Quellen entnommen wurden, sind als solche kenntlich gemacht. Diese Arbeit hat in gleicher oder ähnlicher Form noch keiner Prüfungsbehörde vorgelegen.

Darmstadt, den 13.12.2012

(D. Weber)

Zusammenfassung

Realistische Nukleon-Nukleon-Potentiale sind ein wesentlicher Bestandteil moderner mikroskopischer Vielteilchen-Rechnungen. Diese Potentiale können auf zwei unterschiedliche Arten dargestellt werden: **Operatordarstellung** oder **Matrixelementdarstellung**. In Operatordarstellung wird das Potential durch einen Satz quantenmechanischer Operatoren repräsentiert, während es in Matrixelementdarstellung durch die Matrixelemente in einer vorgegebenen Basis definiert ist.

Viele moderne Potentiale werden direkt in der Matrixelementdarstellung konstruiert. Während sich die Matrixelementdarstellung aus der Operatordarstellung berechnen lässt, ist die Bestimmung einer Operatordarstellung aus den Matrixelementen schwieriger. Da man sich bei der Wahl der Basis immer auf einen endlich-dimensionalen Hilbert-Raum beschränken muss, ist die Abbildung von Matrixelement- auf Operatordarstellung auch nicht eindeutig. Einige Methoden zur Lösung des nuklearen Vielteilchen-Problems wie die **Fermionische Molekulardynamik** (FMD) oder die **Green's Funktion Monte Carlo** (GFMC) Methode benötigen jedoch explizit die Operatordarstellung eines Potentials, da sie nicht mit einer festen Vielteilchenbasis arbeiten. Es ist also wünschenswert, auch für die in Matrixelementen vorliegenden Wechselwirkungen eine Operatordarstellung zu erzeugen.

In dieser Arbeit wird eine Methode vorgestellt, eine approximative Operatordarstellung aus den Partialwellen-Matrixelementen eines Potentials zu bestimmen. Dazu wird ein Ansatz für die Operatordarstellung gewählt und die Parameter darin werden aus einem Fit an die Matrixelemente bestimmt.

Da mit einem endlichen Satz von Operatoren im Allgemeinen keine perfekte Reproduktion der Matrixelemente erreicht werden kann und die Resultate von der Wahl des Ansatzes abhängen, wird die erhaltene Operatordarstellung in Vielteilchen-Rechnungen untersucht und die Ergebnisse werden mit denen der Matrixelementdarstellung des Ausgangspotentials verglichen. Zur Berechnung der Nukleon-Nukleon-Streuphasen und der Eigenschaften des Deuterons wird ein Computercode verwendet, der im Rahmen dieser Arbeit geschrieben wurde. Zur Untersuchung größerer Kerne werden das **No-Core-Schalenmodell** (NCSM) und die FMD verwendet.

Die beschriebene Methode zur Berechnung der Operatordarstellung wird für verschiedene sogenannte **effektive realistische Potentiale** angewendet. Sie wird einerseits verwendet, um Potentiale mit bekannter Operatorform möglichst gut durch einen reduzierten Satz von Operatoren zu beschreiben und andererseits, um eine Operatordarstellung für nur durch Matrixelemente definierte Potentiale zu generieren.

Zunächst wird das mit der **Methode der Unitären Korrelatoren** (UCOM) transformierte **Argonne V18** Potential betrachtet. Dessen bekannte, aber im Vergleich zum Argonne-Potential umfangreichere Operatordarstellung, enthält insbesondere nichtlokale Terme mit polynomialen Impulsabhängigkeiten. Im Ansatz für die Operatordarstellung wird ein optimierter Operatorsatz verwendet, der kleiner als der des UCOM-Potentials ist. Durch den Fit dieses Ansatzes an die Matrixelemente des UCOM-Potentials erhält man das sogenannte **reduzierte UCOM** Potential. Im Fit werden Partialwellen mit kleinen Bahndrehimpulsen L höher gewichtet, sodass das reduzierte UCOM-Potential Streuphasen mit $L \leq 2$ genauso gut wie das volle UCOM-transformierte Argonne-Potential beschreibt und nur bei höheren L kleinere Abweichungen auftreten. Es gelingt auch die Eigenschaften leichter Kerne ebenso gut wie mit dem exakten UCOM-Potential zu reproduzieren.

Als Nächstes wird eine Operatordarstellung des mit der **Ähnlichkeits-Renormierungs-Gruppe** (SRG) transformierten Argonne-Potentials bestimmt. Dabei wird ein Ansatz basierend auf den Operatoren des Argonne-Potentials verwendet. Es werden jedoch zur Beschreibung der durch die SRG induzierten Impulsabhängigkeit nichtlokale Radialfunktionen im Ansatz für die Operatordarstellung eingeführt. Anhand von Zwei- und Vielteilchen-Rechnungen wird gezeigt, dass die Operatordarstellung und die exakte Matrixelementdarstellung zu den gleichen Ergebnissen für leichte Kerne und Streuphasen mit Bahndrehimpulsen $L \leq 2$ führen und die Operatordarstellung somit das SRG transformierte Argonne-Potential in den betrachteten Hilberträumen ausreichend gut beschreibt. Außerdem werden die FMD Matrixelemente für diesen nichtlokalen Ansatz analytisch ausgearbeitet.

Abschließend wird eine Operatordarstellung der JISP16-Wechselwirkung, welche speziell auf die harmonische Oszillatorbasis zugeschnitten ist, bestimmt. Dazu wird der gleiche Ansatz wie im Falle des SRG transformierten Argonne-Potentials verwendet. Die nichtlokalen Radialfunktionen in diesem Ansatz erlauben eine adäquate Beschreibung der Matrixelemente einzelner Partialwellen. Mit dem verwendeten Satz von Operatoren gelingt es jedoch nicht, die in jeder Partialwelle individuell konstruierte JISP16-Wechselwirkung in allen Partialwellen ausreichend gut zu reproduzieren. Man kann lediglich so viele Partialwellen reproduzieren, wie im Ansatz linear unabhängige Operatoren (und somit freie Parameter) zur Verfügung stehen, weshalb die extrahierte Operatordarstellung auch nur begrenzt in der Lage ist, die Streuphasen und die Eigenschaften leichter Kerne zu reproduzieren. Alternative Ansätze für die Operatordarstellung, die sich mehr an der Struktur der Wechselwirkung orientieren (wie zum Beispiel die Verwendung von Projektionsoperatoren auf die verschiedenen Partialwellen), erlauben hingegen eine bessere Beschreibung der JISP16-Wechselwirkung.

Zusammenfassend lässt sich sagen, dass für die unterschiedlichen effektiven Wechselwirkungen nicht ein allgemeiner Satz von Operatoren verwendet werden kann, bei dem man nur die Radialabhängigkeiten anpasst. Trotzdem ist es möglich, selbst bei effektiven Operatoren, die spezifisch auf numerische Handhabbarkeit ausgerichtet sind und die einzelnen Partialwellen separat behandeln, eine brauchbare Operatordarstellung zu konstruieren.

Abstract

Realistic nucleon-nucleon potentials are an essential ingredient of modern microscopic many-body calculations. These potentials can be represented in two different ways: **operator representation** or **matrix element representation.** In operator representation the potential is represented by a set of quantum mechanical operators while in matrix element representation it is defined by the matrix elements in a given basis.

Many modern potentials are constructed directly in matrix element representation. While the matrix element representation can be calculated from the operator representation, the determination of the operator representation from the matrix elements is more difficult. Furthermore, when choosing a basis one always has to restrict oneself to a finite dimensional Hilbert space so that the mapping from matrix elements to operator representation is not unique. Some methods to solve the nuclear many-body problem, such as **Fermionic Molecular Dynamics** (FMD) or the **Green's Function Monte Carlo** (GFMC) method, however require explicitly the operator representation of the potential, as they do not work in a fixed many-body basis. It is therefore desirable to derive an operator representation also for the interactions given by matrix elements.

In this work a method is presented which allows the derivation of an approximate operator representation starting from the momentum space partial wave matrix elements of the interaction. For that purpose an ansatz for the operator representation is chosen. The parameters in the ansatz are determined by a fit to the partial wave matrix elements.

Since a perfect reproduction of the matrix elements in general cannot be achieved with a finite number of operators and the quality of the results depends on the choice of the ansatz, the obtained operator representation is tested in nuclear many-body calculations and the results are compared with those from the initial interaction matrix elements. For the calculation of the nucleon-nucleon scattering phase shifts and the deuteron properties a computer code written within this work is used. For larger nuclei the **No Core Shell Model** (NCSM) and FMD are applied.

The described method to calculate the operator representation is applied to different **effective realistic potentials.** It is used to describe potentials with a known operator representation as precisely as possible with a reduced set of operators and to generate an operator representation from potentials defined by matrix elements only.

In a first application the **Argonne V18** potential, transformed by means of the **Unitary Correlation Operator Method** (UCOM), is considered. Its known, but in comparison to the Argonne potential richer operator representation, contains nonlocal terms with a polynomial momentum dependence. In the ansatz for the operator representation one uses an optimized set of operators which is a subset of the one of the UCOM potential. By fitting this ansatz to the matrix elements of the exact potential, one obtains the so called **reduced UCOM** potential. In the fit partial waves with small orbital angular momenta L are weighted higher, so that the reduced UCOM potential describes the phase shifts for $L \leq 2$ with the same accuracy as the full UCOM transformed Argonne potential and only for higher L rather small deviations occur. It also succeeds in reproducing the properties of light nuclei as accurately as the exact UCOM transformed Argonne potential.

As second application an operator representation of the **Similarity Renormalization Group** (SRG) transformed Argonne potential is obtained. For this, an ansatz based on the operators of the Argonne potential is used. To describe the complex momentum dependence of the potential nonlocal radial functions are introduced. By means of two- and many-body calculations it is shown that the operator representation and the exact matrix element representation lead to the same results for light nuclei and the same phase shifts for $L \leq 2$. Thus, the operator representation describes adequately the SRG transformed Argonne potential in the considered Hilbert spaces. Furthermore, the FMD matrix elements for this nonlocal ansatz are worked out analytically.

Finally an operator representation of the **JISP16** interaction, which is specifically designed for the harmonic oscillator basis, is derived by using the same ansatz as for the SRG transformed Argonne

potential. The nonlocal radial functions allow an adequate description of the matrix elements for a given partial wave. However, with the used set of operators one does not succeed in accurately reproducing all partial waves of the JISP16 interaction, which is constructed for each partial wave individually. It is only possible to describe as many partial waves as there are linearly independent operators (and thereby free parameters) available. Consequently, the extracted operator representation is of limited quality in reproducing phase shifts and properties of light nuclei. Alternative choices for the ansatz of the operator representation that are more adapted to the structure of the interaction, such as working with projection operators on the partial wave channels, allow a better description of the JISP16 interaction.

Summing up, there is no general set of operators which can be used to describe all the different effective interactions by just adjusting the particular radial functions. However, it is possible to find a suitable operator representation, even for effective operators that are specifically designed for numerical feasibility and are treating each partial wave separately.

Contents

1 Introduction

Quarks and gluons are considered to be the most elementary degrees of freedom in the description of hadrons. Their dynamics are described by **Quantum Chromo Dynamics** (QCD). The strong interaction between the quarks is mediated by gluons which couple to the color charge of the quarks. As the gluons carry color as well, they interact also with themselves. In nature only colorless objects are observed. This leads to the so called confinement: quarks and gluons are confined into colorless baryons and mesons. At low energies only the lightest baryons, the proton and the neutron, are present. Thus, for low energy nuclear structure physics, considered in this work, protons and neutrons, or more general nucleons[*], are the relevant degrees of freedom. The interaction between the color neutral nucleons is the residual strong interaction between two complex QCD objects, similar to the residual electromagnetic interaction between two neutral atoms. At relative distances of a few fm[†] the interaction is mediated by the exchange of virtual pions. At distances smaller than about 2 fm polarization effects occur and contribute to the residual interaction. In this region one utilizes symmetries of the underlying QCD and form factors to get the form of the interaction. Parameters are adjusted to fit measured phase shifts and other observables.

The idea of nuclear **ab-initio methods** is to solve the nuclear many-body problem by using the same basic nuclear interaction – without further assumptions and approximations specific to the considered nuclear application. The aim is to describe a wide range of nuclear properties in a unified picture. The solution of the many-body problem requires two ingredients: the interaction between the nucleons and the representation (e.g. a basis) in the many-body Hilbert space, in which the problem is to be solved.

In recent years, several methods to solve the nuclear many-body problem have been developed, such as the **Faddeev-Yakubovsky** equations [2], the **Hyperspherical Harmonics** basis [3], the **Green's Function Monte Carlo** (GFMC) method [4], the **No Core Shell Model** (NCSM) [5–9], **Coupled Cluster** methods [10] or **Fermionic Molecular Dynamics** (FMD) [11–13] and **Antisymmetrized Molecular Dynamics** (AMD) [14]. All of these models are suitable to describe light nuclei, but show in practice different strengths and limitations concerning the size and the structure of nuclear systems they can be applied to. FMD for example is a very powerful method to describe exotic structures like cluster and halo states which are often not accessible to other methods.

The second ingredient to a nuclear ab-initio calculation is the nucleon-nucleon (NN) potential. Since the interaction between the nucleons originates from the quark and gluon substructure, a calculation within QCD would be desirable. This however is presently not fully possible, neither conceptually nor numerically [15]. Nevertheless the structure of the NN interaction may be based on QCD considerations, like chiral symmetry and pion-exchange, where the unknown parameters, like coupling strengths or cut-offs in form factors, have to be determined from scattering data and bound state properties of the two-nucleon system or few-body systems. In recent years it has become clear that also three-nucleon interactions have to be included [9, 16]. They appear whenever three nucleons are close enough that their pairwise polarization, which is included in the two-body interaction, is distorted by the presence of the third nucleon.

One can construct different **realistic NN potentials**. "Realistic" in this context means, that the potential describes the experimentally known two-nucleon scattering data up to the pion threshold and the deuteron properties with high precision. All these different potentials have in common certain symmetries (for example invariance under parity transformation, translation and rotation) and show characteristic features such as a contribution from a central force, a spin-orbit force and a tensor force which is sensitive to the orientation of the spins of the nucleons with respect to their distance vector [17]. The various potentials can be quite different in their detailed structure, especially at small distances. The **Argonne V18** potential [18] explicitly includes pion exchange at larger distances, while the short range part is parameterized phenomenologically. The **JISP16** potential [19] is constructed in the harmonic

---

[*] In this work the isospin formalism [1] is used. Protons and neutrons are unified as nucleons with the isospin quantum number $m_t = +\frac{1}{2}$ and $m_t = -\frac{1}{2}$, respectively.

[†] In nuclear physics the unit femto-meter (fm) is the natural length scale. Often the denotation "Fermi" is used instead of fm.

oscillator basis such, that it has a simple tridiagonal structure which is advantageous for NCSM applications. The **CD Bonn** potential [20], as another example, is based completely on the meson exchange picture, while the so called **chiral** potentials [21–23] are constructed by means of chiral perturbation theory in an effective field theory concept with explicit treatment of the pion exchange. All these realistic potentials succeed in describing the two-nucleon properties with comparable accuracy. This reflects the fact that these two-nucleon properties are not sufficient to determine an unambiguous NN potential and there exists an infinite number of phase shift equivalent potentials. This is due to the fact that the short range behaviour corresponding to energies above the pion threshold is not determined by low energy NN scattering phase shifts and that NN scattering experiments are only sensitive to the so called on-shell behaviour of the interaction. This means that the asymptotic absolute value of the relative momentum or energy of the initial and the scattered system are the same. In the nucleus in the presence of more than two nucleons a pair of two nucleons does not have a sharp energy since the nucleons of the pair are interacting with other nucleons as well. Thus, in the nucleus not only the on-shell but also the off-shell behaviour of the interaction is relevant. Consequently, different realistic potentials with different off-shell behaviour yield different results in calculations for larger nuclei, yet describing the two-nucleon system with the same accuracy.

The restriction to protons and neutrons as degrees of freedom and thereby neglecting the QCD substructure of the nucleons leads to genuine three-body forces. One example is the **Fujita-Myazawa** term [24] induced by the strong coupling to intermediate Δ excitations. In general the explicit form and strength of the three-body forces depend on the corresponding two-body potential and its off-shell behaviour. By the inclusion of these three-body forces one can achieve improved results in many-body calculations [25, 26]. The potentials based on chiral effective field theory contain in the next-to-next-to-leading order (N2LO) also such three-body terms. It is interesting to note that one can construct a potential whose off-shell behaviour is such, that the three-body contributions to the energy are minimal in the three- and four-body system [27].

Realistic nuclear potentials show a strong repulsion at short distances and a strong tensor force which induce correlations in the nuclear many-body state. In a representation using Slater determinants, like in the NCSM or FMD, these correlations can only be described by including a large number of basis states in the calculation. This however demands a rapidly increasing numerical effort for systems with more than about 4 particles. Modern methods approach this problem by means of **effective interactions** that are obtained by unitary transformations. They are devised such that they exhibit the same phase shifts as the initial interaction but require much smaller model spaces in nuclear many-body calculations. The **Unitary Correlation Operator Method** (UCOM) [28–34] is one example of such a technique. The correlations induced by the repulsive core and the tensor force are imprinted by a unitary correlation operator acting on the simple model states. When acting with the correlation operator on the Hamiltonian one obtains an UCOM transformed interaction which by construction has the same phase shifts as the original Hamiltonian. Alternatively one can derive effective realistic interactions by means of renormalization techniques. In a momentum space picture, the short ranged central and tensor interactions connect low relative momentum states to states with high momentum, so that the matrix elements of the interaction show strong off-diagonal contributions. Consequently, the high momentum states have to be included in the model space, also for the calculation of low energy observables. Transformation methods such as V_{lowk} [35, 36] and the **Similarity Renormalization Group** (SRG) [37] allow to decouple the high and low momentum part of the interaction and therefore to work in smaller low momentum model spaces only. The same holds true for the UCOM transformed interaction. It should be emphasized that all these methods create effective realistic interactions for low momentum Hilbert spaces which do not depend explicitly on the exact size or truncation of the model space, as it is the case for example for the Lee-Suzuki transformation [38].

Since several methods to solve the nuclear many-body problem, as well as effective realistic interactions, are available for ab-initio calculations, it is desirable to be able to compare different methods and interactions in order to draw conclusions on their quality in describing nuclear many-body systems. For this, one needs to be able to apply different NN potentials in a certain nuclear many-body method.

The effective realistic potentials discussed above are either formulated in the **operator representation** or in a **matrix element representation.** In operator representation the potential is represented by a quantum mechanical operator $\underset{\sim}{V}$. In matrix element representation the potential is given by the matrix elements $\langle\, \alpha \,|\, \underset{\sim}{V} \,|\, \alpha' \,\rangle$ of the operator in a Hilbert space basis, where $|\, \alpha \,\rangle$ describes the relative motion of two nucleons. These two different types of representations are illustrated in Fig. 1.1 for the Argonne potential. The left-hand side shows the operator structure of the potential, the right-hand side some of the corresponding matrix elements in the partial wave basis in momentum space which is explained in Appendix A.2.3. Both representations describe the same physics. The operator representation however has the advantage that it can be used in any basis representation and by the explicit operator form it provides a much more intuitive understanding than looking at the matrix elements. For example, some features of the potential like a spin-orbit ($\underset{\sim}{\vec{L}} \cdot \underset{\sim}{\vec{S}}$) or tensor component ($\underset{\sim}{S}_{12}$) and their radial range are immediately visible while this cannot be directly identified in the partial wave representation.

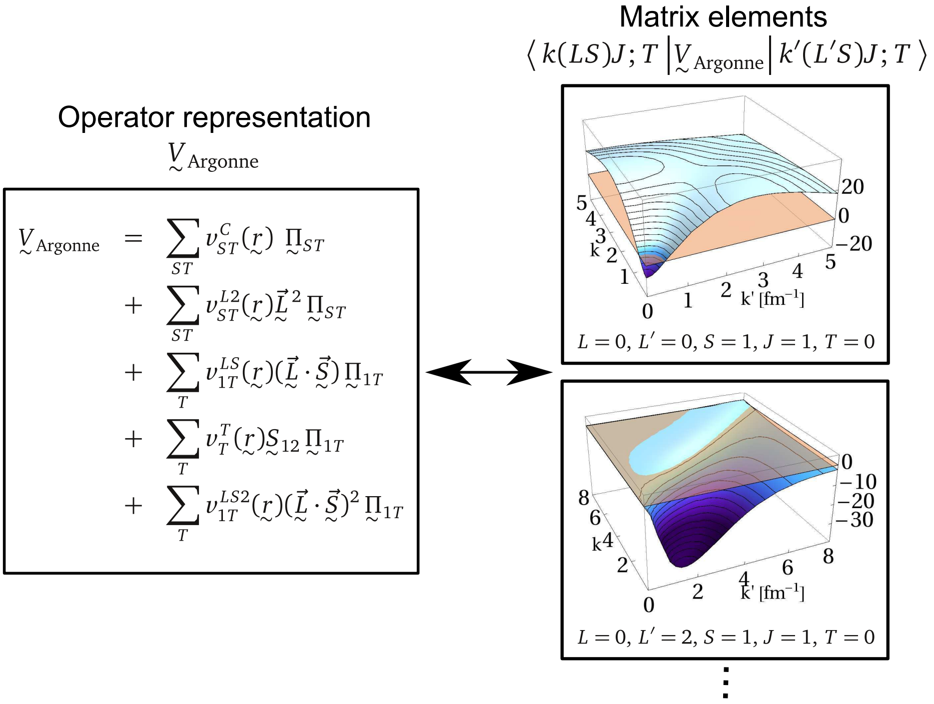

Figure 1.1: Operator representation and partial wave matrix elements (in units of MeVfm^3) of the Argonne potential.

Most of the modern effective realistic interactions are constructed directly in a matrix element representation, which restricts their use to many-body methods that are based on a predetermined basis representation, such as the NCSM or the Coupled Cluster approach. In such methods the basis states are expanded in a fixed basis, for example the harmonic oscillator basis. In this case the matrix elements can be calculated from the momentum space partial wave matrix element representation of the potential once before being used for all many-body calculations. Other many-body approaches, like FMD, AMD or GFMC do not expand their basis states in a fixed basis. For these models it is not possible to use pre-calculated matrix elements. Furthermore the basis states might not be angular momentum eigenstates. For an efficient calculation of these matrix elements it is necessary to have the operator representation of the interaction. In order to give those models access to modern interactions, a transformation between the two types of representations is needed.

The aim of this work is to develop a method to derive an approximate operator representation from the partial wave matrix elements of a potential. To achieve this, an ansatz for the operator representation is chosen, which is supposed to be able to reproduce the partial wave matrix elements. The free parameters in the ansatz are obtained from a fit to the partial wave matrix elements. The quality of the obtained operator representation depends on the chosen ansatz. To investigate the influence of deviations between the operator representation and the matrix element representation, the results for nuclear two- and few-nucleon systems obtained with both representations are compared. For the description of the two-nucleon system, the deuteron properties and the NN scattering phase shifts, a computer code was written, which allows to calculate the two-nucleon properties directly from the given partial wave matrix elements of a potential. For the operators used in this work the calculation of the matrix elements of the derived operator representation is straightforward. Thus, the code can also calculate the two-nucleon properties for the obtained operator representation. The properties of bound few-nucleon systems are calculated within the NCSM and FMD.

In Sec. 2 the many-body methods used in this work are presented. The calculation of the deuteron properties and NN scattering phase shifts is discussed and the computer code written to solve the two-nucleon problem is illustrated. Furthermore, NCSM and FMD are presented in greater detail.

Sec. 3 focuses on effective realistic potentials for nuclear ab-initio calculations. First, the UCOM transformation is introduced. This method is used to obtain the UCOM transformed Argonne potential whose properties are discussed. Next, the focus is on potentials with an unknown operator representation. The SRG transformation and the SRG transformed Argonne potential are presented and the JISP16 potential is discussed. The origin of the complicated momentum dependence of these potentials is illustrated.

In Sec. 4 the method to derive an operator representation starting from the partial wave matrix elements of a potential is demonstrated. This method is applied to derive operator representations for the effective realistic potentials discussed in Sec. 3. Starting from the matrix elements of the UCOM transformed Argonne potential, the so called reduced UCOM potential is derived. This is a potential containing a smaller set of operators than the exact UCOM transformed potential. The reduced UCOM potential is tested by using the many-body methods discussed in Sec. 2 and the results are compared to those obtained with the exact potential. Then the SRG transformed Argonne potential and the JISP16 potential are considered. To describe the more complex momentum dependence of these potentials, nonlocal radial functions are introduced in the ansatz for the operator representation. Using this nonlocal ansatz, the operator representations for both potentials are obtained and tested in two- and few-nucleon calculations.

In Sec. 5 concluding remarks on the method to derive an operator representation and its results for the considered effective realistic interactions are given. The section is closed with an outlook on further tasks and questions.

The thesis is supplemented by three appendices. In Appendix A basic definitions and the partial wave basis states are introduced. Appendix B focuses on technical details of the methods to calculate the deuteron properties and NN phase shifts (discussed in Sec. 2.2.1). In Appendix C details of the obtained operator representations of the reduced UCOM potential and the SRG transformed Argonne potential are presented. The weights which are used in the fits to the partial wave matrix elements and the parameters of the radial functions are listed explicitly. Furthermore, analytic expressions for the partial wave matrix elements and the FMD matrix elements of the operator representations are presented.

2 Probing nucleon-nucleon interactions

The nucleon-nucleon (NN) potential itself is not an observable. To judge the ability of a given potential to describe the properties of a physical system, it is necessary to evaluate measurable physical properties and compare those to experimental data. In this section a “toolbox” of techniques to calculate such expectation values and propabilities for selected two- and few-nucleon systems is introduced. These methods are used later to investigate the potentials discussed in Sec. 3.

2.1 Properties of few-nucleon systems

To describe nuclear properties, one has to solve the Schrödinger equation

$$\left(\underset{\sim}{T}+\underset{\sim}{V}\right)\left|\,\Phi_n\,\right\rangle = E_n\left|\,\Phi_n\,\right\rangle \tag{2.1}$$

for the potential $\underset{\sim}{V}$ under investigation. This way one obtains the energy eigenvalues E_n and the corresponding many-body eigenstates $\left|\,\Phi_n\,\right\rangle$. The energies E_n can then be compared to experimental values. For example, in bound nucleon systems the lowest energy eigenvalue E_0 has to be compared with the binding energy E_B obtained from mass measurements. Furthermore, if excited states exist, it is possible to compare the experimental energy spectrum with the corresponding calculated energy eigenvalues E_n.

The eigenstates $\left|\,\Phi_n\,\right\rangle$ are used to obtain other physical observables B by evaluating the expectation value of the corresponding quantum mechanical operator $\underset{\sim}{B}$ as

$$B_n = \left\langle\,\Phi_n\left|\underset{\sim}{B}\right|\Phi_n\,\right\rangle \tag{2.2}$$

or for transition amplitudes

$$B_{nn'} = \left\langle\,\Phi_n\left|\underset{\sim}{B}\right|\Phi_{n'}\,\right\rangle. \tag{2.3}$$

In this work, the following observables B are considered:

- the square point-matter radius R^2 with the corresponding operator

$$\underset{\sim}{R}^2 = \sum_{i=1}^{A}\underset{\sim}{\vec{r}}'^2(i),$$

- the square point-proton radius* R_p^2 with the corresponding operator

$$\underset{\sim}{R}_p^2 = \sum_{i=1}^{A}\underset{\sim}{\vec{r}}'^2(i)\,\underset{\sim}{\Pi}_p(i),$$

- the magnetic dipole moment μ with the corresponding operator

$$\underset{\sim}{\mu} = \sqrt{\frac{3}{4\pi}}\mu_N\sum_{i=1}^{A}\left[g_p\underset{\sim}{s}_z(i)+\underset{\sim}{l}'_z(i)\right]\underset{\sim}{\Pi}_p(i)+g_n\underset{\sim}{s}_z(i)\,\underset{\sim}{\Pi}_n(i),$$

---

[*] For the calculation of the point-proton radius R_p the nucleons are considered to be point-like particles. The experimentally measured charge radius R_c however contains contributions from the finite size of the nucleons and is related to the point-proton radius by $R_c^2 = R_p^2 + \langle\, r_p^2\,\rangle + N/Z\langle\, r_n^2\,\rangle$ [39], with the charge radius of the proton $\langle\, r_p^2\,\rangle^{1/2} = 0.895(18)\,\mathrm{fm}$ [40] and the mean-square charge radius of the neutron $\langle\, r_n^2\,\rangle = -0.120(5)\,\mathrm{fm}^2$ [41].

- the electric quadrupole moment Q with the corresponding operator

$$\underset{\sim}{Q} = e \sum_{i=1}^{A} \underset{\sim}{\vec{r}}'^2(i) Y_{20}(\vartheta'(i))\, \underset{\sim}{\Pi}_p(i).$$

Here $\vec{r}'(i)$ is the coordinate with respect to the center-of-mass $\vec{R}_{c.m.}$ of the A-nucleon system, e the charge of the proton, $\mu_N = \frac{e\hbar}{2m_p}$ the nuclear magneton and $g_n = -3.8263$ and $g_p = 5.5855$. $\underset{\sim}{\Pi}_p(i)$ and $\underset{\sim}{\Pi}_n(i)$ are projectors on protons and neutrons, respectively.

As the deuteron is the only bound two-nucleon system, most of the information on the potential comes from scattering properties which are measured in terms of cross sections. From a theoretical point of view it is convenient to calculate phase shifts (explained in more detail in Sec. 2.2) for all channels. All cross sections can be obtained from those. The calculated phase shifts have then to be compared to the phase shifts which are extracted from the experimental cross section fits. It should be noted that phase shifts are not a direct observable but can be mapped into the two-nucleon cross sections which are observables. This is demonstrated later in Eq. (2.34). However, for lab energies higher than 300 MeV (which corresponds to the threshold for pion production) inelastic scattering sets in. Thus, the extraction of the elastic part becomes increasingly complicated and limits the information at high momentum transfer which leads to a finite resolution in the length scale.

It must be noted that even if the phase shifts of the two-body system were precisely known at all energies, the potential is not unambiguously determined. Different momentum-dependent potentials can yield exactly the same phase shifts. Those potentials differ in the so called “off-shell” behaviour* to which the two-nucleon phase shifts are not sensitive. Consequently two realistic potentials describing the two nucleon system with the same precision can show a very different behaviour for many-body systems. Thus, it is necessary to consider not only the two-nucleon but also few-nucleon systems in order to gain additional information about the off-shell properties and many-body forces.

In the following methods to solve the nuclear two- and few-body problem are discussed.

2.2 Solving the many-body problem

2.2.1 Two-nucleon systems

As already mentioned, a “realistic” NN potential is defined as a potential which describes the experimentally known two-nucleon properties with very high accuracy. Thus, for constructing as well as transforming or modifying realistic NN potentials, it is crucial to have a tool to compute two-nucleon properties. This way it is possible to test and ensure that the experimental two-nucleon data is reproduced accurately.

The deuteron

The deuteron is a weakly bound system consisting of a proton and a neutron. Only the ground state with $J^\pi = 1^+$ is bound. The ground state properties are presented in Tab. 2.1.

E_B [MeV]	$\mu\,[\mu_N]$	$Q\,[e\,\text{fm}^2]$	$\sqrt{R_c^2}$ [fm]
2.224644±0.000046	0.8574382308±0.0000000072	0.2860±0.0015	1.9635±0.0045

Table 2.1: Experimental deuteron properties, taken from Ref. [42].

---

* For the definition of “on”- and “off-shell” by means of the T-Matrix see page 16.

To calculate the deuteron properties for a given potential $\underset{\sim}{V}$, a short computer code, which uses the partial wave matrix elements $\left\langle k(LS)J;TM_T \middle| \underset{\sim}{V} \middle| k'(L'S)J;TM_T \right\rangle$ (for the definition of the basis see Appendix A.2.3) of the potential as input to the Schrödinger equation, was written.

Since the deuteron ground state has the quantum numbers $J = 1$ and $T = 0$, the major part of the ground state has the orbital angular momentum quantum number $L = 0$ (the so called S-wave, see Appendix A.2.4) and spin $S = 1$. A small component with $L = 2$ (D-wave) is admixed by the tensor force, so that the ground state has the form

$$\left| \phi_D \right\rangle = c_0 \left| \phi_0(01)1;00 \right\rangle + c_2 \left| \phi_2(21)1;00 \right\rangle. \tag{2.4}$$

Projecting the Schrödinger equation

$$\left(\underset{\sim}{T} + \underset{\sim}{V} \right) \left| \phi_D \right\rangle = E_B \left| \phi_D \right\rangle \tag{2.5}$$

onto $\left\langle k(01)1;00 \right|$ and $\left\langle k(21)1;00 \right|$ leads to the Rarita-Schwinger equations [43], here written in momentum space representation:

$$\begin{aligned} \frac{k^2}{2\mu}\tilde{\phi}_0(k) \quad &+ \int_0^\infty \mathrm{d}k'\, k'^2 \left\langle k(01)1;00 \middle| \underset{\sim}{V} \middle| k'(01)1;00 \right\rangle \tilde{\phi}_0(k') \\ &+ \int_0^\infty \mathrm{d}k'\, k'^2 \left\langle k(01)1;00 \middle| \underset{\sim}{V} \middle| k'(21)1;00 \right\rangle \tilde{\phi}_2(k') = E_B\, \tilde{\phi}_0(k) \end{aligned} \tag{2.6a}$$

$$\begin{aligned} \frac{k^2}{2\mu}\tilde{\phi}_2(k) \quad &+ \int_0^\infty \mathrm{d}k'\, k'^2 \left\langle k(21)1;00 \middle| \underset{\sim}{V} \middle| k'(01)1;00 \right\rangle \tilde{\phi}_0(k') \\ &+ \int_0^\infty \mathrm{d}k'\, k'^2 \left\langle k(21)1;00 \middle| \underset{\sim}{V} \middle| k'(21)1;00 \right\rangle \tilde{\phi}_2(k') = E_B\, \tilde{\phi}_2(k). \end{aligned} \tag{2.6b}$$

This system of two coupled equations contains the matrix elements of the potential and the unknown radial functions $\tilde{\phi}_0(k) = c_0 \left\langle k(01)1;00 \middle| \phi_0(01)1;00 \right\rangle$ and $\tilde{\phi}_2(k) = c_2 \left\langle k(21)1;00 \middle| \phi_2(21)1;00 \right\rangle$. These are the L-projected radial parts of the deuteron wave function in momentum representation.

To solve the equations the momentum coordinate is discretized on an equidistant grid which transforms the Rarita-Schwinger equations to matrix form and thereby the integral equations to an eigenvalue problem. By solving the eigenvalue problem one obtains the energy eigenvalue and the functions $\tilde{\phi}_0(k)$ and $\tilde{\phi}_2(k)$ on the momentum grid. The functions $\tilde{\phi}_0(k)$ and $\tilde{\phi}_2(k)$ are Fourier-Bessel transformed to obtain the solutions $\phi_0(r)$ and $\phi_2(r)$ in position space. Furthermore, magnetic dipole moment and electric quadrupole moment are calculated. More details can be found in Appendix B.1. Fig. 2.1 shows the radial solutions in momentum and position space calculated with the matrix elements of the Argonne V18 interaction. The obtained fraction of the D-wave is 5.7%.

The deuteron wave function is only sensitive to the ${}^3\mathrm{S}_1$* and the ${}^3\mathrm{D}_1$ channel, so that only matrix elements with $L = \{0, 2\}$, $S = 1$, $J = 1$ and $T = 0$ can be examined. To probe the properties of a potential in this and the other channels of the two-nucleon system at various momenta or at positive energies, one has to consider the phase shifts.

---

* For the definition of the spectroscopic notation see Appendix A.2.4

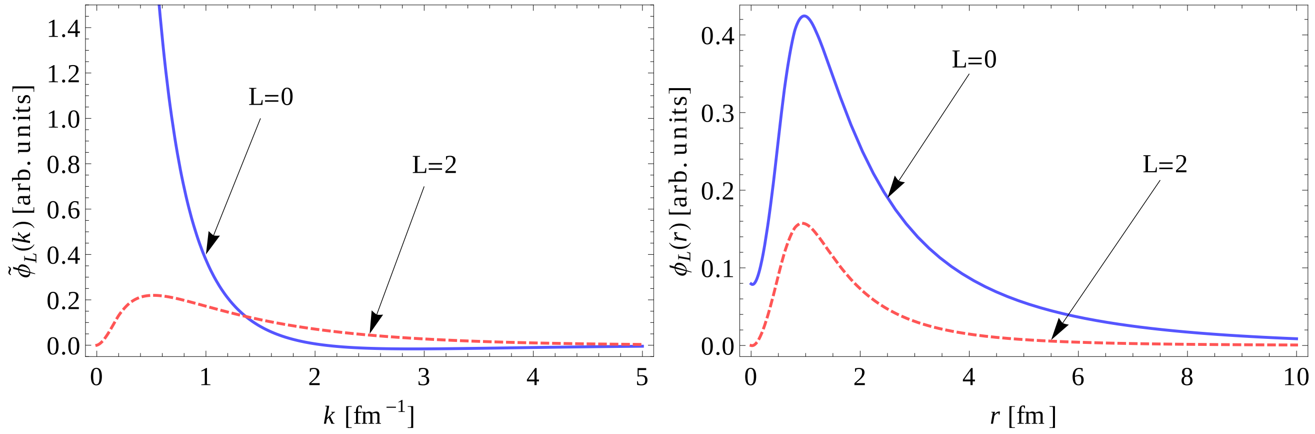

Figure 2.1: The radial part of the Deuteron ground state calculated with the Argonne potential in momentum space (left) and position space (right). The blue solid blue curve shows the S-wave ($L = 0$) component, the dashed red curve the D-wave ($L = 2$) component of the solution.

Nucleon-nucleon phase shifts

In this section, the phase shifts for the elastic NN scattering by means of $\underset{\sim}{V}$ are derived. Since the NN interaction only depends on the relative coordinates, it is convenient to work in relative and center-of-mass (c.m.) coordinates and consider the problem in the c.m.-frame. The nuclear interaction[*] has a finite range R of a few fm. Thus, for $r \gg R$ (or $r \to \infty$), where the measurement is done, the particles are moving freely[†]. To describe the scattering experiment, the boundary conditions of the quantum state have to reflect the physical situation.

The isospin quantum numbers $m_t(1)$ and $m_t(2)$ show, which kind of nucleons take part in the scattering process. For an experimental setup with given $m_t(1)$ and $m_t(2)$ the isospin part can be written in terms of total isospin eigenstates using Clebsch-Gordan coefficients (see Appendix A.2.2):

$$\left| m_t(1), m_t(2) \right\rangle = \sum_T C \left(\begin{array}{cc|c} \frac{1}{2} & \frac{1}{2} & T \\ m_t(1) & m_t(2) & M_T \end{array} \right) \left| T M_T \right\rangle. \tag{2.7}$$

For proton-proton scattering for example, $m_t(1) = m_t(2) = \frac{1}{2}$ and $M_T = m_t(1) + m_t(2) = 1$ so that only $T = 1$ contributes. For proton-neutron scattering $M_T = 0$ and a linear combination of $T = 0$ and $T = 1$ has to be taken.

The spin quantum numbers S and M_S are defined in an analogue way as T and M_T above. In contrast to the isospin, the experiment in general does not prepare a pure spin state, but a statistical ensemble of spin states with different orientations. Thus, when calculating the cross section one has to work with a statistical operator $\underset{\sim}{\rho}{}^{M_T}_{\vec{k}}$ to describe the averaging over the initial states. For the incoming particles one has

$$\underset{\sim}{\rho}{}^{M_T}_{in,\vec{k}} = \sum_{m_s(1),m_s(2)} D_{m_s(1),m_s(2)} \sum_{T,T'} C^{m_t(1)m_t(2)}_{TT'M_T} \left| \phi_{in,\vec{k}}, m_s(1)m_s(2); TM_T \right\rangle \left\langle \phi_{in,\vec{k}}, m_s(1)m_s(2); T'M_T \right|, \tag{2.8}$$

---

[*] The Coulomb interaction is not taken into consideration. Consequently the nuclear phase shifts are compared to experimental data from which the known Coulomb effects are already subtracted.

[†] In case of two protons, they interact by the Coulomb force.

where $\phi_{in,\vec{k}}$ describes the spatial part of the two-nucleon state with relative momentum $\vec{k}$[*], $m_s(1)$ and $m_s(2)$ are the spin quantum numbers of the nucleons. Furthermore the definition

$$C^{m_t(1)m_t(2)}_{TT'M_T} := C\left(\begin{array}{cc|c} \frac{1}{2} & \frac{1}{2} & T \\ m_t(1) & m_t(2) & M_T \end{array}\right) C\left(\begin{array}{cc|c} \frac{1}{2} & \frac{1}{2} & T' \\ m_t(1) & m_t(2) & M_T \end{array}\right) \tag{2.9}$$

is used. The parameters $D_{m_s(1),m_s(2)}$ represent the experimental setup. For unpolarized scattering for example, $D_{m_s(1),m_s(2)} = \frac{1}{4}$ for all possible combinations of $m_s(1)$ and $m_s(2)$.

Written in a coupled spin basis with the quantum numbers S and $M_S = m_s(1)+m_s(2)$, Eq. (2.8) reads

$$\underset{\sim}{\rho}^{M_T}_{in,\vec{k}} = \sum_{m_s(1),m_s(2)} D_{m_s(1),m_s(2)} \sum_{\substack{S,S'\\T,T'}} C^{m_s(1)m_s(2)}_{SS'M_S} C^{m_t(1)m_t(2)}_{TT'M_T} \left|\, \phi_{in,\vec{k}}, SM_S; TM_T \right\rangle \left\langle \phi_{in,\vec{k}}, S'M_S; T'M_T \,\right|. \tag{2.10}$$

$C^{m_s(1)m_s(2)}_{TT'M_T}$ is defined in an analogue way as $C^{m_t(1)m_t(2)}_{TT'M_T}$ in Eq. (2.9). In the following it is sufficient to regard only the spin and isopsin eigenstates states $\left|\, \phi_{in,\vec{k}}, SM_S; TM_T \right\rangle$ from which the statistical operator $\underset{\sim}{\rho}^{M_T}_{in,\vec{k}}$ in Eq. (2.10) can be constructed by means of the parameters $D_{m_s(1),m_s(2)}$ corresponding to the experimental setup.

For $r > R$, the spatial part of the wave function of the incoming nucleons can be described by a plane wave with momentum $\vec{k}$, so that one finds in the c.m. system:

$$\left\langle \vec{r} \,\middle|\, \phi_{in,\vec{k}}, SM_S; TM_T \right\rangle \xrightarrow{r \gg R} e^{i\vec{k}\cdot\vec{r}} \left|\, SM_S; TM_T \right\rangle. \tag{2.11}$$

For the scattered system $\left|\, \phi^{M_S}_{scat,\vec{k}}, S; TM_T \right\rangle$ the spatial wave function outside the range of the potential is given by a spherical wave[†] with momentum $k = |\vec{k}|$, centered around the center of mass and multiplied by an angle-dependent amplitude $f^{SM'_S TM_T}_{\vec{k}}(\widehat{\vec{r}})$. Since the nuclear interaction connects different M_S, the scattered state does not possess good M_S[‡]

$$\left\langle \vec{r} \,\middle|\, \phi^{M_S}_{scat,\vec{k}}, S; TM_T \right\rangle \xrightarrow{r \gg R} \sum_{M'_S} f^{SM'_S TM_T}_{\vec{k}}(\widehat{\vec{r}}) \frac{e^{ikr}}{r} \left|\, SM'_S; TM_T \right\rangle. \tag{2.12}$$

The two-nucleon state $\left|\, \phi^{M_S}_{\vec{k}}, S; TM_T \right\rangle$ describes the superposition of the incoming and the scattered wave:

$$\left|\, \phi^{M_S}_{\vec{k}}, S; TM_T \right\rangle = \left|\, \phi_{in,\vec{k}}, SM_S; TM_T \right\rangle + \left|\, \phi^{M_S}_{scat,\vec{k}}, S; TM_T \right\rangle. \tag{2.13}$$

The spatial part of the two-nucleon scattering state is illustrated in Fig. 2.2.

---

[*] The energy in the c.m. system is $E = \frac{\vec{k}^2}{2\mu}$

[†] In case of two protons $\frac{e^{ikr}}{r}$ has to be replaced by the corresponding Coulomb scattering solution.

[‡] The index M_S in the scattered state $\left|\, \phi^{M_S}_{scat,\vec{k}}, S; TM_T \right\rangle$ only indicates that this state originates from a system with the quantum number M_S but does not imply that the scattered state has this quantum number.

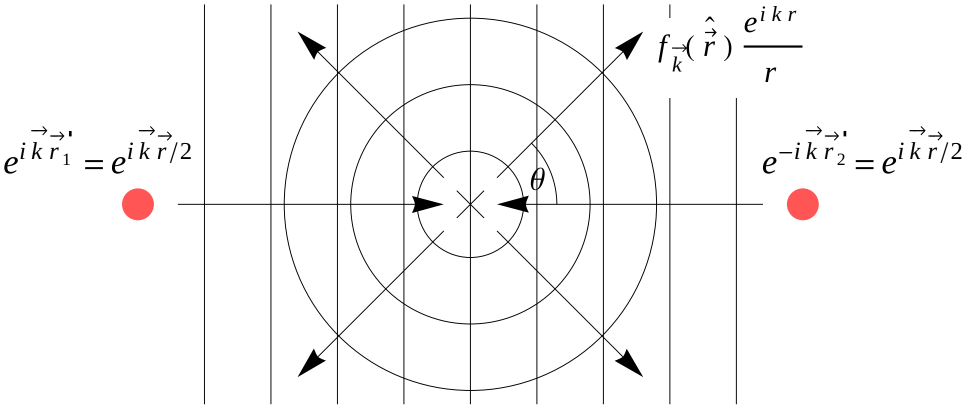

Figure 2.2: Illustration of the nucleon-nucleon scattering problem in the x-z-plane of the center-of-mass frame. The incoming particles are represented by a plane wave $e^{i\vec{k}\vec{r}}$, the scattered particles are described by a spherical wave $\frac{e^{ikr}}{r}$ around the center of mass, modulated by an angle-dependent scattering amplitude $f_{\vec{k}}(\widehat{\vec{r}})$.

Partial wave decomposition

Due to the symmetries of the NN interaction it is convenient to perform a partial wave expansion and consider each angular momentum partial wave separately. For convenience, one can assume that $\vec{k}$ points in z-direction. The plane wave can be written as

$$\begin{aligned} \left\langle \vec{r} \,\middle|\, \phi_{in,\vec{k}}, SM_S; TM_T \right\rangle &= e^{i\vec{k}\vec{r}} \left| SM_S; TM_T \right\rangle \\ &= \sum_{L=0}^{\infty} a^{LST} i^L \, j_L(kr) \, Y^L_{M=0}(\theta) \left| SM_S; TM_T \right\rangle \\ &= \sum_{J=0}^{\infty} \sum_{L=|J-S|}^{J+S} a^{LST} i^L \, j_L(kr) \, C\left(\begin{array}{cc|c} L & S & J \\ 0 & M_S & M_S \end{array} \right) \left\langle \vec{r} \,\middle|\, (LS)JM_S; TM_T \right\rangle . \quad (2.14) \end{aligned}$$

In the last row of Eq. (2.14) the incoming wave is decomposed in partial waves which are characterized by the quantum numbers L, S, J, M_S, T and M_T. The spherical Bessel function $j_L(kr)$ describes the radial dependence and $\left\langle \widehat{\vec{r}} \,\middle|\, (LS)JM_S; TM_T \right\rangle$ denotes the angular part of the wave function for each partial wave. The factor a^{LST} is given by

$$a^{LST} := \frac{1}{2}\left(1 - (-1)^{S+T+L}\right) \sqrt{4\pi}\sqrt{2L+1}, \quad (2.15)$$

and ensures the antisymmetry of the two-nucleon state. Asymptotically one finds (see Ref. [44])

$$\begin{aligned} \left\langle \vec{r} \,\middle|\, \phi_{in,\vec{k}}, SM_S; TM_T \right\rangle \xrightarrow[kr \gg L]{r \gg R} \sum_{J=0}^{\infty} \sum_{L=|J-S|}^{J+S} a^{LST} \left(i^L \frac{\sin(kr - \pi L/2)}{kr} \right) \cdot \\ C\left(\begin{array}{cc|c} L & S & J \\ 0 & M_S & M_S \end{array} \right) \left\langle \widehat{\vec{r}} \,\middle|\, (LS)JM_S; TM_T \right\rangle \quad (2.16a) \end{aligned}$$

$$= \sum_{J=0}^{\infty} \sum_{L=|J-S|}^{J+S} a^{LST} \frac{1}{2ikr} \left((-1)^{L+1} e^{-ikr} + e^{ikr} \right) \cdot$$

$$C \left(\begin{array}{cc|c} L & S & J \\ 0 & M_S & M_S \end{array} \right) \langle \hat{\vec{r}} \,|\, (LS)JM_S; TM_T \rangle. \quad (2.16b)$$

The nuclear interaction $\underset{\sim}{V}$ is almost diagonal in the partial wave basis used above. Only the tensor force connects different partial waves such, that $\left| (L{=}J-1\,1)JM; TM_T \right\rangle$ and $\left| (L{=}J+1,1)JM; TM_T \right\rangle$ states are mixed. $S=1$ states with $L=J$ in contrast are not mixed with other states. The latter can be explained by parity conservation and the fact that only states with the same total angular momentum J are connected by the nuclear interaction. For $S=0$ states the interaction is already diagonal in the partial wave basis since the tensor force does not act in these channels. One can define a new basis $\left| k\,\alpha, SJM; TM_T \right\rangle$ for each k and J such, that the NN interaction is completely diagonal. To do this, the new quantum number α running from 0 to 3 is introduced and replaces the angular momentum quantum number L. The transformation is given by

$$\left| k\,\alpha{=}0, 0JM; TM_T \right\rangle = \left| k\,(J0)JM; TM_T \right\rangle \quad (2.17a)$$

$$\left| k\,\alpha{=}1, 1JM; TM_T \right\rangle = \cos\epsilon_J(k) \left| k\,(J-1\,1)JM; TM_T \right\rangle - \sin\epsilon_J(k) \left| k\,(J+1\,1)JM; TM_T \right\rangle \quad (2.17b)$$

$$\left| k\,\alpha{=}2, 1JM; TM_T \right\rangle = \left| k\,(J1)JM; TM_T \right\rangle \quad (2.17c)$$

$$\left| k\,\alpha{=}3, 1JM; TM_T \right\rangle = \sin\epsilon_J(k) \left| k\,(J-1\,1)JM; TM_T \right\rangle + \cos\epsilon_J(k) \left| k\,(J+1\,1)JM; TM_T \right\rangle. \quad (2.17d)$$

For the channels in which $\underset{\sim}{V}$ is already diagonal the new basis states $\left| k\,0, 0JM; TM_T \right\rangle$ and $\left| k\,2, 0JM; TM_T \right\rangle$ are just identical to the partial wave states $\left| k\,(J0)JM; TM_T \right\rangle$ and $\left| k\,(J1)JM; TM_T \right\rangle$. The states $\left| k\,1, 1JM; TM_T \right\rangle$ and $\left| k\,3, 1JM; TM_T \right\rangle$ of the new basis are a superposition of the partial wave basis states of the mixed channels $\left| (J-1\,1)JM; TM_T \right\rangle$ and $\left| (J+1,1)JM; TM_T \right\rangle$ such that $\underset{\sim}{V}$ is diagonal in this basis. The parameter $\epsilon_J(k)$ is called “mixing angle”.

Writing down Eq. (2.16b) in the new basis, given by Eqs. (2.17), leads to

$$\langle \vec{r} \,|\, \phi_{in,\vec{k}}, SM_S; TM_T \rangle \xrightarrow[kr \gg J]{r \gg R} \sum_{J=0}^{\infty} \sum_{\alpha=0}^{3} \frac{1}{2ikr} c^{\alpha,SJT} \left((-1)^{J+\alpha+1} e^{-ikr} + e^{ikr} \right) \langle \hat{\vec{r}} \,|\, \alpha, SJM_S; TM_T \rangle \quad (2.18)$$

with the parameters

$$c^{\alpha,SJT} = \sum_{L=|J-S|}^{J+S} a^{LST} C \left(\begin{array}{cc|c} L & S & J \\ 0 & M_S & M_S \end{array} \right) \langle \alpha, SJM_S; TM_T \,|\, (LS)JM_S; TM_T \rangle. \quad (2.19)$$

The scattered wave $\langle \vec{r} \,|\, \phi^{M_S}_{scat,\vec{k}}, S; TM_T \rangle$ can be written in terms of the new basis as

$$\langle \vec{r} \,|\, \phi^{M_S}_{scat,\vec{k}}, S; TM_T \rangle \xrightarrow[kr \gg J]{r \gg R} \sum_{J=0}^{\infty} \sum_{\alpha=0}^{3} c^{\alpha,SJT} f_k^{\alpha SJTM_T} \frac{e^{ikr}}{r} \langle \hat{\vec{r}} \,|\, \alpha, SJM_S; TM_T \rangle, \quad (2.20)$$

where

$$f_k^{\alpha SJTM_T} = \left(c^{\alpha,SJT} \frac{e^{ikr}}{r} \right)^{-1} \langle \alpha, SJM_S; TM_T \,|\, \phi_{scat,\vec{k}}, SM_S; TM_T \rangle. \quad (2.21)$$

For the total wave function Eq. (2.13) one obtains by combining Eqs. (2.18) and (2.20)

$$\begin{aligned} \left\langle \vec{r} \,\middle|\, \phi_{\vec{k}}^{M_S}, S; TM_T \right\rangle &\xrightarrow[kr\gg J]{r\gg R} \sum_{J=0}^{\infty}\sum_{\alpha=0}^{3} \frac{1}{2ikr} c^{\alpha,SJT} \left((-1)^{J+\alpha+1} e^{-ikr} + (1+2ikf_k^{\alpha SJTM_T}) e^{ikr} \right) \cdot \\ &\qquad \left\langle \hat{\vec{r}} \,\middle|\, \alpha, SJM_S; TM_T \right\rangle \qquad (2.22a) \\ &= \sum_{J=0}^{\infty}\sum_{\alpha=0}^{3} \frac{1}{2ikr} c^{\alpha,SJT} \left((-1)^{J+\alpha+1} e^{-ikr} + S_{\alpha SJT}(k) e^{ikr} \right) \cdot \\ &\qquad \left\langle \hat{\vec{r}} \,\middle|\, \alpha, SJM_S; TM_T \right\rangle. \qquad (2.22b) \end{aligned}$$

In Eq. (2.22b) $\left\langle \vec{r} \,\middle|\, \phi_{\vec{k}}^{M_S}, S; TM_T \right\rangle$ is written in terms of the S-Matrix element[*] [45]:

$$S_{\alpha SJT}(k) := \left\langle k\,\alpha, SJM; TM_T \,\middle|\, \underset{\sim}{S} \,\middle|\, k\,\alpha, SJM; TM_T \right\rangle = 1 + 2if_k^{\alpha SJTM_T}. \tag{2.23}$$

The S-Matrix imprints the (asymptotic) effects of the scattering on the outgoing wave. Since the interaction is diagonal in the basis $\left| k\,\alpha, SJM; TM_T \right\rangle$, for each part of the sum in Eq. (2.22b) the amplitude of the outgoing wave has to be the same as the one of the incoming wave. Thus,

$$|S_{\alpha SJT}(k)| = 1. \tag{2.24}$$

One can parameterize the S-Matrix by the phase shift $\tilde{\delta}_{\alpha,SJT}(k)$

$$S_{\alpha SJT}(k) = e^{2i\tilde{\delta}_{\alpha,SJT}(k)}. \tag{2.25}$$

Rewriting Eq. (2.22b) by making use of relation Eq. (2.25) leads to

$$\begin{aligned} \left\langle \vec{r} \,\middle|\, \phi_{\vec{k}}, SM_S; TM_T \right\rangle &\xrightarrow[kr\gg J]{r\gg R} \sum_{J=0}^{\infty}\sum_{\alpha=0}^{3} \frac{c^{\alpha,SJT}}{2ikr} e^{i\tilde{\delta}_{\alpha,SJT}(k)} \left((-1)^{J+\alpha+1} e^{-i(kr+\tilde{\delta}_{\alpha,SJT}(k))} + e^{i(kr+\tilde{\delta}_{\alpha,SJT}(k))} \right) \cdot \\ &\qquad \left\langle \hat{\vec{r}} \,\middle|\, \alpha, SJM_S; TM_T \right\rangle. \end{aligned} \tag{2.26}$$

Comparing the scattered wave and the free plane-wave in the basis given by Eqs. (2.26) and (2.18), the origin of the name phase shift becomes clear: For each channel, the solution of the scattered nucleons Eq. (2.26) is shifted by a phase $\tilde{\delta}_{\alpha,SJT}(k)$ compared to the solution of the free nucleons Eq. (2.18). The whole impact of the NN potential far away from the point of scattering is described completely by the phase shift $\tilde{\delta}_{\alpha,SJT}(k)$.

The phase shifts are defined in the eigenbasis given in Eqs. (2.17) in which the S-Matrix is diagonal. For the $S = 0$ states, the eigenstate $\left| k\,0, 0JM; TM_T \right\rangle$ is identical to the partial wave state $\left| k(L{=}J0)JM; TM_T \right\rangle$ so that the phase shift $\tilde{\delta}_{0,0JT}(k)$ can be referred to this partial wave. One can write it as $\delta_{(L0)JT}(k)$ with the indices of the partial wave. The same holds when $S = 1$ and $L = J$:

$$\begin{aligned} e^{2i\delta_{(J1)JT}(k)} &:= \left\langle k(L{=}J1)JM; TM_T \,\middle|\, \underset{\sim}{S} \,\middle|\, k(L{=}J1)JM; TM_T \right\rangle \\ &= \left\langle k\,\alpha{=}2, 1JM; TM_T \,\middle|\, \underset{\sim}{S} \,\middle|\, k\,\alpha{=}2, 1JM; TM_T \right\rangle = e^{2i\tilde{\delta}_{2,1JT}(k)}. \end{aligned} \tag{2.27}$$

---

[*] The S-Matrix does not depend explicitly on M since the NN interaction is invariant under rotations. As the NN interaction shows a weak charge dependence, the S-Matrix in principle depends on M_T as well. However, in this work only charge independent potentials are used. In this case the S-Matrix element is also independent of M_T and the index M_T is omitted. The S-Matrix is diagonal in the eigenbasis $\left| k\,\alpha, SJM; TM_T \right\rangle$ of $\underset{\sim}{V}$.

For $S=1$ and $L=J\pm 1$ the S-Matrix however is not diagonal in the partial wave basis due to the mixing of these channels caused by the tensor force, leading to

$$\begin{aligned}
&S^{1JT}(k) := \\
&\begin{pmatrix}
\langle k(J{-}1\,1)J;TM_T|\underset{\sim}{S}|k(J{-}1\,1)J;TM_T\rangle & 0 & \langle k(J{-}1\,1)J;TM_T|\underset{\sim}{S}|k(J{+}1\,1)J;TM_T\rangle \\
0 & \langle k(J\,1)J;TM_T|\underset{\sim}{S}|k(J\,1)J;TM_T\rangle & 0 \\
\langle k(J{+}1\,1)J;TM_T|\underset{\sim}{S}|k(J{-}1\,1)J;TM_T\rangle & 0 & \langle k(J{+}1\,1)J;TM_T|\underset{\sim}{S}|k(J{+}1\,1)J;TM_T\rangle
\end{pmatrix} \\
&= U_J^{-1} e^{2i\Delta_{JT}} U_J,
\end{aligned} \tag{2.28}$$

with the matrix U_J containing the mixing angle

$$U_J = \begin{pmatrix} \cos\epsilon_J(k) & 0 & \sin\epsilon_J(k) \\ 0 & 1 & 0 \\ -\sin\epsilon_J(k) & 0 & \cos\epsilon_J(k) \end{pmatrix}, \tag{2.29}$$

and the matrix Δ_{JT}

$$\Delta_{JT} = \begin{pmatrix} \tilde{\delta}_{1,1JT}(k) & 0 & 0 \\ 0 & \tilde{\delta}_{2,1JT}(k) & 0 \\ 0 & 0 & \tilde{\delta}_{3,1JT}(k) \end{pmatrix}, \tag{2.30}$$

containing the phase shifts in the eigen basis $|k\,\alpha, SJM; TM_T\rangle$.

Instead of the "eigen" phase shifts defined by Eqs. (2.25) and (2.28), one can use the so called "bar" phase shifts, which are, in contrast to Eq. (2.28) defined by

$$S^{1JT}(k) = e^{i\bar{\Delta}_{JT}} \bar{U}_J e^{i\bar{\Delta}_{JT}}, \tag{2.31}$$

with

$$\bar{U}_J = \begin{pmatrix} \cos 2\bar{\epsilon}_J(k) & 0 & i\sin 2\bar{\epsilon}_J(k) \\ 0 & 1 & 0 \\ i\sin 2\bar{\epsilon}_J(k) & 0 & \cos 2\bar{\epsilon}_J(k) \end{pmatrix} \tag{2.32}$$

$$\bar{\Delta}_{JT} = \begin{pmatrix} \bar{\delta}_{1,1JT}(k) & 0 & 0 \\ 0 & \bar{\delta}_{2,1JT}(k) & 0 \\ 0 & 0 & \bar{\delta}_{3,1JT}(k) \end{pmatrix}. \tag{2.33}$$

The relation between eigen and bar phase shifts can be found in Ref. [46] and in Appendix B.2. For the non-mixed case ($L=J$), the eigen and bar phase shifts are identical. Fig. 2.3 shows both types of phase shifts calculated with the Argonne potential for selected partial waves. In contrast to eigen phase shifts the bar phase shift description allows an easy separation of the Coulomb and the nuclear part of the S-Matrix. Thus, phase shifts extracted from scattering data tend to be given as bar phase shifts. In this work, theoretical phase shifts will be compared to the bar phase shifts from the Nijmegen partial wave analysis [47]. As a consequence all calculated phase shifts shown in this work (except the eigen phase shifts in Fig. 2.3) are bar phase shifts.

In general for both types of phase shifts, one cannot define a phase shift for L in the mixed partial wave channels due to the coupling between the $L=J\mp 1$ channels. The outgoing waves with the phase shifts $\tilde{\delta}_{1,1JT}(k)$ and $\tilde{\delta}_{3,1JT}(k)$ contain contributions from both, the $L=J-1$ and the $L=J+1$ partial wave. They are not associated to a certain L anymore, but only the total angular momentum J. The mixing is described by the mixing angle $\epsilon_J(k)$.

If $\epsilon_J(k)$ is small, $\tilde{\delta}_{1,1JT}(k)$ is dominated by the $L = J - 1$ channel and $\tilde{\delta}_{3,1JT}(k)$ by $L = J + 1$. Thus, one often uses a sloppy notation and labels $\tilde{\delta}_{1,1JT}(k)$ with $L = J - 1$ and $\tilde{\delta}_{3,1JT}(k)$ with $L = J + 1$. As shown above, this is not quite correct. To indicate this, in this work the labels of those phase shifts containing contributions from different partial waves are written in quotation marks. An example of this notation can be seen in Fig. 2.3. Since the nuclear interaction connects the ^{3}P$_2$ and the ^{3}F$_2$ channel, there exist no independent phase shifts for these channels, but phase shifts $\tilde{\delta}_{1,121}(k)$ and $\tilde{\delta}_{3,121}(k)$ with contributions from both channels. Nevertheless, one labels $\tilde{\delta}_{1,121}(k)$ with ”^{3}P$_2$” and $\tilde{\delta}_{3,121}(k)$ with ”^{3}F$_2$”, keeping in mind that there still is a mixing between the partial waves, described by the angle $\epsilon_2(k)$. The label of the pure ^{3}P$_1$ channel is written without any quotation marks as it only contains contributions from this single partial wave.

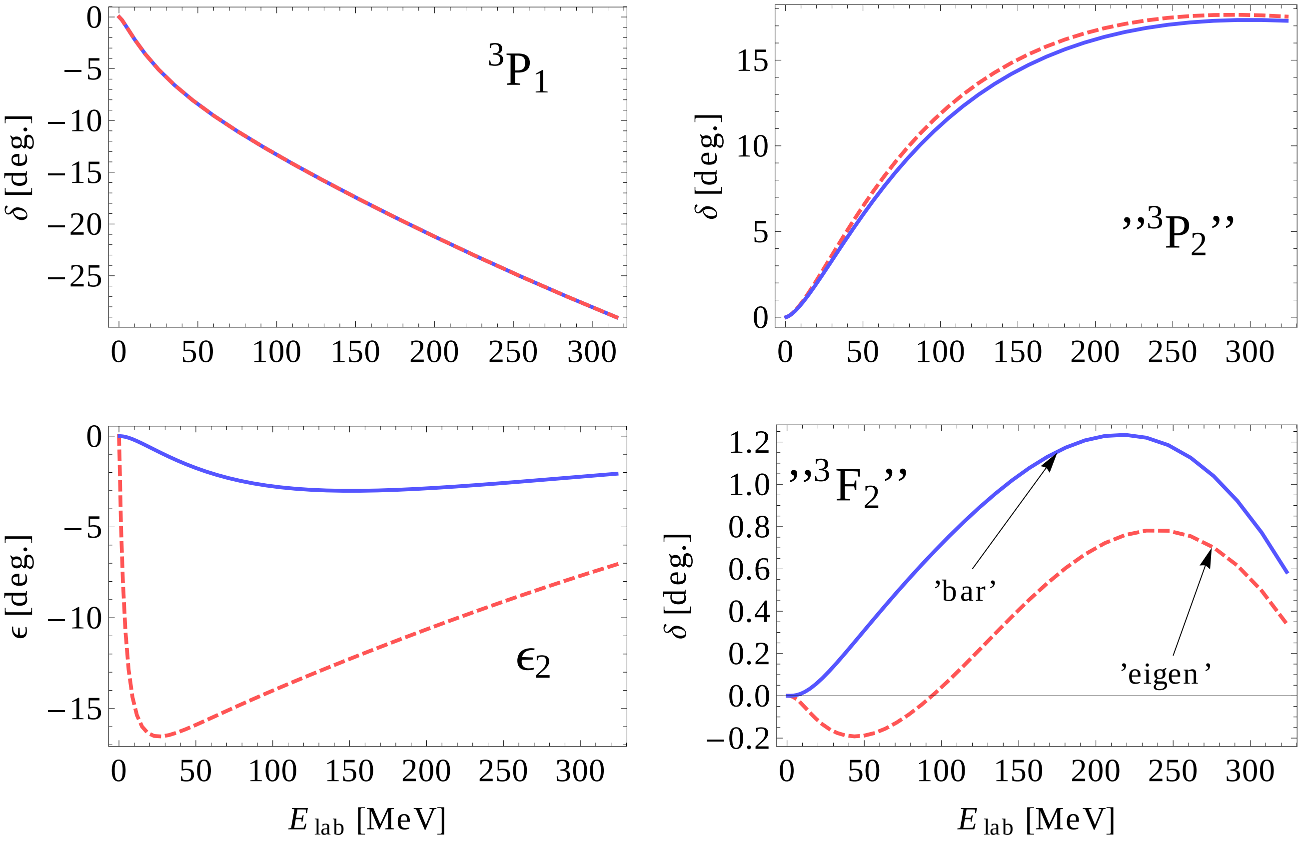

Figure 2.3: The eigen (red dashed line) and bar (blue solid line) phase shifts for selected partial waves, calculated with the Argonne potential.

Since neither a wave function nor a phase shift in the wave function are directly observable, it is helpful to link this concept to properties which are accessible by experiments. For a scattering experiment with a beam described by the statistical operator given by Eq. (2.8), the differential cross section is:

$$
\begin{aligned}
\frac{d\sigma_{\vec{k}}}{d\Omega}(\widehat{\vec{r}}) &= \sum_{m_s(1),m_s(2)} D_{m_s(1)m_s(2)} \sum_{S,T} C^{m_s(1)m_s(2)}_{SSM_S} C^{m_t(1)m_t(2)}_{TTM_T} \left| \left\langle \widehat{\vec{r}} \,\middle|\, \phi^{SM_S}_{scat,\vec{k}}; TM_T \right\rangle \right|^2 \\
&= \sum_{m_s(1),m_s(2)} D_{m_s(1)m_s(2)} \sum_{S,T} C^{m_s(1)m_s(2)}_{SSM_S} C^{m_t(1)m_t(2)}_{TTM_T} \\
&\qquad \cdot \left| \sum_{J=0}^{\infty} \sum_{\alpha=0}^{3} \frac{1}{k} c^{\alpha,SJT} \sin \tilde{\delta}_{\alpha,SJT}(k)\, e^{i\tilde{\delta}_{\alpha,SJT}(k)} \left\langle \widehat{\vec{r}} \,\middle|\, \alpha, SJM_S; TM_T \right\rangle \right|^2 . \qquad (2.34)
\end{aligned}
$$

Starting from known two-nucleon scattering data, it is possible to extract the corresponding phase shifts [47]. Such a phase shift analysis provides an interface between experimental results and theoretical calculations. It is sufficient to calculate the two-nucleon phase shifts for a potential $\underset{\sim}{V}$ and compare those to the phase shifts extracted from the experimental data. If the phase shifts agree, due to Eq. (2.34) the theoretical cross sections obtained with $\underset{\sim}{V}$ and the experimental cross sections will agree as well.

Calculation of phase shifts from interaction matrix elements

Now that the ingredients necessary to describe the scattering process are defined, one has to calculate the phase shifts from the matrix elements of the interaction. Let $\underset{\sim}{H}_0$ be the Hamiltonian for particles without any interaction

$$
\underset{\sim}{H}_0 \left| \vec{k}, SM_S; TM_T \right\rangle = \frac{\vec{k}^2}{2\mu} \left| \vec{k}, SM_S; TM_T \right\rangle \qquad (2.35)
$$

and $\underset{\sim}{H} = \underset{\sim}{H}_0 + \underset{\sim}{V}$ the full Hamiltonian with an scattering eigenstate $\left| \phi_{\vec{k}}, SM_S; TM_T \right\rangle$:

$$
\underset{\sim}{H} \left| \phi_{\vec{k}}, SM_S; TM_T \right\rangle = \left(\underset{\sim}{H}_0 + \underset{\sim}{V} \right) \left| \phi_{\vec{k}}, SM_S; TM_T \right\rangle = \frac{\vec{k}^2}{2\mu} \left| \phi_{\vec{k}}, SM_S; TM_T \right\rangle . \qquad (2.36)
$$

Combining these two equations yields the Lippmann-Schwinger equation [48]

$$
\left| \phi_{\vec{k}}, SM_S; TM_T \right\rangle = \left| \vec{k}, SM_S; TM_T \right\rangle + \left(\frac{k^2}{2\mu} - \underset{\sim}{H}_0 + i\epsilon \right)^{-1} \underset{\sim}{V} \left| \phi_{\vec{k}}, SM_S; TM_T \right\rangle . \qquad (2.37)
$$

Here $+i\epsilon$ is added to prevent the inverse operator on the right-hand side of Eq. (2.37) to create singularities. This corresponds to outgoing boundary conditions[*]. By defining the T-Matrix

$$
\underset{\sim}{T}^{(+)}(k) \left| \vec{k}, SM_S; TM_T \right\rangle = \underset{\sim}{V} \left| \phi_{\vec{k}}, SM_S; TM_T \right\rangle \qquad (2.38)
$$

and multiplying Eq. (2.37) from the left by $\underset{\sim}{V}$, one obtains

$$
\underset{\sim}{T}^{(+)}(k) \left| \vec{k}, SM_S; TM_T \right\rangle = \underset{\sim}{V} \left| \vec{k}, SM_S; TM_T \right\rangle + \underset{\sim}{V} \left(\frac{k^2}{2\mu} - \underset{\sim}{H}_0 + i\epsilon \right)^{-1} \underset{\sim}{T}^{(+)}(k) \left| \vec{k}, SM_S; TM_T \right\rangle . \qquad (2.39)
$$

---

[*] This means, that the asymptotic solution for $r \to \infty$ is a superposition of a plane wave plus an outgoing spherical wave.

Written in the momentum partial wave basis, Eq. (2.39) reads

$$\begin{aligned}\left\langle k(LS)JT \left| \underset{\sim}{T}^{(+)}(k') \right| k'(L'S)JT \right\rangle &= \left\langle k(LS)JT \left| \underset{\sim}{V} \right| k'(L'S)JT \right\rangle \\ &+ \sum_{L''=|J-S|}^{J+S} \int_0^\infty \mathrm{d}q\, q^2 \frac{\left\langle k(LS)JT \left| \underset{\sim}{V} \right| q(L''S)JT \right\rangle \left\langle q(L''S)JT \left| \underset{\sim}{T}^{(+)}(k') \right| k'(L'S)JT \right\rangle}{\frac{k'^2}{2\mu} - \frac{q^2}{2\mu} + i\epsilon}. \end{aligned} \tag{2.40}$$

The energy-on-shell T-Matrix element* $\left\langle k\alpha, SJT \left| \underset{\sim}{T}^{(+)}(k) \right| k\alpha, SJT \right\rangle$ in the eigenbasis Eqs. (2.17) contains the phase shift $\tilde{\delta}_{\alpha,SJT}(k)$ [48]:

$$\left\langle k\alpha, SJT \left| \underset{\sim}{T}^{(+)}(k) \right| k\alpha, SJT \right\rangle = -\frac{\pi}{2} \frac{1}{2\mu k} e^{i\tilde{\delta}_{\alpha,SJT}(k)} \sin\left(\tilde{\delta}_{\alpha,SJT}(k)\right). \tag{2.41}$$

Formally, one would have to solve Eq. (2.40) for a given potential $\underset{\sim}{V}$ to obtain the on-shell matrix elements of the T-Matrix from which the phase shifts can be extracted by using the relation Eq. (2.41). Practically, to get rid of the imaginary part in Eq. (2.40), it is convenient to define a new operator $\underset{\sim}{R}(k)$ by the equation

$$\begin{aligned}\left\langle k(LS)JT \left| \underset{\sim}{R}(k') \right| k'(L'S)JT \right\rangle &= \left\langle k(LS)JT \left| \underset{\sim}{V} \right| k'(L'S)JT \right\rangle \\ &+ \sum_{L''=|J-S|}^{J+S} \mathscr{P} \int_0^\infty \mathrm{d}q\, q^2 \frac{\left\langle k(LS)JT \left| \underset{\sim}{V} \right| q(L''S)JT \right\rangle \left\langle q(L''S)JT \left| \underset{\sim}{R}(k') \right| k'(L'S)JT \right\rangle}{\frac{k'^2}{2\mu} - \frac{q^2}{2\mu}}. \end{aligned} \tag{2.42}$$

$\mathscr{P}$ denotes a Cauchy principal value integral (see Eq. (A.2) in Appendix B.2).

In Eq. (2.42), one easily recognizes that the matrix elements of $\underset{\sim}{R}(k)$ can be chosen to be real numbers because $\underset{\sim}{V}$ is hermitian. It can be shown that the on-shell matrix elements of $\underset{\sim}{T}^{(+)}(k)$ and $\underset{\sim}{R}(k)$ in the eigenbasis (2.17) are connected by the simple relation [49]:

$$\left\langle k\alpha, SJT \left| \underset{\sim}{R}(k) \right| k\alpha, SJT \right\rangle = \left(\cos\tilde{\delta}_{\alpha,SJT}(k)\right)^{-2} \mathrm{Re}\left[\left\langle k\alpha, SJT \left| \underset{\sim}{T}^{(+)}(k) \right| k\alpha, SJT \right\rangle\right]. \tag{2.43}$$

Thus, by using Eq. (2.41), one finds

$$\left\langle k\alpha, SJT \left| \underset{\sim}{R}(k) \right| k\alpha, SJT \right\rangle = -\frac{\pi}{2} \frac{1}{2\mu k} \tan\left(\tilde{\delta}_{\alpha,SJT}(k)\right). \tag{2.44}$$

Instead of solving Eq. (2.40) for the T-Matrix, one can solve Eq. (2.42) and obtain the phase shifts by the relation Eq. (2.44). The phase shifts presented in this work are calculated by solving Eq. (2.42) on an equidistant momentum grid. Technical details like the treatment of the Cauchy principal value integral or coupled partial wave channels can be found in Appendix B.2.

2.2.2 Few-nucleon systems

Phase shifts and deuteron properties alone do not restrain the NN potential enough to use it without further considerations in nuclear ab-initio calculations. In fact, two realistic NN potentials which (by definition) reproduce the two-nucleon properties with the same precision can exhibit differing features already in the three- or four-nucleon system. Thus, it is important to have ab-initio many-body methods available which allow to investigate the properties of a given potential in different few-nucleon systems. In this work, the **No Core Shell Model** and **Fermionic Molecular Dynamics** are applied.

---

* The T-Matrix element $\left\langle k \left| \underset{\sim}{T}^{(+)}(k_0) \right| k' \right\rangle$ is called "(energy-)on-shell matrix element" if $k = k' = k_0$.

No Core Shell Model

In the **No Core Shell Model** (NCSM), the Schrödinger equation is solved by diagonalization of the (intrinsic) Hamiltonian in a harmonic oscillator (HO) basis.

To introduce a truncation scheme for the NCSM model spaces, one uses the eigenstates $\left|\Phi_n^{\text{mf}}\right\rangle$ of the mean field Hamiltonian

$$\underset{\sim}{H}^{\Omega}_{\text{mf}} = \sum_{i=1}^{A}\left(\frac{\underset{\sim}{\vec{p}}_i^{\,2}}{2m} + \frac{1}{2}m\Omega^2\underset{\sim}{\vec{r}}_i^{\,2}\right). \tag{2.45}$$

The eigenstates $\left|\Phi_n^{\text{mf}}\right\rangle$ are Slater determinants describing a configuration of A nucleons occupying certain HO energy shells. As an example, the energetically lowest configuration for the ^{6}Li case, a system of 3 protons and 3 neutrons, is shown in Fig. 2.4.

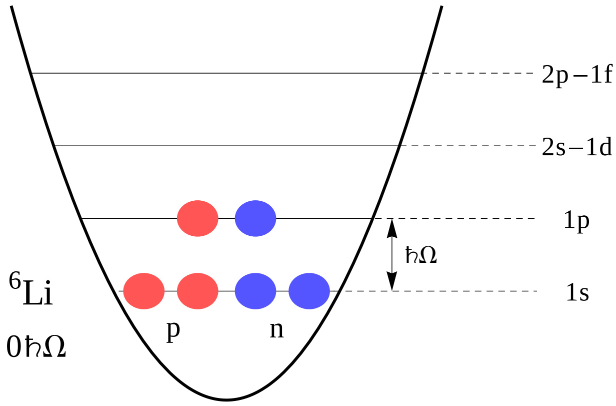

Figure 2.4: The $0\hbar\Omega$ configuration for ^{6}Li: The lowest lying energy HO shells are filled (respecting the Pauli principle) with 3 protons (p) and 3 neutrons (n).

The eigenstates of $\underset{\sim}{H}^{\Omega}_{\text{mf}}$ serve as a representation for the Hamiltonian $\underset{\sim}{H}$ of the A-nucleon system one aims to describe. One can expand eigenstates of the Hamiltonian $\underset{\sim}{H}$ in the eigenstates $\left|\Phi_n^{\text{mf}}\right\rangle$ of $\underset{\sim}{H}^{\Omega}_{\text{mf}}$ which are Slater determinants. For numerical reasons this expansion has to be truncated. One only includes basis states $\left|\Phi_n^{\text{mf}}\right\rangle$ whose mean-field energy does not lie more than $N_{max}\hbar\Omega$ above the energy of the lowest energy state $\left|\Phi_0^{\text{mf}}\right\rangle$:

$$\left\langle\Phi_n^{\text{mf}}\middle|\underset{\sim}{H}^{\Omega}_{\text{mf}}\middle|\Phi_n^{\text{mf}}\right\rangle - \left\langle\Phi_0^{\text{mf}}\middle|\underset{\sim}{H}^{\Omega}_{\text{mf}}\middle|\Phi_0^{\text{mf}}\right\rangle \le N_{max}\hbar\Omega. \tag{2.46}$$

This truncation scheme allows a decoupling of the relative and the c.m. part of the Hamiltonian [50]. Fig. 2.5 shows the configurations $2\hbar\Omega$ above the ground-state for ^{6}Li. A NCSM calculation with $N_{max} = 2$ uses a model space consisting of the Slater determinants with the $0\hbar\Omega$ configuration depicted in Fig. 2.4 and the $2\hbar\Omega$ configurations[*] in Fig. 2.5. In this model space, the Schrödinger equation is solved by diagonalizing the Hamilton matrix.

The truncation to N_{max} creates an Ω- dependence of the intrinsic properties. This dependence is shown in Fig. 2.6. It weakens with increasing model space size but can still be recognized in the $N_{max} = 12$ model space. Nonetheless the calculation is variational. One can calculate the energies for different frequencies Ω and take the lowest energy as the best approximation to the exact energy value. Note, that

---

[*] $1\hbar\Omega$ configurations have a different parity than the $0\hbar\Omega$ and $2\hbar\Omega$ configurations. Since parity is a good quantum number for atomic nuclei, only configurations with either even or odd numbers of HO quanta contribute to nuclear states with even or odd parity, respectively.

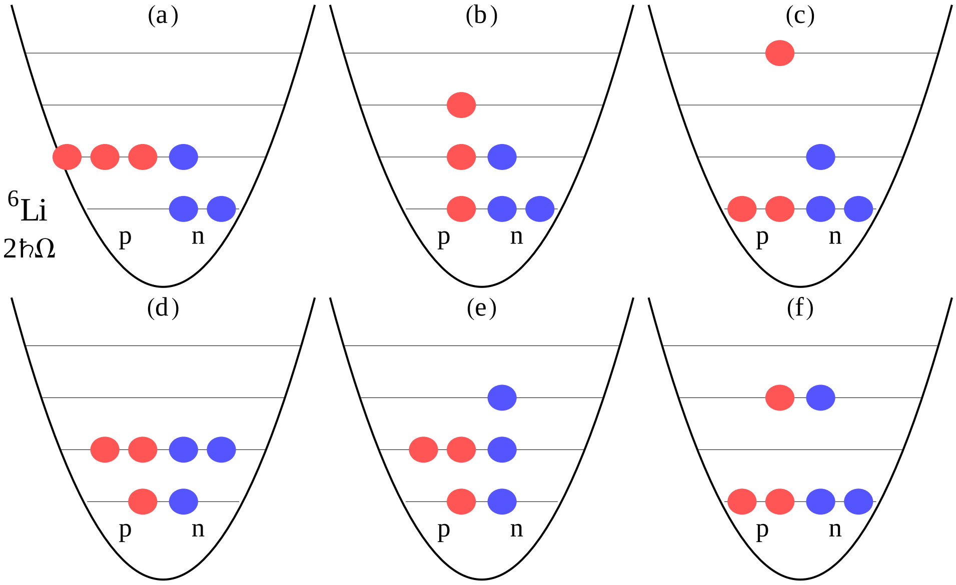

Figure 2.5: Configurations for ^{6}Li with an energy $2\,\hbar\Omega$ above the HO ground-state energy. Note that for (a), (b), (c) and (e) not only the depicted configuration but also a configuration with protons and neutrons exchanged exists.

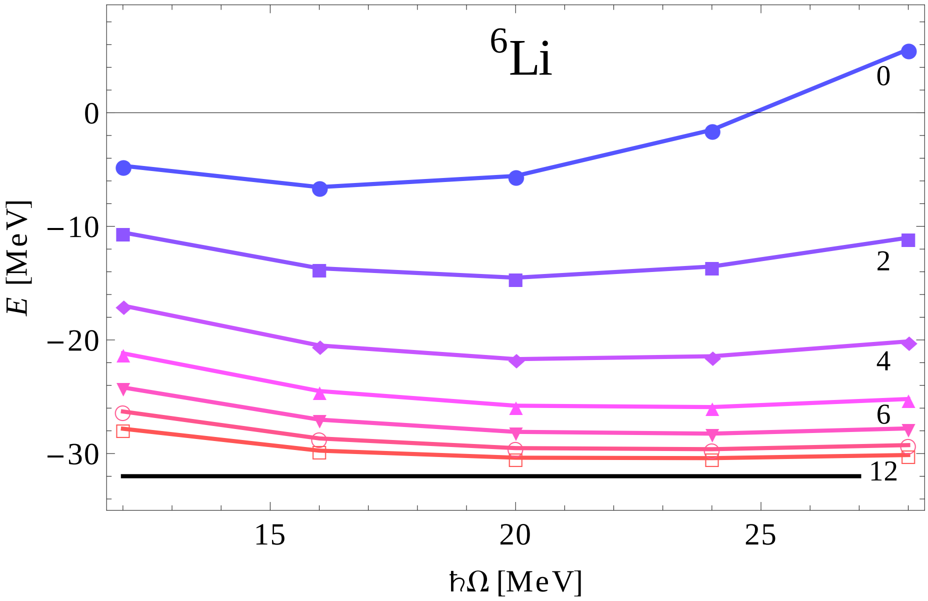

Figure 2.6: The results of a NCSM calculation for the ground state of ^{6}Li using the UCOM(SRG) transformed Argonne potential. The binding energy is plotted as a function of the HO frequency. Each line represents a calculation with a truncation at N_{max} from 0 (upper graph) to 12 (lower graph). The constant black line indicates the experimental value.

for different model space sizes N_{max}, the lowest energy occurs at different frequencies Ω. For example in Fig. 2.6, the lowest energy for $N_{max} = 0$ is found for $\hbar\Omega = 16\,\text{MeV}$ while for $N_{max} = 12$ the energy is minimal for $\hbar\Omega = 24\,\text{MeV}$. Once Ω is fixed by the minimal energy for a given truncation N_{max}, the solutions of the Schrödinger equation in this model space (defined by N_{max} and Ω) can be used to calculate expectation values and transition matrix elements for further observables.

In principle N_{max} has to be chosen large enough, so that the results do not change anymore by increasing the model space. In practice this means that one often has to handle Hilbert spaces with huge dimensions, since the amount of possible configurations increases exponentially with higher N_{max}. In fact the numerical treatment of the occurring large matrices limits the applicability of the NCSM to nuclei up to ^{12}C, where matrices with dimensions of the order of 10^8 or 10^9 have to be handled. By using approximations like the importance truncation [8] one can reach larger mass numbers A. For the NCSM calculations presented in this thesis, convergence is achieved for ^{3}H and ^{3}He in model spaces with $N_{max} = 40^*$ and in some cases, depending on the interaction, for ^{4}He with $N_{max} = 18$. The energies for ^{6}He, ^{6}Li and ^{7}Li do not perfectly converge in the used model space sizes with $N_{max} = 12$ or 10. This is shown in Fig. 2.7 for a ^{6}Li calculation. The binding energy still depends on the model space size and decreases with increasing N_{max}.

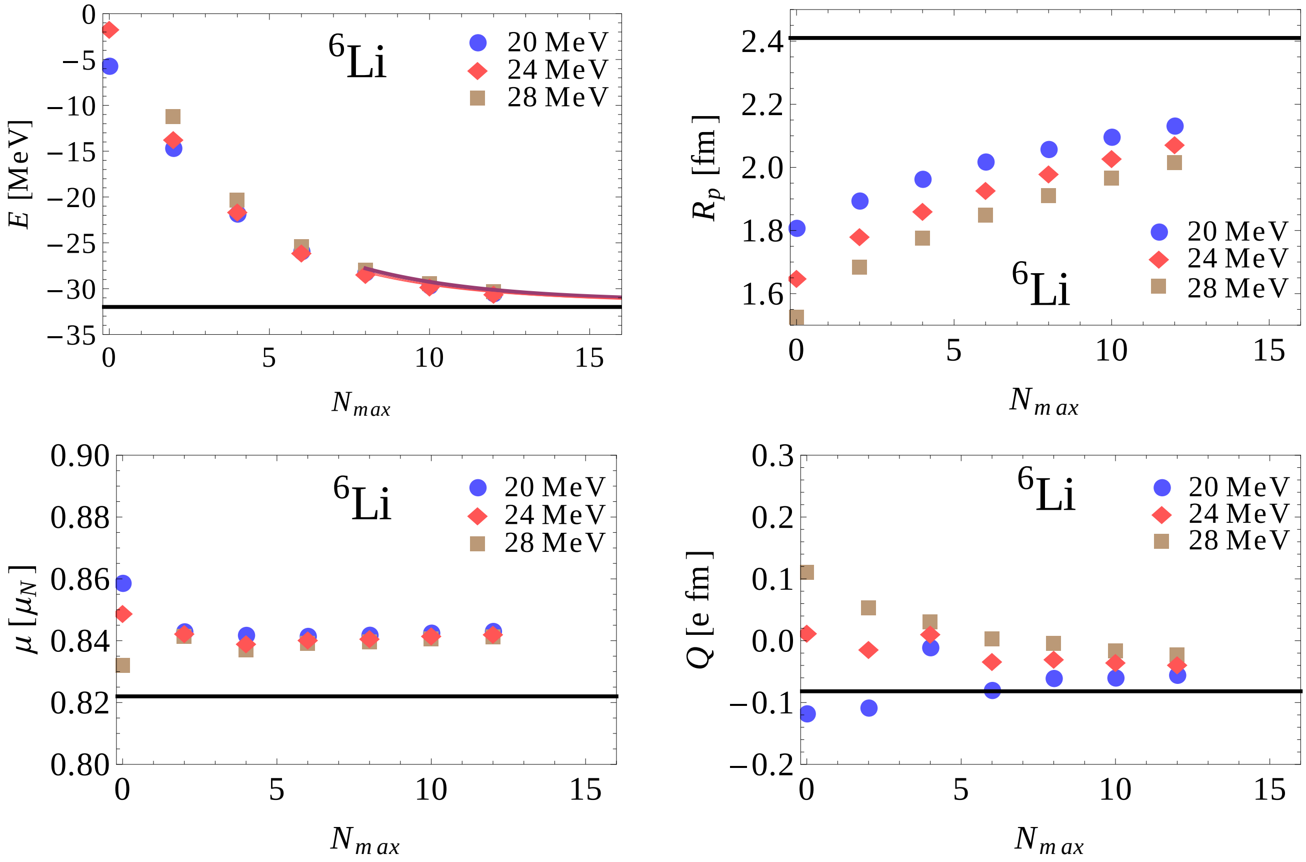

Figure 2.7: Results of a NCSM calculation for the ground state of ^{6}Li using the UCOM(SRG) transformed Argonne potential. The binding energy E, the point-proton radius R_p, the magnetic moment μ and the electric quadrupole moment Q are plotted as a function of the model space size, described by the parameter N_{max}. The black constant lines indicate the experimental values, taken from [51] and [52].

For model spaces with dimensions beyond numerical feasibility one can extrapolate the almost converged energies to infinite model space size by the exponential ansatz

$$E_\Omega(N_{max}) = A_\Omega \exp\left(-\lambda_\Omega N_{max}\right) + B_\Omega, \qquad N_{max} \geq N_0 \tag{2.47}$$

where the parameters A_Ω, B_Ω and λ_Ω are fitted to the calculated energies from model spaces with N_{max} larger than a chosen $N_0{}^\dagger$. The parameter B_Ω gives the extrapolated binding energies for $N_{max} \to \infty$. In Fig. 2.7 the result of such an extrapolation for the binding energies is shown.

---

[*] For most interactions, convergence is already achieved in model spaces smaller than $N_{max} = 40$.

[†] Usually the three data points with the largest N_{max} are used to obtain the extrapolation function.

Note, that convergence of the ground state in a certain model space does not imply, that other observables like excitation energies or radii are converged as well. Fig. 2.7 shows that the results for some observables of a state (in this example the magnetic moment, the electric quadrupole moment and point proton radius) can show a faster or slower convergence than the energies.

For the nuclei with $A \leq 4$ the NCSM calculation in this work are performed with the *ManyEff* code by Petr Navrátil [5]. For larger systems the *Antoine* shell model code was employed [6, 7].

Fermionic Molecular Dynamics

The NCSM is a very powerful tool to calculate properties of light nuclei. Nevertheless there is not only the limitation to nuclei with $A \lesssim 12$ discussed in the last section. Also exotic states of nuclei like pronounced cluster and halo states require huge model spaces. Therefore it is helpful to treat such exotic states in a more appropriate basis, allowing to describe these states in much smaller model spaces.

The **Fermionic Molecular Dynamics** model (FMD) [11–13] is such an approach. FMD can be applied to several physical problems, such as the description of nuclei, nuclear reactions and bulk fermion systems like for example the neutron star crust [53]. In this work FMD is used to calculate the properties of light nuclei by solving the nuclear many-body problem in the so called FMD basis.

In FMD, an A-body trial state $\left| Q \right\rangle$ is given by a Slater determinant

$$\left| Q \right\rangle = \underset{\sim}{\mathcal{A}} \left(\left| q_1 \right\rangle \otimes \left| q_2 \right\rangle \otimes \cdots \otimes \left| q_A \right\rangle \right). \tag{2.48}$$

The single-particle FMD basis states are given by

$$\left| q \right\rangle = \sum_{k=1}^{n} c_k \left| a_k \, \vec{b}_k, \chi_k; \xi \right\rangle, \tag{2.49}$$

where χ_k denotes a two-component spinor and ξ is the isospin of the nucleon. The spatial part is parameterized by Gaussian wave packets

$$\left\langle \vec{r} \middle| a \, \vec{b} \right\rangle = \exp \left\{ -\frac{(\vec{r} - \vec{b})^2}{2a} \right\}, \tag{2.50}$$

where the complex parameters a and $\vec{b}$ encode the width and mean position of the nucleon. In the most simple case a, $\vec{b}$, c and χ are determined variationally by a minimization of the intrinsic energy:

$$E = \frac{\left\langle Q \middle| \underset{\sim}{\hat{H}} - \underset{\sim}{T}_{\mathrm{c.m.}} \middle| Q \right\rangle}{\left\langle Q \middle| Q \right\rangle} \to \mathrm{min}. \tag{2.51}$$

With these trial states not only shell-model like states but also cluster and halo configurations can be described. Thus, FMD is an important tool for the theoretical investigation of such exotic states.

The intrinsic state $\left| Q \right\rangle$ obtained from the minimization Eq. (2.51) does not need to have good total angular momentum J and parity $\pi = \pm$. In order to restore the symmetries, one projects on these quantum numbers by means of the following projection operators:

$$\underset{\sim}{P}^{\pi} = \frac{1}{2} \left(1 + \pi \underset{\sim}{\Pi} \right), \tag{2.52a}$$

$$\underset{\sim}{P}^{J}_{MK} = \int \mathrm{d}\alpha \, \mathrm{d}(\cos\beta) \, \mathrm{d}\gamma \, D^{J*}_{MK}(\alpha, \beta, \gamma) \underset{\sim}{R}(\alpha, \beta, \gamma), \tag{2.52b}$$

where $\underset{\sim}{\Pi}$ performs an inversion at the origin of the coordinate system centered at the c.m. position and $\underset{\sim}{R}(\alpha,\beta,\gamma)$ a rotation with the Euler angles α, β and γ:

$$\underset{\sim}{R}(\alpha,\beta,\gamma) = e^{-i\alpha \underset{\sim}{J}_z} e^{-i\beta \underset{\sim}{J}_y} e^{-i\gamma \underset{\sim}{J}_z}. \tag{2.53}$$

D^J_{MK} is the Wigner D-matrix

$$D^J_{MK} = \left\langle JM \left| e^{-i\alpha \underset{\sim}{J}_z} e^{-i\beta \underset{\sim}{J}_y} e^{-i\gamma \underset{\sim}{J}_z} \right| JK \right\rangle. \tag{2.54}$$

In practice the integration in Eq. (2.52b) is performed numerically.

The projections can be applied either before the variation or afterwards. The first case is called “variation after projection” (VAP), the second one “projection after variation” (PAV). A VAP calculation is computational more demanding. It is therefore restricted to lighter nuclei. In addition the FMD code allows to perform the minimization on a submanifold of the parameters. These may be defined through constraints of physical properties during the variation, such as dipole or quadrupole moments. Solutions obtained with different constraints or optimized for certain angular momenta are used to create linearly independent many-body states as input for a multi-configuration calculation.

After solving the eigenvalue problem for a given Hamiltonian in the Hilbert space spanned by those states, the resulting eigenstates can be used to evaluate further physical properties like densities, radii, magnetic and electric moments or transitions. Fig. 2.8 shows the proton and neutron density of the (unprojected) intrinsic ^{6}Li state, obtained from a PAV minimization using the UCOM transformed Argonne potential.

FMD requires a NN potential which can be written in an operator representation, for example as a sum of radial functions $V^P_{ST}(\underset{\sim}{r})$ multiplied with corresponding operators $\underset{\sim}{\mathcal{O}}_P$.

$$\underset{\sim}{V}_{\mathrm{NN}} = \sum_P \sum_{S,T} \frac{1}{2} \left[\underset{\sim}{\mathcal{O}}_P V^P_{ST}(\underset{\sim}{r}) + V^P_{ST}(\underset{\sim}{r}) \underset{\sim}{\mathcal{O}}_P \right] \tag{2.55}$$

$\underset{\sim}{\mathcal{O}}_p$ can be any operator depending on relative momentum, angular momentum, spin and isospin of the nuclear pair, for example $\underset{\sim}{1}$, $\underset{\sim}{\vec{L}} \cdot \underset{\sim}{\vec{S}}$, the tensor operator $\underset{\sim}{S}_{12}$ or $\underset{\sim}{\vec{p}}^{\,2}$. Since the required precise numerical evaluation of the FMD matrix elements is computationally demanding, one prefers analytical expressions of the matrix elements of the interaction. Therefore, the radial functions $V^P_{ST}(r)$ are parameterized by a sum of gaussians $G_\mu(r)$:

$$G_\mu(r) = \exp\left\{ -\frac{r^2}{2\kappa_\mu} \right\}, \tag{2.56}$$

so that

$$V^P_{ST}(\underset{\sim}{r}) = \sum_\mu \gamma^P_{ST,\mu} G_\mu(\underset{\sim}{r}). \tag{2.57}$$

The FMD matrix element is given by the sum

$$\begin{aligned} \left\langle q_k, q_l \left| \underset{\sim}{V}_{\mathrm{NN}} \right| q_m, q_n \right\rangle &= \\ \sum_P \sum_{S,T} \sum_\mu \frac{1}{2} \gamma^P_{ST,\mu} &\left[\left\langle q_k, q_l \left| \underset{\sim}{\mathcal{O}}_P G_\mu(\underset{\sim}{r}) + G_\mu(\underset{\sim}{r}) \underset{\sim}{\mathcal{O}}_P \right| q_m, q_n \right\rangle \right], \end{aligned} \tag{2.58}$$

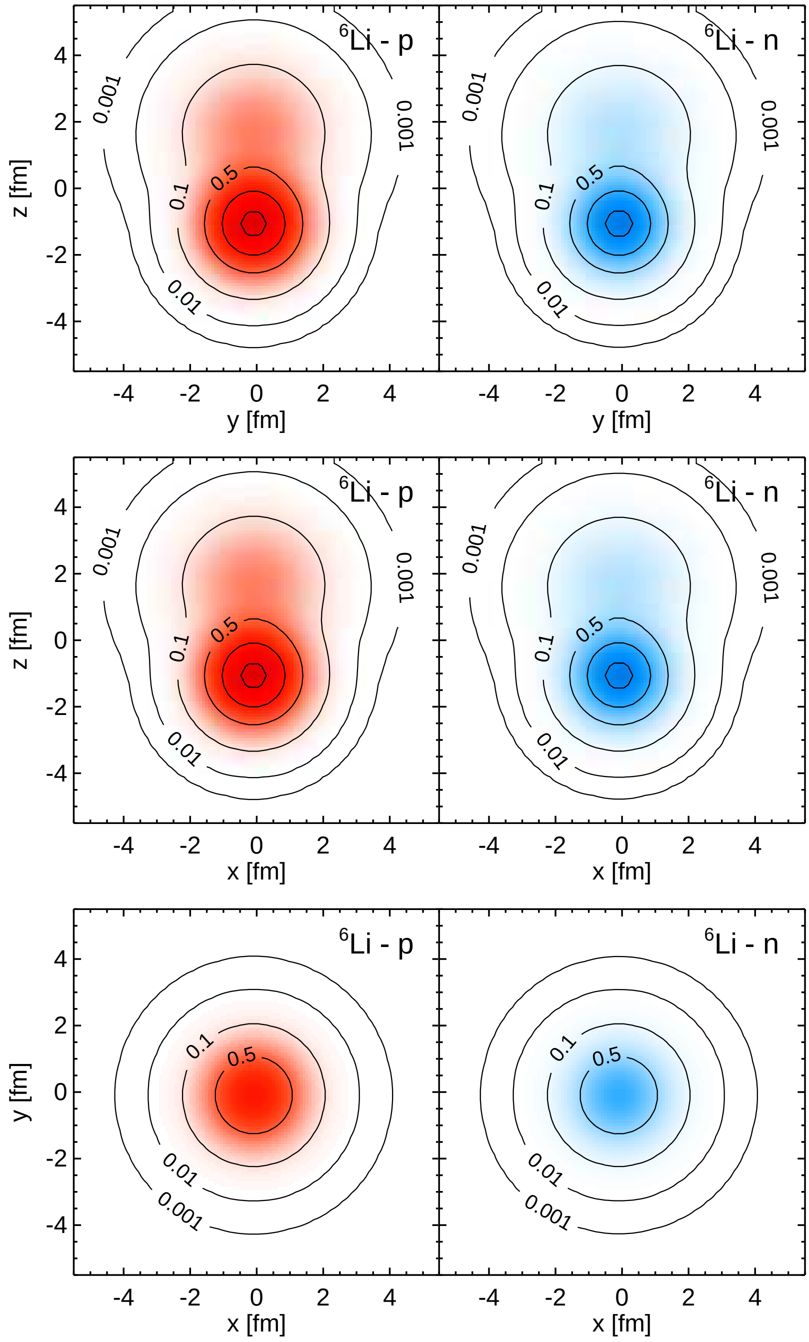

Figure 2.8: Proton (left) and neutron density (right) of the intrinsic ^{6}Li state from an FMD PAV calculation with the UCOM transformed Argonne potential. The two-dimensional plots are shown in planes perpendicular to the axes of inertia of the nucleus.

so that only the expressions for the matrix elements

$$\left\langle q_k, q_l \left| G_\mu(\underset{\sim}{r})\underset{\sim}{\mathcal{O}}_P + G_\mu(\underset{\sim}{r})\underset{\sim}{\mathcal{O}}_P \right| q_m, q_n \right\rangle \tag{2.59}$$

for a standard set of Gaussians $G_\mu(r)$ have to be calculated*.

However, for most effective realistic interactions an operator form such as Eq. (2.55) is not explicitly known. Thus, FMD up to now was limited to the UCOM transformed Argonne potential, which provides an explicit operator representation and is discussed in more detail in Sec. 3. To calculate the FMD matrix elements Eq. (2.59) of the potential, the parameterization given by Eq. (2.57) is used. Only in case of the tensor operators $\underset{\sim}{S}_{12}$, $\bar{S}_{12}(\underset{\sim}{\vec{q}}_\Omega, \underset{\sim}{\vec{q}}_\Omega)$ and $S_{12}(\underset{\sim}{\vec{r}}, \underset{\sim}{\vec{q}}_\Omega)$ occurring in the potential (see Eq. (3.22)), it is more convenient to parameterize the radial functions as

$$
\begin{aligned}
V_{ST}^{T/Tqq}(\underset{\sim}{r}) &= \sum_\mu \gamma_{ST,\mu}^{T/Tqq}\, \underset{\sim}{r}^2 G_\mu(\underset{\sim}{r}) && (2.60a)\\
V_{ST}^{Trq}(\underset{\sim}{r}) &= \sum_\mu \gamma_{ST,\mu}^{Trq}\, \underset{\sim}{r}^3 G_\mu(\underset{\sim}{r}). && (2.60b)
\end{aligned}
$$

The analytic expressions of the FMD matrix elements Eq. (2.59) have been worked out and can be found in Ref. [13] and Appendix C.3.3 and C.4.2.

The parameters $\gamma_{ST,\mu}^P$ and κ_μ can be obtained from a fit to the radial functions in the operator form of the UCOM transformed Argonne potential or from a fit to the partial wave matrix elements of the interaction. The second method is explained in detail in Sec. 4.2 and Ref. [54]. The advantage of the second method is, that it also allows the implementation of interactions in FMD calculations that are only given by partial wave matrix elements. A successful operator representation requires an ansatz rich and flexible enough to describe all partial wave matrix elements of the interaction.

In general, the momentum dependence of a NN potential can be very complicated. Consequently, an operator representation with only local radial functions $V_{ST}^P(r)$, as in Eq. (2.57), is often not flexible enough to describe the momentum dependence of the potential properly. Thus, in this work not only local radial functions but also potentials with nonlocal radial functions $V_{ST}^P(\underset{\sim}{\vec{r}}, \underset{\sim}{\vec{p}})$ are used:

$$
\underset{\sim}{V}_{\mathrm{NN}} = \sum_P \sum_{S,T} \frac{1}{2}\left[\underset{\sim}{\mathcal{O}}_P V_{ST}^P(\underset{\sim}{\vec{r}}, \underset{\sim}{\vec{p}}) + V_{ST}^P(\underset{\sim}{\vec{r}}, \underset{\sim}{\vec{p}})\underset{\sim}{\mathcal{O}}_P\right]. \tag{2.61}
$$

The nonlocal functions do not only depend on the relative distance operator $\underset{\sim}{\vec{r}}$ but also the relative momentum operator $\underset{\sim}{\vec{p}}$. The nonlocal functions are parameterized by the hermitian form

$$
V_{ST}^P(\underset{\sim}{\vec{r}}, \underset{\sim}{\vec{p}}) = \sum_{\mu,\nu} \gamma_{ST,\mu\nu}^P \left(\frac{\kappa_\mu}{\kappa_\mu - \lambda_\nu/4}\right)^{3/2} \exp\left\{-\frac{\lambda_\nu}{4}\underset{\sim}{\vec{p}}^2\right\} \exp\left\{-\frac{\underset{\sim}{\vec{r}}^2}{2(\kappa_\mu - \lambda_\nu/4)}\right\} \exp\left\{-\frac{\lambda_\nu}{4}\underset{\sim}{\vec{p}}^2\right\}, \tag{2.62}
$$

where the additional parameters λ_ν describe the momentum dependence. For $\lambda_\nu = 0$, Eq. (2.62) is identical with the local case in Eq. (2.56). This parameterization is be discussed in more detail in Sec. 4.3.1. Similar to the case of local radial functions Eq. (2.59), one can obtain analytical expressions for the FMD matrix elements for the nonlocal radial functions. The results for the operators used in this work are presented in Appendix C.4.2. The parameters κ_μ, λ_ν and $\gamma_{ST,\mu\nu}^P$ in Eq. (2.62) are obtained by a fit to the partial wave matrix elements of the interaction and presented explicitly in Sec. 4.3.1 and Appendix C.4.1.

In the following different realistic effective NN potentials are discussed. Furthermore, a method is presented which allows to derive the radial functions Eq. (2.56) or (2.62) of an operator representation from the partial wave matrix elements of the potential. It should be emphasized again, that these

---

* In fact, only the matrix element $\langle\, q_k, q_l \,|G_\mu(\underset{\sim}{r})|\, q_m, q_n \,\rangle$ and its derivatives with respect to the parameters a and $\vec{b}$, have to be calculated to obtain the expressions for $\langle\, q_k, q_l \,|\underset{\sim}{\mathcal{O}}_P G_\mu(\underset{\sim}{r}) + G_\mu(\underset{\sim}{r})\underset{\sim}{\mathcal{O}}_P|\, q_m, q_n \,\rangle$. This is shown in detail in Appendix C.4.2.

radial functions are needed to calculate the matrix elements of the NN potential in the FMD basis analytically. Therefore the radial functions are the basic ingredient necessary to use a NN potential in FMD calculations.

3 Effective realistic potentials

Besides the representation of the many-body Hilbert space, the NN potential is the second ingredient to solve the nuclear may-body problem. All realistic NN potentials show a strong repulsion at short relative distances and a dependence on the orientation of the spin of the nucleons. This is illustrated in Fig. 3.1 for the Argonne V18 potential. The repulsive core and the tensor force induce strong correlations in nuclear many-body states which cannot be described by Slater determinants. Methods working in a Slater determinant basis, such as the **No Core Shell Model** (NCSM) or **Fermionic Molecular Dynamics** (FMD), consequently require unmanageable large model spaces to represent the correlations induced by these potentials. All modern methods to deal with this problem employ a unitary transformation of the realistic NN potential to obtain a so called **effective realistic potential** which can be applied in much smaller model spaces. These unitary transformations however induce many-body forces which have to be controlled as they rapidly increase the numerical effort to diagonalize the effective Hamiltonian and calculate other observables which also have to undergo the same unitary transformation. This is subject of present investigations and no final completely satisfying solution has been found yet. In this work only two-body interactions are considered.

In this section different effective realistic potentials are considered. The **Unitary Correlation Operator Method** (UCOM) and the **Similarity Renormalization Group** (SRG) are discussed and applied to the **Argonne V18** potential. Finally the **JISP16** interaction, which can be used without further transformations, is discussed. For all these potentials operator representation are derived later in Sec. 4.

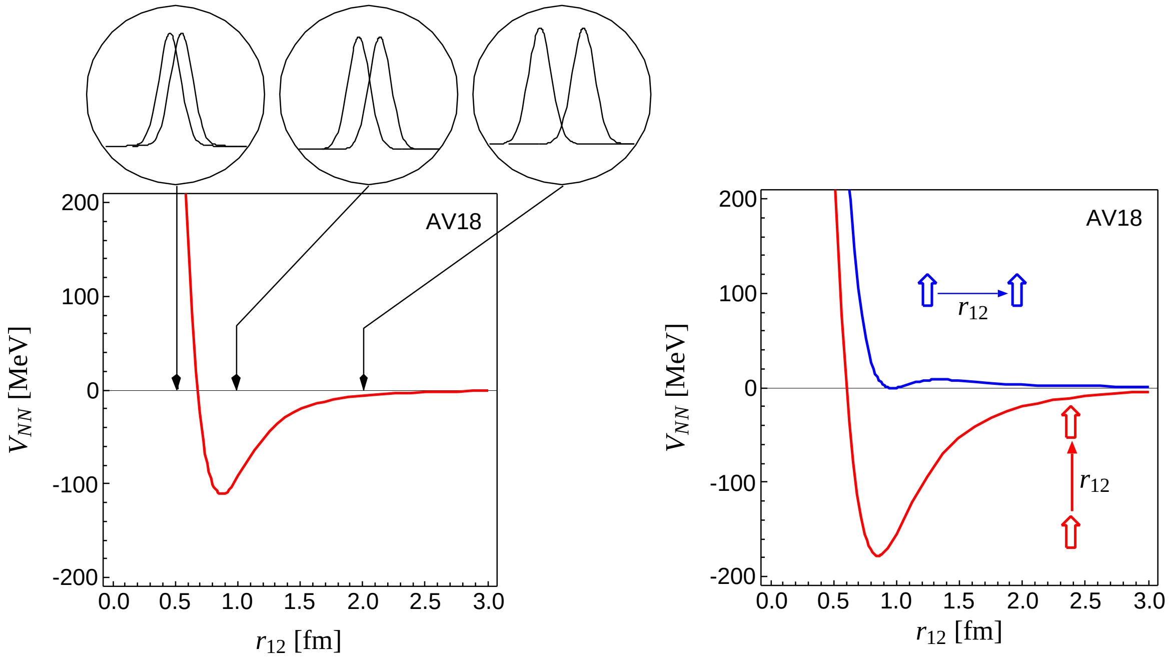

Figure 3.1: Illustration of the short-range repulsion and the tensor force in case of the Argonne V18 potential for relative momentum zero. The left picture shows the potential for $S = 0$ and $T = 1$. At short relative distances r_{12}, where the nucleons strongly overlap, the potential becomes highly repulsive. The right picture shows the potential for $S = 1$ and $T = 0$. The interaction depends, due to the tensor force, significantly on the orientation of the nucleon spins. Figure taken from Ref. [32].

3.1 The Unitary Correlation Operator Method

The concept of the **Unitary Correlation Operator Method** (UCOM) [28–32] is to imprint the short-range central and tensor correlations induced by the nuclear interaction on "simple" many-body states $\left|\Psi\right\rangle$, such as Slater determinants or shell model basis states. The unitary operator $\underset{\sim}{C}$ describes the transformation between the uncorreleated many-body state $\big|\,\Psi\,\big\rangle$ and the state $\big|\,\widehat{\Psi}\,\big\rangle$ which contains central and tensor correlations:

$$\big|\,\widehat{\Psi}\,\big\rangle = \underset{\sim}{C}\,\big|\,\Psi\,\big\rangle. \tag{3.1}$$

To calculate the matrix element $\big\langle\,\widehat{\Psi}\,\big|\underset{\sim}{B}\big|\,\widehat{\Psi}'\,\big\rangle$ of an arbitrary operator $\underset{\sim}{B}$ one can either work with the bare operator $\underset{\sim}{B}$ and correlated states $\big|\,\widehat{\Psi}\,\big\rangle$ or use a correlated operator

$$\widehat{\underset{\sim}{B}} = \underset{\sim}{C}^{-1}\underset{\sim}{B}\,\underset{\sim}{C} = \underset{\sim}{C}^{\dagger}\underset{\sim}{B}\,\underset{\sim}{C} \tag{3.2}$$

and uncorrelated states $\big|\,\Psi\,\big\rangle$ instead:

$$\big\langle\,\widehat{\Psi}\,\big|\underset{\sim}{B}\big|\,\widehat{\Psi}'\,\big\rangle = \big\langle\,\Psi\,\big|\underset{\sim}{C}^{\dagger}\underset{\sim}{B}\,\underset{\sim}{C}\big|\,\Psi'\,\big\rangle = \big\langle\,\Psi\,\big|\widehat{\underset{\sim}{B}}\big|\,\Psi'\,\big\rangle. \tag{3.3}$$

Both methods are equivalent, but it is generally more convenient to correlate the operators and work with uncorrelated, simple states.

The correlation operator $\underset{\sim}{C}$ is decomposed into unitary operators $\underset{\sim}{C}_{\Omega}$ and $\underset{\sim}{C}_{r}$ describing the tensor and central correlations, respectively:

$$\underset{\sim}{C} = \underset{\sim}{C}_{\Omega}\underset{\sim}{C}_{r}. \tag{3.4}$$

The following ansatz

$$\underset{\sim}{C}_{\Omega} = \exp\Big\{ -i\sum_{i<j}\underset{\sim}{g}_{\Omega,ij}\Big\} \tag{3.5a}$$

$$\underset{\sim}{C}_{r} = \exp\Big\{ -i\sum_{i<j}\underset{\sim}{g}_{r,ij}\Big\} \tag{3.5b}$$

with hermitian two-body generators $\underset{\sim}{g}_{r}$ and $\underset{\sim}{g}_{\Omega}$ is used. The form of these generators determines the structure of the central and tensor correlations.

Form of the generators

The short-range repulsion of the interaction prevents the nucleons from approaching each other closer than the extent of the repulsive core. That means, the two-body density at short relative distances will be strongly suppressed in the correlated many-body state. This effect can be achieved by a distance-dependent shift of the radial wave function. Using the projection of the relative momentum $\vec{p} = \frac{1}{2}(\vec{p}_1 - \vec{p}_2)$ on the relative distance vector $\vec{r} = \vec{r}_1 - \vec{r}_2$

$$\underset{\sim}{p}_{r} = \frac{1}{2}\Big[\underset{\sim}{\vec{p}}\,\frac{\vec{r}}{\underset{\sim}{r}} + \frac{\vec{r}}{\underset{\sim}{r}}\,\underset{\sim}{\vec{p}}\Big], \tag{3.6a}$$

which in coordinate representation reads

$$\underset{\sim}{p}_r \overset{\mathbf{r}}{\Longrightarrow} \frac{-i}{r}\frac{\partial}{\partial r} r, \tag{3.6b}$$

together with the shift function $s_{ST}(r)$ describing the amplitude of the radial shift for each spin-isospin channel, the generator can be written as

$$\underset{\sim}{g}_r = \sum_{ST} \frac{1}{2}\left[\underset{\sim}{p}_r s_{ST}(\underset{\sim}{r}) + s_{ST}(\underset{\sim}{r})\underset{\sim}{p}_r\right] \underset{\sim}{\Pi}_{ST}, \tag{3.7}$$

where $\underset{\sim}{\Pi}_{ST}$ is a projector on spin S and isospin T.

The tensor force induces correlations between the orientation of the total spin and that of the relative distance vector $\vec{r}$ of a pair of nucleons. These correlations can be achieved by a tangential shift perpendicular to $\vec{r}$, generated by the “orbital momentum” operator

$$\underset{\sim}{\vec{p}}_\Omega = \underset{\sim}{\vec{p}} - \frac{\vec{r}}{\underset{\sim}{r}}\underset{\sim}{p}_r. \tag{3.8}$$

The generator is given by

$$\underset{\sim}{g}_\Omega = \sum_T \vartheta_T(r) S_{12}(\underset{\sim}{\vec{r}}, \underset{\sim}{\vec{p}}_\Omega)\, \underset{\sim}{\Pi}_{1T}. \tag{3.9}$$

Here the function $\vartheta_T(r)$ describes (like $s_{ST}(r)$ for the central correlations) the distance dependence of the tensor correlations and the generating operator $S_{12}(\underset{\sim}{\vec{r}}, \underset{\sim}{\vec{p}}_\Omega)$, defined by

$$S_{12}(\underset{\sim}{\vec{a}}, \underset{\sim}{\vec{b}}) = \frac{3}{2}\left[(\underset{\sim}{\vec{\sigma}}_1 \cdot \underset{\sim}{\vec{a}})(\underset{\sim}{\vec{\sigma}}_2 \cdot \underset{\sim}{\vec{b}}) + (\underset{\sim}{\vec{\sigma}}_1 \cdot \underset{\sim}{\vec{b}})(\underset{\sim}{\vec{\sigma}}_2 \cdot \underset{\sim}{\vec{a}})\right] - \frac{1}{2}(\underset{\sim}{\vec{\sigma}}_1 \cdot \underset{\sim}{\vec{\sigma}}_2)(\underset{\sim}{\vec{a}} \cdot \underset{\sim}{\vec{b}} + \underset{\sim}{\vec{b}} \cdot \underset{\sim}{\vec{a}}). \tag{3.10}$$

The effect of the central and tensor correlation operators are illustrated in Fig. 3.2. The two-body density calculated with the uncorrelated trial state is not able to describe central and tensor correlations: it has its maximum at a relative distance of zero and shows no dependence on the angular orientation of the nucleons. By applying the central correlation operator $\underset{\sim}{C}_r$ on the trial state, the density at short relative distances is lowered so that the correlations induced by the repulsive core are described by the transformed state. Similarly, the tensor correlation operator $\underset{\sim}{C}_\Omega$ performs an angular shift by which the tensor correlations are imprinted.

The correlation functions $s_{ST}(r)$ and $\vartheta_T(r)$ are specific to the used NN interaction. They can be determined for example by performing an energy minimization in the lowest angular momentum channels, called UCOM(var.) [29, 30]. Another method is to extract them from SRG calculations (UCOM(SRG)) [55]. In this work a UCOM(SRG) transformed interaction is used. Except when noted otherwise, the SRG flow parameter used to obtain the UCOM correlation functions is $s = 0.04\,\mathrm{fm}^4$. For this parameter the ^{3}H and ^{4}He binding energies are optimally reproduced without three- or four-nucleon forces.

The UCOM transformed Argonne potential

The formalism described above can be applied to correlate the nuclear Hamiltonian in two-body approximation. The starting point is an uncorrelated two-body Hamiltonian

$$\underset{\sim}{H} = \underset{\sim}{H}_{\text{int}} + \underset{\sim}{T}_{\text{c.m.}} = \underset{\sim}{T}_{\text{int}} + \underset{\sim}{V} + \underset{\sim}{T}_{\text{c.m.}} \tag{3.11}$$

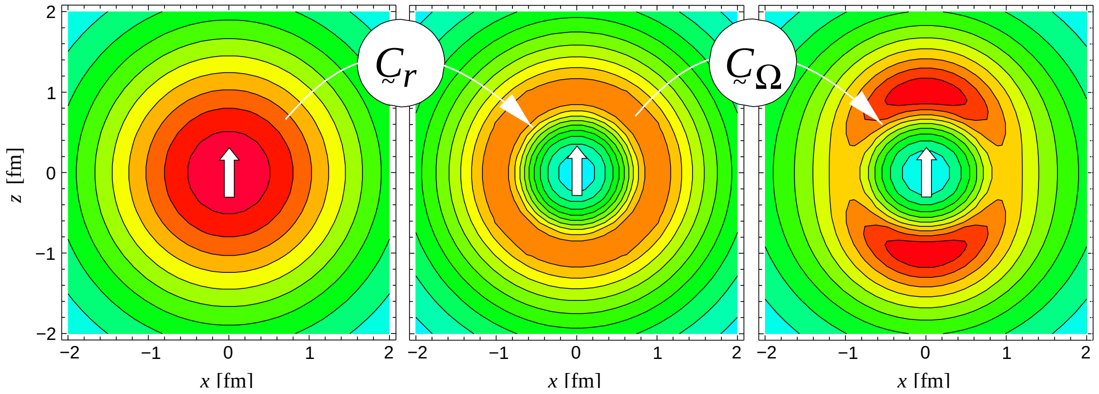

Figure 3.2: The two-body density of ^{4}He for $T = 0$, $S = 1$ and $M_S = +1$. The left picture shows the density calculated with an uncorrelated trial state, the picture in the middle shows the density after applying radial correlations to the same trial state and the right picture the density with additional tensor correlations. Figure taken from Ref. [29].

where the kinetic energy is decomposed into a center-of-mass contribution $\underset{\sim}{T}_{\text{c.m.}}$ and the intrinsic part $\underset{\sim}{T}_{\text{int}}$. $\underset{\sim}{V}$ is a realistic two-body potential. Here the charge independent part of the **Argonne V18** potential [18] is used. It can be written as a sum of functions $v^P_{ST}(\underset{\sim}{r})$ (depending only on the relative distance of two nucleons) multiplied with the corresponding operators*

$$\underset{\sim}{\mathcal{O}}_p \in \{\underset{\sim}{1},\ \underset{\sim}{\vec{L}}^2,\ (\underset{\sim}{\vec{L}}\cdot\underset{\sim}{\vec{S}}),\ \underset{\sim}{S}_{12},\ S_{12}(\underset{\sim}{\vec{L}},\underset{\sim}{\vec{L}})\} \tag{3.12}$$

which act on angular momentum and spin degrees of freedom:

$$\underset{\sim}{V}_{\text{Argonne}} = \sum_P \sum_{ST} v^P_{ST}(\underset{\sim}{r})\underset{\sim}{\mathcal{O}}_P\,\underset{\sim}{\Pi}_{ST}. \tag{3.13}$$

In the operator form Eq. (3.13) the quadratic spin-orbit operator $(\underset{\sim}{\vec{L}}\cdot\underset{\sim}{\vec{S}})^2$ used in Ref. [18] was replaced by the tensor operator $S_{12}(\underset{\sim}{\vec{L}},\underset{\sim}{\vec{L}})$ by means of the relation

$$(\underset{\sim}{\vec{L}}\cdot\underset{\sim}{\vec{S}})^2 = \frac{1}{6}S_{12}(\underset{\sim}{\vec{L}},\underset{\sim}{\vec{L}}) + \frac{2}{3}\underset{\sim}{\vec{L}}^2\underset{\sim}{\Pi}_{S=1} - \frac{1}{2}(\underset{\sim}{\vec{L}}\cdot\underset{\sim}{\vec{S}}).$$

The Argonne potential reads explicitly

$$\begin{aligned}\underset{\sim}{V}_{\text{Argonne}} &= \sum_{ST} v^C_{ST}(\underset{\sim}{r})\,\underset{\sim}{\Pi}_{ST}\\ &+ \sum_{ST} v^{L2}_{ST}(\underset{\sim}{r})\underset{\sim}{\vec{L}}^2\,\underset{\sim}{\Pi}_{ST}\\ &+ \sum_{T} v^{LS}_{1T}(\underset{\sim}{r})(\underset{\sim}{\vec{L}}\cdot\underset{\sim}{\vec{S}})\,\underset{\sim}{\Pi}_{1T}\\ &+ \sum_{T} v^{T}_{1T}(\underset{\sim}{r})\underset{\sim}{S}_{12}\,\underset{\sim}{\Pi}_{1T}\\ &+ \sum_{T} v^{Tll}_{1T}(\underset{\sim}{r})S_{12}(\underset{\sim}{\vec{L}},\underset{\sim}{\vec{L}})\,\underset{\sim}{\Pi}_{1T}.\end{aligned} \tag{3.14}$$

---

* $\underset{\sim}{S}_{12}$ in Eq. (3.12) stands for $S_{12}(\frac{\vec{r}}{\underset{\sim}{r}}, \frac{\vec{r}}{\underset{\sim}{r}})$.

The UCOM transformation is performed in the two-body space. Carried out in an A-body space, the UCOM transformation induces also many-body forces up to A-body forces. Since the UCOM transformation only acts at short ranges, those induced forces are of short range as well. Considering nuclear densities, the probability of three or more nucleons being close enough to see these forces is small. Furthermore, the range of the UCOM tensor correlator in the UCOM(var.) or the flow parameter in the UCOM(SRG) method can be chosen to minimize the effect of induced three- and four-body forces. Thus, a treatment only on the two-body level will be considered in the following.

Central correlations

To derive the central correlated Hamiltonian $\underset{\sim}{C}_r^\dagger \underset{\sim}{H} \underset{\sim}{C}_r$, one has to calculate the correlated kinetic energy $\underset{\sim}{C}_r^\dagger \underset{\sim}{T} \underset{\sim}{C}_r$ and the correlated interaction $\underset{\sim}{C}_r^\dagger \underset{\sim}{V} \underset{\sim}{C}_r$. As the generator $\underset{\sim}{g}_r$ commutes with the operators $\underset{\sim}{O}_P$ occuring in the Argonne potential, only the correlated radial dependencies have to be calculated [28]:

$$\underset{\sim}{C}_r^\dagger \left(v(\underset{\sim}{r})\underset{\sim}{O} \right) \underset{\sim}{C}_r = v(\underset{\sim}{C}_r^\dagger \underset{\sim}{r} \underset{\sim}{C}_r)\, \underset{\sim}{O} = v(R_+(\underset{\sim}{r}))\, \underset{\sim}{O}. \tag{3.15}$$

The correlation function $R_+(r)$ is connected to the shift function $s(r)$ in Eq. (3.7) by the relation $\int_r^{R_+(r)} \frac{\mathrm{d}\xi}{s(\xi)} = 1$.

The central correlation of the kinetic energy results in a sum of one- and many-body operators:

$$\underset{\sim}{C}_r^\dagger \underset{\sim}{T} \underset{\sim}{C}_r = \underset{\sim}{T} + \underset{\sim}{\widehat{T}}^{[2]} + \underset{\sim}{\widehat{T}}^{[3]} \cdots \tag{3.16}$$

In two-body approximation (C2) only the one- and two-body terms are considered

$$\underset{\sim}{C}_r^\dagger \underset{\sim}{T} \underset{\sim}{C}_r \overset{C2}{=} \underset{\sim}{T} + \underset{\sim}{\widehat{T}}^{[2]}. \tag{3.17}$$

While the one-body term is identical to the uncorrelated kinetic energy operator, the two-body term $\underset{\sim}{\widehat{T}}^{[2]}$ contains besides a central and an $\underset{\sim}{\vec{L}}^2$-operator term a contribution with a quadratic momentum dependence:

$$\frac{1}{2}\left[\underset{\sim}{\vec{p}}^2 V_{ST}^{p2}(\underset{\sim}{r}) + V_{ST}^{p2}(\underset{\sim}{r})\underset{\sim}{\vec{p}}^2\right], \tag{3.18}$$

where $V_{ST}^{p2}(\underset{\sim}{r})$ is expressed in terms of $R_+(r)$ and its derivatives.

Tensor correlations

The transformation of the Hamiltonian with the tensor correlation operator can be evaluated by means of the Baker-Campbell-Hausdorff expansion:

$$\underset{\sim}{C}_\Omega^\dagger \underset{\sim}{H} \underset{\sim}{C}_\Omega = \underset{\sim}{H} + i\left[\underset{\sim}{g}_\Omega, \underset{\sim}{H}\right] + \frac{i^2}{2}\left[\underset{\sim}{g}_\Omega, \left[\underset{\sim}{g}_\Omega, \underset{\sim}{H}\right]\right] + \cdots \; . \tag{3.19}$$

Calculating the commutator of $\underset{\sim}{g}_\Omega$ with the operators $\underset{\sim}{T}$, $\underset{\sim}{\vec{L}}^2$, $(\underset{\sim}{\vec{L}} \cdot \underset{\sim}{\vec{S}})$, $\underset{\sim}{S}_{12}$, $S_{12}(\underset{\sim}{\vec{L}}, \underset{\sim}{\vec{L}})$ occuring in the Hamiltonian creates additional central, spin-orbit and tensor contributions. In addition, new operators like

$$\bar{S}_{12}(\underset{\sim}{\vec{p}}_\Omega, \underset{\sim}{\vec{p}}_\Omega) = 2\underset{\sim}{r}^2 S_{12}(\underset{\sim}{\vec{p}}_\Omega, \underset{\sim}{\vec{p}}_\Omega) + S_{12}(\underset{\sim}{\vec{L}}, \underset{\sim}{\vec{L}}) - \frac{1}{2}\underset{\sim}{S}_{12} \tag{3.20}$$

and $S_{12}(\underset{\sim}{\vec{r}}, \underset{\sim}{\vec{p}}_\Omega)$ appear [30].

Different from the central correlator, the commutator algebra is not closed for the tensor correlator and higher orders lead to further new operators with the structure $\underset{\sim}{\vec{L}}^{2n}(\underset{\sim}{\vec{L}}\cdot\underset{\sim}{\vec{S}})$, $\underset{\sim}{\vec{L}}^{2n}\underset{\sim}{S}_{12}(\underset{\sim}{\vec{L}},\underset{\sim}{\vec{L}})$ and $\underset{\sim}{\vec{L}}^{2n}\bar{S}_{12}(\underset{\sim}{\vec{p}}_{\Omega},\underset{\sim}{\vec{p}}_{\Omega})$, with $n = 1, 2, 3, \cdots$. The contributions of terms with higher-order angular momentum operators will become important with increasing angular momentum quantum numbers L. However, for large values of L, due to the centrifugal barrier the relative wave function moves more and more outside the range of $\vartheta_T(r)$. Therefore the action of $\underset{\sim}{C}_{\Omega}$ ceases and one may perform a partial summation in Eq. (3.19) neglecting all terms beyond the third order of angular momentum $\underset{\sim}{\vec{L}}$.

Operator representation of the UCOM potential

The UCOM potential V_{UCOM} is defined as the two-body part of the correlated Hamiltonian

$$\underset{\sim}{C}_r^{\dagger}\underset{\sim}{C}_{\Omega}^{\dagger}\underset{\sim}{H}\underset{\sim}{C}_{\Omega}\underset{\sim}{C}_r = \underset{\sim}{C}_r^{\dagger}\underset{\sim}{C}_{\Omega}^{\dagger}\left(\underset{\sim}{T}+\underset{\sim}{V}\right)\underset{\sim}{C}_{\Omega}\underset{\sim}{C}_r \overset{C2}{=} \underset{\sim}{T} + \underset{\sim}{\widehat{T}}^{[2]} + \underset{\sim}{\widehat{V}}^{[2]} =: \underset{\sim}{T} + \underset{\sim}{V}_{\text{UCOM}}. \tag{3.21}$$

For the Argonne potential as initial potential one finds, using the relations discussed above, the structure [31]

$$\begin{aligned}
\underset{\sim}{V}_{\text{UCOM}} &= \sum_{ST} V_{ST}^{C}(\underset{\sim}{r})\,\underset{\sim}{\Pi}_{ST} \\
&+ \sum_{ST} V_{ST}^{L2}(\underset{\sim}{r})\underset{\sim}{\vec{L}}^{2}\,\underset{\sim}{\Pi}_{ST} \\
&+ \sum_{ST} \frac{1}{2}\left[\underset{\sim}{\vec{p}}^{2}V_{ST}^{p2}(\underset{\sim}{r}) + V_{ST}^{p2}(\underset{\sim}{r})\underset{\sim}{\vec{p}}^{2}\right]\underset{\sim}{\Pi}_{ST} \\
&+ \sum_{T} V_{1T}^{LS}(\underset{\sim}{r})(\underset{\sim}{\vec{L}}\cdot\underset{\sim}{\vec{S}})\,\underset{\sim}{\Pi}_{1T} \\
&+ \sum_{T} V_{1T}^{L2LS}(\underset{\sim}{r})\underset{\sim}{\vec{L}}^{2}(\underset{\sim}{\vec{L}}\cdot\underset{\sim}{\vec{S}})\,\underset{\sim}{\Pi}_{1T} \\
&+ \sum_{T} V_{1T}^{T}(\underset{\sim}{r})\underset{\sim}{S}_{12}\,\underset{\sim}{\Pi}_{1T} \\
&+ \sum_{T} V_{1T}^{Tll}(\underset{\sim}{r})S_{12}(\underset{\sim}{\vec{L}},\underset{\sim}{\vec{L}})\,\underset{\sim}{\Pi}_{1T} \\
&+ \sum_{T} V_{1T}^{Tpp}(\underset{\sim}{r})\bar{S}_{12}(\underset{\sim}{\vec{p}}_{\Omega},\underset{\sim}{\vec{p}}_{\Omega})\,\underset{\sim}{\Pi}_{1T} \\
&+ \sum_{T} \frac{1}{2}\left[\underset{\sim}{p}_r V_{1T}^{Trp}(\underset{\sim}{r}) + V_{1T}^{Trp}(\underset{\sim}{r})\underset{\sim}{p}_r\right]S_{12}(\underset{\sim}{\vec{r}},\underset{\sim}{\vec{p}}_{\Omega})\,\underset{\sim}{\Pi}_{1T} \\
&+ \sum_{T} \frac{1}{2}V_{1T}^{L2Tpp}(\underset{\sim}{r})\left[\underset{\sim}{\vec{L}}^{2}\bar{S}_{12}(\underset{\sim}{\vec{p}}_{\Omega},\underset{\sim}{\vec{p}}_{\Omega}) + \bar{S}_{12}(\underset{\sim}{\vec{p}}_{\Omega},\underset{\sim}{\vec{p}}_{\Omega})\underset{\sim}{\vec{L}}^{2}\right]\underset{\sim}{\Pi}_{1T}.
\end{aligned} \tag{3.22}$$

The new radial functions* $V_{ST}^{P}(r)$ depend on the initial potential and the correlation functions $s_{ST}(r)$ and $\vartheta_T(r)$. Compared to the bare potential Eq. (3.14) the operator structure is more complicated and contains the additional spin-orbit and tensor operators $\underset{\sim}{\vec{L}}^{2}(\underset{\sim}{\vec{L}}\cdot\underset{\sim}{\vec{S}})$, $\bar{S}_{12}(\underset{\sim}{\vec{p}}_{\Omega},\underset{\sim}{\vec{p}}_{\Omega})$, $S_{12}(\underset{\sim}{\vec{r}},\underset{\sim}{\vec{p}}_{\Omega})$ (plus all the higher-order angular momentum operators neglected in the partial summation) and the explicitly momentum dependent operators $\underset{\sim}{\vec{p}}^{2}$ and $\underset{\sim}{p}_r S_{12}(\underset{\sim}{\vec{r}},\underset{\sim}{\vec{p}}_{\Omega})$. The momentum dependence originates from the

---

[*] To indicate the differences between the radial functions of the initial Argonne potential and the UCOM transformed potential, the radial functions of the Argonne potential are written in lower-case letters $v_{ST}^{P}(r)$ while those of the UCOM interaction are written in capital letters $V_{ST}^{P}(r)$.

transformed kinetic energy operator. Therefore the UCOM potential* $\underset{\sim}{V}_{\mathrm{UCOM}}$ is always nonlocal, even if the initial interaction is local. The UCOM transformed potential is "softer" than the initial Argonne potential. That means the short range repulsion and tensor is weakend and replaced by momentum dependent operators. The operator representation of the UCOM transformed Argonne potential in Eq. (3.22) gives a good impression of the general structure of the interaction. The more complex structure compared to the initial potential is the price one pays for the ability to work with simple model states.

Matrix elements of the UCOM potential

In practical applications one often uses a fixed many-body basis and works with a matrix representation. In those cases it is not necessary to derive the operator representation because one can perform the UCOM transformation directly for the matrix elements. The derivation of the matrix elements of a UCOM transformed interaction in basis representation is discussed in the following.

In matrix representation with basis states that possess good angular momentum and spin quantum numbers, like in the shell model or the partial wave basis in momentum space, the operator structure and its truncation is not explicitly needed. In that case it is possible to perform the UCOM transformation exactly in the given basis. With the relations given in Ref. [31] one finds for the matrix elements of the correlated interaction terms with the operators $\underset{\sim}{\mathcal{O}}$ in Eq. (3.12) in the partial wave basis† $\left| k(LS)J;T \right\rangle$

$$\left\langle k(JS)J;T \left| \underset{\sim}{C}_r^{\dagger} \underset{\sim}{C}_{\Omega}^{\dagger} \underset{\sim}{v}(\underset{\sim}{r}) \underset{\sim}{\mathcal{O}} \underset{\sim}{C}_{\Omega} \underset{\sim}{C}_r \right| k'(JS)J;T \right\rangle = \frac{2}{\pi} \int_0^{\infty} \mathrm{d}r\, r^2\, j_J(kr) \widehat{v}(r) j_J(k'r) \left\langle (JS)J;T \left| \underset{\sim}{\mathcal{O}} \right| (JS)J;T \right\rangle \tag{3.23a}$$

$$\begin{aligned} \left\langle k(J\mp 1S)J;T \left| \underset{\sim}{C}_r^{\dagger} \underset{\sim}{C}_{\Omega}^{\dagger} \underset{\sim}{v}(\underset{\sim}{r}) \underset{\sim}{\mathcal{O}} \underset{\sim}{C}_{\Omega} \underset{\sim}{C}_r \right| k'(J\mp 1S)J;T \right\rangle = {} & \frac{2}{\pi} \int_0^{\infty} \mathrm{d}r\, r^2\, j_{J\mp 1}(kr) \widehat{v}(r) j_{J\mp 1}(k'r) \cdot \\ & \Big[\left\langle (J\mp 1S)J;T \left| \underset{\sim}{\mathcal{O}} \right| (J\mp 1S)J;T \right\rangle \left(\cos\widehat{\Theta}(r)\right)^2 \\ & + \left\langle (J\pm 1S)J;T \left| \underset{\sim}{\mathcal{O}} \right| (J\pm 1S)J;T \right\rangle \left(\sin\widehat{\Theta}(r)\right)^2 \\ & \pm \left\langle (J\mp 1S)J;T \left| \underset{\sim}{\mathcal{O}} \right| (J\pm 1S)J;T \right\rangle 2\cos\widehat{\Theta}(r)\sin\widehat{\Theta}(r) \Big] \end{aligned} \tag{3.23b}$$

$$\begin{aligned} \left\langle k(J\mp 1S)J;T \left| \underset{\sim}{C}_r^{\dagger} \underset{\sim}{C}_{\Omega}^{\dagger} \underset{\sim}{v}(\underset{\sim}{r}) \underset{\sim}{\mathcal{O}} \underset{\sim}{C}_{\Omega} \underset{\sim}{C}_r \right| k'(J\pm 1S)J;T \right\rangle = {} & \frac{2}{\pi} \int_0^{\infty} \mathrm{d}r\, r^2\, j_{J\mp 1}(kr) \widehat{v}(r) j_{J\pm 1}(k'r) \cdot \\ & \Big[\left\langle (J\mp 1S)J;T \left| \underset{\sim}{\mathcal{O}} \right| (J\pm 1S)J;T \right\rangle \left(\cos\widehat{\Theta}(r)\right)^2 \\ & - \left\langle (J\pm 1S)J;T \left| \underset{\sim}{\mathcal{O}} \right| (J\mp 1S)J;T \right\rangle \left(\sin\widehat{\Theta}(r)\right)^2 \\ & \mp \left\langle (J\mp 1S)J;T \left| \underset{\sim}{\mathcal{O}} \right| (J\mp 1S)J;T \right\rangle \cos\widehat{\Theta}(r)\sin\widehat{\Theta}(r) \\ & \pm \left\langle (J\pm 1S)J;T \left| \underset{\sim}{\mathcal{O}} \right| (J\pm 1S)J;T \right\rangle \cos\widehat{\Theta}(r)\sin\widehat{\Theta}(r) \Big], \end{aligned} \tag{3.23c}$$

---

[*] In the following, the UCOM correlated Argonne potential will be often called, for reasons of simplification, just "UCOM potential". Note that a UCOM transformed potential always depends on the initial interaction, so that the structure of the UCOM transformed Argonne potential differs from the structure of other UCOM transformed potentials.

[†] See Appendix A.2.3.

where the abbreviations $\widehat{\Theta}(r) = 3\sqrt{J(J+1)}\vartheta(R_+(r))$ and $\widehat{v}(r) = v(R_+(\underset{\sim}{r}))$ were used[*].

The correlated kinetic energy matrix elements can be written as

$$\begin{aligned}
\langle k(JS)J;T \left| \underset{\sim}{C}_r^\dagger \underset{\sim}{C}_\Omega^\dagger \underset{\sim}{T} \underset{\sim}{C}_\Omega \underset{\sim}{C}_r \right| k'(JS)J;T \rangle \;=\;& \frac{2}{\pi}\int_0^\infty \mathrm{d}r\, r^2 \Big\{ j_J(kr) j_J(k'r) \Big[\frac{W(r)}{2\widehat{\mu}_r(r)} + \frac{\widehat{\mu}_r'(r)}{2\left(\widehat{\mu}_r(r)\right)^2}\frac{R_+''(r)}{\left(R_+'(r)\right)^2}\Big] \\
& -\frac{1}{2}\left[j_J''(kr)j_J(k'r) + j_J(kr)j_J''(k'r)\right] \frac{1}{2\widehat{\mu}_r(r)\left(R_+'(r)\right)^2}\Big\}
\end{aligned} \tag{3.23d}$$

$$\begin{aligned}
\langle k(J\mp 1S)J;T \left| \underset{\sim}{C}_r^\dagger \underset{\sim}{C}_\Omega^\dagger \underset{\sim}{T} \underset{\sim}{C}_\Omega \underset{\sim}{C}_r \right| k'(J\mp 1S)J;T \rangle \;=\;& \frac{2}{\pi}\int_0^\infty \mathrm{d}r\, r^2 \Big\{ j_{J\mp 1}(kr) j_{J\mp 1}(k'r) \cdot \\
& \Big[\frac{W(r)}{2\widehat{\mu}_r(r)} + \frac{\left(\widehat{\Theta}'(r)\right)^2}{2\widehat{\mu}_r(r)} + \frac{\widehat{\mu}_r'(r)}{2\left(\widehat{\mu}_r(r)\right)^2}\frac{R_+''(r)}{\left(R_+'(r)\right)^2}\Big] \\
& -\frac{1}{2}\left[j_{J\mp 1}(kr)j_{J\mp 1}''(k'r) + j_{J\mp 1}''(kr)j_{J\mp 1}(k'r)\right] \\
& \cdot \frac{1}{2\widehat{\mu}_r(r)\left(R_+'(r)\right)^2}\Big\}
\end{aligned} \tag{3.23e}$$

$$\begin{aligned}
\langle k(J\mp 1S)J;T \left| \underset{\sim}{C}_r^\dagger \underset{\sim}{C}_\Omega^\dagger \underset{\sim}{T} \underset{\sim}{C}_\Omega \underset{\sim}{C}_r \right| k'(J\pm 1S)J;T \rangle \;=\;& \pm\frac{2}{\pi}\int_0^\infty \mathrm{d}r\, r^2 \left[j_{J\mp 1}(kr)j_{J\pm 1}'(k'r) + j_{J\mp 1}'(kr)j_{J\pm 1}(k'r)\right] \cdot \\
& \frac{\left(\widehat{\Theta}'(r)\right)^2}{2\widehat{\mu}_r(r)\left(R_+'(r)\right)^2}.
\end{aligned} \tag{3.23f}$$

$f'(kr)$, $f''(kr)$ and $f'''(kr)$ here denote the partial derivatives with respect to r and the definitions

$$\begin{aligned}
W(r) &= \frac{7R_+''(r)^2}{4\left(R_+'(r)\right)^4} - \frac{R_+'''(r)}{2\left(R_+'(r)\right)^3} \\
\frac{1}{2\mu_r(r)} &= \frac{1}{2\mu}\left(\frac{1}{\left(R_+'(r)\right)^2} - 1\right)
\end{aligned}$$

are used. Using the relations Eqs. (3.23), the matrix elements of $\underset{\sim}{V}_{\mathrm{UCOM}}$ can be calculated by

$$\langle k(LS)J;T \left| \underset{\sim}{V}_{\mathrm{UCOM}} \right| k'(L'S)J;T \rangle = \langle k(LS)J;T \left| \underset{\sim}{C}_r^\dagger \underset{\sim}{C}_\Omega^\dagger \underset{\sim}{H}_{\mathrm{int}} \underset{\sim}{C}_\Omega \underset{\sim}{C}_r - \underset{\sim}{T}_{\mathrm{int}} \right| k'(L'S)J;T \rangle. \tag{3.24}$$

Fig. 3.3 shows the matrix elements of the bare Argonne potential and the matrix elements of the UCOM transformed Argonne potential for the ${}^3\mathrm{S}_1$ and the ${}^3\mathrm{S}_1$–${}^3\mathrm{D}_1$ channel. In momentum space representation the short range repulsion and tensor force result in large off-diagonal matrix elements and therefore in

---

[*] Note that $R_+(r)$, $\widehat{v}(r)$ and $\widehat{\Theta}(r)$ in Eqs. (3.23) depend on S and T ($\widehat{\Theta}(r)$ additionally depends on J). For reasons of a shorter notation this is not indicated explicitly.

a coupling of low momentum modes to high momentum modes. The UCOM transformation leads to significant lowering of the off-diagonal matrix elements. Hence, in the picture of momentum space matrix elements the softening of the short range repulsion and tensor can be seen as a suppression of the off-diagonal matrix elements.

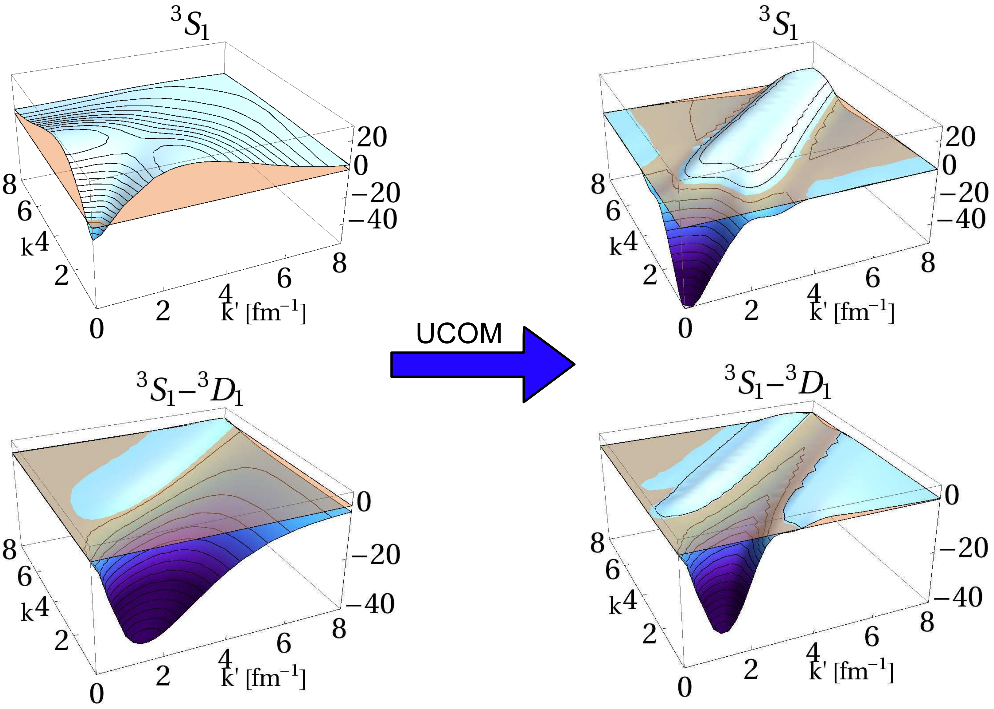

Figure 3.3: The partial wave matrix elements (in MeVfm^3) of the $^3S_1$ and $^3S_1 -^3 D_1$ channel of the bare Argonne potential (left) and the UCOM transformed Argonne potential (right).

The matrix elements obtained by the expression Eq. (3.24) and Eqs. (3.23) are exact on the two-body level and include no approximations like the partial summation of the Baker-Campbell-Hausdorff expansion in the operator representation. For models which use interaction matrix elements as input for the calculation one can directly calculate the UCOM matrix elements and if necessary transform them into the used basis (e.g. harmonic oscillator basis for the shell model) without considering the operator structure. Nevertheless, models such as FMD or Antisymmetrized Molecular Dynamics (AMD) [14] require the operator representation Eq. (3.22). For these models the operator structure and the radial dependencies are needed.

The UCOM transformed Argonne potential is the only phase shift equivalent effective interaction for which an operator representation is explicitly known. Another advantage is that it contains only a quadratic momentum dependence. For all other effective realistic potentials no operator representation exists and their momentum dependence goes beyond a simple quadratic form. In the following two examples for which only matrix element representations are available, namely a Similarity Renormalization Group generated effective potential and the JISP16 interaction, are discussed.

3.2 Similarity Renormalization Group

The **Similarity Renormalization Group** [37, 56–58] is used to derive an effective (intrinsic) Hamiltonian $\underset{\sim}{H}_s$ related to the initial Hamiltonian $\underset{\sim}{H}$ by a unitary transformation

$$\underset{\sim}{H}_s = \underset{\sim}{U}(s)\underset{\sim}{H}\underset{\sim}{U}^\dagger(s) = \underset{\sim}{T}_{\text{int}} + \underset{\sim}{V}_s \tag{3.25}$$

with the flow parameter s. $\underset{\sim}{H}_s$ evolves according to the flow equation

$$\frac{d\underset{\sim}{H}_s}{ds} = \left[\underset{\sim}{\eta}_s, \underset{\sim}{H}_s\right], \tag{3.26}$$

where $\underset{\sim}{\eta}_s$ is the anti-hermitian generator which specifies the transformation:

$$\underset{\sim}{\eta}_s = \frac{d\underset{\sim}{U}(s)}{ds}\underset{\sim}{U}^{\dagger}(s) = -\underset{\sim}{\eta}^{\dagger}. \tag{3.27}$$

The generator itself is expressed by the commutator of a meta-generator $\underset{\sim}{G}_s$ and the evolved Hamiltonian:

$$\underset{\sim}{\eta}_s = \left[\underset{\sim}{G}_s, \underset{\sim}{H}_s\right]. \tag{3.28}$$

The meta-generator has to be chosen such, that the desired renormalization is achieved. The choice of the meta-generator is still a subject of present research. In most applications a generator proportional to the intrinsic kinetic energy operator $\underset{\sim}{T}_{\text{int}}$ is taken, e.g.

$$\underset{\sim}{\eta}_s = m^2\left[\underset{\sim}{T}_{\text{int}}, \underset{\sim}{H}_s\right], \tag{3.29}$$

as proposed in Ref. [58]. Other choices (e.g. those presented in Refs. [59, 60]) are possible as well. But in the following, only the generator defined in Eq. (3.29) is used.

In two-body space, under the assumption of equal masses, the kinetic energy decomposes into

$$\underset{\sim}{T} = \frac{1}{2m}\left(\underset{\sim}{\vec{p}}_1^{\,2} + \underset{\sim}{\vec{p}}_2^{\,2}\right) = \frac{1}{4m}\underset{\sim}{\vec{P}}_{\text{c.m.}}^{\,2} + \frac{1}{m}\underset{\sim}{\vec{p}}^{\,2} \tag{3.30}$$

with $\vec{P}_{\text{c.m.}} = \vec{p}_1 + \vec{p}_2$ and $\vec{p} = \frac{1}{2}\left(\vec{p}_1 - \vec{p}_2\right)$. As the partial wave basis describes the relative motion, only the relative kinetic energy $\underset{\sim}{T}_{\text{rel}} = \frac{1}{m}\underset{\sim}{\vec{p}}^{\,2}$ enters. For a given NN potential $\underset{\sim}{V}$ one finds for the evolved two nucleon interaction $\underset{\sim}{V}_s$ the flow equation for the partial wave matrix elements

$$\begin{aligned}\frac{d}{ds}\langle\, k(LS)J;T\left|\underset{\sim}{V}_s\right|k'(L'S)J;T\,\rangle \;\; &= \;\; -(k^2-k'^2)^2\,\langle\, k(LS)J;T\left|\underset{\sim}{V}_s\right|k'(L'S)J;T\,\rangle \\ +m\sum_{L''=J-1}^{J+1}\int_0^{\infty} & dq\,q^2(k^2-2q^2+k'^2)\langle\, k(LS)J;T\left|\underset{\sim}{V}_s\right|q(L''S)J;T\,\rangle\langle\, q(L''S)J;T\left|\underset{\sim}{V}_s\right|k'(L'S)J;T\,\rangle\end{aligned} \tag{3.31}$$

with $\underset{\sim}{V}_0 = \underset{\sim}{V}$. This equation can be solved numerically to obtain the matrix elements of the SRG evolved interaction.

$\underset{\sim}{V}_{s=0} = \underset{\sim}{V}$ does not connect different S, J, M, T and M_T. This symmetry property is conserved by the flow equation for all s because the meta-generator $\underset{\sim}{T}$ also possesses the same symmetries. In Eq. (3.31) these symmetries are used.

Since the SRG transformation is carried out directly in matrix element representation (see Eq. (3.31)), the operator representation of the transformed interaction is unknown*. For the SRG transformed Argonne potential, for example, the operator representation is not known although the operator representation of the initial bare Argonne potential Eq.(3.22) is known.

---

* It is interesting to note that in the first evolution step ds the SRG result is of the same structure as the UCOM result [55, 61].

Fixed-point of the SRG evolution

From Eq. (3.26) follows, that the SRG evolution has a fixed-point s_{fix} for which

$$\frac{d\underset{\sim}{H}_s}{ds} = \left[\underset{\sim}{\eta}_{s_{\text{fix}}}, \underset{\sim}{H}_{s_{\text{fix}}}\right] = \underset{\sim}{0} \tag{3.32}$$

and hence the SRG evolution would stop. Eq. (3.32) is trivially fulfilled for

$$\underset{\sim}{\eta}_{s_{\text{fix}}} = \left[\underset{\sim}{T}, \underset{\sim}{H}_{s_{\text{fix}}}\right] = \underset{\sim}{0}. \tag{3.33}$$

That would mean that $\underset{\sim}{H}_{s_{\text{fix}}}$ and $\underset{\sim}{T}$ have a common eigenbasis and $\underset{\sim}{H}_{s_{\text{fix}}}$ can be written as

$$\begin{aligned}\underset{\sim}{H}_{s_{\text{fix}}} &= \sum_M \left| s_{\text{fix}}; \tilde{d}\, S{=}1\, J{=}1\, M; T{=}0\, M_T{=}0 \right\rangle E_d \left\langle s_{\text{fix}}; \tilde{d}\, S{=}1\, J{=}1\, M; T{=}0\, M_T{=}0 \right| \\ &\quad + \int_0^\infty dk k^2 \sum_{J,M} \sum_{T,M_T} \sum_S \sum_\alpha \left| s_{\text{fix}}; k, \alpha SJM; TM_T \right\rangle \frac{k^2}{2\mu} \left\langle s_{\text{fix}}; k, \alpha SJM; TM_T \right|, \end{aligned} \tag{3.34}$$

where $\left| s_{\text{fix}}; k, \alpha SJM; TM_T \right\rangle$ are the tensor mixed states given in Eqs. (2.17). As $\left| s_{\text{fix}}; k, \alpha SJM; TM_T \right\rangle$ are also eigenstates of $\underset{\sim}{p}^2$ they cannot have any phase shifts because otherwise the states would not be regular at the origin. E_d is the binding energy of the deuteron which is negative. The eigenstate $\left| s_{\text{fix}}; \tilde{d}\, S{=}1\, J{=}1\, M; T{=}0\, M_T{=}0 \right\rangle$ should also be an eigenstate of $\underset{\sim}{p}^2$ and therefore be completely delocalized in contrast to the localized deuteron wave function. These considerations show already that the evolution most likely will not reach this fixed point for a finite s.

The other possibility that $\left[\underset{\sim}{\eta}_{s_{\text{fix}}}, \underset{\sim}{H}_{s_{\text{fix}}}\right] = \underset{\sim}{0}$ implies that

$$\begin{aligned}\left\langle s_{\text{fix}}; k, \alpha SJM; TM_T \right| \left[\underset{\sim}{\eta}_{s_{\text{fix}}}, \underset{\sim}{H}_{s_{\text{fix}}}\right] \left| s_{\text{fix}}; k', \alpha SJM; TM_T \right\rangle &= \\ = \left(k^2 - k'^2\right)^2 \left\langle s_{\text{fix}}; k, \alpha SJM; TM_T \right| \frac{\underset{\sim}{\vec{p}}^2}{2\mu} \left| s_{\text{fix}}; k', \alpha SJM; TM_T \right\rangle &= 0, \end{aligned} \tag{3.35}$$

where $\left| s_{\text{fix}}; k', \alpha SJM; TM_T \right\rangle$ are eigenstates of $\underset{\sim}{H}_{s_{\text{fix}}}$ for the positive energies

$$\underset{\sim}{H}_{s_{\text{fix}}} \left| s_{\text{fix}}; k, \alpha SJM; TM_T \right\rangle = \frac{k^2}{2\mu} \left| s_{\text{fix}}; k, \alpha SJM; TM_T \right\rangle. \tag{3.36}$$

Condition Eq. (3.35) implies

$$\left\langle s_{\text{fix}}; k, \alpha SJM; TM_T \right| \underset{\sim}{\vec{p}}^2 \left| s_{\text{fix}}; k', \alpha SJM; TM_T \right\rangle \propto \delta\left(k - k'\right), \tag{3.37}$$

because either k has to be equal k' or the matrix element has to be zero. This means that $\underset{\sim}{\vec{p}}^2$ has to be diagonal in this basis which leads back to condition Eq. (3.32) where $\underset{\sim}{\vec{p}}^2$ and $\underset{\sim}{H}_{s_{\text{fix}}}$ commute.

Altogether one can say that s determines in how far one evolves in smoothing the wave functions $\left\langle r(LS)JM; TM_T \middle| s; k, \alpha SJM; TM_T \right\rangle$ or reducing the high momentum components in $\left\langle k'(LS)JM; TM_T \middle| s; k, \alpha SJM; TM_T \right\rangle$. But it is also clear that one should evolve not too far because eigenstates of $\underset{\sim}{\vec{p}}^2$ are certainly not an adequate representation of bound nuclear many-body states.

The SRG transformed Argonne potential

The Argonne potential is evolved by means of the SRG flow equation Eq. (3.31). The evolved matrix elements in the $^1S_0$ channel are shown in Fig. 3.4 for different flow parameters s. With increasing s the potential evolves to a band diagonal structure and the absolute value of the off-diagonal matrix elements is successively lowered. This is basically driven by the first term on the left-hand side of Eq. (3.31). Similar to the UCOM transformation (see Fig. 3.3), the SRG transformation leads to a decoupling of high and low momentum (or energy) modes by suppressing off-diagonal matrix elements. This has the advantage, that calculations for low energy properties with the SRG transformed interaction require smaller model spaces, since matrix elements with higher momentum do not need to be considered.

The reduction of the off-diagonal matrix elements is dominated by the first term on the r.h.s of the SRG flow equation Eq. (3.31), $-(k^2-k'^2)^2 \left\langle k(LS)J;T \middle| \underset{\sim}{V}_s \middle| k'(L'S)J;T \right\rangle$. Since this term is proportional to the matrix element itself, it decreases in an exponential fashion. Due to the factor $(k^2-k'^2)^2$, the lowering is additionally suppressed at small momenta k and k' and for matrix elements which are "almost" diagonal. Consequently with increasing flow parameter s the speed of the evolution goes down exponentially. Reaching the fixed-point, at which only diagonal matrix elements remain, would therefore require extremely large s.

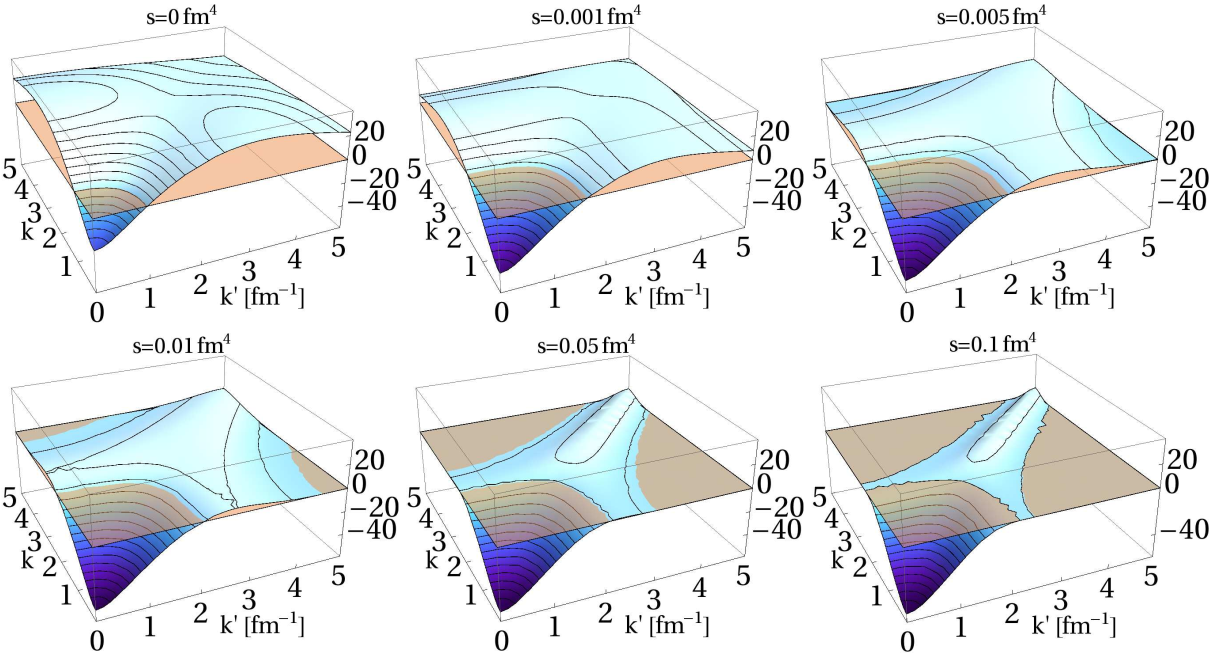

Figure 3.4: Illustration of the SRG evolution in the $^1S_0$ channel. The initial Argonne potential partial wave matrix elements are shown in the upper left picture. The other plots show the SRG-evolved matrix elements for a given flow parameter s. All matrix elements are plotted in units of MeVfm^3.

If the SRG transformation of the interaction is performed in the two-body space only, one finds a dependence of the results of few-nucleon calculations on the flow parameter s. This is due to three- and four-nucleon forces which are induced in the SRG transformation, but are not considered on the two-body level. Thus, one would have to perform the SRG transformation in three-body [62] or even more body spaces. Therefore, it is not desirable to evolve the interaction too far because then the spatial range of the SRG action gets too large and strong many-body forces are induced.

One has found that the effects of induced three-body interactions cancel to a certain extend the genuine three-body interactions. Thus, one chooses the flow parameter s for a two-body SRG evolution such, that the effect of many-body forces is minimized. One works with the parameter s for which one obtains the best description of the experimental binding energies of ^{3}H and ^{4}He with a pure two-body potential. Starting from the Argonne potential this is reached for a flow parameter of $s = 0.03\,\mathrm{fm}^4$, which is used in all calculations shown later.

Momentum dependence

The SRG transformation of the Argonne potential creates a more complex momentum dependence than the one obtained in the UCOM transformation Eq. (3.22), which only contains the nonlocal operators $\underset{\sim}{\vec{p}}^{\,2}$ and $\underset{\sim}{p}_r S_{12}(\underset{\sim}{\vec{r}}, \underset{\sim}{\vec{p}}_\Omega)$. As mentioned before the operator representation of the SRG transformed potential is not known. Nevertheless, one can gain some information about the momentum dependence of the SRG transformed Argonne potential by calculating explicitly the generators and potentials for the first steps of the SRG flow.

For a certain partial wave channel the Argonne potential can be represented by one, or three where mixing occurs, local potentials $V^{C(0)}_{LL'SJ}(r)$ which contain all the local radial functions occurring in Eq. (3.14) multiplied with the appropriate values of the matrix elements of the corresponding operators in that channel. For example in the ^{1}D$_2$ channel, the potential $V^{C(0)}_{2202}(r)$ would be $V^{C(0)}_{2202}(r) = v^{C}_{01}(r) + 6\,v^{L2}_{01}(r)$. The generator $\underset{\sim}{\eta}_0$ at $s = 0$ given by[*]

$$\underset{\sim}{\eta}_0 = m^2 \left[\underset{\sim}{T}_{\mathrm{rel}}, V^{C(0)}_{LLSJ}(\underset{\sim}{r})\right] = -i\,m \left(\underset{\sim}{p}_r V^{C(0)\prime}_{LLSJ}(\underset{\sim}{r}) + V^{C(0)\prime}_{LLSJ}(\underset{\sim}{r}) \underset{\sim}{p}_r \right), \tag{3.38}$$

has the same structure as the central UCOM generator from Eq. (3.7) (see Refs. [55, 61]). The potential evolves by

$$\begin{aligned} d\underset{\sim}{V}_0 &= \left[\underset{\sim}{\eta}_0, V^{C(0)}_{LLSJ}(\underset{\sim}{r})\right] ds \\ &= m \Bigg\{ \frac{2}{m} \left(\underset{\sim}{\vec{p}}^{\,2} V^{C(0)\prime\prime}_{LLSJ}(\underset{\sim}{r}) + V^{C(0)\prime\prime}_{LLSJ}(\underset{\sim}{r}) \underset{\sim}{\vec{p}}^{\,2} \right) + \frac{1}{m} \left(\frac{V^{C(0)\prime}_{LLSJ}(\underset{\sim}{r})}{r^3} - \frac{V^{C(0)\prime\prime}_{LLSJ}(\underset{\sim}{r})}{r^2} \right) \underset{\sim}{\vec{L}}^2 \\ &\qquad + \frac{V^{C(0)\prime\prime\prime\prime}_{LLSJ}(\underset{\sim}{r})}{m} - 2 \left(V^{C(0)\prime}_{LLSJ}(\underset{\sim}{r}) \right)^2 \Bigg\} ds. \end{aligned} \tag{3.39}$$

To clarify the structure of this potential, one can use the abbreviations
$V^{C(1)}_{LLSJ}(r) = V^{C(0)\prime\prime\prime\prime}_{LLSJ}(r) - 2m\left(V^{C(0)\prime}_{LLSJ}(r)\right)^2$, $V^{p2(1)}_{LLSJ}(r) = \frac{1}{4} V^{C(0)\prime\prime}_{LLSJ}(r)$ and
$V^{L2(1)}_{LLSJ}(r) = \frac{V^{C(0)\prime}_{LLSJ}(r)}{r^3} - \frac{V^{C(0)\prime\prime}_{LLSJ}(r)}{r^2}$ and finds

$$\begin{aligned} \underset{\sim}{V}_{ds} &= \underset{\sim}{V}_0 + d\underset{\sim}{V}_0 \\ &= \left(V^{C(0)}_{LLSJ}(\underset{\sim}{r}) + V^{C(1)}_{LLSJ}(\underset{\sim}{r})\, ds \right) + \frac{1}{2} \left(\underset{\sim}{\vec{p}}^{\,2} \left(V^{p2(1)}_{LLSJ}(\underset{\sim}{r})\, ds \right) + \left(V^{p2(1)}_{LLSJ}(\underset{\sim}{r})\, ds \right) \underset{\sim}{\vec{p}}^{\,2} \right) + V^{L2(1)}_{LLSJ}(\underset{\sim}{r})\, ds\, \underset{\sim}{\vec{L}}^2. \end{aligned} \tag{3.40}$$

Since the generators have the same structure, the SRG evolved potential $\underset{\sim}{V}_{ds}$ in Eq. (3.40) has the same quadratic momentum structure as the UCOM potential Eq. (3.22). But in contrast to the UCOM

---

[*] For reasons of simplicity, only the situation in the absence of mixing between states with different L is considered.

generator, the SRG generator is dynamically changing. In the next step, the generator $\underset{\sim}{\eta}_{ds}$ uses the evolved potential $\underset{\sim}{V}_{ds}$ as input so that the new generator is given by

$$\begin{aligned}\underset{\sim}{\eta}_{ds} \;=\; m^2\Big[\underset{\sim}{T}_{\text{rel}},\Big(V^{C(0)}_{LLSJ}(\underset{\sim}{r})+V^{C(1)}_{LLSJ}(\underset{\sim}{r})\,ds\Big)+\frac{1}{2}\Big(\underset{\sim}{\vec{p}}^{\,2}\Big(V^{p2(1)}_{LLSJ}(\underset{\sim}{r})\,ds\Big)+\Big(V^{p2(1)}_{LLSJ}(\underset{\sim}{r})\,ds\Big)\underset{\sim}{\vec{p}}^{\,2}\Big).\\ +V^{L2(1)}_{LLSJ}(\underset{\sim}{r})\,ds\,\underset{\sim}{\vec{L}}^{2}\Big]\end{aligned}\tag{3.41}$$

This leads to a more complex momentum dependence than the one in Eq. (3.38). For the second step of the evolution, one finds an interaction with the structure

$$\begin{aligned}\underset{\sim}{V}_{2ds} &= \underset{\sim}{V}_{ds}+d\underset{\sim}{V}_{ds}\\ &= \Big(V^{C(0)}_{LLSJ}(\underset{\sim}{r})+V^{C(1)}_{LLSJ}(\underset{\sim}{r})\,ds+V^{C(2)}_{LLSJ}(\underset{\sim}{r})\,ds^2\Big)+\Big(V^{L2(1)}_{LLSJ}(\underset{\sim}{r})\,ds+V^{L2(2)}_{LLSJ}(\underset{\sim}{r})\,ds^2\Big)\underset{\sim}{\vec{L}}^{2}+V^{L4(2)}_{LLSJ}(\underset{\sim}{r})\,ds^2\,\underset{\sim}{\vec{L}}^{4}\\ &\quad+\frac{1}{2}\Big(\underset{\sim}{\vec{p}}^{\,2}\Big(V^{p2(1)}_{LLSJ}(\underset{\sim}{r})\,ds+V^{p2(2)}_{LLSJ}(\underset{\sim}{r})\,ds^2\Big)+\Big(V^{p2(1)}_{LLSJ}(\underset{\sim}{r})\,ds+V^{p2(2)}_{LLSJ}(\underset{\sim}{r})\,ds^2\Big)\underset{\sim}{\vec{p}}^{\,2}\Big)\\ &\quad+\frac{1}{2}\Big(\underset{\sim}{\vec{p}}^{\,2}\Big(V^{p2L2(2)}_{LLSJ}(\underset{\sim}{r})\,ds^2\Big)+\Big(V^{p2L2(2)}_{LLSJ}(\underset{\sim}{r})\,ds^2\Big)\underset{\sim}{\vec{p}}^{\,2}\Big)\underset{\sim}{\vec{L}}^{2}\\ &\quad+\frac{1}{2}\Big(\underset{\sim}{\vec{p}}^{\,4}\Big(V^{p4(2)}_{LLSJ}(\underset{\sim}{r})\,ds^2\Big)+\Big(V^{p4(2)}_{LLSJ}(\underset{\sim}{r})\,ds^2\Big)\underset{\sim}{\vec{p}}^{\,4}\Big),\end{aligned}\tag{3.42}$$

which contains terms of the fourth power of the momentum operator. This shows that during the SRG evolution contributions with higher and higher powers of the relative momentum operator are created. In the next step of the evolution terms with $\vec{p}^{\,6}$ appear, followed by terms with $\vec{p}^{\,8}$ and so on. Thus, the momentum dependence of the SRG evolved Argonne potential is more complicated than the one of the UCOM transformed potential.

Another difference between UCOM and SRG is the fact that the SRG transformation is performed in each partial wave with given L, S, J and T separately, while the UCOM generator only depends on spin S and isospin T. This and the momentum dependence play a important role in the choice of the ansatz for the operator representation discussed later in Sec. 4.3.2.

3.3 The JISP16 interaction

The **J-matrix inverse scattering potential** JISP16 [19, 63, 64] is a realistic NN interaction constructed in the harmonic oscillator (HO) basis. The J-matrix inverse scattering approach (see Ref. [63]) is used to construct a potential which reproduces the experimental NN scattering phase shifts. Furthermore several phase equivalent transformations are applied in a way that the binding energies and spectra of nuclei with A $\leq$ 16 are reproduced. Since not only properties of the two-nucleon and some few-nucleon systems, but data from the whole range of nuclei one aims to describe, are used to obtain the interaction, the JISP16 interaction is called an “ab-exitu” approach.

The JISP16 interaction is tailored for NCSM calculations. The J-matrix inverse scattering approach yields a tridiagonal matrix in the HO partial wave basis. The phase equivalent transformations applied to reproduce the binding energies of selected nuclei create additional nonvanishing matrix elements in the HO basis which, by construction, only connect states with radial quantum numbers $n-n'=0, \pm 1, \pm 2$. Thus, the potential can be represented in the HO partial wave basis (see Appendix A.2.3) as

$$\underset{\sim}{V}_{\text{JISP16}}=\sum_{S,T=0}^{1}\sum_{J=0}^{4}\sum_{L,L'=J-1}^{J+1}\sum_{n=0}^{4}\sum_{n'=n-2}^{n+2}\big|\,n(LS)J;T\,\big\rangle V^{LL'SJT}_{nn'}\big\langle\,n'(L'S)J;T\,\big|\tag{3.43}$$

with the matrix elements $V_{nn'}^{LL'SJT}$ from Refs. [19, 64].

The $^1S_0$ partial wave HO matrix elements of the potential are presented in Fig. 3.5. The almost tridiagonal form in the HO basis, with only a few interaction matrix elements not being zero, leads to a rapid convergence in NCSM calculations. In contrast to many other realistic potentials, like for example the Argonne V18, the JISP16 interaction shows no coupling of low and high momentum states as can be seen in Fig. 3.5. Consequently, the bare JISP16 interaction can be used directly in nuclear many-body calculations and further renormalization methods like UCOM and SRG are not necessary as they are already included in the construction procedure.

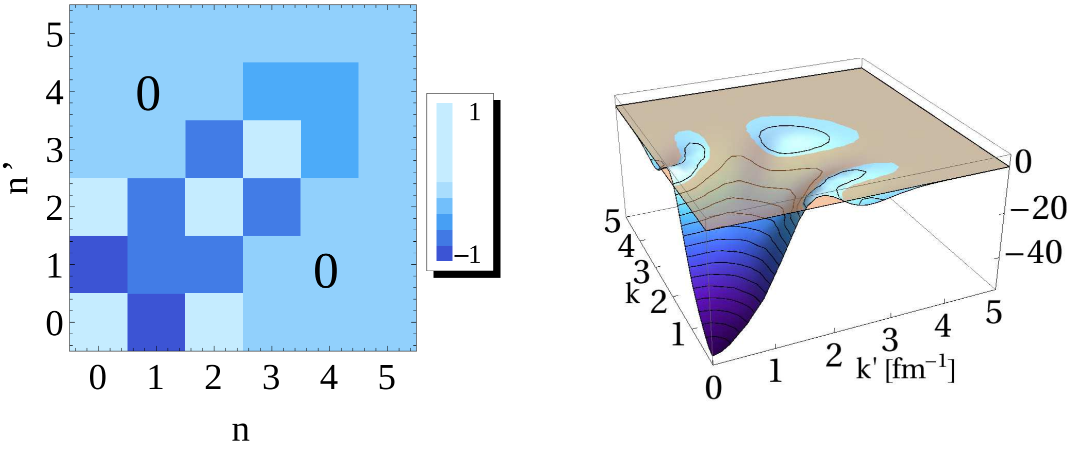

Figure 3.5: The $^1S_0$ partial wave matrix elements of the JISP16 interaction [19, 64]. The left picture shows a plot of the harmonic oscillator matrix elements with radial quantum numbers n and n' (in arbitrary units). The right picture shows the corresponding momentum space matrix elements in units of $\mathrm{MeV\,fm}^3$ [65].

The JISP16 potential is constructed directly in the harmonic oscillator basis and therefore its operator representation is not known. The potential has by construction a simple and convenient structure in the harmonic oscillator basis. Since there are no constraints on the momentum dependence in the construction procedure of the potential, one has to expect a complicated nonlocal structure. Furthermore it is constructed for each partial wave individually, so that no simple dependence on the partial wave quantum numbers L, S and J can be expected.

In the next section operator representations for the three presented effective realistic potentials are derived.

4 Operator representations from partial wave matrix elements

In this section the method to derive an operator representation from the partial wave matrix elements of a potential is presented. In the following the strategy to obtain an operator representation by a fit to the matrix elements of the potential is discussed.

4.1 Method

One starts by defining an ansatz for the operator representation of the potential given in matrix element representation. This ansatz has the form

$$\underset{\sim}{V}_{\text{ansatz}} = \sum_{P} \sum_{ST} \frac{1}{2} \left[\underset{\sim}{\mathcal{O}}_P \mathcal{V}^P_{ST}(\underset{\sim}{\vec{r}}, \underset{\sim}{\vec{p}}) + \mathcal{V}^P_{ST}(\underset{\sim}{\vec{r}}, \underset{\sim}{\vec{p}}) \underset{\sim}{\mathcal{O}}_P \right] \underset{\sim}{\Pi}_{ST} \tag{4.1}$$

with a certain set of operators $\underset{\sim}{\mathcal{O}}_p$ acting on the angular and spin part of the Hilbert space (for example the spin orbit operator $\underset{\sim}{\vec{L}} \cdot \underset{\sim}{\vec{S}}$ or the tensor operator $\underset{\sim}{S}_{12}$) and the corresponding radial functions $\mathcal{V}^P_{ST}(\underset{\sim}{\vec{r}}, \underset{\sim}{\vec{p}})$. The radial functions depend on scalar products of the relative distance operator $\underset{\sim}{\vec{r}}$ and the relative momentum operator $\underset{\sim}{\vec{p}}$, for example $\underset{\sim}{\vec{r}}^2$, $\underset{\sim}{\vec{p}}^2$ or $\underset{\sim}{p}_r$ defined in Eq. (3.6a), which do not act on the angular part of the nuclear relative motion.

For some potentials, like the Argonne potential Eq. (3.14) or the UCOM transformed Argonne potential Eq. (3.22), which contain by construction only local radial functions or local radial functions and a polynomial momentum dependence, it is sufficient to work with an ansatz with local radial functions. This means that these functions do not explicitly depend on the momentum operator $\underset{\sim}{\vec{p}}$ and therefore can be written as $\mathcal{V}^P_{ST}(\underset{\sim}{r})$, where $\underset{\sim}{r} = \sqrt{\underset{\sim}{\vec{r}}^2}$. For potentials with a nonlocal structure beyond a polynomial momentum dependence nonlocal radial functions $\mathcal{V}^P_{ST}(\underset{\sim}{\vec{r}}, \underset{\sim}{\vec{p}})$ depending on both, the relative position and momentum operator, are used.

The choice of the set of operators $\underset{\sim}{\mathcal{O}}_p$ is motivated by the information available on the structure of the potential. For example for the UCOM transformed Argonne potential the known operator structure Eq. (3.22) can be used as a guideline for the ansatz. For the SRG transformed Argonne potential one can try to represent the complicated momentum dependence by an adequate choice of the radial functions $\mathcal{V}^P_{ST}(\underset{\sim}{\vec{r}}, \underset{\sim}{\vec{p}})$. Another ansatz is to use as many linearly independent $\underset{\sim}{\mathcal{O}}_p$ as one wants to fit channels for low values of L and J. The form of operators can also be motivated by the application of the operator representation. For FMD calculations the operator representation should for example contain operators which can be treated analytically in the FMD basis.

The radial functions are not known *a priori* and have to be parameterized in an appropriate way to describe the potential under consideration. Once an ansatz for the operator representation is chosen, one has to determine the unknown parameters in the radial functions $\mathcal{V}^P_{ST}(\underset{\sim}{\vec{r}}, \underset{\sim}{\vec{p}})$. It is important to chose the operators $\underset{\sim}{\mathcal{O}}_p$ and the parameterization of the radial functions such, that one has analytical expressions for the partial wave matrix elements of the ansatz. By a fit of these analytical expressions to the given partial wave matrix elements, one obtains the parameters of the radial functions and thereby the operator representation with the chosen set of operators. The whole procedure is depicted schematically in Fig. 4.1.

Obviously not all partial wave channels can be included in the fit. In partial waves with high angular momentum quantum numbers L, the kinetic energy is dominant[*] and the contribution from the potential is small in comparison. Since the low L channels are more important in nuclear structure applications,

---

[*] This results from the centrifugal barrier of the kinetic energy. It is proportional to $\frac{L(L+1)}{r^2}$ and therefore becomes large for high angular momentum L.

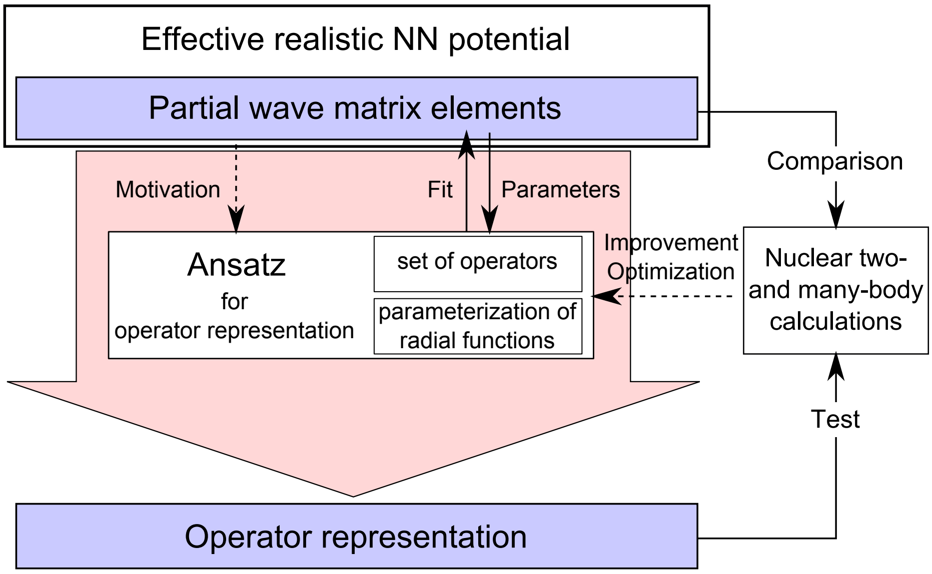

Figure 4.1: A schematic picture of method used to derive an operator representation from the partial wave matrix elements of an effective realistic NN potential.

it is reasonable to focus more on these partial waves. In the fit only partial wave channels with L up to 4 are considered. Due to the dominance of the kinetic energy in channels with higher L, deviations between the fitted and the exact potential, have only a minor effect. If large deviations in the phase shifts occur the ansatz most likely contains unreasonable momentum or angular momentum terms. In the fit of the ansatz to the partial wave matrix elements weight factors are used. These weights are chosen to favour lower angular momentum partial waves (the S-, P- and D-wave) so that these matrix elements are reproduced best.

It should be noted that the success of the presented method strongly depends on the choice of the operators and the parameterization of the radial functions. By working with a set of operators which is not big enough or inappropriate to describe a certain potential, the obtained operator representation will not reproduce well enough the matrix elements. The obtained operator representation is tested by calculating nuclear properties by means of the methods discussed in Sec. 2 and comparing those with the results obtained from the matrix element representation. This comparison allows to draw conclusions on the quality of the derived operator representation and possible improvement or optimization of the used ansatz.

In the following the discussed method is applied for different effective realistic potentials and the choice of the set of operators and the parameterization of the radial functions is illustrated for these cases.

4.2 UCOM potential with reduced set of operators

As shown in Sec. 3.1, the UCOM transformed Argonne potential is one of the few effective realistic potentials for which the operator representation as well as the partial wave matrix element representation is known. The operator representation of the UCOM transformed Argonne potential V_{UCOM} Eq. (3.22) is more complicated than the operator representation of the initial Argonne potential (3.14), even though terms with large powers of the angular momentum operator have been neglected already. It has been shown in Ref. [30] that these neglected terms are not important. The question arises if one can reduce the number of operators further without loosing accuracy.

For this purpose, the method presented in Sec. 4.1 is used to derive a simplified operator representation of the UCOM transformed Argonne potential which reproduces the matrix elements of the lowest angular momentum channels with the same accuracy as the exact matrix elements given (Eq. (3.24)). The known operator representation Eq. (3.22) serves as a motivation for an ansatz with a different set of operators, in particular a subset.

4.2.1 Ansatz for the operator representation

The exact partial wave matrix elements in momentum space of the UCOM transformed Argonne potential are used as input to derive the corresponding operator representation. The procedure presented in Sec. 4.1 is applied. The operator representation of the UCOM transformed Argonne potential Eq. (3.22) contains only a quadratic momentum dependence in the central and tensor part of type $\left(\underset{\sim}{\vec{p}}^2 V(\underset{\sim}{r}) + V(\underset{\sim}{r})\underset{\sim}{\vec{p}}^2\right)$ and $\left(\underset{\sim}{p}_r V(\underset{\sim}{r}) + V(\underset{\sim}{r})\underset{\sim}{p}_r\right) S_{12}(\underset{\sim}{\vec{r}}, \underset{\sim}{\vec{p}}_\Omega)$, respectively. Thus, one can add the momentum dependent operators $\underset{\sim}{\vec{p}}^2$ and $\underset{\sim}{p}_r S_{12}(\underset{\sim}{\vec{r}}, \underset{\sim}{\vec{p}}_\Omega)$ explicitly to the set of operators $\underset{\sim}{\mathcal{O}}_p$ and write the ansatz with local radial functions $\mathcal{V}^P_{ST}(\underset{\sim}{r})$:

$$\underset{\sim}{V}_{\text{ansatz}} = \sum_P \sum_{ST} \frac{1}{2} \left[\underset{\sim}{\mathcal{O}}_P \mathcal{V}^P_{ST}(\underset{\sim}{r}) + \mathcal{V}^P_{ST}(\underset{\sim}{r}) \underset{\sim}{\mathcal{O}}_P \right] \underset{\sim}{\Pi}_{ST}. \tag{4.2}$$

Radial functions

The radial functions $\mathcal{V}^P_{ST}(r)$ are parameterized by a sum of gaussians, in analogy to the parameterization used in FMD (Eqs. (2.57), (2.60a), (2.60b)):

$$\mathcal{V}^P_{ST}(r) = \sum_\mu \gamma^P_{ST,\mu}\, r^{n^P} \exp\left\{ -\frac{r^2}{2\kappa_\mu} \right\}, \tag{4.3}$$

with $n^p = 0$, 2 or 3, depending on the operator $\underset{\sim}{\mathcal{O}}_P$.

In principle one can use $\gamma^P_{ST,\mu}$ and κ_μ as free parameters which have to be obtained from the fit. But to avoid ambiguities it is more convenient to choose a fixed set of parameters κ and only have the $\gamma^P_{ST,\mu}$ as free parameters. This set has to cover the whole range in which the radial functions are not zero. Here the geometrical sequence

$$\kappa_\mu = \kappa_1 \cdot b^{\mu-1}$$

with $\kappa_1 = 0.05\,\text{fm}^2$ and $b = \sqrt{2}$ is used, which leads to

$$\kappa = \{0.05,\, 0.05 \cdot \sqrt{2},\, 0.1,\, \cdots,\, 6.4\}\text{fm}^2.$$

These parameters cover the relevant range of the interaction which is only a few Fermi.

Matrix elements

The parameters $\gamma^P_{ST,\mu}$ have to be obtained by fitting the ansatz to the partial wave matrix elements of V_{UCOM}. The matrix elements of V_{ansatz} for the local radial functions can be written as

$$\left\langle k(LS)J;T \left| \underset{\sim}{V}_{\text{ansatz}} \right| k'(L'S)J;T \right\rangle = \sum_P \left\langle k(LS)J;T \left| \frac{1}{2} \left[\underset{\sim}{\mathcal{O}}_P \mathcal{V}^P_{ST}(\underset{\sim}{r}) + \mathcal{V}^P_{ST}(\underset{\sim}{r}) \underset{\sim}{\mathcal{O}}_P \right] \right| k'(L'S)J;T \right\rangle. \tag{4.4}$$

For operators $\underset{\sim}{\mathcal{O}}_P$ that act only in angular momentum and spin space (e.g. all the operators occurring in the Argonne potential Eq. (3.12) and $\underset{\sim}{\vec{L}}^2(\underset{\sim}{\vec{L}} \cdot \underset{\sim}{\vec{S}})$ and $\bar{S}_{12}(\underset{\sim}{\vec{q}}_\Omega, \underset{\sim}{\vec{q}}_\Omega)$ in the UCOM transformed Argonne potential Eq. (3.22)), $\underset{\sim}{\mathcal{O}}_P$ and its radial function $\mathcal{V}^P_{ST}(\underset{\sim}{r})$ commute. Thus, one has to calculate the matrix elements of the operator $\underset{\sim}{\mathcal{O}}_P$ and an integral over the radial functions. With the parameterization Eq. (4.3) for the radial functions one finds

$$\left\langle k(LS)J;T \left| \mathcal{V}^P_{ST}(\underset{\sim}{r})\underset{\sim}{\mathcal{O}}_P \right| k'(L'S)J;T \right\rangle = \sum_\mu \gamma^P_{ST,\mu} \frac{2}{\pi} \int_0^\infty dr\, r^2 j_L(kr)\, r^{n^P} \exp\left\{-\frac{r^2}{2\kappa_\mu}\right\} j_{L'}(k'r) \cdot \left\langle (LS)J;T \left| \underset{\sim}{\mathcal{O}}_P \right| (L'S)J;T \right\rangle . \tag{4.5a}$$

Due to the parameterization in terms of gaussians, the integral can be solved analytically. A recursion relation for the solution of the integral is given in Appendix C.3.2.

For the momentum dependent terms with the operators $\underset{\sim}{\vec{p}}^2$ and $\underset{\sim}{p}_r S_{12}(\underset{\sim}{\vec{r}}, \underset{\sim}{\vec{p}}_\Omega)$ one finds

$$\left\langle k(LS)J;T \left| \frac{1}{2}\left[\underset{\sim}{\vec{p}}^2 \mathcal{V}^{p2}_{ST}(\underset{\sim}{r}) + \mathcal{V}^{p2}_{ST}(\underset{\sim}{r})\underset{\sim}{\vec{p}}^2\right] \right| k'(L'S)J;T \right\rangle = \sum_\mu \gamma^{p2}_{ST,\mu} \frac{2}{\pi} \int_0^\infty dr\, r^2 j_L(kr) \exp\left\{-\frac{r^2}{2\kappa_\mu}\right\} j_L(k'r) \cdot \frac{1}{2}(k^2 + k'^2)\delta_{LL'} \tag{4.5b}$$

and

$$\left\langle k(LS)J;T \left| \frac{1}{2}\left[\underset{\sim}{p}_r \mathcal{V}^{Trp}_{1T}(\underset{\sim}{r}) + \mathcal{V}^{Trp}_{1T}(\underset{\sim}{r})\underset{\sim}{p}_r\right] S_{12}(\underset{\sim}{\vec{r}}, \underset{\sim}{\vec{p}}_\Omega) \right| k'(L'S)J;T \right\rangle = \sum_\mu \gamma^{Trp}_{ST,\mu} \frac{i}{\pi} \left[\int_0^\infty dr\, r^2 \left(\frac{1}{r}\frac{\partial}{\partial r} r j_L(kr)\right) r^3 \exp\left\{-\frac{r^2}{2\kappa_\mu}\right\} j_{L'}(k'r) - \int_0^\infty dr\, r^2 j_L(kr)\, r^3 \exp\left\{-\frac{r^2}{2\kappa_\mu}\right\} \left(\frac{1}{r}\frac{\partial}{\partial r} r j_{L'}(k'r)\right) \right] \cdot \left\langle k(LS)J;T \left| S_{12}(\underset{\sim}{\vec{r}}, \underset{\sim}{\vec{p}}_\Omega) \right| k'(L'S)J;T \right\rangle . \tag{4.5c}$$

As in Eq. (4.5a), the integrals and the matrix elements of the operators can be calculated analytically. Details are shown in Appendix C.3.2.

4.2.2 Choice of the operators

As already mentioned, the choice of the operators in Eq. (4.2) plays a crucial role for the quality of the fitted operator representation. Up to now, the set of operators $\underset{\sim}{\mathcal{O}}_P$ was not specified. A first ansatz is to include all operators which occur in the operator representation of the UCOM potential Eq. (3.22). The UCOM potential given in partial wave representation (Eq. (3.24)) is taken as input in order to test if the fitting procedure contains enough momentum space matrix elements to fix uniquely the parameters γ^P_{ST} of the radial functions Eq. (4.3). It has been shown in Ref. [54] that the obtained radial functions $\mathcal{V}^P_{ST}(r)$ agree with the exact radial functions from Eq. (3.22). This proves the applicability of the fitting procedure.

Reduced set of operators

In this work, as a next step, an ansatz for the operator representation with only a subset of the operators in $\underset{\sim}{V}_{\mathrm{UCOM}}$ (Eq. (3.22)) is considered. The radial functions are obtained from a fit to the exact partial wave matrix elements of the UCOM transformed Argonne potential. Obviously a fit with less operators will not reproduce perfectly the matrix elements of the exact potential. But as already discussed before, for higher angular momenta L the centrifugal barrier becomes dominant and the contributions from the interaction are small in comparison. Thus, one can optimize the potential with the reduced set of operators for the lowest angular momentum channels and afterwards make sure (by testing the interaction with the methods described in Sec. 2) that the deviations in the higher angular momentum channels do not affect the phase shifts and the properties of finite nuclei calculated with the potential.

There is no unique choice of a reduced set of operators describing correctly the lowest angular momentum channels. It is convenient to use as few operators as possible but still maintain correct matrix elements and nuclear properties. An ansatz with the following reduced set of operators is discussed:

$$\begin{aligned}
\underset{\sim}{V}^{(\text{red.UCOM})}_{\text{ansatz}} &= \sum_{ST} \mathcal{V}^{C}_{ST}(\underset{\sim}{r})\, \underset{\sim}{\Pi}_{ST} \\
&+ \sum_{ST} \mathcal{V}^{L2}_{ST}(\underset{\sim}{r})\underset{\sim}{\vec{L}}^{2}\, \underset{\sim}{\Pi}_{ST} \\
&+ \sum_{ST} \frac{1}{2}\left[\underset{\sim}{\vec{p}}^{2}\mathcal{V}^{p2}_{ST}(\underset{\sim}{r}) + \mathcal{V}^{p2}_{ST}(\underset{\sim}{r})\underset{\sim}{\vec{p}}^{2}\right] \underset{\sim}{\Pi}_{ST} \\
&+ \sum_{T} \mathcal{V}^{LS}_{1T}(\underset{\sim}{r})(\underset{\sim}{\vec{L}}\cdot\underset{\sim}{\vec{S}})\, \underset{\sim}{\Pi}_{1T} \\
&+ \sum_{T} \mathcal{V}^{T}_{1T}(\underset{\sim}{r})\underset{\sim}{S}_{12}\, \underset{\sim}{\Pi}_{1T} \\
&+ \sum_{T} \mathcal{V}^{Tll}_{1T}(\underset{\sim}{r})S_{12}(\underset{\sim}{\vec{L}},\underset{\sim}{\vec{L}})\, \underset{\sim}{\Pi}_{1T} \\
&+ \sum_{T} \frac{1}{2}\left[\underset{\sim}{p}_{r}\mathcal{V}^{Trp}_{1T}(\underset{\sim}{r}) + \mathcal{V}^{Trp}_{1T}(\underset{\sim}{r})\underset{\sim}{p}_{r}\right] S_{12}(\underset{\sim}{\vec{r}},\underset{\sim}{\vec{p}}_{\Omega})\, \underset{\sim}{\Pi}_{1T}\,. \qquad (4.6)
\end{aligned}$$

Compared to the full UCOM potential Eq. (3.22) this **reduced UCOM potential** Eq. (4.6) lacks the operators $\underset{\sim}{\vec{L}}^{2}(\underset{\sim}{\vec{L}}\cdot\underset{\sim}{\vec{S}})$, $\bar{S}_{12}(\underset{\sim}{\vec{p}}_{\Omega},\underset{\sim}{\vec{p}}_{\Omega})$, $\underset{\sim}{\vec{L}}^{2}\bar{S}_{12}(\underset{\sim}{\vec{p}}_{\Omega},\underset{\sim}{\vec{p}}_{\Omega})$ and all the high-order angular momentum terms already neglected in Eq. (3.22). Compared to the operator set of the initial Argonne potential Eq. (3.14) it is supplemented by the momentum dependent operators $\underset{\sim}{\vec{p}}^{2}$ and $\underset{\sim}{p}_{r}S_{12}(\underset{\sim}{\vec{r}},\underset{\sim}{\vec{p}}_{\Omega})$. It turns out that in this ansatz the tensor operator $S_{12}(\underset{\sim}{\vec{L}},\underset{\sim}{\vec{L}})$ is only needed for $T=0$. The radial function for $T=1$, $\mathcal{V}^{Tll}_{11}(\underset{\sim}{r})$, can be set to zero without impairing the quality of the fit.

The partial wave matrix elements of this ansatz (calculated by means of Eqs. (4.5)) are fitted to the exact partial wave matrix elements of the UCOM transformed Argonne potential. Not all matrix elements can be considered in this fit, so that one has to restrict oneself to a certain range of momenta and angular momenta. It is important to include all states with momentum k relevant for low energy nuclear structure physics and also states with higher momentum which are connected to those by the NN interaction. In case of the UCOM transformed Argonne potential and the other effective realistic potentials considered in this work it is sufficient to take the matrix elements with momenta k up to $10\,\text{fm}^{-1}$. Since the kinetic energy becomes dominant with increasing angular momentum L, only matrix elements with L up to 4 are used to perform the fit. The computer code for the fitting procedure weights the considered partial wave channels differently in order to optimize the fit for certain channels one wants to reproduce with high accuracy. Channels with higher angular momentum are weighted lower than those with low angular momentum (e.g. for $S=1$ and $T=0$, the S and D wave matrix elements are weighted by a factor 10 more than those of the F wave) to provide optimal results for low angular momenta. Details of the used weights can be found in Appendix C.2. The parameters $\gamma^{p}_{ST,\mu}$ obtained from the fit are shown in Appendix C.3.1. These parameters define in combination with the operator representation Eq. (4.6) and the parameterization of the radial functions Eq. (4.3) the reduced UCOM potential.

Fig. 4.2 shows the matrix elements for selected partial waves of the reduced UCOM potential compared to the exact matrix elements of the UCOM potential. As one requires, by means of the weight factors, more accuracy for low angular momentum partial waves than for those with higher angular momenta, the deviations between the exact UCOM matrix elements and the matrix elements of the potential with the reduced set of operators are very small in the $^{3}\text{S}_{1}$ and $^{3}\text{S}_{1}$-$^{3}\text{D}_{1}$ channel, while in the $^{3}\text{F}_{3}$ channel

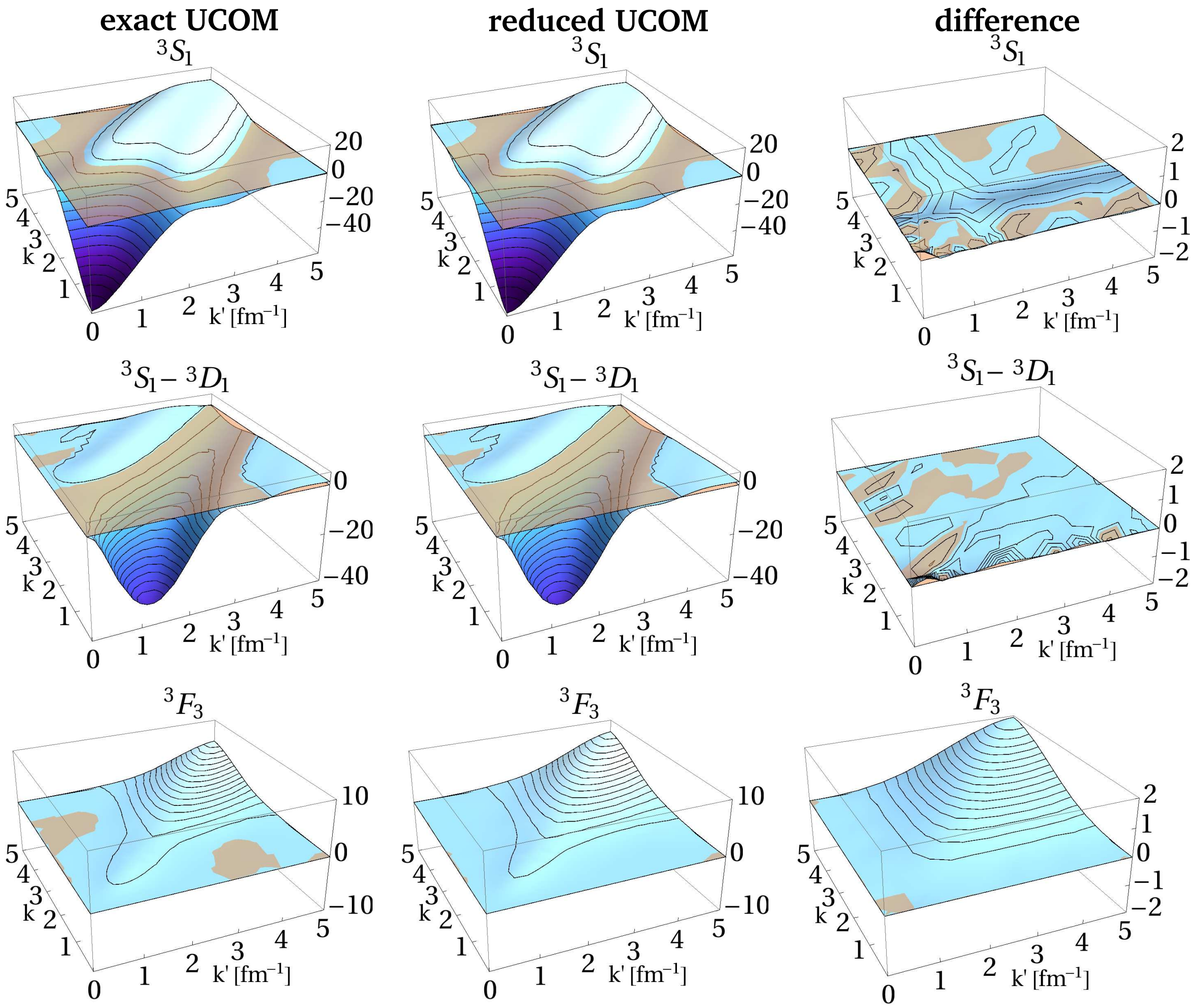

Figure 4.2: Exact matrix elements $\left\langle k(LS)J;T \left| V_{\text{UCOM}} \right| k'(L'S)J;T \right\rangle$ (in $\text{MeV}\,\text{fm}^3$) of the UCOM potential (left), matrix elements $\left\langle k(LS)J;T \left| V^{(\text{red.})}_{\text{UCOM}} \right| k'(L'S)J;T \right\rangle$ obtained by a fit using the reduced ansatz (4.6) (middle) and the difference between the matrix elements (right) for the $^3S_1$, $^3S_1$-$^3D_1$ and $^3F_3$ channel. The reddish plane marks the position of the zero-plane.

differences between the exact UCOM matrix elements and those of the reduced UCOM occur. The small deviations in the $^3S_1$ and $^3S_1$-$^3D_1$ channel are also reflected in the phase shifts displayed in Fig. 4.3. Exact UCOM and reduced UCOM result in the same phase shifts for $L=0$ and 2, $S=1$, $J=1$ and $T=0$ up to $E_{\text{lab}} = 300\,\text{MeV}$. They also reproduce the measured data (Nijmegen 1993 np [47]) which is to be expected, as UCOM is by construction phase shift equivalent to the initial Argonne potential. For the $^3F_3$ channel, which shows deviations between the matrix elements of the exact and the reduced UCOM potential (Fig. 4.2), the phase shifts in Fig. 4.7 consequently differ at higher energies. In the following the quality of an operator representation for a partial wave is often discussed in terms of phase shifts which is analogue to a discussion in terms of partial wave matrix elements since the phase shifts are calculated from those. Deviations between the matrix elements of the derived operator representation and the exact potential result in deviations for the calculated phase shifts in the considered partial wave channel. Vice versa, a bad description of the phase shifts by the derived operator representation implies deviations between the matrix elements of this operator representation and the exact potential.

It should be emphasized that the radial functions $\mathcal{V}^{P}_{ST}(r)$ of the reduced UCOM potential Eq. (4.6) generally differ from the corresponding radial dependencies $V^{P}_{ST}(r)$ in the full operator representation of the UCOM potential Eq. (3.22). For instance, the spin-orbit term $\mathcal{V}^{LS}_{ST}(r)$ in $\underset{\sim}{V}^{(\text{red.})}_{\text{UCOM}}$ can absorb for $L=1$ and 2 the contribution that came from the neglected $\underset{\sim}{\vec{L}}^{2}(\underset{\sim}{\vec{L}}\cdot\underset{\sim}{\vec{S}})$ term such, that for $L=1$, $T=1$ and $L=2$, $T=0$

$$\left\langle k(L1)JT \left| \mathcal{V}^{LS}_{1T}(\underset{\sim}{r})(\underset{\sim}{\vec{L}}\cdot\underset{\sim}{\vec{S}}) \right| k'(L1)JT \right\rangle = \left\langle k(L1)JT \left| V^{LS}_{1T}(\underset{\sim}{r})(\underset{\sim}{\vec{L}}\cdot\underset{\sim}{\vec{S}}) + V^{L2LS}_{1T}(\underset{\sim}{r})\underset{\sim}{\vec{L}}^{2}(\underset{\sim}{\vec{L}}\cdot\underset{\sim}{\vec{S}}) \right| k'(L1)JT \right\rangle \quad (4.7)$$

and differences occur only for $L=3$ and higher. On the other hand, since no operators of the central part of the interaction ($\underset{\sim}{1}$, $\underset{\sim}{\vec{L}}^{2}$, $\underset{\sim}{\vec{p}}^{2}$) are neglected in ansatz Eq. (4.6), no terms of the central part have to be absorbed by others and the results of the fit reproduce the exact radial functions. In Appendix C.3.1 (Fig. C.1 to C.5), the radial functions $\mathcal{V}^{P}_{ST}(r)$ of the reduced UCOM potential are plotted as a function of the relative distance and compared with the radial functions $V^{P}_{ST}(r)$ of the full UCOM potential.

If one simply neglects the omitted operators $\underset{\sim}{\vec{L}}^{2}(\underset{\sim}{\vec{L}}\cdot\underset{\sim}{\vec{S}})$, $\bar{S}_{12}(\underset{\sim}{\vec{q}}_{\Omega},\underset{\sim}{\vec{q}}_{\Omega})$ and $\underset{\sim}{\vec{L}}^{2}\bar{S}_{12}(\underset{\sim}{\vec{q}}_{\Omega},\underset{\sim}{\vec{q}}_{\Omega})$ in the UCOM potential Eq. (3.22) (UCOM-neglected in Fig. 4.3) without refitting the radial functions, one sees a substantial difference. This means that the contribution of the operators neglected in the reduced UCOM potential is not small but is absorbed in the refitted radial dependencies of the reduced set of operators.

Other sets of operators

As already mentioned, there are different possibilities to choose a reduced set of operators. An overview of possible sets of operators is given in Tab. 4.1.

It turns out that it is necessary to have at least the set of operators already present in the initial Argonne potential* plus the momentum dependent operators originating from the correlated kinetic energy $\underset{\sim}{\vec{p}}^{2}$ and $\underset{\sim}{p}_{r}S_{12}(\underset{\sim}{\vec{r}},\underset{\sim}{\vec{p}}_{\Omega})$. The contributions from the momentum dependent terms cannot be absorbed in the radial functions of the other operators because all these terms in the UCOM transformed Argonne potential are local and therefore not able to describe this momentum dependence. The quadratic momentum dependence is a characteristic feature of the UCOM potential. These terms replace the strong short range repulsion and the short range tensor which are responsible for undesired scattering to high momentum states and it is necessary to include them in the reduced set of operators. Fig. 4.4 shows the phase shifts

set	operator structure										pw's	
no.	C	$L2$	$p2$	LS	$L2LS$	T	TLL	Tpp	Trp	$L2Tpp$	$L\leq 2$	remarks
(1)	✓	✓	✓	✓	✓	✓	✓	✓	✓	✓	✓	full set of operators
(2)	✓	✓	×	✓	✓	✓	✓	✓	×	✓	×	without momentum (see Fig. 4.4)
(3)	✓	✓	✓	✓	×	✓	✓	✓	✓	×	✓	
(4)	✓	✓	✓	✓	×	✓	✓	×	✓	×	✓	
(5)	✓	✓	✓	✓	×	✓	✓,×	×	✓	×	✓	same as (4), but TLL only for $T=0$
(6)	✓	✓	✓	✓	×	✓	×	✓	✓	×	✓	
(7)	✓	✓	✓	✓	×	✓	×	×	✓	×	×	deviations in D-wave channels
(8)	✓	✓	✓	✓	×	×	×	×	✓	×	×	deviations in P-wave channels

Table 4.1: Different sets of operators used in V_{ansatz} (for the abbreviations see Eq. (3.22)). The matrix elements, phase shifts and deuteron properties calculated with the fitted interaction are compared to those of the exact UCOM potential. A check mark in the column "pw's $L\leq 2$" indicates that the set is able to reproduce the exact results in the partial waves with L up to 2.

---

[*] As an exception, the contributions of the operator $S_{12}(\underset{\sim}{\vec{L}},\underset{\sim}{\vec{L}})$ can be absorbed by other tensor operators, for example in set no. (6) in Tab. 4.1.

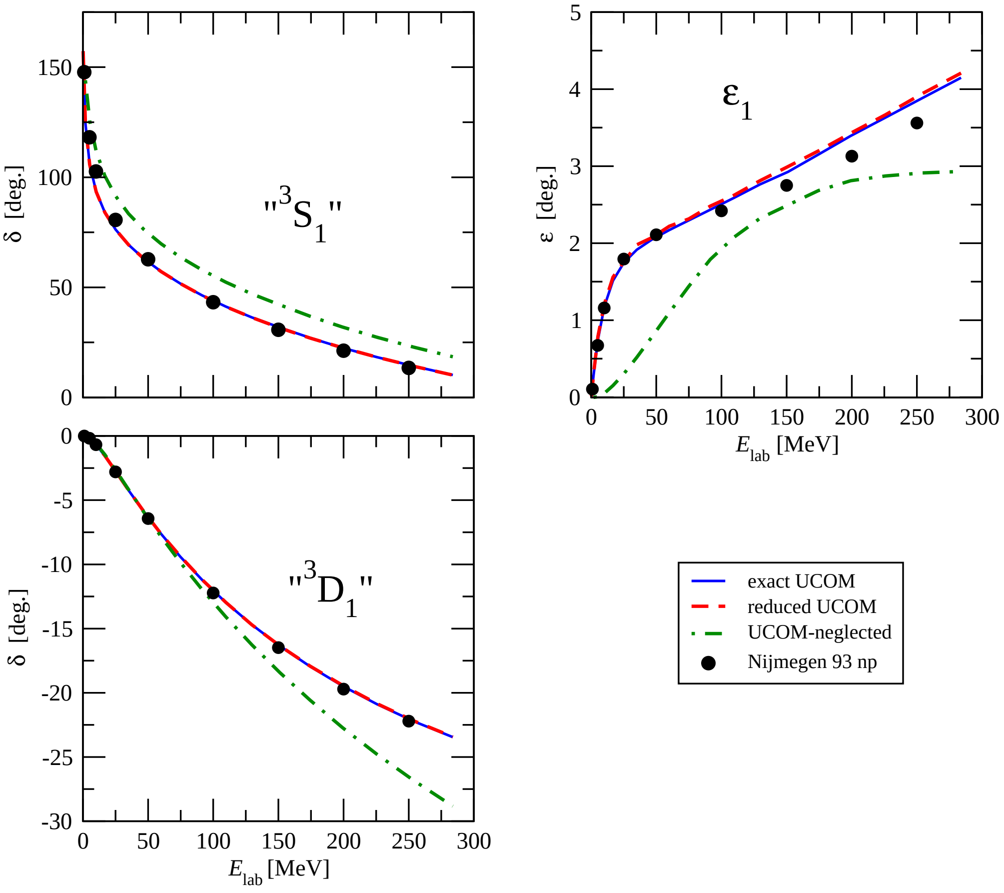

Figure 4.3: Nucleon-nucleon phase shifts calculated with the exact matrix elements of the UCOM transformed Argonne potential (blue solid line), the reduced UCOM potential (red dashed line) and the UCOM transformed Argonne potential neglecting the terms with $\vec{L}^2(\vec{L}\cdot\vec{S})$, $\bar{S}_{12}(\vec{p}_\Omega,\vec{p}_\Omega)$ and $\vec{L}^2\bar{S}_{12}(\vec{p}_\Omega,\vec{p}_\Omega)$ (green dot-dashed line). The dots indicate the results of the 1993 Nijmegen partial wave analysis [47].

calculated with a refitted operator representation excluding the momentum dependent operators (corresponding to set no. (2) in Tab. 4.1). From this results it is obvious, that it is not possible to reproduce the phase shifts of the exact UCOM potential without using momentum dependent operators in the ansatz.

Other choices of operators in $\underset{\sim}{V}_{\text{ansatz}}$ are also possible. An ansatz using $\bar{S}_{12}(\underset{\sim}{\vec{p}}_\Omega,\underset{\sim}{\vec{p}}_\Omega)$ instead of $S_{12}(\underset{\sim}{\vec{L}},\underset{\sim}{\vec{L}})$ (set no. (6) in Tab. 4.1) for example leads to results comparable to those obtained with the set in Eq. (4.6). For smaller sets of operators the matrix elements and two-nucleon properties of the fitted interaction do not agree well with the initial UCOM transformed Argonne potential, even for the lowest angular momenta (set no. (7) and (8)). In that sense, the presented choice of operators for the reduced UCOM potential Eq. (4.6) (corresponding to set no. (4) and (5) in Tab. 4.1) provides a minimal set of operators which reproduces matrix elements and properties of the UCOM potential for angular momenta up to $L = 2$ and with small deviations also in the F-wave ($L = 3$). Thus, the set of operators no. (5), which is used in this work, is (among set no. (4) and (6)) the best choice for the reduced UCOM potential.

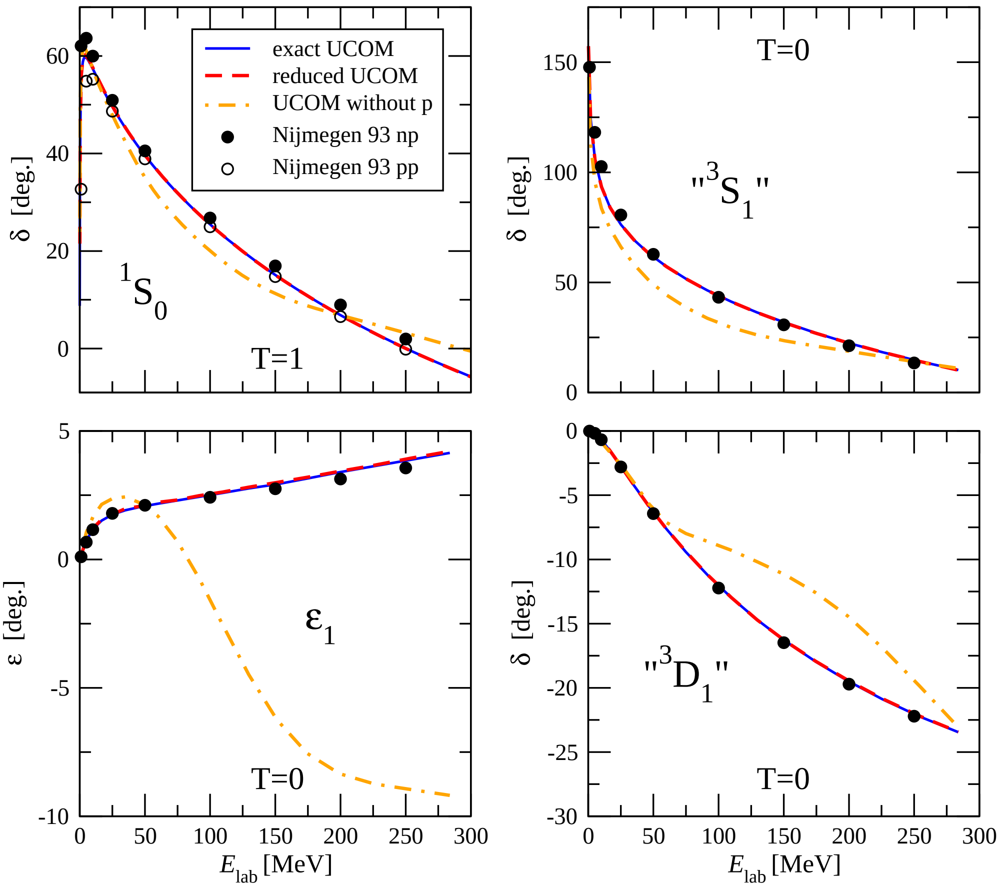

Figure 4.4: Nucleon-nucleon phase shifts calculated with the exact matrix elements of the UCOM transformed Argonne potential (blue solid line), the reduced UCOM (red dashed line) and an UCOM potential with refitted radial functions excluding explicitly momentum dependent operators (corresponding to set no. (2) in Tab. 4.1) (orange dot-dashed line). The dots indicate the results of the 1993 Nijmegen partial wave analysis [47].

4.2.3 Results for two- and few-nucleon systems

To evaluate the quality of the UCOM potential with the reduced set of operators discussed above, the many-body methods discussed in Sec. 2 are used with the reduced UCOM potential and, to have a reference point, with the exact UCOM transformed Argonne matrix elements. The results of these calculations are shown in this section.

Two-nucleon systems

The initial Argonne potential is a realistic NN interaction: it reproduces the NN scattering phase shifts and the properties of the deuteron. The short-ranged unitary UCOM transformation does not affect these properties and leads to the effective realistic UCOM transformed Argonne potential. The reduced UCOM interaction has to reproduce the deuteron properties and phase shifts in the same quality as the exact UCOM interaction, at least for angular momenta up to $L = 2$. The computer code discussed in Sec. 2.2.1 and Appendix B is used to calculate the two-nucleon properties. Since the code uses the partial wave matrix elements as input, the matrix elements of the reduced UCOM potential are needed. The calculation of these matrix elements from the operator representation can be easily performed by using Eqs. (4.5).

Fig. 4.3 and 4.5 - 4.7 show the phase shifts calculated with the exact UCOM transformed Argonne potential and the reduced UCOM potential. The results for the deuteron can be found in Tab. 4.2.

^{2}H	E_B [MeV]	$\mu\,[\mu_N]$	$Q\,[e\,\mathrm{fm}^2]$
exact UCOM	2.23	0.847	0.270
reduced UCOM	2.23	0.847	0.270
Experiment	2.2246	0.8574	0.2860

Table 4.2: Binding energy E_B, magnetic dipole moment μ and electric quadrupole moment Q of the deuteron for the exact UCOM transformed Argonne potential (exact UCOM) and the reduced UCOM potential (reduced UCOM) compared with experimental data. The results for μ and Q have been obtained with correlated operators.

The phase shifts show very good agreement up to the D-wave. Deviations occur for $L = 3$ and above, especially at higher laboratory energies. These deviations are in general rather small compared to the absolute value of the phase shifts. Only the ^{3}D$_3$-wave phase shifts of the reduced UCOM potential are poorly reproduced. The large deviations originate from the coupling to G-wave matrix elements which is not reproduced well by the reduced set of operators. The D-wave matrix elements of the reduced UCOM potential themselves are correct, as can be seen in the other D-wave channels.

The deuteron properties, which are sensitive only to the ^{3}S$_1$- and ^{3}D$_1$-wave channels, are described very well by both interactions.

This shows that the reduced UCOM potential and the exact UCOM potential have the same features at low angular momenta: phase shifts and deuteron properties calculated with both interactions are in good agreement. At higher angular momenta L, the reduced UCOM potential is less precise in reproducing the correct phase shifts than the exact UCOM interaction, but the obtained phase shifts are of the same order of magnitude as the correct ones. By studying light nuclei, one can investigate if the deviations for higher L have an effect on the quality of the reduced UCOM potential for those systems.

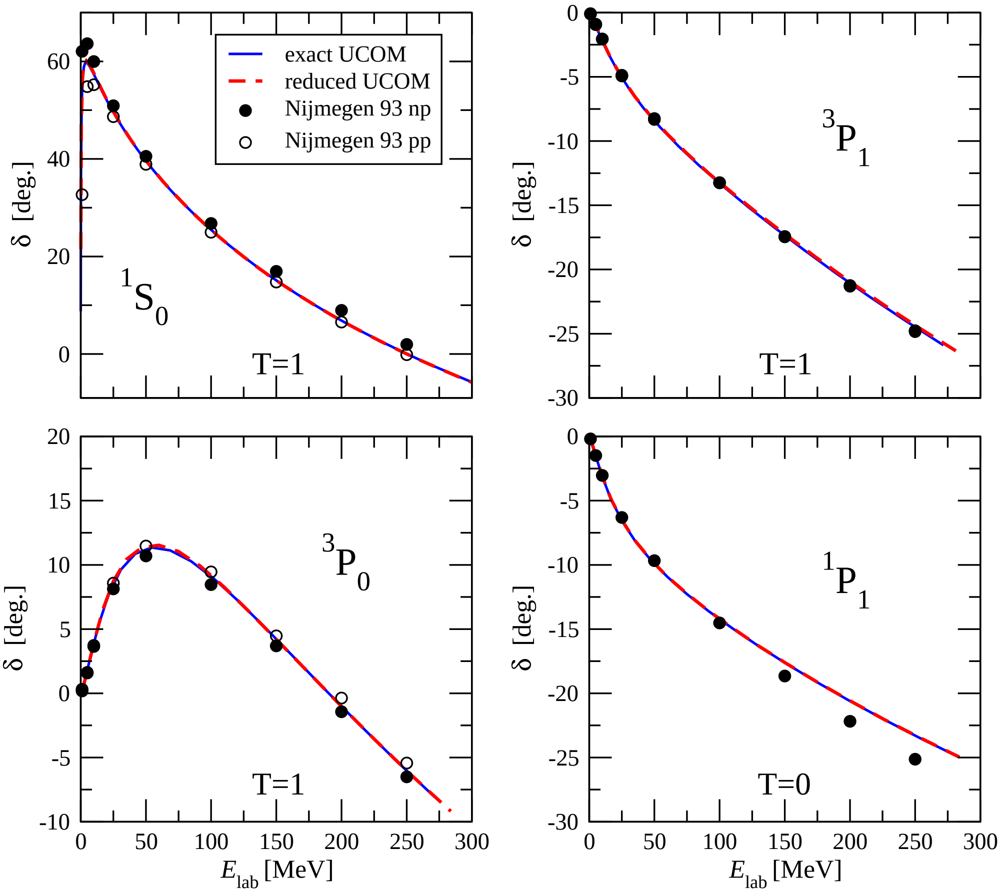

Figure 4.5: Nucleon-nucleon phase shifts for total angular momentum $J = 0$ $(T = 1)$ and $J = 1$ $(T = 0$ and $1)$ calculated with the exact matrix elements of the UCOM transformed Argonne potential (blue solid line) and the UCOM potential with a reduced set of operators (red dashed line). The dots indicate the results of the 1993 Nijmegen partial wave analysis [47]. The phase shifts of the original Argonne potential are identical with those of the UCOM correlated Argonne potential.

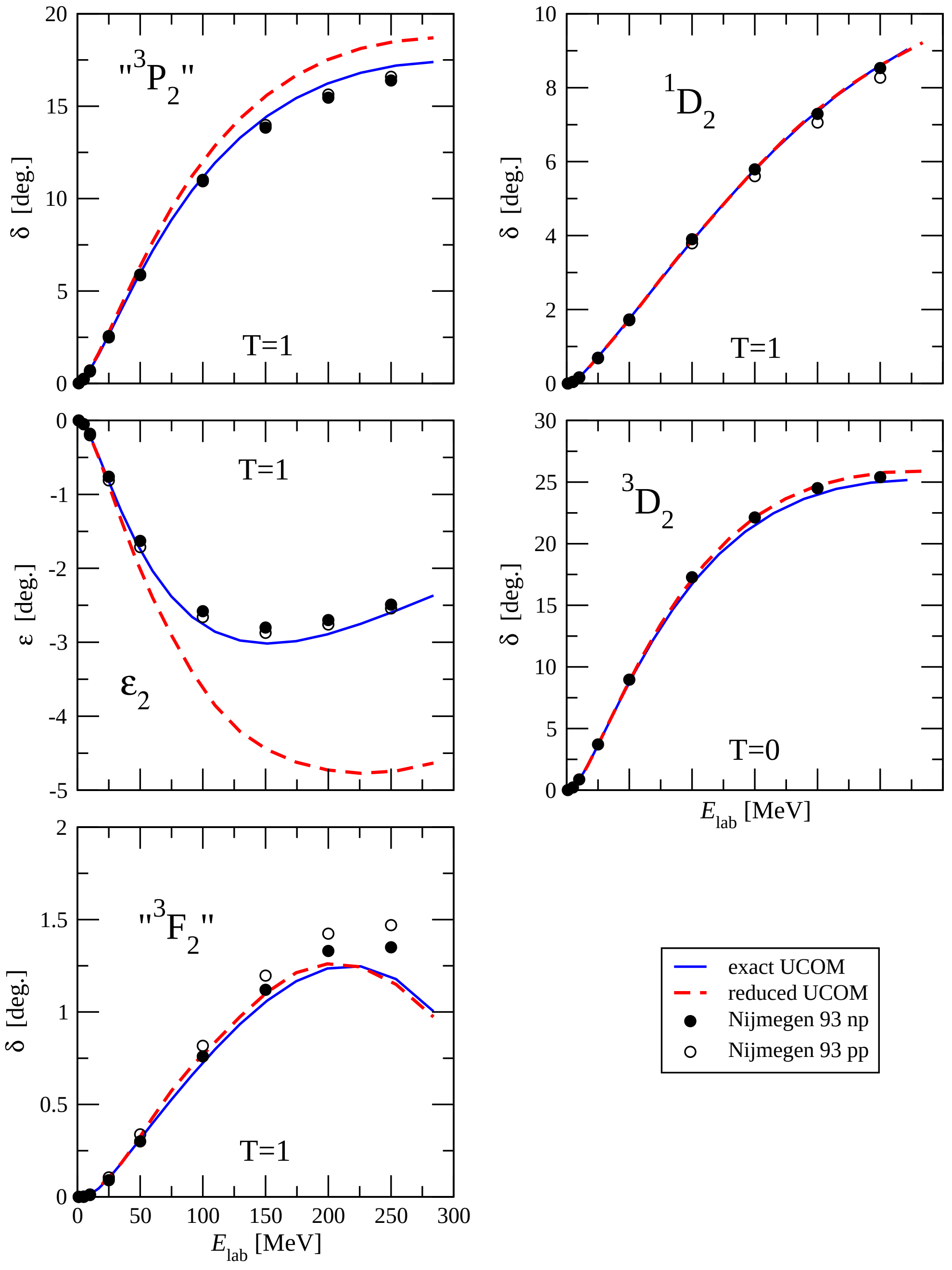

Figure 4.6: Same as Fig. 4.5, but for $J = 2$ and $T = 0, 1$.

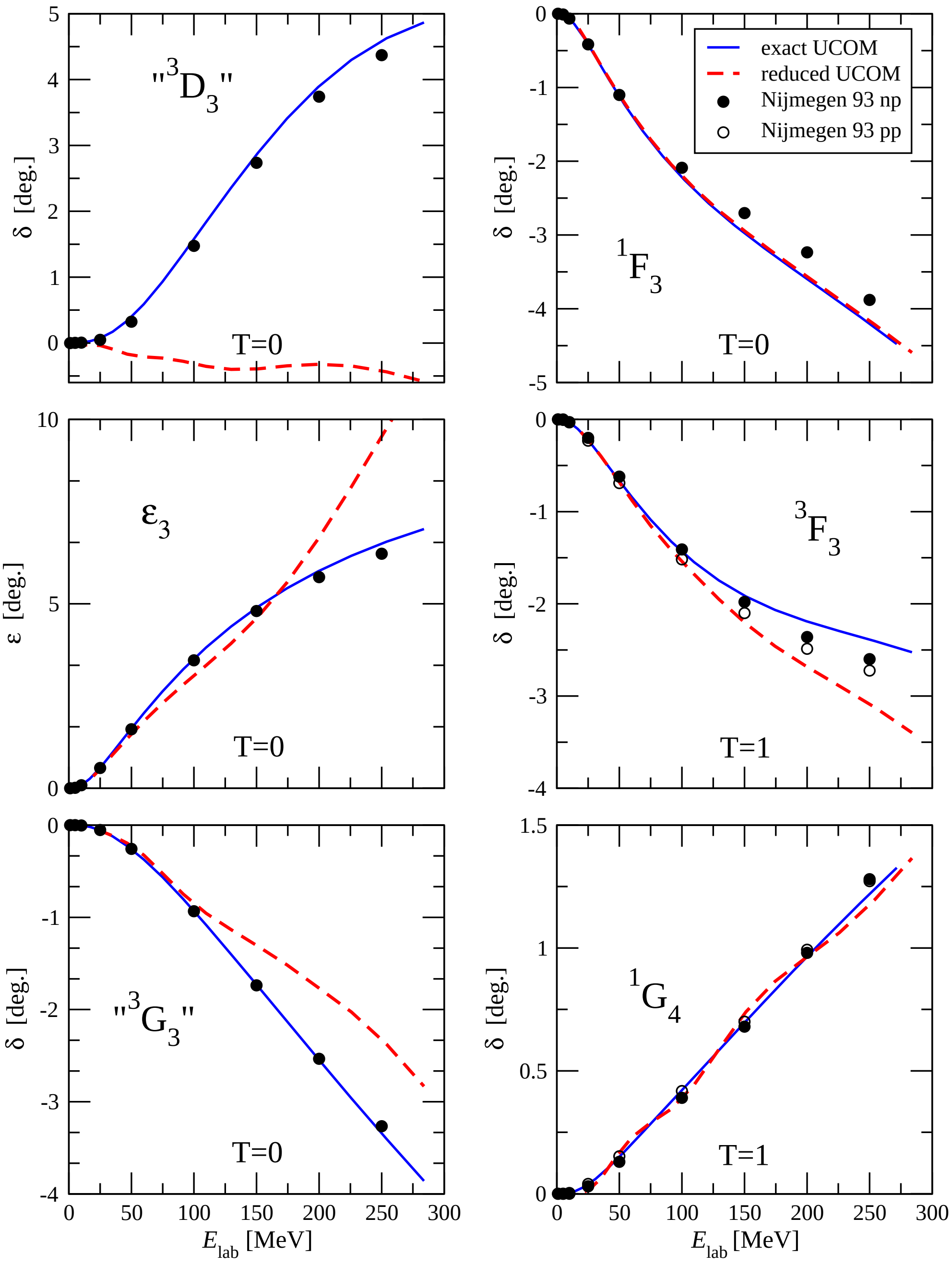

Figure 4.7: Same as Fig. 4.5, but for $J = 3$, $T = 0$ and 1 and $J = 4$, $T = 1$.

No Core Shell Model

The reduced UCOM potential and the exact UCOM potential are used in the No Core Shell Model (NCSM). First, the binding energies of selected light nuclei are calculated. The extrapolated binding energies for some light nuclei up to ^{7}Li are shown in Tab. 4.3. Energies obtained from a $0\hbar\omega$ calculation for larger nuclei are presented in Tab. 4.4. Other observables than binding energies are considered as well. Results for the point proton radius, the magnetic dipole moment and the electric quadrupole moment of the ^{6}Li and ^{7}Li ground states are listed in Tab. 4.5.

	^{3}H	^{3}He	^{4}He	^{6}He	^{6}Li	^{7}Li
exact UCOM	8.38(1)	7.67(1)	28.53(1)	28.4(2)	31.5(2)	38.6(4)
reduced UCOM	8.37(1)	7.67(1)	28.51(2)	28.6(2)	31.7(2)	38.8(4)
Experiment	8.482	7.718	28.296	29.269	31.995	39.245

Table 4.3: Binding energies (in MeV) of some light nuclei calculated in the NCSM with the exact matrix elements of the UCOM transformed Argonne potential (exact UCOM) and the UCOM potential with a reduced set of operators (reduced UCOM). The results for the ^{4}He, ^{6}He, ^{6}Li and ^{7}Li energies are obtained by an extrapolation to infinite model space size. The error estimates are obtained from comparison of energies using different oscillator frequencies.

	^{9}Be	^{10}B	^{11}B	^{12}C	^{13}C	^{14}N	^{15}N	^{16}O
exact UCOM	15.6	16.6	24.9	37.3	39.0	46.3	60.0	72.3
reduced UCOM	15.7	16.7	25.0	37.3	39.1	46.4	60.0	72.3

Table 4.4: Binding energies (in MeV) of light nuclei calculated in the NCSM in a $0\hbar\omega$ model space with the exact matrix elements of the UCOM transformed Argonne potential (exact UCOM) and the reduced UCOM potential (reduced UCOM).

	Nucleus	E_B [MeV]	R_p [fm]	μ [μ_N]	Q [$e\,\mathrm{fm}^2$]
exact UCOM	^{6}Li	31.5(2)	2.1(1)	0.843(2)	-0.04(2)
reduced UCOM		31.7(2)	2.1(1)	0.842(1)	-0.03(3)
Experiment		31.995	2.41(3)	0.8220	-0.0818(17)
exact UCOM	^{7}Li	38.6(4)	2.0(1)	2.988(3)	-2.6(3)
reduced UCOM		38.8(4)	2.0(1)	2.987(2)	-2.5(3)
Experiment		39.245	2.26(2)	3.2564	-4.06(8)

Table 4.5: Properties of ^{6}Li and ^{7}Li. Binding energy E_B, point-proton radius R_p, magnetic dipole moment μ and electric quadrupole moment Q, calculated in the NCSM with the exact UCOM matrix elements (exact UCOM) and the reduced UCOM potential (reduced UCOM). The energies are obtained from an extrapolation to infinite model space size. The other properties are calculated in a model space size of $12\hbar\Omega$ for ^{6}Li and $10\hbar\Omega$ for ^{7}Li with an oscillator frequency of $\hbar\Omega = 24\,\mathrm{MeV}$ and by means of uncorrelated operators. Error estimates are from comparison of results with different oscillator frequencies. Experimental data from [51] and [52].

The results for the binding energy obtained with the reduced set of operators in Tab. 4.3 lie within a range of 200 keV around those calculated with the exact UCOM potential.

The results of the $0\hbar\omega$ calculations for stable nuclei up to ^{16}O in Tab. 4.4 are far from the point of convergence, so that the comparison with the experimental values is not very meaningful. However, one can compare the energies obtained with the reduced and the exact UCOM potential. As already seen for the converged NCSM results in Tab. 4.3, reduced and the exact UCOM potential lead to exactly the same results, even for the larger systems.

A good agreement can also be seen for calculated ground state properties in Tab. 4.5. The radii of ^{6}Li and ^{7}Li and the quadrupole moment of ^{7}Li in these calculations still depend on the size of the model space, but good agreement between the results from the exact and reduced UCOM potential is observed. The nuclear spectra of ^{6}Li and ^{7}Li calculated with the reduced UCOM potential and the exact UCOM potential are shown in Fig. 4.8. One has to compare the $12\hbar\Omega$ results of the reduced UCOM potential with the exact UCOM result for ^{6}Li and the $10\hbar\Omega$ results for ^{7}Li*. Both interactions clearly lead to almost identical energy spectra.

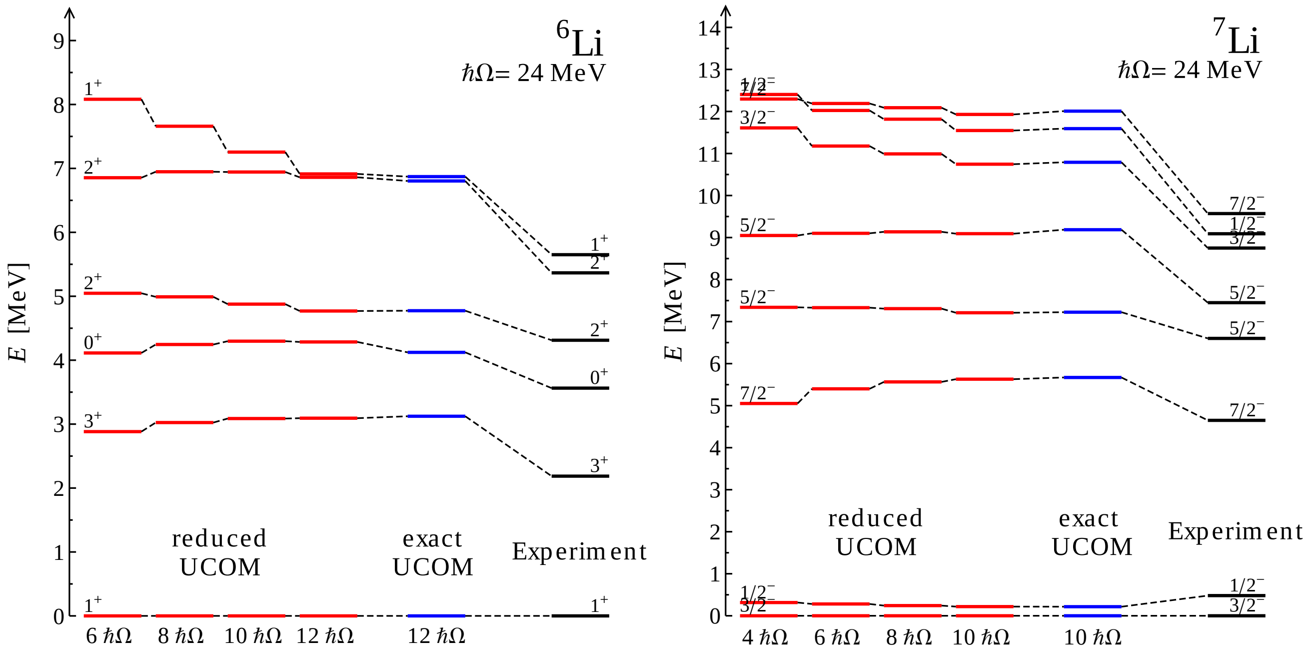

Figure 4.8: Spectra of ^{6}Li and ^{7}Li. The red lines show the results of a NCSM calculation with the matrix elements of the reduced UCOM potential for different model spaces up to $12\,\hbar\Omega$ for ^{6}Li and up to $10\,\hbar\Omega$ for ^{7}Li in comparison with the results of the exact UCOM matrix elements (blue lines) in a $12\,\hbar\Omega$ and $10\,\hbar\Omega$ model space and the experiment [51].

Summing up, one sees that for all calculated observables the reduced UCOM potential yields the same results as the exact UCOM transformed Argonne potential, although having a less complicated operator structure.

---

* The reduced UCOM results for the smaller model space sizes are also depicted to show how good the results for a given energy level are converged.

Fermionic Molecular Dynamics

Finally, the full* UCOM potential Eq. (3.22) and the reduced UCOM potential Eq. (4.6) are tested in **Fermionic Molecular Dynamics** (FMD) calculations.

The potentials are tested in a VAP† calculation for ^{4}He. The results are shown in Tab. 4.6. The difference between the results of the full UCOM and the reduced UCOM potential are around one hundred keV and thereby not much bigger than those obtained in the NCSM. However, both interactions are noticeably underbinding the ^{4}He ground state. This effect is due to the fact, that some of the long-ranged tensor correlations induced by the potential cannot be described in the FMD basis.

By using a UCOM potential with a longer ranged tensor correlator, the induced tensor correlations are lowered and can be described better by the used FMD basis states. For FMD calculations one usually uses a UCOM(SRG)‡ transformed Argonne potential obtained with a flow parameter of $s = 0.2\,\text{fm}^4$ (UCOM(0.2)) rather than the potential obtained with $s = 0.04\,\text{fm}^4$ which was discussed so far. The UCOM potential obtained with $s = 0.2\,\text{fm}^4$ has the advantage to induce less tensor correlations. Both UCOM transformed Argonne potentials have the same operator structure (given by Eq. (3.22)), but different radial functions. The usage of the UCOM(0.2) potential in the VAP FMD calculation discussed above results in a higher binding energy than for the UCOM(SRG) potential with $s = 0.04\,\text{fm}^4$. By using the method discussed in Sec. 4.2.1, one can derive an operator representation for the UCOM(0.2) potential with the same reduced set of operators Eq. (4.6) which was used for the UCOM potential with $s = 0.04\,\text{fm}^4$. The parameters of this potential, which in the following will be called **reduced UCOM(0.2)**, are listed in Appendix C.3.1.

The results for the binding energy of ^{4}He binding energy obtained with the full set of operators (full UCOM(0.2)) and the reduced set (reduced UCOM(0.2)) are given in Tab. 4.6. They lie again very close and in addition show a better agreement with the experiment.

^{4}He	E_B [MeV]
full UCOM	26.38
reduced UCOM	26.29
full UCOM(0.2)	27.42
reduced UCOM(0.2)	27.51
Experiment	28.296

Table 4.6: Binding energies (in MeV) of ^{4}He, calculated in a FMD VAP calculation with the full UCOM transformed Argonne potential (full UCOM), the UCOM potential with a reduced set of operators (red. UCOM), the UCOM transformed Argonne potential obtained with a correlation function from a SRG transformation with flow parameter $s = 0.2\,\text{fm}^4$ (full UCOM(0.2) and the reduced UCOM(0.2) potential (red. UCOM(0.2)).

The operator representations can be tested in further FMD calculations. Energy spectra from simple FMD PAV calculations with only one intrinsic state using the full and reduced UCOM and UCOM(0.2) potential are presented in Fig. 4.9 and 4.10. The ^{6}Li and ^{7}Li results obtained with the UCOM interaction show the same underbinding effect seen for ^{4}He. The spectra however show good agreement with the experimental data. A more important point is, that only negligible differences between the energy levels calculated with the full UCOM potential and the reduced UCOM potential occur. The same can be seen for the full and reduced UCOM(0.2) potential, which is here illustrated for ^{6}He in Fig. 4.10.

---

[*] The expression "full UCOM" refers to the operator representation Eq. (3.22). "Exact UCOM" refers to the exact UCOM matrix elements Eq. (3.24). Due to the partial summation the full UCOM is not identical to the exact UCOM potential, although the differences are very small.

[†] For the definition see Sec. 2.2.2.

[‡] See Ref. [55].

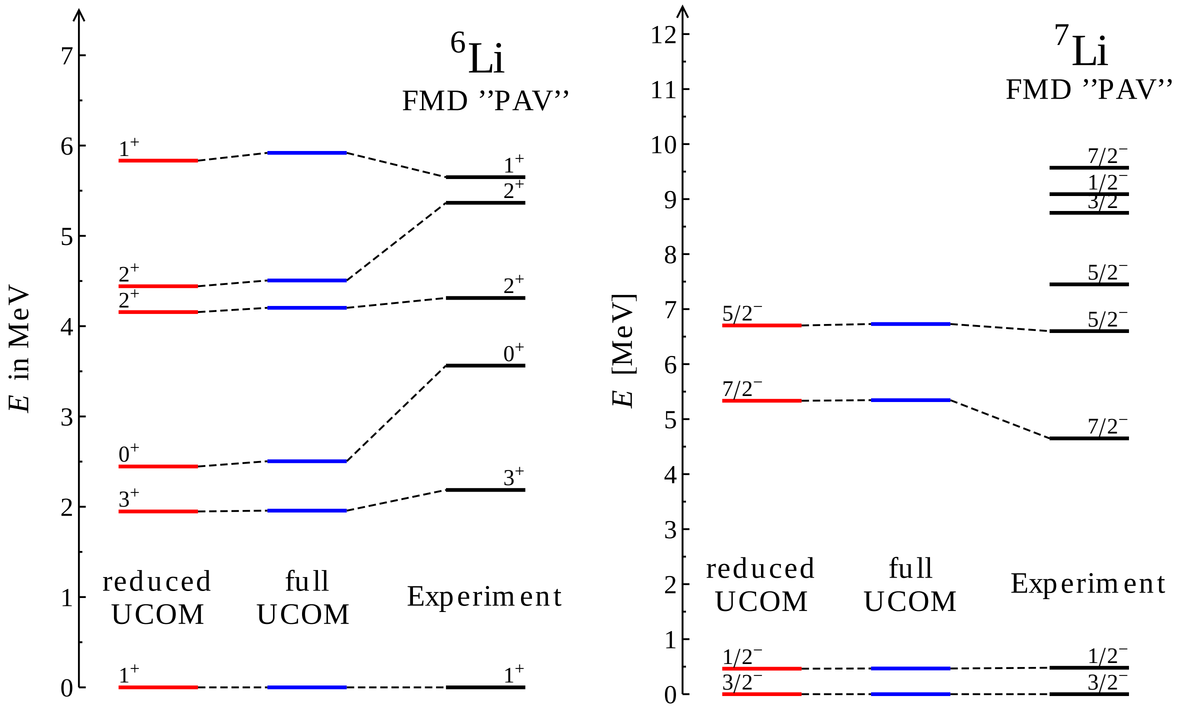

Figure 4.9: Spectra of ^{6}Li and ^{7}Li. The red lines show the results of a simple FMD PAV calculation with the reduced UCOM potential in comparison with the results of the full UCOM potential (blue lines) and the experiment [51].

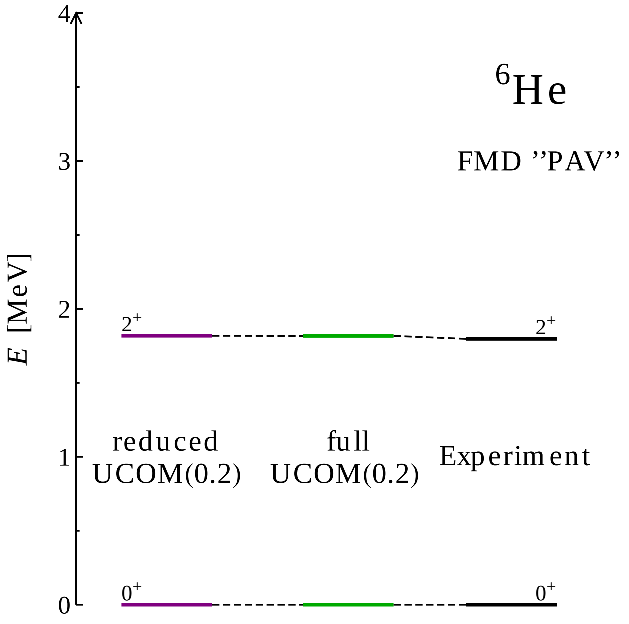

Figure 4.10: Spectrum of ^{6}He, calculated in a FMD PAV calculation with the reduced UCOM(0.2) potential (purple lines) and the full UCOM(0.2) potential (green lines). The black lines show the experimental results [51].

4.2.4 Closing remarks on the reduced UCOM potential

The derived reduced UCOM potential contains less operators than the full UCOM transformed Argonne potential.

In calculations of two-nucleon systems discussed in Sec. 4.2.3, reduced UCOM and the matrix elements of the exact UCOM transformed Argonne potential show the same results for the deuteron and the phase shifts up to the D-wave and slight deviations in the phase shifts with higher angular momenta. The latter can be traced back to the fact that the reduced set of operators cannot describe perfectly the exact UCOM potential in all partial waves and that the fitting method favors low angular momentum matrix elements to be reproduced as accurate as possible. The small deviations for higher angular momenta however have no effect on the results on the few-nucleon systems investigated by means of NCSM and FMD calculations. The reduced UCOM potential yields the same results as the exact UCOM transformed Argonne potential for a wide range of different physical properties of light nuclei, such as binding energies, energy level spectra, radii, magnetic dipole and electric quadrupole moments.

From these results one can conclude that the reduced UCOM potential contains all important features of the exact UCOM transformed Argonne potential which are relevant to describe the light nuclear systems discussed. It describes light nuclei with the same precision as the UCOM transformed Argonne potential, but contains a smaller set of operators. Due to this reduced set of operators, the reduced UCOM potential allows to perform FMD calculations for light nuclei with a reduced computational effort and without loosing accuracy at the same time.

Furthermore, the structure of the reduced UCOM potential allows to draw conclusions on the importance of the operators in the UCOM transformed Argonne potential Eq. (3.22). Although many new operators are created by the UCOM transformation, one succeeds in describing the important features of the potential by the set of operators already present in the bare Argonne potential plus the two momentum dependent operators in Eq. (3.22). This points out that especially the momentum dependent operators replacing short-range repulsion and tensor correlations play an essential role for the potential and have to be included in the reduced set of operators. The influence of the other operators created by the UCOM transformation is either small or can be absorbed by other operators without altering two- and few-nucleon properties significantly, so that these operators do not have to be considered explicitly in the reduced set of operators.

4.3 Operator representation for the SRG transformed Argonne potential

In this section, an operator representation of the SRG transformed Argonne potential is derived. As for the UCOM transformed Argonne potential, the method presented in Sec. 4.1 is applied. At first one hast to choose an ansatz for the operator representation.

4.3.1 Ansatz for the operator representation

In contrast to the UCOM transformed Argonne potential, the operator representation for the SRG transformed Argonne potential is not available. As discussed in Sec. 3.2, a complicated momentum dependence is expected, so that one would prefer to work with nonlocal radial functions $\mathcal{V}^{P}_{ST}(\underset{\sim}{\vec{r}}, \underset{\sim}{\vec{p}})$ to be flexible enough to describe the nonlocal behaviour. The ansatz for the operator representation is then given by Eq. 4.1.

Radial functions

The nonlocal radial functions $\mathcal{V}^{P}_{ST}(\underset{\sim}{\vec{r}},\underset{\sim}{\vec{p}})$ have to be parameterized. This can be done in different ways. An ansatz using a polynomial expansions in terms of $\underset{\sim}{\vec{p}}^{2}$, such as

$$\mathcal{V}^{P}_{ST}(\underset{\sim}{\vec{r}},\underset{\sim}{\vec{p}}) = \sum_{n=0}^{n_{max}} \sum_{\mu} \gamma^{n,P}_{ST,\mu} \left[\underset{\sim}{\vec{p}}^{2n}\, e^{-\frac{\underset{\sim}{\vec{r}}^{2}}{2\kappa_\mu}} + e^{-\frac{\underset{\sim}{\vec{r}}^{2}}{2\kappa_\mu}}\, \underset{\sim}{\vec{p}}^{2n} \right], \tag{4.8}$$

is not suitable, since in this case matrix elements $\langle\, k(LS)J;T \left| V^{P}_{ST}(\underset{\sim}{\vec{r}},\underset{\sim}{\vec{p}}) \right| k'(L'S)J;T \,\rangle$ with large k and k' are needed in the fit to prevent the polynomial ansatz from creating unphysical coupling to high momentum states outside the fitting region. A momentum dependence with a controlled range in the momentum space is important to prevent undesired unphysical effects at large momenta. This can be achieved by a momentum dependent operator having a gaussian structure*:

$$\mathcal{V}^{P}_{ST}(\underset{\sim}{\vec{r}},\underset{\sim}{\vec{p}}) = \sum_{\nu} \sum_{\mu} \gamma^{P}_{ST,\mu\nu} \left(\frac{\kappa_\mu}{\kappa_\mu - \lambda_\nu/4} \right)^{3/2} e^{-\frac{\lambda_\nu}{4}\underset{\sim}{\vec{p}}^{2}}\, e^{-\frac{\underset{\sim}{\vec{r}}^{2}}{2(\kappa_\mu - \lambda_\nu/4)}}\, e^{-\frac{\lambda_\nu}{4}\underset{\sim}{\vec{p}}^{2}}. \tag{4.9}$$

In position space basis representation this ansatz becomes

$$\langle\, \vec{r} \left| \mathcal{V}^{P}_{ST}(\underset{\sim}{\vec{r}},\underset{\sim}{\vec{p}}) \right| \vec{r}\,' \,\rangle = \sum_{\nu,\mu} \gamma^{P}_{ST,\mu\nu} \left(\frac{1}{2\pi\lambda_\nu} \right)^{3/2} e^{-\frac{1}{2\lambda_\nu}(\vec{r}-\vec{r}\,')^{2}}\, e^{-\frac{1}{2\kappa_\mu}\left(\frac{\vec{r}+\vec{r}\,'}{2}\right)^{2}}. \tag{4.10}$$

For $\lambda = 0$, the first exponential in Eq. (4.10) reduces to a delta function

$$\left(\frac{1}{2\pi\lambda} \right)^{3/2} e^{-\frac{1}{2\lambda}(\vec{r}-\vec{r}\,')^{2}} \xrightarrow{\lambda\to 0} \delta^{3}(\vec{r}-\vec{r}\,') \tag{4.11}$$

and one ends up at the local parameterization Eq. (4.3) used for the UCOM transformed Argonne potential. For parameters $\lambda > 0$ however, also nonlocal components are included.

The range of the momentum dependence in Eq. (4.9) in the partial wave basis in momentum space is controlled and restricted by the parameters λ_ν. One can choose these parameters such that the range of the momentum dependence does not exceed the momenta of the matrix elements to which the operator representation is fitted. This ensures that no unphysical behaviour at large momenta k outside the fit can appear. For $\lambda = 0$, the radial functions Eq. (4.9) reduce, as already seen in the position basis, to the local functions $\mathcal{V}_{ST}(\underset{\sim}{r})$ (Eq. (4.3)) used in the operator representation of the UCOM potential. For small

---

[*] The maybe somewhat complicated notation using the expression $\kappa_\mu - \lambda_\nu/4$ in the denominator of the argument of the exponential function in Eq. (4.9) has historical reasons. The nonlocal radial functions were originally defined in the position space basis by Eq. (4.10) in which κ_μ and λ_ν occur only separately. The corresponding operator form Eq. (4.9) was used later.

parameters λ (with $\lambda k_F^2 \ll 1$), one obtains, by using a truncated Taylor expansion of $e^{-\frac{\lambda_\nu}{4}\vec{p}^2}$ in Eq. (4.9), an ansatz with a quadratic momentum dependence:

$$\begin{aligned}
\mathcal{V}^P_{ST}(\utilde{\vec{r}},\utilde{\vec{p}}) &= \sum_\nu \sum_\mu \gamma^P_{ST,\mu\nu} \left(\frac{\kappa_\mu}{\kappa_\mu - \lambda_\nu/4} \right)^{3/2} e^{-\frac{\lambda_\nu}{4}\utilde{\vec{p}}^2}\, e^{-\frac{\utilde{\vec{r}}^2}{2(\kappa_\mu-\lambda_\nu/4)}}\, e^{-\frac{\lambda_\nu}{4}\utilde{\vec{p}}^2} \\
&\overset{\lambda_\nu k_F^2 \ll 1}{\simeq} \sum_\nu \sum_\mu \gamma^P_{ST,\mu\nu} \left(\frac{\kappa_\mu}{\kappa_\mu - \lambda_\nu/4} \right)^{3/2} \Bigg[e^{-\frac{\utilde{\vec{r}}^2}{2(\kappa_\mu-\lambda_\nu/4)}} \\
&\qquad + \frac{1}{4} \left(\utilde{\vec{p}}^2\, \lambda_\nu e^{-\frac{\utilde{\vec{r}}^2}{2(\kappa_\mu-\lambda_\nu/4)}} + \lambda_\nu e^{-\frac{\utilde{\vec{r}}^2}{2(\kappa_\mu-\lambda_\nu/4)}}\, \utilde{\vec{p}}^2 \right) \Bigg]. \qquad (4.12)
\end{aligned}$$

This shows that the ansatz Eq. (4.6) with local radial functions and quadratic momentum dependence, used for the UCOM potential, is included in the nonlocal ansatz Eq. (4.9). In contrast to the ansatz for the UCOM potential, the nonlocal parameterization Eq. (4.9) is able to tackle more complicated momentum dependences as well.

Matrix elements

One advantage of choosing the parameterization Eq. (4.9) is, that the matrix elements $\langle\, k(LS)J;T \,|\utilde{V}_{\text{ansatz}}|\, k'(L'S)J;T \,\rangle$ of the ansatz with nonlocal radial functions Eq. (4.1) can be calculated very similar to those of the ansatz with local radial functions Eq. (4.3). One finds for the matrix elements $\langle\, k(LS)J;T \,|\mathcal{V}^P_{ST}(\utilde{\vec{r}},\utilde{\vec{p}})\utilde{\mathcal{O}}_P|\, k'(L'S)J;T \,\rangle$ the expression

$$\begin{aligned}
\langle\, k(LS)J;T \,|\mathcal{V}^P_{ST}(\utilde{\vec{r}},\utilde{\vec{p}})\utilde{\mathcal{O}}_P|\, k'(L'S)J;T \,\rangle &= \sum_{\mu,\nu} \gamma^P_{ST,\mu\nu} \frac{2}{\pi} \left(\frac{\kappa_\mu}{\kappa_\mu - \lambda_\nu/4} \right)^{3/2} e^{-\frac{\lambda_\nu}{4}(\vec{k}^2+\vec{k}'^2)} \,\cdot \\
&\quad \int_0^\infty dr\, r^2 j_L(kr) j_{L'}(k'r) \exp\left\{ -\frac{r^2}{2(\kappa_\mu-\lambda_\nu/4)} \right\} \langle\, (LS)J;T \,|\utilde{\mathcal{O}}_P|\, (L'S)J;T \,\rangle.
\end{aligned}$$

$$(4.13)$$

Compared to the expression for the local radial function Eq. (4.5a), this matrix element contains the same integral over spherical Bessel functions and a gaussian* and is only supplemented by a factor of $\left(\frac{\kappa_\mu}{\kappa_\mu-\lambda_\nu/4}\right)^{3/2} e^{-\frac{\lambda_\nu}{4}(\vec{k}^2+\vec{k}'^2)}$. Thus, the solutions of the integral for the local case, which are discussed in Appendix C.3.2, can be used in the nonlocal case as well.

For the tensor part, a slightly different parameterization combining the radial part and the tensor operator is used:†

$$\utilde{\mathcal{V}}^T_{1T}(\utilde{\vec{r}},\utilde{\vec{p}},\utilde{S}_{12}) = \sum_\nu \sum_\mu \gamma^T_{1T,\mu\nu} \left(\frac{\kappa_\mu}{\kappa_\mu - \lambda_\nu/4} \right)^{3/2} e^{-\frac{\lambda_\nu}{4}\utilde{\vec{p}}^2}\, \utilde{\vec{r}}^2\, e^{-\frac{\utilde{\vec{r}}^2}{2(\kappa_\mu-\lambda_\nu/4)}}\, \utilde{S}_{12}\, e^{-\frac{\lambda_\nu}{4}\utilde{\vec{p}}^2}. \qquad (4.14)$$

---

* In this case the width parameter is $\kappa_\mu - \lambda_\nu/4$ instead of just κ_μ in the local case.

† This parameterization has technical advantages in the calculation of partial wave and FMD matrix elements and provides the same accuracy in the description of the partial wave matrix elements as the maybe more suggesting parametrization of the form $\utilde{\mathcal{V}}^T_{1T}(\utilde{\vec{r}},\utilde{\vec{p}},\utilde{S}_{12}) := \utilde{S}_{12}\mathcal{V}^T_{1T}(\utilde{\vec{r}},\utilde{\vec{p}}) + \mathcal{V}^T_{1T}(\utilde{\vec{r}},\utilde{\vec{p}})\utilde{S}_{12}$.

The partial wave matrix element is given by

$$\left\langle k(LS)J;T \left| \underset{\sim}{\mathscr{V}}{}^{T}_{1T}(\underset{\sim}{\vec{r}},\underset{\sim}{\vec{p}},\underset{\sim}{S}_{12}) \right| k'(L'S)J;T \right\rangle = \sum_{\mu,\nu} \gamma^{P}_{ST,\mu\nu} \frac{2}{\pi} \left(\frac{\kappa_\mu}{\kappa_\mu - \lambda_\nu/4}\right)^{3/2} e^{-\frac{\lambda_\nu}{4}(\vec{k}^2+\vec{k}'^2)} \cdot$$
$$\int_0^\infty dr r^2 j_L(kr) j_{L'}(k'r)\, r^2 \exp\left\{-\frac{r^2}{2(\kappa_\mu - \lambda_\nu/4)}\right\} \left\langle (LS)J;T \left| \underset{\sim}{S}_{12} \right| (L'S)J;T \right\rangle. \tag{4.15}$$

This is again the expression for the local case multiplied by $\left(\frac{\kappa_\mu}{\kappa_\mu - \lambda_\nu/4}\right)^{3/2} e^{-\frac{\lambda_\nu}{4}(\vec{k}^2+\vec{k}'^2)}$. Thus, the results for the matrix elements of the ansatz with the local radial functions (Eq. (4.5a)) can be used directly to calculate the analytical expression of the matrix elements for the nonlocal ansatz. Furthermore, the parameterization using gaussians allows to derive analytical expressions for the matrix elements in the FMD basis which are presented in Appendix C.4.2.

4.3.2 Choice of the operators

As discussed in Sec. 3.2 the SRG transformation evolves the potential in each channel defined by the quantum numbers L, S, J and T separately because the SRG generator $\underset{\sim}{\eta}_s = [\underset{\sim}{T}_{\text{rel}}, \underset{\sim}{V}_s]$ itself depends on $\underset{\sim}{V}_s$ and therefore has a different form in each partial wave. Only between $S = 1$, $L = J \pm 1$ channels, due to the tensor force, mixing occurs and the channels are evolved together. Since each partial wave is evolved individually with its own generator, one has to expect that during the SRG evolution a more complicated dependence on the quantum numbers L, S and J than in the initial Argonne potential Eq. (3.14) is created. The question is now, whether one can still describe the SRG transformed Argonne matrix elements, at least approximately, with the set of operators from the Argonne potential or if only a description in terms of projection operators $\underset{\sim}{\Pi}_{LSJT}$ on the quantum numbers of each partial wave is able to represent the evolution in each partial wave with sufficient precision.

An ansatz working with projection operators and representing the SRG evolved matrix elements by nonlocal radial functions would be very flexible but requires in general more parameters, though probably much less than the number of matrix elements themselves. An ansatz with the operators from the Argonne potential in contrast contains less radial functions $\mathscr{V}^{P}(\underset{\sim}{\vec{r}},\underset{\sim}{\vec{p}})$ and is more transparent. Also for FMD, for which the operator representation is designated, it is difficult to calculate analytically the matrix elements of projectors on L and J in the FMD basis. Thus, an ansatz with the operators from the Argonne potential, but nonlocal radial functions, is used.

The ansatz reads explicitly

$$\begin{aligned}
\underset{\sim}{V}{}^{\text{SRG}}_{\text{ansatz}} &= \sum_{ST} \mathscr{V}^{C}_{ST}(\underset{\sim}{\vec{r}},\underset{\sim}{\vec{p}})\, \underset{\sim}{\Pi}_{ST} \\
&+ \sum_{ST} \mathscr{V}^{L2}_{ST}(\underset{\sim}{\vec{r}},\underset{\sim}{\vec{p}})\, \underset{\sim}{\vec{L}}{}^{2}\, \underset{\sim}{\Pi}_{ST} \\
&+ \sum_{T} \mathscr{V}^{LS}_{1T}(\underset{\sim}{\vec{r}},\underset{\sim}{\vec{p}})(\underset{\sim}{\vec{L}} \cdot \underset{\sim}{\vec{S}})\, \underset{\sim}{\Pi}_{1T} \\
&+ \sum_{T} \underset{\sim}{\mathscr{V}}{}^{T}_{1T}(\underset{\sim}{\vec{r}},\underset{\sim}{\vec{p}},\underset{\sim}{S}_{12})\, \underset{\sim}{\Pi}_{1T} \\
&+ \sum_{T} \mathscr{V}^{Tll}_{1T}(\underset{\sim}{\vec{r}},\underset{\sim}{\vec{p}}) S_{12}(\underset{\sim}{\vec{L}},\underset{\sim}{\vec{L}})\, \underset{\sim}{\Pi}_{1T}.
\end{aligned} \tag{4.16}$$

The parameters κ and λ in the nonlocal functions $\mathcal{V}^{P}_{ST}(r,p)$ are chosen to be

$$\begin{aligned}\kappa &= \{0.1, 0.2, 0.4, \cdots, 6.4\}\mathrm{fm}^2. \\ \lambda &= \left\{0, \frac{1}{16}, \frac{\sqrt{2}}{16}, \frac{1}{8}, \frac{\sqrt{2}}{8}, \frac{1}{4}\right\}\mathrm{fm}^2.\end{aligned}$$

With the set of parameters κ one is able to cover the range of the NN potential. The parameters λ are chosen such that they can describe local potentials (for $\lambda = 0$) as well as more complicated momentum dependences for $\lambda > 0$.

Following the procedure discussed in Sec. 4.1, the partial wave matrix elements of the ansatz Eq. (4.16) are to be calculated by means of Eqs. (4.13) and (4.15) and fitted to the partial wave matrix elements of the SRG transformed Argonne potential with $s = 0.03\,\mathrm{fm}^4$. As for the UCOM transformed Argonne potential, partial wave matrix elements with momenta up to $10\,\mathrm{fm}^{-1}$ and angular momentum up to $L = 4$ are included in the fit. Partial waves with small angular momentum quantum numbers L are weighted higher in the fit in order to obtain optimal results for these channels. At the same time one has to take care that by optimizing the fit for the lowest angular momenta the deviations for bigger L do not become too large. Thus, often a compromise between a perfect description of the partial waves with low L and a not too bad description of the other partial wave matrix elements has to be achieved. The used weights are listed in Appendix C.2. The parameters γ^{P}_{ST} obtained from this fit are listed in Appendix C.4.1.

Other operators

Recalling the connections between UCOM and SRG (Ref. [55, 61]), one expects that the operators of the UCOM potential Eq. (3.22) appear during the SRG transformation as well – maybe in a more complicated form due to the dynamically changing generator. Thus, one could include them in the ansatz for the operator form of the SRG transformed Argonne potential Eq. (4.16). In general, the inclusion of these operators gives more freedom to the fit to describe the different partial waves correctly. But since one aims to keep the number of parameters as low as possible, only the set in Eq. (4.16) and its extension by the momentum dependent operator $S_{12}(\underset{\sim}{\vec{r}}, \underset{\sim}{\vec{p}_\Omega})$ is studied in this work. The operator $S_{12}(\underset{\sim}{\vec{r}}, \underset{\sim}{\vec{p}_\Omega})$ results in the UCOM transformation from the tensor correlation operator $\underset{\sim}{C}_\Omega$. It has only off-diagonal matrix elements between $L = J \pm 1$ and one expects that it will help to reproduce the reduction of the tensor coupling caused by the SRG evolution.

The necessity to include the operator $S_{12}(\underset{\sim}{\vec{r}}, \underset{\sim}{\vec{p}_\Omega})$ for a correct description of the partial wave matrix elements can be seen in the ${}^3\mathrm{S}_1 - {}^3\mathrm{D}_1$ channel. A fit of the ansatz without $S_{12}(\underset{\sim}{\vec{r}}, \underset{\sim}{\vec{p}_\Omega})$ Eq. (4.16) to the partial wave matrix elements of this channel is not able to reproduce the matrix elements of the SRG transformed Argonne potential correctly. Increasing the number of parameters κ and λ in the fit does not improve the result, which indicates that without $S_{12}(\underset{\sim}{\vec{r}}, \underset{\sim}{\vec{p}_\Omega})$ one is not able to describe perfectly the matrix elements in this channel. This effect can also be seen by means of the phase shifts, presented in Fig. 4.11. The deviations in the matrix elements of the ${}^3\mathrm{S}_1 - {}^3\mathrm{D}_1$ channel result in deviations between the mixing angle ϵ_1 calculated with the exact SRG transformed Argonne matrix elements and the operator representation. By supplementing the ansatz Eq. (4.16) by a term similar to the tensor term Eq. (4.14), but containing the operator $S_{12}(\underset{\sim}{\vec{r}}, \underset{\sim}{\vec{p}_\Omega})$:

$$\begin{aligned}&\underset{\sim}{\mathcal{V}}^{Trp}_{1T}(\underset{\sim}{\vec{r}}, \underset{\sim}{\vec{p}}, S_{12}(\underset{\sim}{\vec{r}}, \underset{\sim}{\vec{p}_\Omega})) = \\ &\qquad \sum_{\nu}\sum_{\mu}\gamma^{Trp}_{1T,\mu\nu}\left(\frac{\kappa_\mu}{\kappa_\mu - \lambda_\nu/4}\right)^{3/2} e^{-\frac{\lambda_\nu}{4}\underset{\sim}{\vec{p}}^2}\,\frac{1}{2}\left[\underset{\sim}{p}_r \underset{\sim}{r}^3\, e^{-\frac{\underset{\sim}{\vec{r}}^2}{2(\kappa_\mu-\lambda_\nu/4)}} + \underset{\sim}{r}^3\, e^{-\frac{\underset{\sim}{\vec{r}}^2}{2(\kappa_\mu-\lambda_\nu/4)}}\underset{\sim}{p}_r\right] S_{12}(\underset{\sim}{\vec{r}}, \underset{\sim}{\vec{p}_\Omega})\, e^{-\frac{\lambda_\nu}{4}\underset{\sim}{\vec{p}}^2},\end{aligned} \tag{4.17}$$

one obtains a better description of the partial wave channels in which $S_{12}(\underset{\sim}{\vec{r}}, \underset{\sim}{\vec{p}_{\Omega}})$ acts. This results in a better agreement of the phase shifts and especially the mixing angles, shown in Fig. 4.11.

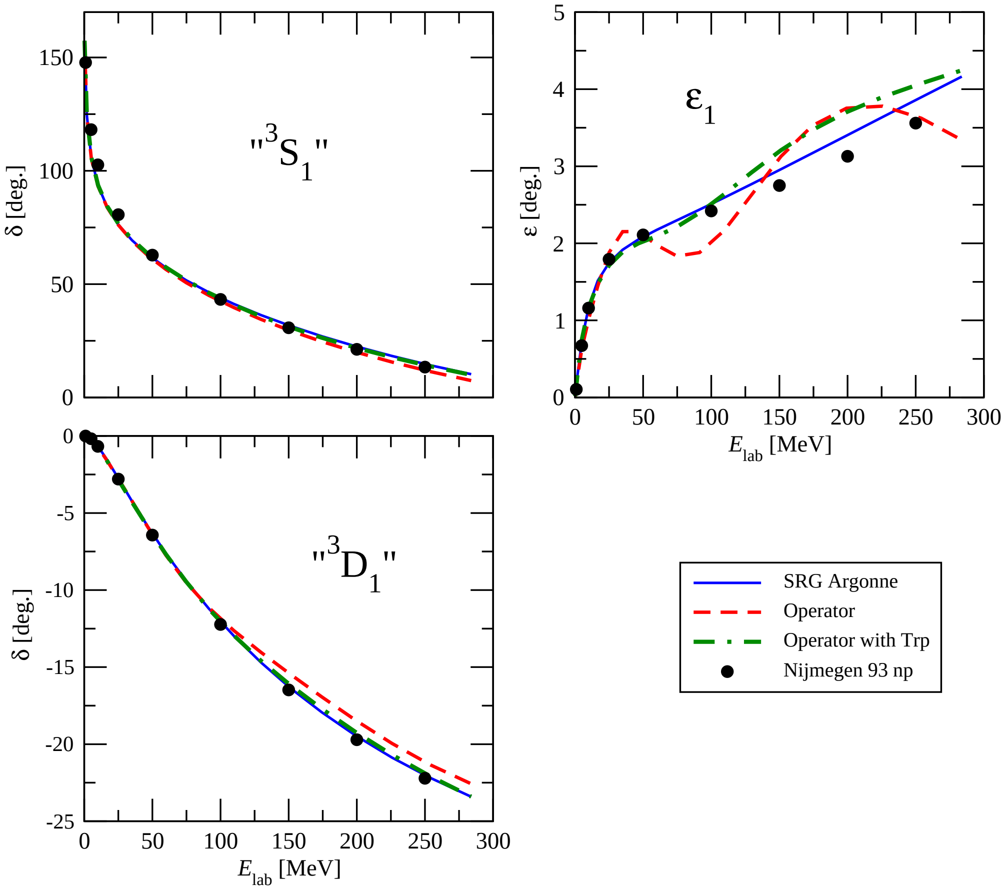

Figure 4.11: Nucleon-nucleon phase shifts of the deuteron channel ($S = 1$, $T = 0$ and $J = 1$) calculated with the SRG transformed Argonne matrix elements (blue solid line), the operator representation Eq. (4.16) (red dashed line) and the operator representation Eq. (4.16) plus the tensor term Eq. (4.17) (green dash-dotted line). The dots indicate the results of the 1993 Nijmegen partial wave analysis [47].

The inclusion of this additional operator in the ansatz however requires more parameters and the complicated analytical expression for the FMD matrix elements of this term has to be derived. Although the mixing angles calculated with the ansatz Eq. (4.16) excluding $S_{12}(\underset{\sim}{\vec{r}}, \underset{\sim}{\vec{p}_{\Omega}})$ do not agree perfectly with those of the SRG transformed Argonne potential and the experimental data, it is not completely off the results of the SRG transformed matrix elements and "oscillates" around the correct value. The deuteron properties calculated with the operator representation, which are sensitive to the same partial wave channels as the phase shifts plotted in Fig. 4.11, are not affected by the absence of the tensor term Eq. (4.17) and agree with those from the exact SRG Argonne potential. Thus, the inclusion of the tensor term Eq. (4.17) does not significantly alter these results which are already well described by the operator set in Eq. (4.16). The same can be seen for other observables of light nuclei (discussed in detail later in Sec. 4.3.3) which are not significantly sensitive to the presence of the additional tensor term Eq. (4.17). Since the tensor term only improves the description of the off-diagonal[*] partial wave matrix elements and the mixing angle but has little effect on other properties calculated with the operator representation, it seems reasonable to drop this term and work in the following with the less complicated operator form Eq. (4.16). One should however keep in mind, that more operators than those in Eq. (4.16) are needed to describe the SRG transformed potential perfectly and that in particular the deviations seen for the ϵ_1 mixing angle are a consequence of neglecting such operators in the used ansatz.

4.3.3 Two- and few-nucleon systems

In the following the operator representation of the SRG transformed Argonne potential is tested by calculating properties of the two- and selected few-nucleon systems. These are compared with the results obtained from the exact SRG transformed Argonne matrix elements.

Two-nucleon systems

The deuteron properties calculated with the matrix elements of the SRG transformed Argonne potential and the operator representation are shown in Tab. 4.7. The NN phase shifts are presented in Fig. 4.12 - 4.14.

^{2}H	E_B [MeV]	μ [μ_N]	Q [$e\,\mathrm{fm}^2$]
bare Argonne	2.23	0.847	0.270
SRG Argonne	2.23	0.847	0.267
Operator	2.23	0.860	0.265
Experiment	2.2246	0.8574	0.2860

Table 4.7: Binding energy E_B, magnetic dipole moment μ and electric quadrupole moment Q of the deuteron, calculated with the Argonne potential (bare Argonne), the exact SRG transformed Argonne matrix elements (SRG Argonne) and its operator representation Eq. (4.16) (Operator) compared to experimental data. The magnetic dipole and electric quadrupole moments are calculated by means of bare operators.

Since the SRG transformed Hamiltonian Eq. (3.25) is used to calculate the deuteron ground state, one would have in principle to use the transformed operators $\underset{\sim}{U}(s)\,\underset{\sim}{\mu}\,\underset{\sim}{U}^{\dagger}(s)$ and $\underset{\sim}{U}(s)\,\underset{\sim}{Q}\,\underset{\sim}{U}^{\dagger}(s)$ (where $\underset{\sim}{U}(s)$ is the unitary operator from Eq. (3.25)) to calculate the magnetic moment and the electric quadruple moment. In that case the results obtained with the SRG transformed Argonne potential and the bare Argonne potential are identical. Here however, the magnetic moment and electric quadrupole moment are calculated with non-transformed bare operators. By comparing the results from the SRG transformed potential by means of bare operators with those from the bare Argonne potential in Tab. 4.7, one sees that working with bare operators for the SRG transformed Argonne causes only a small deviation for the quadrupole moment while the result of the magnetic moment is not noticeably affected.

The results of the deuteron calculation agree apart from small deviations, so that one can conclude that the deuteron is well described by the operator representation. The phase shifts show that the operator representation describes the partial waves with angular momentum up to $L = 2$ also very well. However, clear deviations occur in the partial waves with higher L, for example in the F-wave (see Fig. 4.13 and 4.14). These deviations are bigger than those for the reduced UCOM potential in Sec. 4.2.3 (Fig. 4.6 and 4.7). The reason is that the set of operators in the ansatz Eq. (4.16) is not big enough to describe all partial wave channels correctly. As discussed in Sec. 4.3.2, the weight factors of the partial waves in the

---

[*] In this context “off-diagonal” is used with respect to L.

fit are chosen such, that the low angular momentum partial wave matrix elements (and therefore phase shifts) are reproduced best. In partial waves with higher L however, the phase shifts from the operator representation are significantly different from those of the partial wave matrix elements. The $^3F_3$ partial wave is the most drastic example of this behaviour.

To summarize, the used ansatz for the operator representation is able to describe the properties of two nucleon systems with L up to 2 with high accuracy. At higher angular momenta clear deviations appear, which are in some channels, like e.g. the $^3G_4$, relatively small, but in other channels noticeable large. The question if these deviations affect other nuclear properties is investigated in the next section, where the operator representation and the exact SRG transformed Argonne matrix elements are used in No Core Shell Model calculations for light nuclei and the results of the calculations are compared.

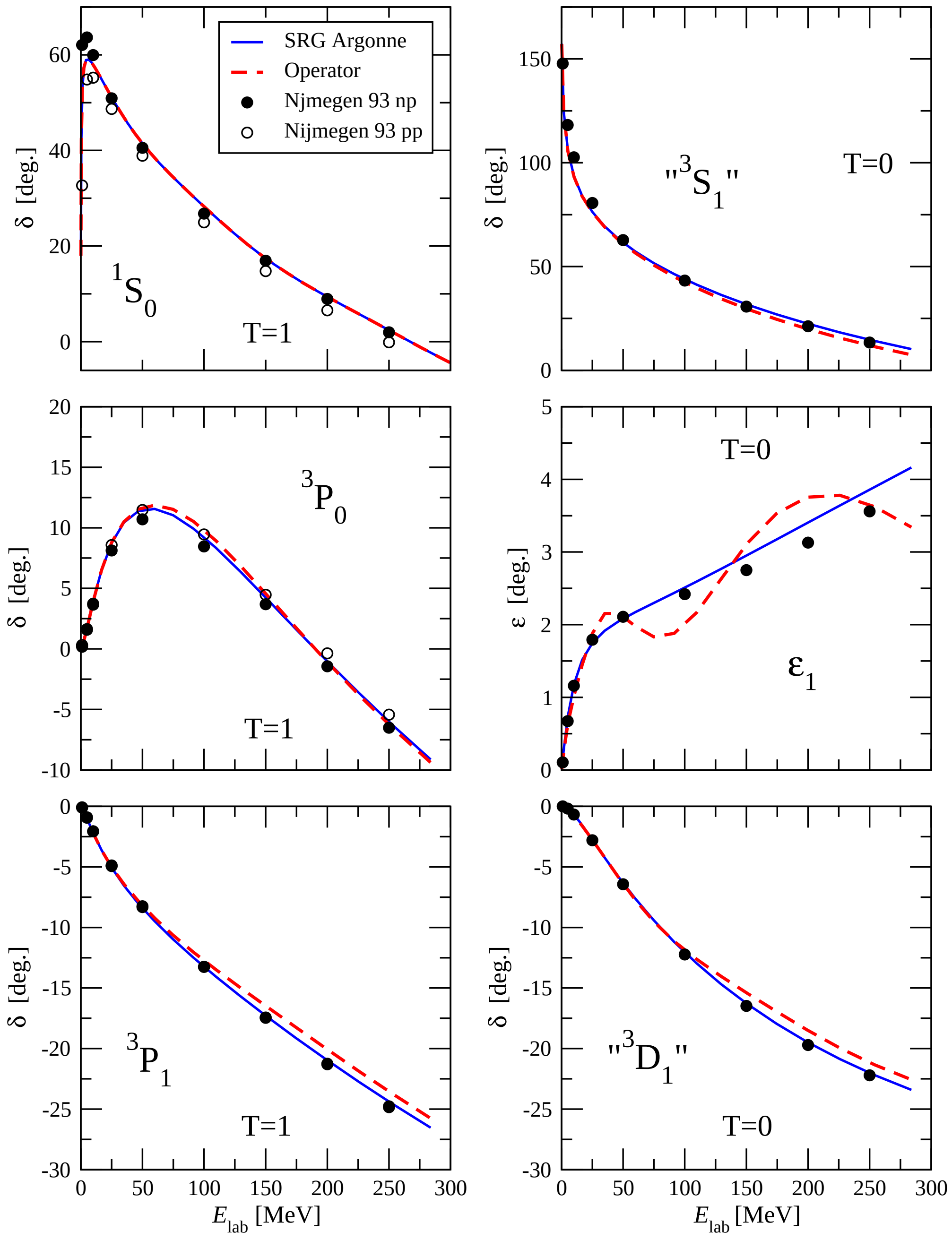

Figure 4.12: Nucleon-nucleon phase shifts for total angular momentum $J = 0$ ($T = 1$) and $J = 1$ ($T = 0$ and 1) calculated with the SRG transformed Argonne matrix elements (identical to the Argonne phase shifts) (blue solid line) and its operator representation Eq. (4.16) (red dashed line). The dots indicate the results of the 1993 Nijmegen partial wave analysis [47].

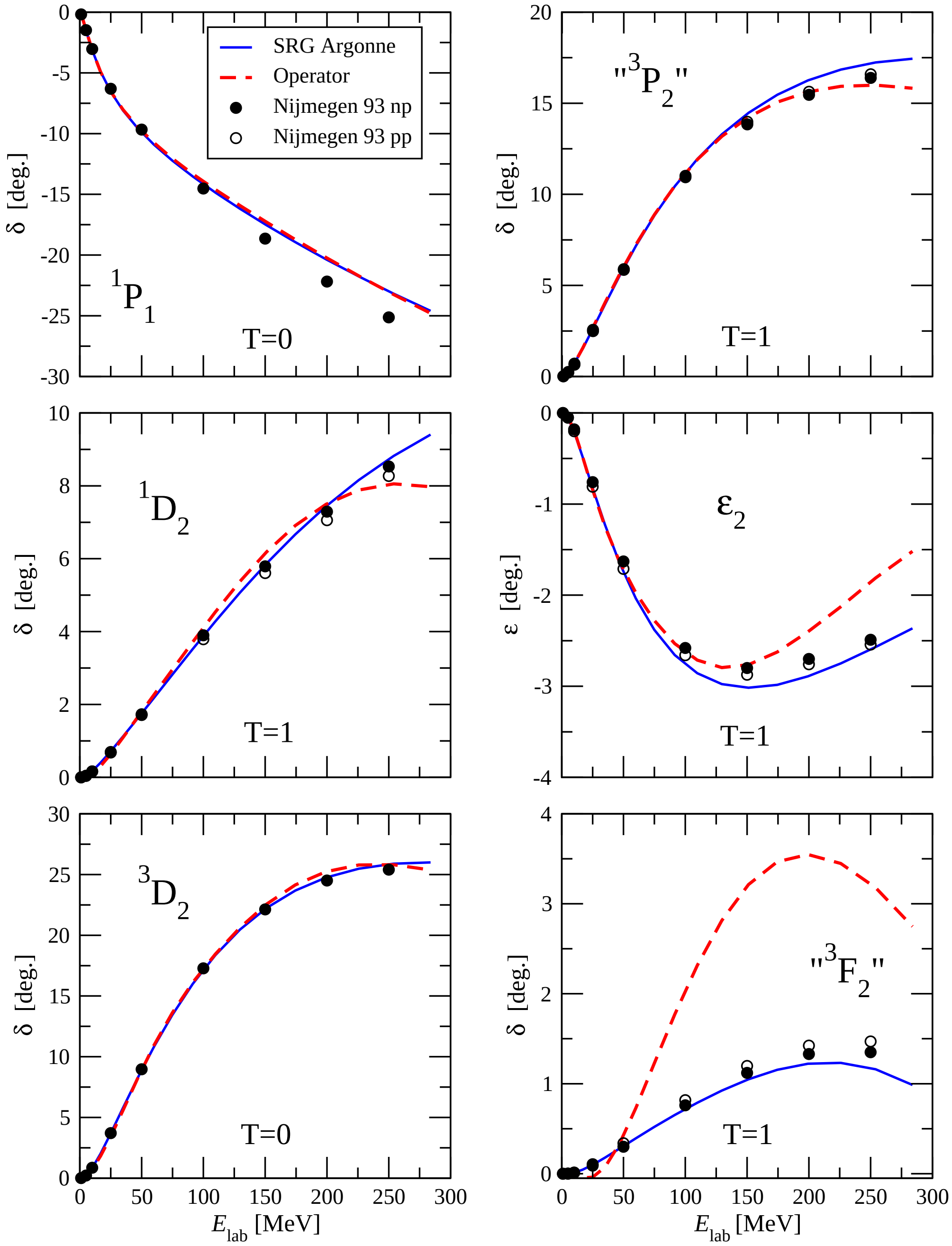

Figure 4.13: Same as Fig. 4.12, but $J = 1, 2$ and $T = 0$ and 1.

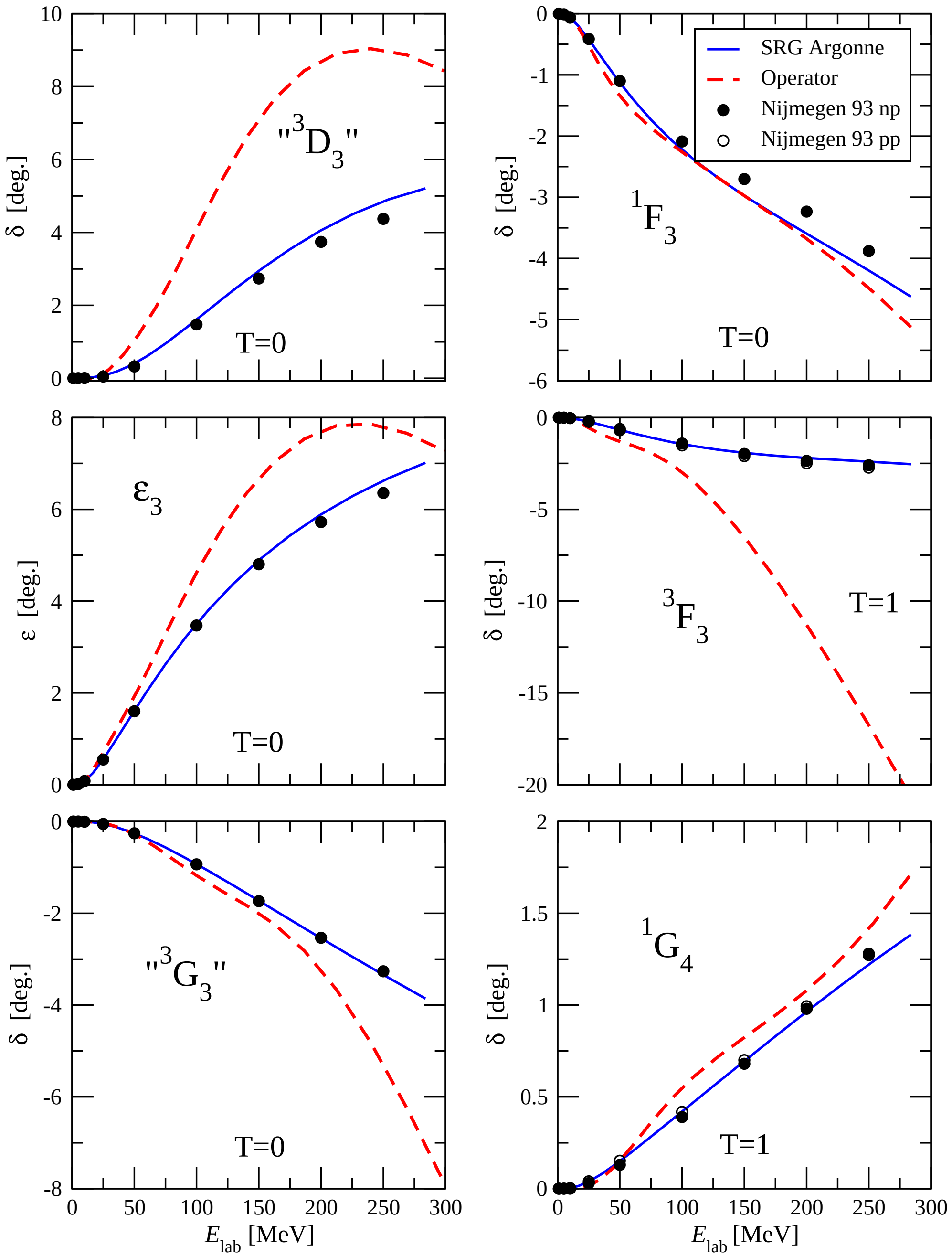

Figure 4.14: Same as Fig. 4.12, but $J = 3$, $T = 0$ and 1 and $J = 4$, $T = 1$.

No Core Shell Model

The operator representation and the matrix elements of the SRG transformed Argonne potential are used in NCSM calculations for the light nuclei discussed in Sec. 4.2.3. Tab. 4.8 shows the binding energies for nuclei with mass number A up to 7. The results of $0\hbar\omega$ calculations for stable nuclei up to ^{16}O are presented in Tab. 4.9. The radii, magnetic and electric quadrupole moments of ^{6}Li and ^{7}Li, calculated with bare operators, are listed in Tab. 4.10. The energy level spectra of these nuclei are presented in Fig. 4.15.

	^{3}H	^{3}He	^{4}He	^{6}He	^{6}Li	^{7}Li
SRG Argonne	8.35(1)	7.62(1)	28.38(1)	28.9(4)	31.8(3)	39.3(5)
Operator	8.33(1)	7.61(1)	28.41(2)	29.0(5)	31.9(3)	39.9(5)
Experiment	8.482	7.718	28.296	29.269	31.995	39.245

Table 4.8: Binding energies (in MeV) of some light nuclei calculated in the NCSM with the SRG transformed Argonne potential (SRG Argonne) and the operator representation (Operator). The error estimates are obtained from calculations with different oscillator frequencies. The results for the ^{4}He, ^{6}He, ^{6}Li and ^{7}Li energies are obtained by an extrapolation to infinite model space size.

	^{9}Be	^{10}B	^{11}B	^{12}C	^{13}C	^{14}N	^{15}N	^{16}O
SRG Argonne	17.5	20.9	31.9	47.1	50.9	61.6	78.0	93.4
Operator	18.3	21.7	31.9	46.0	52.2	63.1	79.7	95.4

Table 4.9: Binding energies (in MeV) of light nuclei calculated in the NCSM with a $0\hbar\omega$ model space for the SRG transformed Argonne matrix elements (SRG Argonne) and its operator representation (Operator).

	Nucleus	E_B [MeV]	R_p [fm]	$\mu\,[\mu_N]$	$Q\,[e\,\text{fm}^2]$
SRG Argonne	^{6}Li	31.8(3)	2.0(2)	0.839(1)	0.01(1)
Operator		31.9(3)	2.0(1)	0.840(2)	0.02(2)
Experiment		31.995	2.41(3)	0.8220	-0.0818(17)
SRG Argonne	^{7}Li	39.3(5)	2.0(1)	2.983(3)	-2.4(2)
Operator		39.5(5)	2.0(1)	2.997(2)	-2.4(3)
Experiment		39.245	2.26(2)	3.2564	-4.06(8)

Table 4.10: Properties of ^{6}Li and ^{7}Li. Binding energy E_B, point-proton radius R_p, magnetic dipole moment μ and electric quadrupole moment Q, calculated in the NCSM with the SRG transformed Argonne matrix elements and the operator representation. A model space with $12\hbar\Omega$ for ^{6}Li and $10\hbar\Omega$ for ^{7}Li and an oscillator frequency of $\hbar\Omega = 24\,\text{MeV}$ was used. The energies are obtained from an extrapolation to infinite model space size. Error estimates are from calculations with different oscillator frequencies. Experimental data from Ref. [51] and [52].

The operator representation leads to very similar results for the binding energies when compared to the exact matrix elements, with a tendency to bind the nuclei slightly more than for the exact matrix

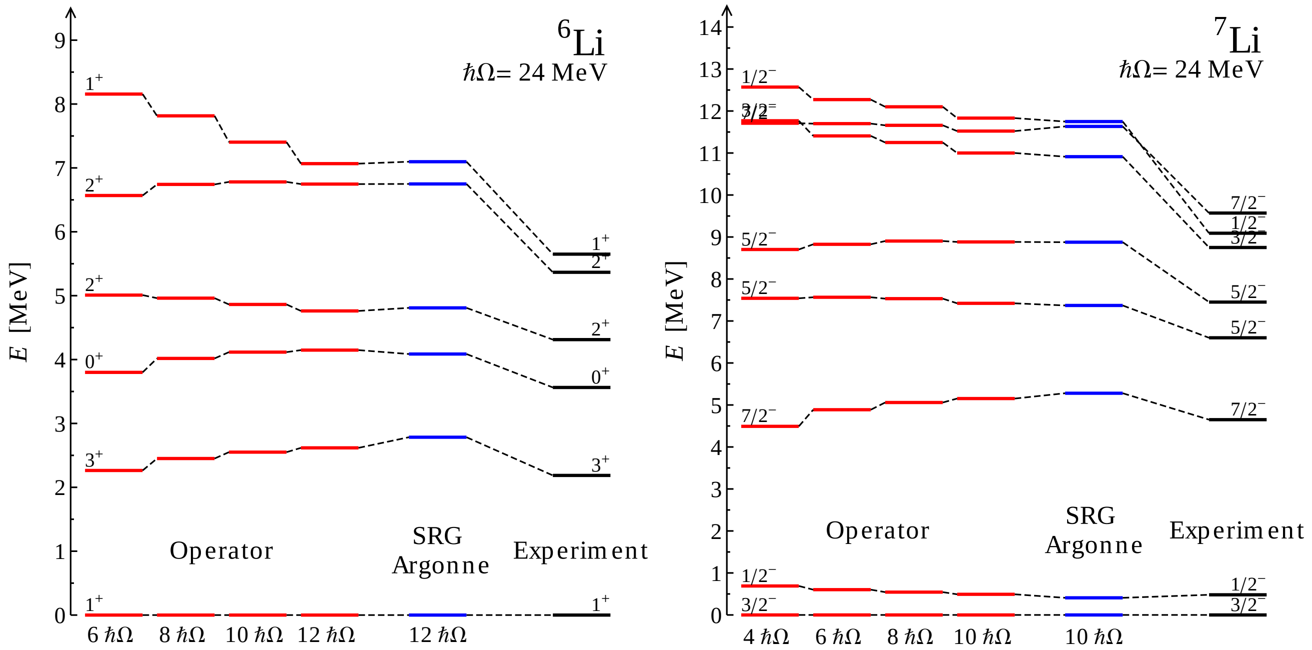

Figure 4.15: Spectra of ^{6}Li and ^{7}Li. The red lines show the results of a NCSM calculation with the operator representation for different model spaces up to $12\hbar\Omega$ for ^{6}Li and up to $10\hbar\Omega$ for ^{7}Li in comparison with the results of the SRG transformed Argonne potential (blue lines) in a $12\hbar\Omega$ and $10\hbar\Omega$ model space and the experiment [51].

elements. These deviations can be traced back to the differences between operator representation and SRG matrix elements at higher angular momenta already discussed for the two-nucleon system. Since the deviations in the binding energies are still relatively small, one can conclude that the binding energies are not very sensitive to partial wave matrix elements of the interactions with higher L and the deviations therein. As already seen for the binding energies, the results for the properties of ^{6}Li and ^{7}Li (Tab. 4.10) obtained with the operator representation and the exact SRG transformed Argonne potential agree very well. Furthermore, Fig. 4.15 shows that both potentials yield the same energy level spectra for these nuclei.

Although the operator does not succeed to describe partial wave matrix elements with $L > 3$ with high precision, it describes the properties of the discussed light nuclei almost as good as the exact matrix elements. The considered nuclear systems are obviously not sensitive to these poorly described partial wave matrix elements, so that the deviations there do not have a significant influence on the calculated properties. Thus, for the considered nuclei (and the corresponding Hilbert spaces) the operator representation provides an adequate description of the exact SRG transformed Argonne matrix elements.

One should however keep in mind, that in larger nuclei larger angular momenta occur and a correct description of high angular momentum partial waves may be important. To investigate these limitations of the derived operator representation, it would be interesting to consider in the future also larger nuclei, for example by applying importance truncation [8] or many-body perturbation theory [66].

Fermionic Molecular Dynamics

As discussed in Sec. 2.2.2, FMD calculations require an analytic expression for the FMD matrix elements of the potential. The expressions for the matrix elements of an operator representation with local radial functions and the operators of the UCOM transformed Argonne potential Eq. (3.22) have been worked out before [13, 67]. The FMD matrix elements for the ansatz Eq. (4.16) with nonlocal radial functions have been derived in this work. These matrix elements and their exact derivation are presented in detail in Appendix C.4.2. The formulas for the FMD matrix elements of the nonlocal radial functions have not been implemented in the FMD code yet. The implementation and the test of operator representations with nonlocal radial functions in the FMD code is a future task.

4.3.4 Representation of the radial functions

The method to derive an operator representation works in a momentum space representation. The fit of the ansatz with nonlocal radial functions with the parameterization Eq. (4.9) is performed in the partial wave basis in momentum space. The partial wave matrix elements in momentum space of the operator representation can be calculated by the relations Eqs. (4.13) and (4.15). These partial wave matrix elements can be used to calculate the deuteron properties, NN phase shifts and harmonic oscillator basis matrix elements for NCSM calculations. Thus, an explicit representation of the potential as a function of the relative distance is not necessary for the derivation of the operator representation and the calculation of the nuclear properties considered in this work. On the other hand one often tends to “think” rather in terms of the position space than in momentum space and a representation of the potential (or the radial functions) in terms of the relative distance of the nucleons would be desirable to gain a more intutive picture of the potential. In the following different methods to represent the nonlocal radial functions $\mathcal{V}^{P}_{ST}(\underset{\sim}{\vec{r}},\underset{\sim}{\vec{p}})$ in position space are investigated.

The local radial functions $\mathcal{V}^{P}_{ST}(\underset{\sim}{r})$ defined by Eq. (4.3) only depend on the relative distance operator and are therefore diagonal in the partial wave basis in position space defined in Appendix A.2.3:

$$\left\langle\, r(LS)J;T \,\middle|\, \mathcal{V}^{P}_{ST}(\underset{\sim}{r}) \,\middle|\, r'(LS)J;T \,\right\rangle = \sum_{\mu} \gamma^{P}_{ST,\mu}\, e^{-\frac{r^2}{2\kappa_\mu}}\, \frac{\delta(r-r')}{r^2} =: \mathcal{V}^{P}_{ST}(r)\frac{\delta(r-r')}{r^2}. \tag{4.18}$$

Thus, one can plot the function $\mathcal{V}^{P}_{ST}(r)$, which is just the matrix element of (the operator) $\mathcal{V}^{P}_{ST}(\underset{\sim}{r})$ in the partial wave basis in position space without the factor $\frac{\delta(r-r')}{r^2}$. These plots are presented in Appendix C.3 for the radial functions of the reduced UCOM potential and compared to those of the full UCOM potential.

The nonlocal radial functions $\mathcal{V}^{P}_{ST}(\underset{\sim}{\vec{r}},\underset{\sim}{\vec{p}})$ additionally depend on the relative momentum operator $\underset{\sim}{\vec{p}}$. Consequently, the matrix elements $\left\langle\, r(LS)J;T \,\middle|\, \mathcal{V}^{P}_{ST}(\underset{\sim}{\vec{r}},\underset{\sim}{\vec{p}}) \,\middle|\, r'(LS)J;T \,\right\rangle$ are not simply diagonal. A representation in terms of such matrix elements depends on the radial quantum numbers r and r' (and the angular momentum L). For the parameterization of the nonlocal radial functions given in Eq. (4.9) one finds for the matrix elements the analytic expression

$$\begin{aligned}\left\langle\, r(LS)J;T \,\middle|\, \mathcal{V}^{P}_{ST}(\underset{\sim}{\vec{r}},\underset{\sim}{\vec{p}}) \,\middle|\, r'(LS)J;T \,\right\rangle = & \sum_{\mu} \gamma^{P}_{ST,\mu\nu_0}\, e^{-\frac{r^2}{2\kappa_\mu}}\, \frac{\delta(r-r')}{r^2} \\ & + 4\pi i^{L} \sum_{\substack{\nu \\ \nu\neq\nu_0}} \sum_{\mu} \gamma^{P}_{ST,\mu\nu}\, e^{-\frac{\kappa_\mu+\lambda_\nu/4}{2\kappa_\mu\lambda_\nu}(r^2+r'^2)}\, j_L\!\left(2i\frac{\kappa_\mu-\lambda_\nu/4}{2\kappa_\mu\lambda_\nu} r r'\right), \end{aligned} \tag{4.19}$$

where ν_0 is the index for which $\lambda_{\nu_0} = 0$. The r.h.s of Eq. (4.19) consists of two parts. The first term originates from the local part ($\lambda_{\nu_0} = 0$) of $\mathcal{V}^{P}_{ST}(\underset{\sim}{\vec{r}},\underset{\sim}{\vec{p}})$ and is identical to the expression Eq. (4.18):

$$\mathcal{V}^{P,\mathrm{loc}}_{ST}(r) = \sum_{\mu} \gamma^{P}_{ST,\mu\nu_0}\, e^{-\frac{r^2}{2\kappa_\mu}}. \tag{4.20a}$$

The second term contains the nonlocal contributions:

$$\mathcal{V}^{P,\,\text{nonloc}}_{LST}(r,r') = 4\pi i^L \sum_{\substack{\nu\\ \nu\neq\nu_0}}\sum_{\mu}\gamma^P_{ST,\mu\nu}\, e^{-\frac{\kappa_\mu+\lambda_\nu/4}{2\kappa_\mu\lambda_\nu}(r^2+r'^2)}\, j_L\left(2i\frac{\kappa_\mu-\lambda_\nu/4}{2\kappa_\mu\lambda_\nu}\, r r'\right). \tag{4.20b}$$

Unfortunately expression Eq. (4.19) is difficult to plot since the first term contains a delta function. The delta function cannot be plotted and "dividing" Eq. (4.19) by $\delta(r-r')$, as it has been done for the local case, is not possible since the delta function is not present in the nonlocal term. The only possibility is to plot the local and the nonlocal part separately. As an example, Fig. 4.16 shows the local part $\mathcal{V}^{C,\,\text{loc}}_{01}(r)$ and the nonlocal part $\mathcal{V}^{C,\,\text{nonloc}}_{001}(r,r')$ (for $L=0$) of the radial function $\mathcal{V}^{C}_{01}(\underset{\sim}{\vec{r}},\underset{\sim}{\vec{p}})$ from the operator representation of the SRG transformed Argonne matrix elements. The local parts of all radial functions in this operator representation are presented in Appendix C.4.1 (Figs. C.11 - C.13). Another way to demonstrate the nonlocal radial functions is the Wigner representation $\mathfrak{V}^P_{ST}(\vec{r},\vec{p})$ [68], defined by

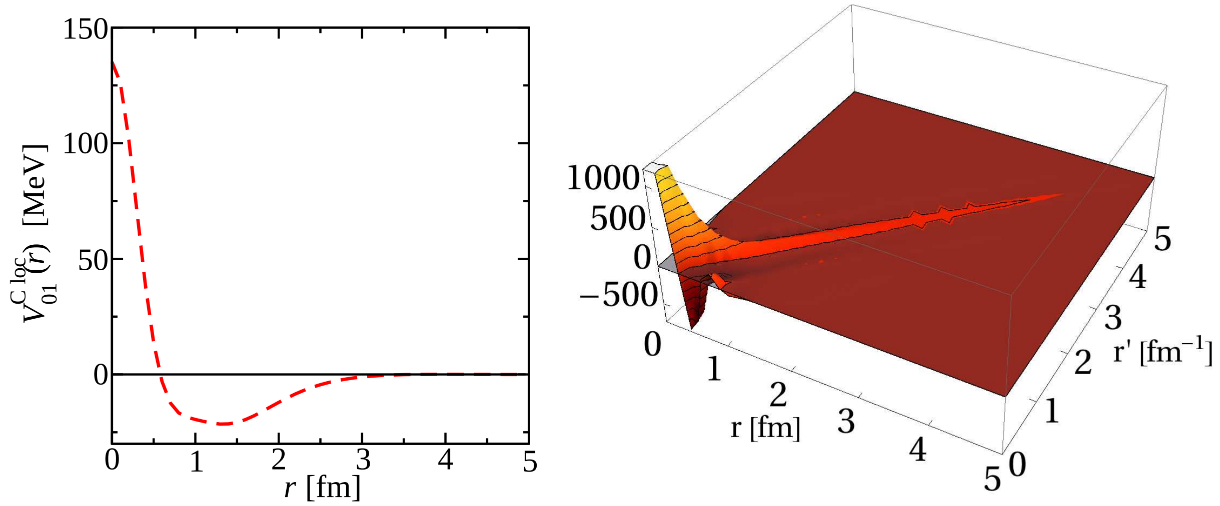

Figure 4.16: The local part $\mathcal{V}^{c,\,\text{loc}}_{01}(r)$ (left) and the nonlocal part $\mathcal{V}^{C,\,\text{nonloc}}_{01}(r,r')$ (right, in units of MeV fm^{-3}) of the central radial function of the SRG Argonne operator representation with $S=0$ and $T=1$. The nonlocal part is shown for $L=0$.

$$\mathfrak{V}^P_{ST}(\vec{r},\vec{p}) = \int_{-\infty}^{\infty} d^3y\, \left\langle \vec{r}-\vec{y}/2 \right| \mathcal{V}^P_{ST}(\underset{\sim}{\vec{r}},\underset{\sim}{\vec{p}}) \left| \vec{r}+\vec{y}/2 \right\rangle e^{i\vec{p}\vec{y}}. \tag{4.21}$$

The Wigner representation is just the classical way (where $\vec{r}$ and $\vec{p}$ commute) one would write the hermitian operator $\mathcal{V}^P_{ST}(\underset{\sim}{\vec{r}},\underset{\sim}{\vec{p}})$. For the parameterization Eq. (4.9) one obtains the expression

$$\mathfrak{V}^P_{ST}(\vec{r},\vec{p}) = \sum_{\nu}\sum_{\mu}\gamma^P_{ST,\mu\nu}\exp\left\{-\left(\frac{1}{2\kappa_\mu}\vec{r}^{\,2}+\frac{\lambda_\nu}{2}\vec{p}^{\,2}\right)\right\}. \tag{4.22}$$

Fig. 4.17 shows the Wigner representation for the central part of the bare Argonne, the UCOM transformed Argonne potential and the operator representation of the SRG transformed Argonne matrix elements. Since the Argonne potential is purely local, the Wigner representation shows no dependence on the relative momentum and is just constant as a function of p. The UCOM transformed Argonne potential exhibits a quadratic momentum dependence leading to a p^2-dependence in the Wigner representation. The nonlocal radial function $\mathcal{V}^{C}_{01}(\underset{\sim}{\vec{r}},\underset{\sim}{\vec{p}})$ of the operator representation for the SRG transformed Argonne matrix elements has a more complicated momentum structure and therefore yields a Wigner representation with a more complex p dependence as well.

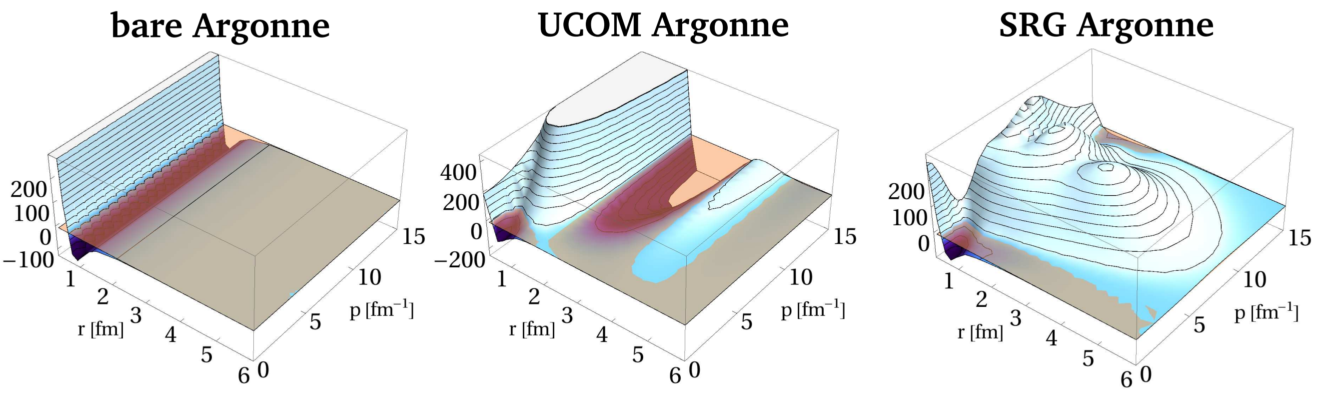

Figure 4.17: The Wigner representation $\mathfrak{V}^{C}_{01}(\vec{r},\vec{p})$ (in MeV) with $S=0$ and $T=1$. Left: For the central part $V^{C}_{01}(r)$ of the bare Argonne potential Eq. (3.14). Middle: For the central part (including momentum dependent terms) $v^{C}_{01}(r)+\frac{1}{2}\left(\vec{p}^{2}\,v^{p2}_{01}(r)+v^{p2}_{01}(r)\,\vec{p}^{2}\right)$ of the UCOM transformed Argonne potential potential Eq. (3.22). Right: For the central part $\mathcal{V}^{C}_{01}(\vec{r},\vec{p})$ of the operator representation of the SRG transformed Argonne matrix elements Eq. (4.16).

The Wigner representation has the advantage, that the contributions from the local and the nonlocal part of $\mathcal{V}^{P}_{ST}(\underset{\sim}{\vec{r}},\underset{\sim}{\vec{p}})$ are represented in an intuitive way. A further task is to compute the Wigner representation also from the interaction matrix elements in order to compare it with the operator representation.

A different way to visualize a "local" part is proposed in Ref. [69]. A so called "local projection" $\mathcal{L}$ is performed which is defined by

$$\mathcal{L}\left[\left\langle\, r(LS)J;T\,\middle|\mathcal{V}^{P}_{ST}(\underset{\sim}{\vec{r}},\underset{\sim}{\vec{p}})\middle|\,r'(LS)J;T\,\right\rangle\right]=\overline{\mathcal{V}}^{P}_{LSJT}(r)\,\frac{\delta(r-r')}{r^{2}},\tag{4.23a}$$

where

$$\overline{\mathcal{V}}^{P}_{LSJT}(r)=\int_{0}^{\infty}dr'r'^{2}\left\langle\, r(LS)J;T\,\middle|\mathcal{V}^{P}_{ST}(\underset{\sim}{\vec{r}},\underset{\sim}{\vec{p}})\middle|\,r'(LS)J;T\,\right\rangle.\tag{4.23b}$$

The local projection maps the matrix element $\left\langle\, r(LS)J;T\,\middle|\mathcal{V}^{P}_{ST}(\underset{\sim}{\vec{r}},\underset{\sim}{\vec{p}})\middle|\,r'(LS)J;T\,\right\rangle$, which depends on the quantum numbers r and r' on the function $\overline{\mathcal{V}}^{P}_{LSJT}(r)$ by integrating over r'. For local radial operators $\mathcal{V}^{P}_{ST}(\underset{\sim}{r})$ one finds that $\overline{\mathcal{V}}^{P}_{LSJT}(r)=\mathcal{V}^{P}_{ST}(r)$. For nonlocal operators $\mathcal{V}^{P}_{ST}(\underset{\sim}{\vec{r}},\underset{\sim}{\vec{p}})$, $\overline{\mathcal{V}}^{P}_{LSJT}(r)$ can be interpreted as the local potential seen by a pair of nucleons with relative momentum zero. One can, in analogy to Eq. (4.23b), also calculate the local projection from the matrix element representation of the considered potential $\underset{\sim}{V}$:

$$\overline{V}_{LSJT}(r)=\int_{0}^{\infty}dr'r'^{2}\left\langle\, r(LS)J;T\,\middle|\underset{\sim}{V}\middle|\,r'(LS)J;T\,\right\rangle.\tag{4.24}$$

The function $\overline{V}_{LSJT}(r)$ can be compared with the corresponding linear combination of the local projection $\overline{\mathcal{V}}^{P}_{LSJT}(r)$ of the nonlocal radial functions $\mathcal{V}^{P}_{ST}(\underset{\sim}{\vec{r}},\underset{\sim}{\vec{p}})$ from the operator representation. For example in the

$^{1}S_{0}$ channel, only the central part contributes and one has to compare $\overline{V}_{0001}(r)$ with $\overline{\mathscr{V}}^{C}_{0001}(r)$. In the $^{1}D_{2}$ channel one has to compare the local projection $\overline{V}_{2021}(r)$ originating from the matrix elements with $\overline{\mathscr{V}}^{C}_{2021}(r)+6\overline{\mathscr{V}}^{L2}_{2021}(r)$ from the operator representation. Fig. 4.18 shows the local projections calculated from the matrix elements and the operator representation for selected partial wave channels. This representation allows to investigate the agreement between operator and matrix element representation. The agreement is remarkable. Deviations only occur below 0.5 fm, a length scale that is not resolved in low energy nuclear physics.

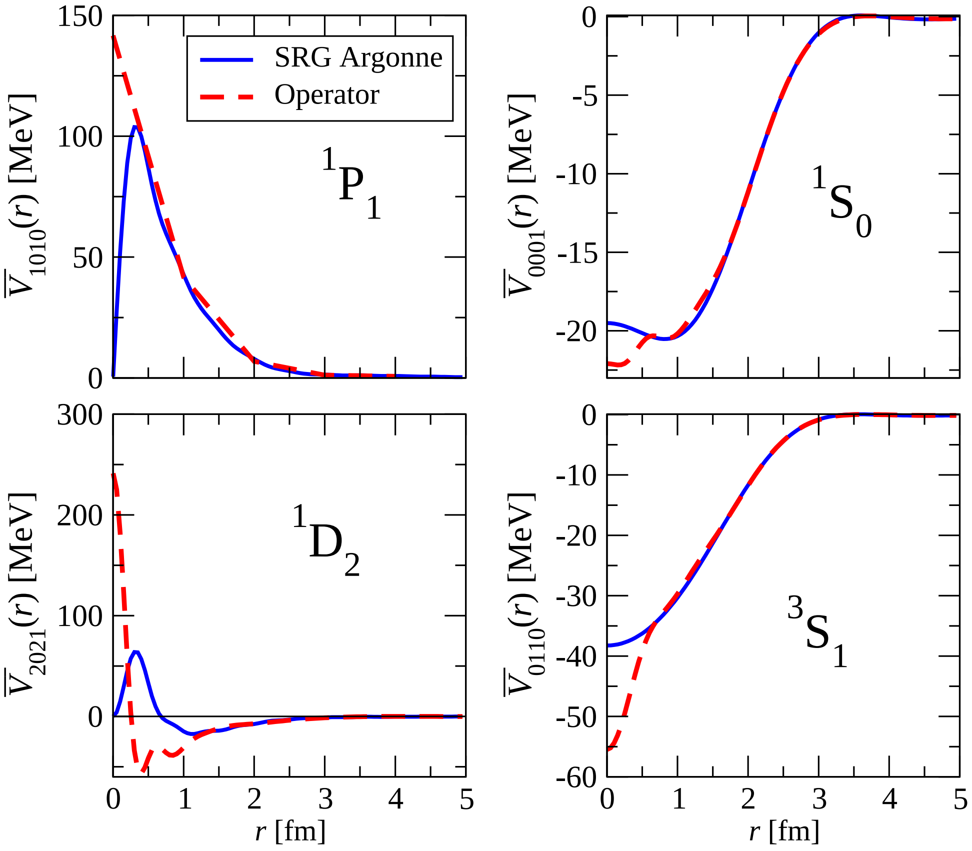

Figure 4.18: Local projections of the SRG transformed Argonne potential obtained from the partial wave matrix elements (blue solid line) and the operator representation (red dashed line) for selected partial wave channels.

Future investigations have to show in how far an intuitively interpretable representation, like the Wigner representation, can help to avoid unphysical peculiarities of the fitting procedure or even undesired features of an SRG evolution.

4.3.5 Closing remarks on the SRG transformed Argonne operator representation

The derived operator representation for the SRG transformed Argonne matrix elements contains the set of operators of the Argonne potential Eq. (3.14), but with nonlocal radial functions Eq. (4.9) to describe the induced complex momentum dependence.

The operator representation, although containing only a small set of operators, describes adequately the properties of the SRG transformed Argonne matrix elements for two-nucleon systems with angular momentum L up to 2. The properties for light nuclei are also very similar for the operator and the matrix element representation. The set of operators is however too limited to describe correctly the SRG transformed Argonne matrix elements in all partial waves. This leads to deviations of the matrix elements and phase shifts for $L \geq 3$. As long as a considered nuclear many-body system is not sensitive to these only poorly described partial waves, as for the nuclei investigated in this work, the obtained operator representation can be used to replace the exact matrix element representation in the many-body calculation. For larger nuclei which contain partial waves with $L \geq 3$ however, the operator representation might not be an adequate representation anymore. In the future, systems with more nucleons should be investigated to find out if the operator representation is still suited.

Another important project is the implementation of the nonlocal radial functions in the FMD code to be finally able to use the extracted operator representation in FMD calculations. The groundwork is done by deriving the analytic expressions for the FMD matrix elements of the terms present in the operator representation Eq. (4.16). Implemented in the FMD code, these expressions (in combination with the presented operator representation) will provide FMD access to the SRG transformed Argonne potential.

4.4 Operator representation of the JISP16 potential

In this section the method described in Sec. 4.1 is applied to derive an operator representation for the JISP16 interaction which is represented as a matrix in harmonic oscillator eigenstates. As discussed in Sec. 3.3 one expects a strong and complicated momentum dependence.

4.4.1 Ansatz for the operator representation

To represent the expected high degree of nonlocality, ansatz Eq. (4.1) containing nonlocal radial functions $\mathscr{V}^{P}_{ST}(\underset{\sim}{\vec{r}},\underset{\sim}{\vec{p}})$ is used. The radial functions are parameterized the same way as for the SRG transformed Argonne potential, described by Eq. (4.9). The strong momentum dependence of the JISP16 potential requires additional parameters λ in the nonlocal radial function in order to describe the partial wave matrix elements. By using the set of parameters:

$$\kappa \;=\; \{0.1, 0.2, 0.4, \cdots, 6.4\}\mathrm{fm}^2$$

and

$$\lambda \;=\; \left\{0, \frac{1}{16}, \frac{1}{8}, \frac{1}{4}, \frac{1}{2}, 1, 2\right\}\mathrm{fm}^2,$$

one succeeds in describing adequately the momentum dependence of the JISP16 interaction. Fig. 4.19 shows as an example the matrix elements of the $^1\mathrm{S}_0$ channel of the JISP16 interaction and the results from the fitted operator representation using the nonlocal radial functions given in Eq. (4.9) with the above set of parameters κ and λ. The fit describes the matrix elements of the JISP16 interaction quite accurately. By adding even more parameters λ to the ansatz, the description can be improved. But since the used set of parameters already yields an accurate description of the phase shifts (see Fig. 4.21), the ansatz is sufficient to describe a given partial wave channel of the JISP16 potential.

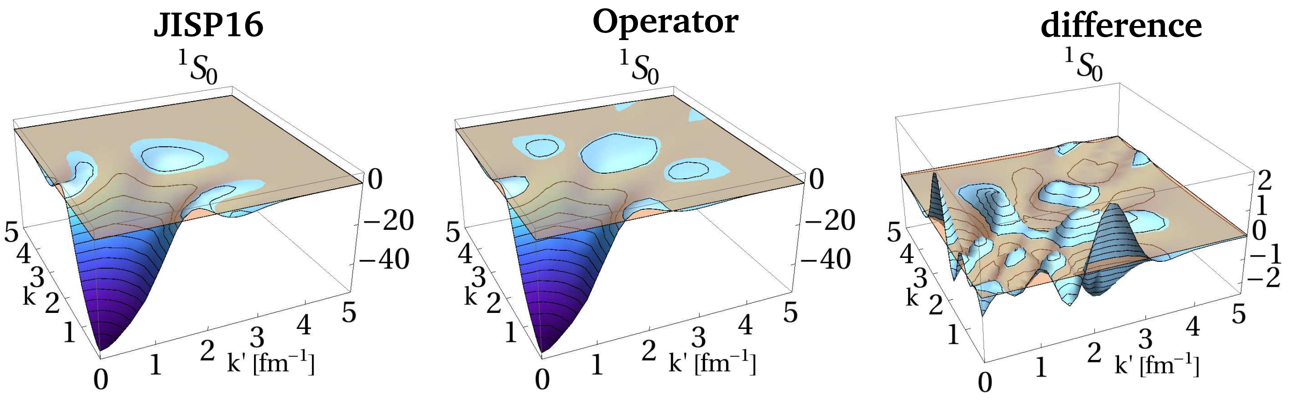

Figure 4.19: Matrix elements $\left\langle k(00)0;1 \middle| V_{\mathrm{JISP16}} \middle| k'(00)0;1 \right\rangle$ (in MeVfm^3) of the JISP16 interaction (left), matrix elements $\left\langle k(00)0;1 \middle| \mathscr{V}(\vec{r},\vec{p}) \middle| k'(00)0;1 \right\rangle$ obtained by a fit using the ansatz for the nonlocal radial functions Eq. (4.9) (middle) and the difference between those (right) in the $^1\mathrm{S}_0$ channel. The reddish plane marks the zero-plane.

In the following, a set of operators for the description of all partial wave channels will be devised.

4.4.2 Choice of the operators

For the SRG transformed Argonne potential at least the operator form of the initial Argonne potential is known and can be used as a guideline to for the set of operators in the ansatz. For the JISP16 potential there is no such hint on a possible operator structure. It is constructed by the J-matrix inverse scattering method and unitary transformations acting independently in each partial wave. Thus, an operator representation in terms of projection operators on the different partial waves would be the most promising choice. As discussed in Sec. 4.3.2, such an ansatz requires many parameters and is hard to employ in FMD calculations. Therefore, an ansatz with the set of operators used for the SRG transformed Argonne potential is also taken for the JISP16 potential:

$$\begin{aligned}\underset{\sim}{V}^{\mathrm{JISP16}}_{\mathrm{ansatz}} &= \sum_{ST} \mathcal{V}^{C}_{ST}(\underset{\sim}{\vec{r}},\underset{\sim}{\vec{p}})\,\underset{\sim}{\Pi}_{ST} \\ &+ \sum_{ST} \mathcal{V}^{L2}_{ST}(\underset{\sim}{\vec{r}},\underset{\sim}{\vec{p}})\underset{\sim}{\vec{L}}^{2}\,\underset{\sim}{\Pi}_{ST} \\ &+ \sum_{T} \mathcal{V}^{LS}_{1T}(\underset{\sim}{\vec{r}},\underset{\sim}{\vec{p}})(\underset{\sim}{\vec{L}}\cdot\underset{\sim}{\vec{S}})\,\underset{\sim}{\Pi}_{1T} \\ &+ \sum_{T} \underset{\sim}{\mathcal{V}}^{T}_{1T}(\underset{\sim}{\vec{r}},\underset{\sim}{\vec{p}},\underset{\sim}{S}_{12})\,\underset{\sim}{\Pi}_{1T} \\ &+ \sum_{T} \mathcal{V}^{Tll}_{1T}(\underset{\sim}{\vec{r}},\underset{\sim}{\vec{p}})S_{12}(\underset{\sim}{\vec{L}},\underset{\sim}{\vec{L}})\,\underset{\sim}{\Pi}_{1T}. \end{aligned} \tag{4.25}$$

The partial wave matrix elements of this ansatz are fitted to the corresponding matrix elements of the JISP16 interaction to obtain the operator representation. As for the SRG transformed Argonne potential, the partial waves are weighted differently to obtain optimal results for the lowest angular momenta L. The weights used in this fit can be found in Appendix C.2.

It turns out that the fit is only able to describe the matrix elements of the partial waves with the lowest angular momenta L. For higher L large deviations between the partial wave matrix elements of the operator representation and the JISP16 interaction matrix elements occur. This is shown in Figs. 4.19 and 4.20. While the S-wave matrix elements are reproduced well and in the D-wave at least fairly well, the matrix elements of the operator representation are much too large in the $^1\mathrm{G}_4$ channel.

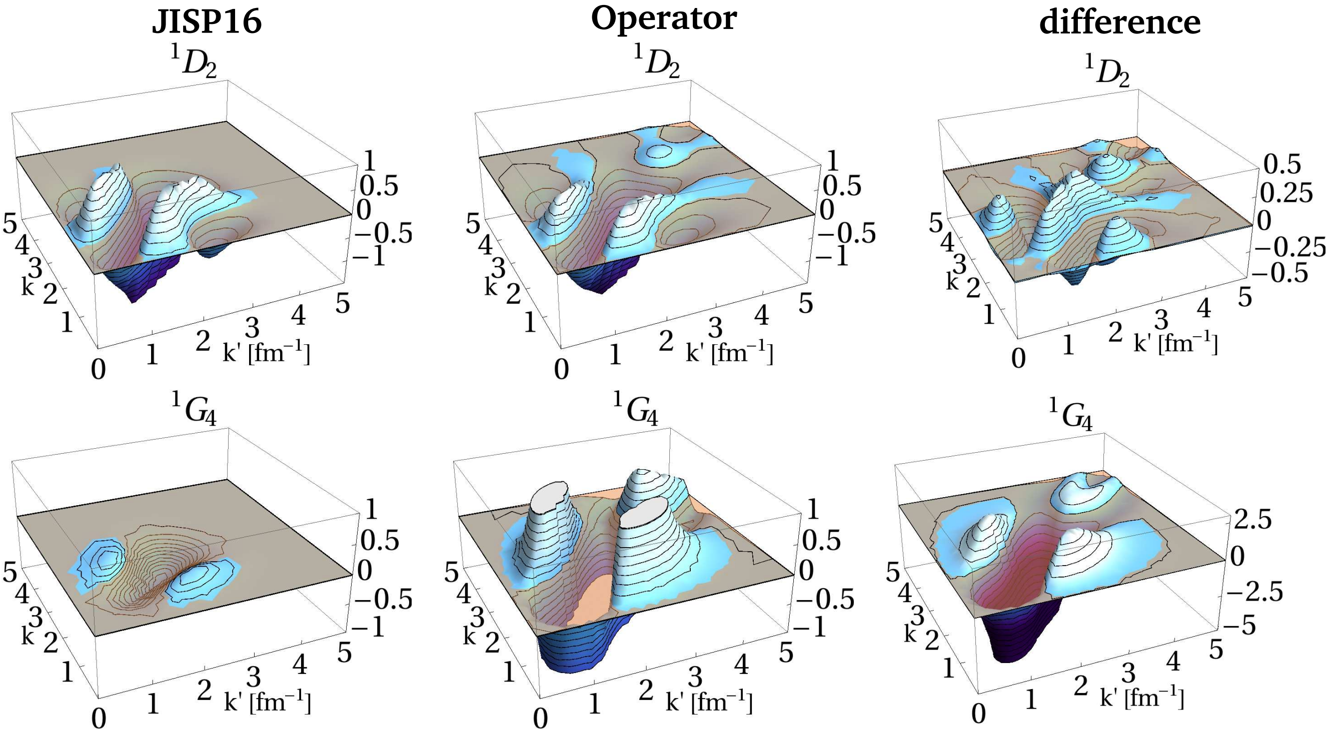

Figure 4.20: Same as Fig. 4.19, but for the $^1\mathrm{D}_2$ and $^1\mathrm{G}_4$ channel.

To study the influence of these deviations and to evaluate the quality of the obtained operator representation, the following subsections investigate the operator representation in two- and few-nucleon calculations.

4.4.3 Two- and few-nucleon systems

Two-nucleon systems

The two-nucleon properties calculated with the matrix elements of the JISP16 interaction and the operator representation are compared. The calculated phase shifts are presented in Fig. 4.21 to 4.23. The calculated deuteron properties can be found in Tab. 4.11.

^{2}H	E_B [MeV]	μ [μ_N]	Q [e fm^2]
JISP16	2.22	0.857	0.279
Operator	2.22	0.857	0.289
Experiment	2.2246	0.8574	0.2860

Table 4.11: Binding energy E_B, magnetic dipole moment μ and electric quadrupole moment Q of the deuteron, calculated with the JISP16 interaction (JISP16) and the operator representation (Operator) and compared to experimental data.

The operator representation describes the deuteron properties as well as the exact JISP16 potential. The phase shifts of the JISP16 interaction and the operator representation agree to some degree up to $L = 2$, although less precise than for the reduced UCOM and SRG transformed Argonne potential. For higher L the operator representation yields completely different phase shifts than the JISP16 interaction which by construction reproduces the experimental values. The reduced UCOM potential and the operator representation of the SRG transformed Argonne potential do also not succeed in describing all partial wave matrix elements and phase shifts for $L \geq 3$ correctly and deviations appear in the F and G wave (see Fig. 4.6 - 4.7 and Fig. 4.13 - 4.14), but these deviations tend to be small or at least of the same order of magnitude as the correct value of the phase shifts. For the operator representation of the JISP16 interaction however one sees large deviations, especially when the phase shifts are small, like in the "^{3}F$_2$", ^{3}F$_3$, "^{3}G$_2$" and ^{1}G$_4$ partial wave. The fit seems to create unphysical pecularities by putting a big weight factor on $L = 0$, 1 and 2, which in turn implies an insufficient or not adequate ansatz for the operator form.

In the following, the operator representation is applied in NCSM calculations to investigate how the wrong behaviour of the operator representation affects the properties of light nuclei.

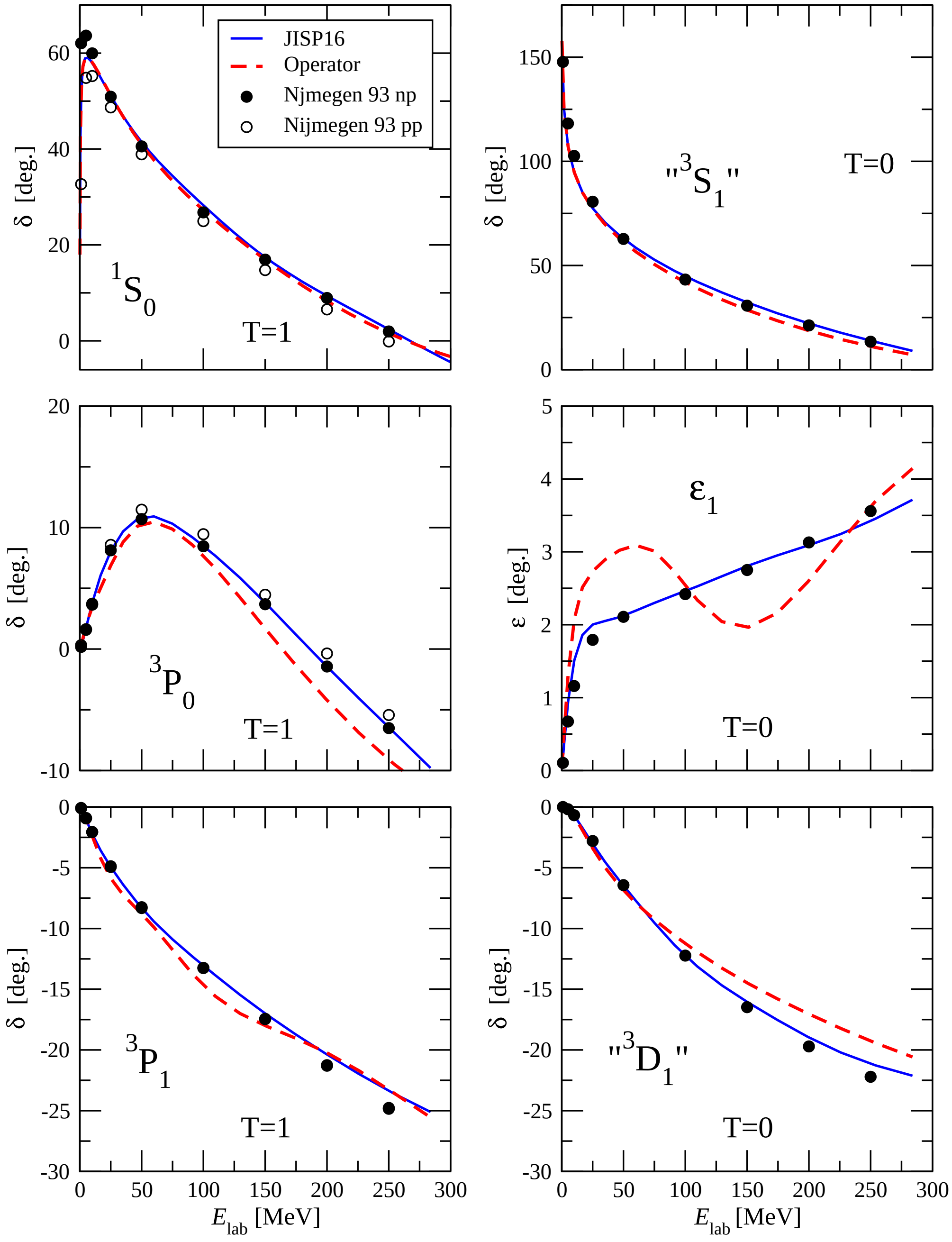

Figure 4.21: Nucleon-nucleon phase shifts for total angular momentum $J = 0$ ($T = 1$) and $J = 1$ ($T = 0$ and 1) calculated with the JISP16 interaction matrix elements (blue solid line) and the fitted operator representation (red dashed line). The dots indicate the results of the 1993 Nijmegen partial wave analysis [47].

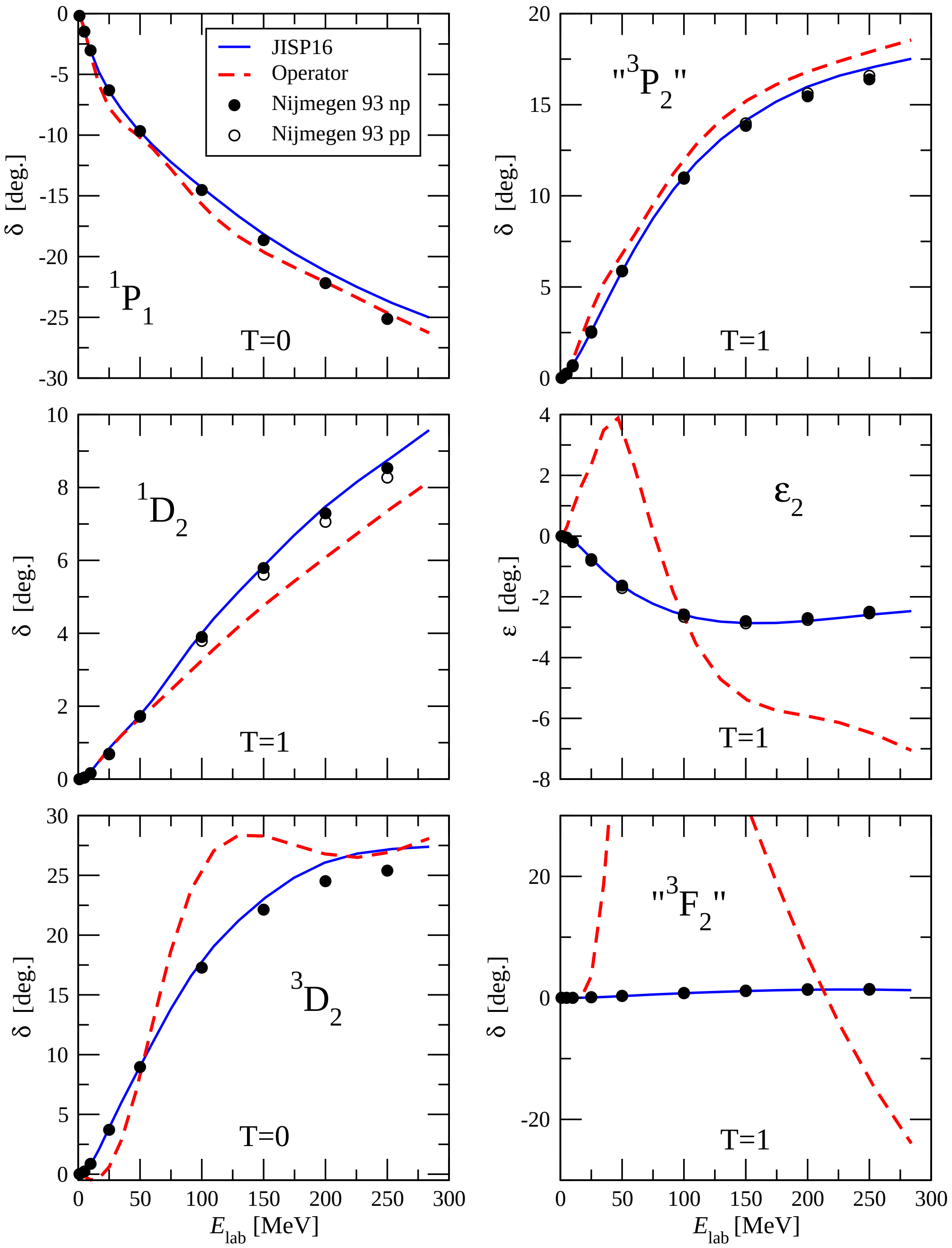

Figure 4.22: Same as Fig. 4.12, but $J = 1, 2$ and $T = 0$ and 1.

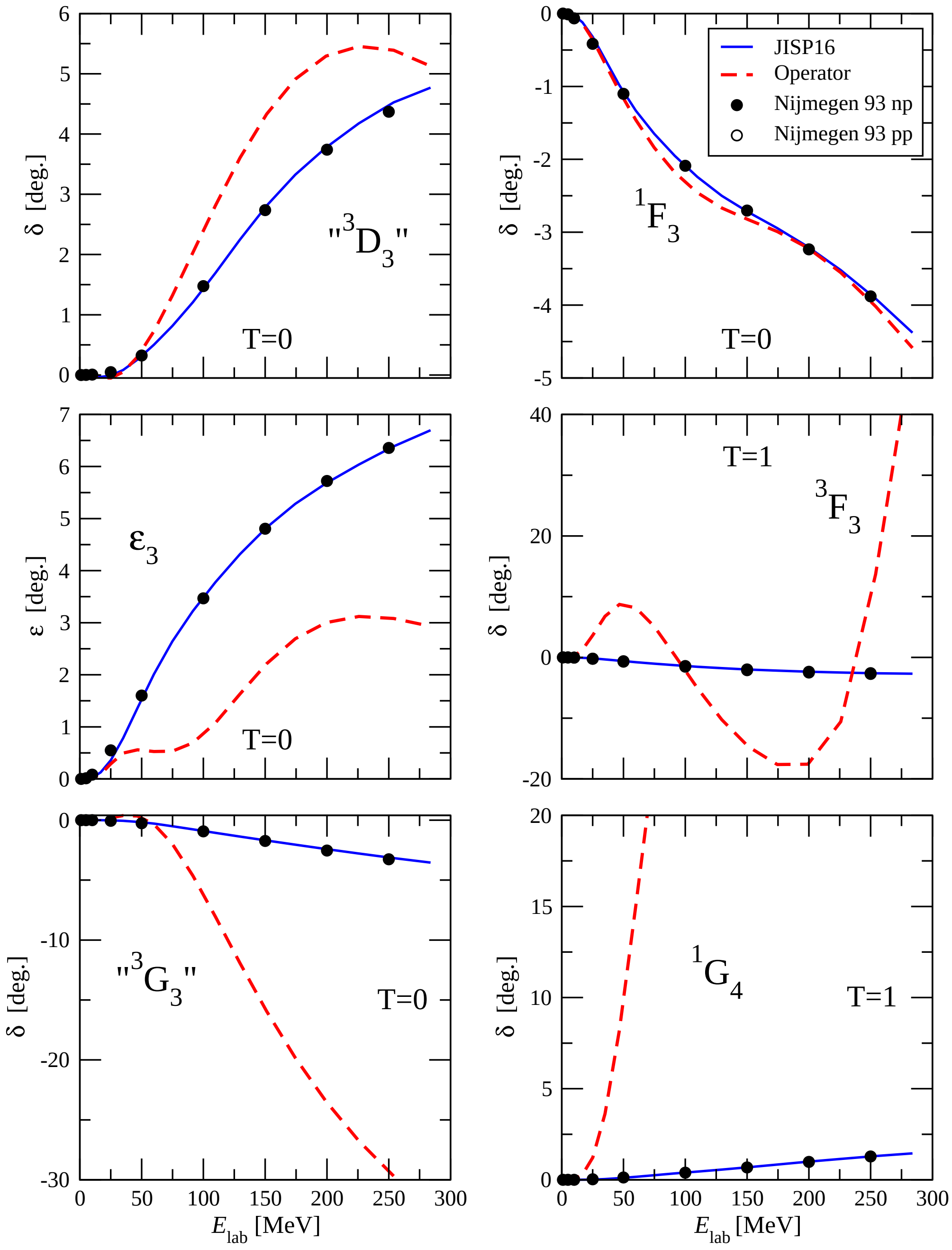

Figure 4.23: Same as Fig. 4.12, but $J = 3$, $T = 0$ and 1 and $J = 4$, $T = 1$.

No Core Shell Model

The NCSM is used to calculate the properties of selected light nuclei. The results for the binding energies of some light nuclei calculated with the JISP16 interaction matrix elements and the operator representation are presented in Tab. 4.12. The ground-state properties of ^{6}Li and ^{7}Li can be found in Tab. 4.13. Fig. 4.15 shows the energy levels of these nuclei.

	^{3}H	^{3}He	^{4}He	^{6}He	^{6}Li	^{7}Li
JISP16	8.37(1)	7.66(1)	28.29(1)	28.8(2)	31.4(2)	38.6(2)
Operator	8.40(1)	7.70(1)	28.48(1)	29.5(2)	32.4(2)	40.0(2)
Experiment	8.482	7.718	28.296	29.269	31.995	39.245

Table 4.12: Binding energies (in MeV) of some light nuclei calculated in the NCSM with the JISP16 interaction matrix elements (JISP16) and its operator representation (Operator). The results for the ^{4}He, ^{6}He, ^{6}Li and ^{7}Li energies are obtained by an extrapolation to infinite model space size. The error estimates are obtained from calculations with different oscillator frequencies.

	Nucleus	E_B [MeV]	R_p [fm]	μ [μ_N]	Q [$e\,\mathrm{fm}^2$]
JISP16	^{6}Li	31.4(3)	2.1(1)	0.838(1)	-0.06(3)
Operator		32.4(2)	2.1(1)	0.836(2)	-0.02(2)
Experiment		31.995	2.41(3)	0.8220	-0.0818(17)
JISP16	^{7}Li	38.6(3)	2.0(2)	2.96(1)	-2.6(2)
Operator		40.0(2)	2.0(1)	3.00(1)	-2.6(3)
Experiment		39.245	2.26(2)	3.2564	-4.06(8)

Table 4.13: Properties of ^{6}Li and ^{7}Li: Binding energy E_B, point-proton radius R_p, magnetic dipole moment μ and electric quadrupole moment Q, calculated in the NCSM with the JISP16 potential (JISP16) and its fitted operator representation (Operator). A model space with $12\hbar\Omega$ for ^{6}Li and $10\hbar\Omega$ for ^{7}Li and an oscillator frequency of $\hbar\Omega = 24\,\mathrm{MeV}$ was used. The energies are obtained from an extrapolation to infinite model space size. Errors are estimated from calculations with different oscillator frequencies. Experimental data are taken from Refs. [51] and [52].

The binding energies of ^{3}H and ^{3}He obtained with the operator representation and the exact JISP16 matrix elements show only small deviations which are however slightly larger than the deviations seen for the reduced UCOM (Tab. 4.3) or the SRG transformed Argonne potential (Tab. 4.8). The calculated energies of ^{4}He, ^{6}He, ^{6}Li and ^{7}Li show deviations of up to more than one MeV. This is distinctly higher than the deviations observed in the calculations with the reduced UCOM potential or the SRG operator representation which are in the order of a up to a few hundred keV. The situation for the other ground state properties of ^{6}Li and ^{7}Li (see Tab. 4.13) is ambiguous: The calculated results for the point-proton radii, the magnetic moment of ^{6}Li and the electric quadrupole moment of ^{7}Li agree. For the magnetic moment of ^{7}Li and the quadrupole moment of ^{6}Li the results however differ.

A look at the energy spectra of the nuclei (Fig. 4.24) shows significant differences between the energy levels calculated with the operator representation and the JISP16 matrix elements. In the ^{6}Li spectrum, the first 2^+ and the second 1^+ excited state calculated with the operator representation are much lower than those obtained with the exact JISP16 matrix elements. These deviations again are much bigger than the deviations seen for the reduced UCOM or the SRG operator representation (Fig. 4.8 and 4.15).

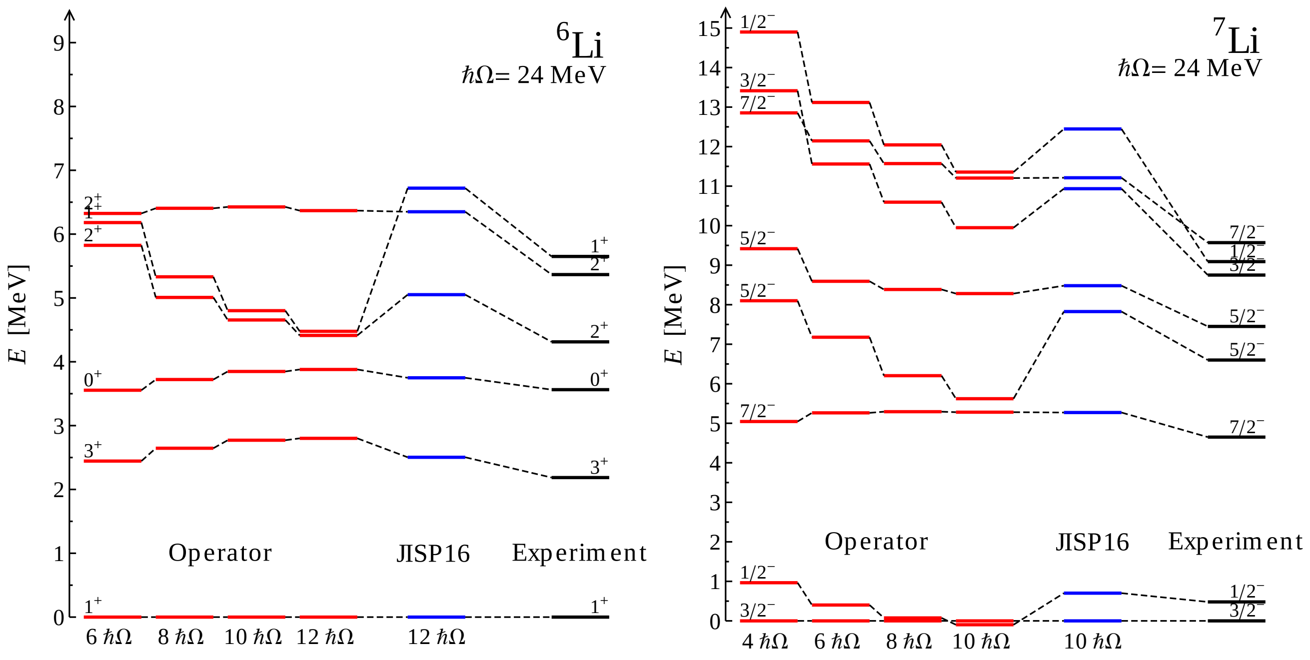

Figure 4.24: Spectra of ^{6}Li and ^{7}Li. The red lines show the results of a NCSM calculation with the fitted operator representation for different model spaces up to $12\hbar\Omega$ for ^{6}Li and up to $10\hbar\Omega$ for ^{7}Li (red lines) in comparison with the results of the JISP16 matrix elements (blue lines) in a $12\hbar\Omega$ and $10\hbar\Omega$ model space and the experiment [51].

In the ^{7}Li spectrum things are even worse: Beside deviations in the results for several energy levels, with increasing Hilbert spaces the $1/2^-$ state slips below the $3/2^-$ ground state indicating that the operator representation has a wrong spin-orbit property.

Summing up, clear deviations are seen between many results obtained with the operator representation and the JISP16 matrix elements. While the partial wave matrix elements and phase shifts agree fairly well for angular momenta up to $L = 2$, large deviations occur at higher L. In contrast to the SRG operator representation, the deviations for the partial waves matrix elements with higher L are not small enough to have only a minor effect on the calculated properties of the many-nucleon systems. The operator representation leads to a significant overbinding effect for most of the considered nuclei and disordered energy levels in the lithium spectra. This can be referred to unphysical attractive components in the poorly reproduced partial waves with $L \geq 3$ which occur in the Hilbert spaces when including larger $N\hbar\Omega$. Thus, the presented JISP16 operator representation does not provide an adequate potential for nuclear two- and few-body calculations. It is obviously not possible to describe all important features of the JISP16 potential for the considered many-body calculations with the ansatz given in Eq. (4.25). It remains to be shown if an improved ansatz, which takes more care of the peculiarities of this interaction, can improve the situation.

4.4.4 Closing remarks on the JISP16 operator representation

The attempted operator representation for the JISP16 potential using the operators of the Argonne potential Eq. (3.14) and nonlocal radial functions Eq. (4.9) fails to describe correctly the partial waves with angular momentum $L \geq 3$ as well as many of the properties of the calculated light nuclei.

The nonlocal radial functions are able to reproduce the momentum dependence of the JISP16 potential only for $L < 3$ (see Fig. (4.19)). The failure to describe the partial waves with $L \geq 3$ shows that the set of operators of ansatz Eq. (4.25) is not appropriate for the "ab-exitu" derived JISP16 interaction.

To illustrate this, one can consider the partial wave channels with $S = 0$ and $T = 1$ of the UCOM transformed Argonne potential, the SRG transformed Argonne potential and the JISP16 interaction. For $S = 0$ tensor and spin-orbit are not present and only the central part contributes. For the UCOM transformed Argonne potential Eq. (3.22) no dependence on L beyond the quadratic angular momentum term occurs and the potential is described only by the operators $\underset{\sim}{1}$ and $\underset{\sim}{\vec{L}}^2$. Consequently an ansatz for the operator representation with only these two operators is able to describe the partial wave matrix elements and phase shifts of all partial waves with $S = 0$ and $T = 1$ ($^1\mathrm{S}_0$, $^1\mathrm{D}_2$, $^1\mathrm{G}_4$, etc.). This can be seen in Figs. 4.5 to 4.7. The SRG transformed Argonne potential exhibits a more complicated dependence on L, although the initial Argonne potential only contains the operators $\underset{\sim}{1}$ and $\underset{\sim}{\vec{L}}^2$. An ansatz with only these two operators, motivated by the form of the initial potential, is not able to describe all partial with $S = 0$ and $T = 1$ correctly but still succeeds in describing at least approximately the partial wave matrix elements and phase shifts of the potential*. Consequently the phase shifts for the $^1\mathrm{S}_0$, $^1\mathrm{D}_2$ and $^1\mathrm{G}_4$ channel, shown in Figs. 4.12 - 4.14, do not agree as well as those for the UCOM transformed Argonne potential, but the deviations between operator representation and exact matrix elements in the $^1\mathrm{D}_2$ and $^1\mathrm{G}_4$ wave are rather small.

For the JISP16 interaction however, there exists no exact or approximate quadratic angular momentum dependence. The interaction is constructed in each partial wave individually and no simple L-dependence can be expected. An ansatz with the operators $\underset{\sim}{1}$ and $\underset{\sim}{\vec{L}}^2$ is not motivated by the available information on the potential as for the UCOM and SRG transformed Argonne potential. For the JISP16 interaction an ansatz with these two operators has to be understood rather as the first order of a polynomial expansions in powers of $\underset{\sim}{\vec{L}}^2$. Such a truncated expansion is able to describe as many partial waves as operators are used but will in general fail to describe the other partial waves. Moreover, a polynomial ansatz is expected to lead to uncontrolled large matrix elements and phase shifts for high L. Exactly this behaviour is seen for the operator representation of the JISP16 interaction. Figs. 4.21 to 4.23 show that the attempt to fit the $^1\mathrm{S}_0$, $^1\mathrm{D}_2$ and $^1\mathrm{G}_4$ partial wave channels with the two operators fails. Fig. 4.25 shows that by using an optimized fit for the $^1\mathrm{S}_0$ and $^1\mathrm{D}_2$ channels (without including the $^1\mathrm{G}_4$ channel in the fit) one succeeds in reproducing perfectly the matrix elements and phase shifts for these channels. The matrix elements and phase shifts of the $^1\mathrm{G}_4$ channel are however much to large. Adding the $\underset{\sim}{\vec{L}}^4$ operator as the next order in the expansion in powers of $\underset{\sim}{\vec{L}}^2$ would allow to reproduce the $^1\mathrm{S}_0$, $^1\mathrm{D}_2$ and $^1\mathrm{G}_4$ channels at the same time, but result in even worse behaviour for partial waves with $L \geq 6$. Thus, adding higher and higher powers of $\underset{\sim}{\vec{L}}^2$ is not an option, since this results in increasingly large matrix elements in partial waves with higher L and therefore unphysical large phase shifts.

The used nonlocal radial functions are flexible enough to describe the momentum dependence of the JISP16 interaction for a given L only. Covering all L requires an ansatz with as many operators as partial waves one aims to describe. To prevent the operator representation from creating uncontrolled large matrix elements in partial waves with high angular momenta L, an ansatz using projection operators on L, S, J and T in combination with the nonlocal radial functions could be used. But this is not what one

---

* In practice one chooses the weights in the fit such that the S-wave matrix elements are reproduced as good as possible and that the deviations in the D- and G-wave are small by finding a compromise between a less accurate description of the D-wave partial wave and a decent description of the G-wave matrix elements.

is aiming at. Alternative possibilities need to be investigated, like a regulator suppressing the operator representation at higher L. This can for example be achieved by the operator $\exp\left\{-\Lambda \underset{\sim}{\vec{L}}^2\right\}$ instead of a polynomial in $\underset{\sim}{\vec{L}}^2$, which prevents large matrix elements and phase shifts for high L. Presently no satisfactory operator representation for the JISP16 interaction has been found.

The failure of the used operator representation for the JISP16 interaction shows that an operator structure like the UCOM transformed Argonne potential is not capable to represent an interaction which is given in a discrete harmonic oscillator basis and reduced to a tri-diagonal form (see Eq.(3.43)). This "ket - bra" type interaction is at variance with the operator form, where the operators contribute in a smooth way to all matrix elements of the HO representation.

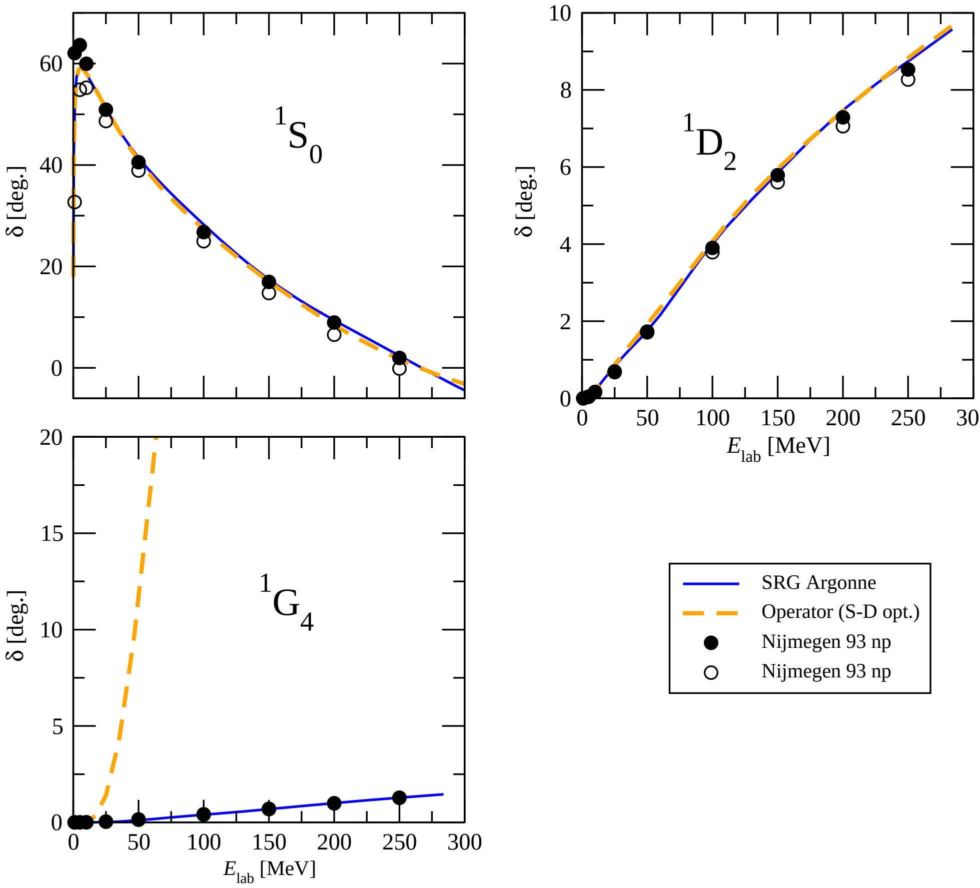

Figure 4.25: Nucleon-nucleon phase shifts for $S = 0$ and $T = 1$, calculated with the JISP16 interaction (blue solid line) and an operator representation fitted only to the $^1S_0$ and $^1D_2$ channel (Operator (S-D-opt.), orange dashed line) and extrapolated to the $^1G_4$ channel. The dots indicate the results of the 1993 Nijmegen partial wave analysis [47].

5 Summary and conclusions

Realistic effective NN potentials for microscopic many-body calculations are either given in operator representation or in matrix element representation. Both representations describe the same physics. While it is always possible to calculate matrix elements from the operator representation, the inverse way is not obvious. But nuclear many-body methods like Fermionic Molecular Dynamics (FMD) or Antisymmetrized Molecular Dynamics (AMD) do not use a fixed basis and thus need an explicit operator representation of the interaction. Since many modern effective NN interactions are constructed in matrix element representation, where the operator representation is not explicitly known, these interactions cannot be used directly in such many-body methods.

In this work a method to derive an operator representation from the partial wave matrix elements of an interaction is presented. By that method matrix element representations can, via their obtained operator representation, also be used in many-body methods that are not based on matrices in a given basis. Furthermore, the obtained operator representation provides insight into the structure of the considered potentials.

To extract the operator representation from the matrix elements, first an ansatz for the operator representation is chosen. This ansatz consists of a set of operators with corresponding radial functions. The exact form of the chosen ansatz is motivated by the available information about the considered potential and the purpose of the operator representation, for example the application in FMD calculations. The radial functions are not known a priori and have to be parameterized. In this work a parameterization formulated as a sum of gaussians which depend on relative distance and momentum is used. The partial wave matrix elements of the ansatz are calculated analytically and the parameters of the radial functions are obtained from a fit to the partial wave matrix elements of the interaction one aims to describe. The task is to find an optimal set of operators which is rich enough to reproduce the interaction adequately in all partial waves. The matrix elements of the partial wave channels with low angular momentum, which play a dominant role in the description of light nuclei, have to be reproduced with the highest accuracy.

The quality of the fitted operator representation is judged by investigating in how far the properties of the two- and few-nucleon systems reproduce the properties calculated directly with the matrix element representation. By this comparison one can improve or, if possible, simplify the ansatz for the operator representation.

To investigate the two-nucleon system in detail, a computer code was written. It allows to calculate the deuteron properties and NN scattering phase shifts by means of the partial wave matrix elements of the NN potential. For three and more nucleons the NCSM and FMD are applied to solve the nuclear many-body problem.

Three different effective realistic NN interactions for low momentum Hilbert spaces are considered: The UCOM transformed Argonne potential, the SRG transformed Argonne potential and the JISP16 interaction. The method described above is used to extract an operator representation from the partial wave matrix elements of these potentials.

For the UCOM transformed Argonne potential the operator representation as well as the partial wave matrix elements are known. Motivated by this known operator representation an ansatz with a subset of the operators present in the UCOM transformed Argonne potential can be chosen. In this work an ansatz based on the operators of the Argonne potential and the momentum dependent operators present in the UCOM transformed potential in combination with local radial functions is discussed. By fitting this ansatz to the partial wave matrix elements of the UCOM transformed Argonne potential a reduced UCOM potential is obtained. The used subset of operators is not able to describe all partial waves perfectly and, since the fit favours partial waves with small angular momentum L, small deviations occur for $L \geq 3$ between the partial wave matrix elements of the exact and the reduced UCOM potential. These deviations are reflected in the results for the phase shifts, where for higher L the reduced UCOM potential reproduces the phase shifts of the UCOM transformed Argonne potential not perfectly. The differences are however rather small. The energies and momenta of the deuteron and several light nuclei calculated in the NCSM and FMD are not sensitive to these deviations and show good agreement with the results from the exact potential. Thus, one can conclude that the obtained operator representation, although consisting of less operators than the exact potential, contains all important features to describe the considered few-nucleon systems. Consequently the reduced UCOM potential with its less complicated structure can be used in FMD calculations without loosing precision but requiring a reduced numerical effort.

The operator structure of the reduced UCOM potential clarifies the importance of the different additional operators created in the UCOM transformation: While the influence of most of the created operators is small or can be absorbed by other terms, the momentum dependent operators are essential to describe the nonlocality of the potential. This nonlocality is introduced by "transforming away" the short range repulsive core and the short range part of the tensor interaction.

For the SRG transformed Argonne potential an operator representation is not available as the SRG evolution is performed in the partial wave basis in momentum space. Only the operator form of the initial Argonne potential is known. To extract an operator representation, an ansatz with the operators present in the Argonne potential multiplied with nonlocal radial functions is used. The replacement of the local radial functions in the Argonne potential by nonlocal ones makes it possible to reproduce the complicated momentum dependence of the SRG transformed potential. The limited set of operators in the ansatz allows to describe the SRG transformed potential for partial waves with low L correctly. The weight factors in the fit are chosen such, that a compromise between an optimal reproduction of the partial waves with low angular momentum and not too large deviations for higher L is achieved. Deviations between the exact potential and the operator representation, which occur for $L \geq 3$, are not or only slightly affecting the results of the NCSM calculations for light nuclei. For the considered nuclei the operator representation and the exact potential lead to the same results. Thus, the operator representation provides an adequate description of the SRG transformed Argonne potential in the Hilbert spaces relevant for these nuclei. In future applications the operator representation should be tested for larger nuclear systems to find possible limits of the validity of the representation.

Analytical expressions for the FMD basis matrix elements of the nonlocal radial functions and the operators present in the used ansatz are derived. After the implementation of these formulas into the FMD code, the obtained operator representation is ready to be used in extensive FMD calculations.

The JISP16 interaction is constructed in terms of a very limited number of harmonic oscillator matrix elements in each partial wave. The matrix elements are the parameters of the interaction so that no simple comprehensive operator structure exists. To devise an operator representation with a limited set of operators, the same ansatz as for the operator representation of the SRG transformed Argonne potential is chosen. One finds that the momentum dependence of a single partial wave can be described by the nonlocal radial functions, but the dependence on the angular momenta L, J and the spin S of the JISP16 interaction is much too complicated to be described by the used finite set of operators. This manifests itself in deviations between the partial wave matrix elements of the operator representation and the exact interaction in the partial waves with $L \geq 3$ and the phase shifts obtained from those. In contrast to the SRG transformed Argonne potential, the deviations are so large that the resulting deviations of calculated many-body properties for light nuclei are not acceptable. Thus, the used set of operators is not able to provide an adequate description of the JISP16 interaction. The used operator representation depends in a smooth way on relative distance, momentum, angular momentum and spin. It has nonvanishing off-diagonal matrix elements in the harmonic oscillator basis for different radial quantum numbers n and n'. But the JISP16 interaction is constructed for each partial wave individually and set to zero for $\left|n - n'\right| > 1$ or 2 and $J > 4$ which makes it difficult to find a useful operator representation.

In summary, the presented method succeeds in constructing an operator representation of an interaction given in terms of partial wave matrix elements. This operator representation is able to describe the two-nucleon system (at low angular momenta) and the considered light nuclei with the same precision as the exact interaction matrix elements. The success of the method significantly depends on the chosen set of operators and the structure of the radial functions employed for the ansatz. This choice is guided by the symmetries of the NN interaction and information about the structure of the interaction, like the momentum dependence.

In this work only two-body interactions are considered. As one knows that three-body interactions, even though their contribution is relatively small, are indispensable, the future task is to develop operator structures for those which then can be fitted to represent given three-body matrix elements. In the future the described method will be applied to derive operator representations of various effective realistic potentials which will emerge from improved renormalization techniques. In particular, the consideration of effective interactions based on chiral potentials is of interest. The expressions for the FMD matrix elements of operator representations with nonlocal radial functions have been worked out. The implementation of these formulas into the FMD code, which will provide the model access to interactions like the SRG transformed Argonne potential or modern chiral interactions and their descendants, remains a future task.

By these developments, all many-body methods that are not based on a fixed basis set can profit from ongoing developments of effective realistic NN interactions.

A Formulas and definitions

In this section, general formulas and definitions used in the thesis are explained.

A.1 Mathematical functions and relations

A.1.1 Definitions

Cauchy principal value integral

If $f(x)$ is a function with one singularity at $x = x_0$ in the interval $a \leq x \leq b$, such that

$$\begin{aligned} \int_a^{x_0} \mathrm{d}x\, f(x) &= \pm\infty \\ \int_{x_0}^{b} \mathrm{d}x\, f(x) &= \mp\infty, \end{aligned} \tag{A.1}$$

the **Cauchy principal value integral** is defined as

$$\mathscr{P}\int_a^b \mathrm{d}x\, f(x) := \lim_{\epsilon\to 0+} \left(\int_a^{x_0-\epsilon} \mathrm{d}x\, f(x) + \int_{x_0+\epsilon}^{b} \mathrm{d}x\, f(x) \right). \tag{A.2}$$

A.1.2 Mathematical functions

Spherical Bessel functions

The **spherical Bessel functions** $j_L(z)$ can be obtained by the recursion relation [70]

$$j_L(z) = (-z)^L \left(\frac{1}{z}\frac{\mathrm{d}}{\mathrm{d}z} \right)^L \frac{\sin z}{z}, \tag{A.3}$$

so that

$$\begin{aligned} j_0(z) &= \frac{\sin z}{z} \\ j_1(z) &= \frac{\sin z}{z^2} - \frac{\cos z}{z} \\ &\vdots \end{aligned} \tag{A.4}$$

The spherical Bessel functions satisfy the orthogonality relation

$$\int_0^\infty \mathrm{d}r\, r^2\, j_L(kr)\, j_L(k'r) = \frac{\pi}{2}\frac{1}{k^2}\delta(k-k'). \tag{A.5}$$

Asymptotically for $z \gg L$, the spherical Bessel functions are given in Ref. [70]

$$j_L(z) \xrightarrow{z\gg L} \frac{\sin(z - \pi L/2)}{z}. \tag{A.6}$$

In this work spherical Bessel functions appear in connection with the partial wave basis in momentum space (see Sec. A.2.3). The radial part of the overlap between the partial wave state $\left| kLM \right\rangle$ and the eigenstate $\left| \vec{r} \right\rangle$ of the position operator is the spherical Bessel function $j_L(kr)$ with $r = |\vec{r}|$ (see Eq. (A.21b)).

Spherical harmonics

The **spherical harmonics** are defined by [70]

$$Y^L_M(\theta,\varphi) = \sqrt{\frac{2L+1}{4\pi}}\sqrt{\frac{(L-M)!}{(L+M)!}}P^L_M(\cos\theta)e^{im\varphi}, \tag{A.7}$$

where $P^L_M(\cos\theta)$ are associated Legendre polynomials. The spherical harmonics with the lowest quantum numbers L and M are given by

$$\begin{aligned}
Y^0_0(\theta,\varphi) &= \frac{1}{2\sqrt{\pi}} \\
Y^1_0(\theta,\varphi) &= \frac{1}{2}\sqrt{\frac{3}{\pi}}\cos\theta \\
Y^1_{-1}(\theta,\varphi) &= \frac{1}{2}\sqrt{\frac{3}{2\pi}}\sin\theta e^{-i\varphi} \\
Y^1_1(\theta,\varphi) &= -\frac{1}{2}\sqrt{\frac{3}{2\pi}}\sin\theta e^{i\varphi} \\
&\vdots
\end{aligned} \tag{A.8}$$

Spherical harmonics satisfy the orthogonality relation

$$\int_0^\pi d\theta \sin\theta \int_0^{2\pi} d\varphi\, \overline{Y}^L_M(\theta,\varphi) Y^{L'}_{M'}(\theta,\varphi) = \delta_{LL'}\delta_{MM'}, \tag{A.9}$$

where $\overline{Y}^L_M(\theta,\varphi)$ denotes the complex conjugate of $Y^L_M(\theta,\varphi)$.

Using the orthogonality Eq. (A.9) one can expand a function $f(r,\theta,\varphi)$ in terms of spherical harmonics:

$$f(r,\theta,\varphi) = \sum_{L=0}^{\infty}\sum_{M=-L}^{L} f^L_M(r) Y^L_M(\theta,\varphi), \tag{A.10}$$

with

$$f^L_M(r) = \int_0^\pi d\theta \sin\theta \int_0^{2\pi} d\varphi\, f(r,\theta,\varphi)\overline{Y}^L_M(\theta,\varphi). \tag{A.11}$$

Spherical harmonics describe the angular part of a state with good angular momentum quantum numbers L and M in position or momentum space:

$$\begin{aligned}
\left\langle \vec{r} \middle| \phi LM \right\rangle &= \phi^L_M(r)\cdot Y^L_M(\widehat{\vec{r}}) \\
\left\langle \vec{k} \middle| \phi LM \right\rangle &= \tilde{\phi}^L_M(k)\cdot Y^L_M(\widehat{\vec{k}}),
\end{aligned} \tag{A.12}$$

where $\phi^L_M(r)$ describes the radial part with $r = \sqrt{\vec{r}^{\,2}}$ and the angular part depends on the direction $\widehat{\vec{r}} = \frac{\vec{r}}{|\vec{r}|}$. The relations for $\vec{k}$, k and $\widehat{\vec{k}}$ are defined in analogy to those for $\vec{r}$ above. An example is the (LS-coupled) partial wave basis in momentum space in Eqs. (A.21).

A.2 Operators and basis

A.2.1 Quantum-mechanical Operators

In this work quantum mechanical **operators** (related to a physical quantity $\mathcal{O}$) are underlined by a tilde: $\underset{\sim}{\mathcal{O}}$.

A.2.2 Angular momentum coupling

Two angular momentum operators $\underset{\sim}{\vec{j}_1}$ and $\underset{\sim}{\vec{j}_2}$ can be added to give the total angular momentum operator

$$\underset{\sim}{\vec{J}} = \underset{\sim}{\vec{j}_1} + \underset{\sim}{\vec{j}_2}. \tag{A.13}$$

Let $\left| j_1 m_1, j_2 m_2 \right\rangle$ be the simultaneous eigenbasis of the operators $\underset{\sim}{\vec{j}^{\,2}_1}$, $\underset{\sim}{j_{1,z}}$, $\underset{\sim}{\vec{j}^{\,2}_2}$ and $\underset{\sim}{j_{2,z}}$:

$$\begin{aligned}
\underset{\sim}{\vec{j}^{\,2}_1}\left| j_1 m_1, j_2 m_2 \right\rangle &= j_1(j_1+1)\left| j_1 m_1, j_2 m_2 \right\rangle \\
\underset{\sim}{j_{1,z}}\left| j_1 m_1, j_2 m_2 \right\rangle &= m_1\left| j_1 m_1, j_2 m_2 \right\rangle \\
\underset{\sim}{\vec{j}^{\,2}_2}\left| j_1 m_1, j_2 m_2 \right\rangle &= j_2(j_2+1)\left| j_1 m_1, j_2 m_2 \right\rangle \\
\underset{\sim}{j_{2,z}}\left| j_1 m_1, j_2 m_2 \right\rangle &= m_2\left| j_1 m_1, j_2 m_2 \right\rangle.
\end{aligned} \tag{A.14}$$

The coupled eigenbasis $\left| (j_1 j_2) J M \right\rangle$ of the total angular momentum operator with

$$\begin{aligned}
\underset{\sim}{\vec{J}^{\,2}}\left| (j_1 j_2) J M \right\rangle &= J(J+1)\left| (j_1 j_2) J M \right\rangle \\
\underset{\sim}{J_z}\left| (j_1 j_2) J M \right\rangle &= M\left| (j_1 j_2) J M \right\rangle \\
\underset{\sim}{\vec{j}^{\,2}_1}\left| (j_1 j_2) J M \right\rangle &= j_1(j_1+1)\left| (j_1 j_2) J M \right\rangle \\
\underset{\sim}{\vec{j}^{\,2}_2}\left| (j_1 j_2) J M \right\rangle &= j_2(j_2+1)\left| (j_1 j_2) J M \right\rangle
\end{aligned} \tag{A.15}$$

can be obtained from the uncoupled basis by means of the Clebsch-Gordan coefficients [44]

$$C\left(\begin{array}{cc|c} j_1 & j_1 & J \\ m_1 & m_2 & M \end{array} \right) := \left\langle j_1 m_1, j_2 m_2 \middle| (j_1 j_2) J M \right\rangle. \tag{A.16}$$

The state $\left| (j_1 j_2) J M \right\rangle$ can be written as

$$\left| (j_1 j_2) J M \right\rangle = \sum_{m_1, m_2} C\left(\begin{array}{cc|c} j_1 & j_1 & J \\ m_1 & m_2 & M \end{array} \right) \left| j_1 m_1, j_2 m_2 \right\rangle. \tag{A.17}$$

It is possible to couple single-particle orbital angular momenta and spins or isospins of different particles. Or one can couple the relative orbital angular momentum L and total spin S to the total angular momentum J. As an example, the partial wave basis $\left| k(LS)JM; TM_T \right\rangle$ in Sec. A.2.3 shows multiple couplings. First, the spin and isospin of the two nucleons are coupled to total spin and total isospin with the quantum numbers S, M_S and T, M_T, respectively. Second, the orbital angular momentum and the total spin are coupled (indicated by the bracket (LS)) to the total angular momentum with quantum numbers J and M.

A.2.3 The partial wave basis in momentum space

The nucleon-nucleon interaction can be represented by matrix elements in a certain basis. In this work, the partial wave basis in momentum space* $\left| k(LS)JM;TM_T \right\rangle$ is mostly used. The unit operator is given by

$$\underset{\sim}{1} = \sum_{\substack{LSJM\\TM_T}} \int_0^\infty dk k^2 \left| k(LS)JM;TM_T \right\rangle \left\langle k(LS)JM;TM_T \right| \tag{A.18}$$

and the overlap between two basis states is

$$\left\langle k(LS)JM;TM_T \middle| k'(L'S')J'M';T'M'_T \right\rangle = \frac{1}{k^2}\delta(k-k')\delta_{LL'}\delta_{SS'}\delta_{JJ'}\delta_{MM'}\delta_{TT'}\delta_{M_TM'_T}. \tag{A.19}$$

The quantum numbers are the momentum quantum number k, angular momentum L, total spin S, the total angular momentum quantum numbers J and M and the total isospin quantum numbers T and M_T:

$$\begin{aligned}
\underset{\sim}{\vec{p}}^{\,2}\left| k(LS)JM;TM_T \right\rangle &= k^2\left| k(LS)JM;TM_T \right\rangle && \text{(A.20a)}\\
\underset{\sim}{\vec{L}}^{\,2}\left| k(LS)JM;TM_T \right\rangle &= L(L+1)\left| k(LS)JM;TM_T \right\rangle && \text{(A.20b)}\\
\underset{\sim}{\vec{S}}^{\,2}\left| k(LS)JM;TM_T \right\rangle &= S(S+1)\left| k(LS)JM;TM_T \right\rangle && \text{(A.20c)}\\
\underset{\sim}{\vec{J}}^{\,2}\left| k(LS)JM;TM_T \right\rangle &= J(J+1)\left| k(LS)JM;TM_T \right\rangle && \text{(A.20d)}\\
\underset{\sim}{J}_z\left| k(LS)JM;TM_T \right\rangle &= M\left| k(LS)JM;TM_T \right\rangle && \text{(A.20e)}\\
\underset{\sim}{\vec{T}}^{\,2}\left| k(LS)JM;TM_T \right\rangle &= T(T+1)\left| k(LS)JM;TM_T \right\rangle && \text{(A.20f)}\\
\underset{\sim}{T}_3\left| k(LS)JM;TM_T \right\rangle &= M_T\left| k(LS)JM;TM_T \right\rangle, && \text{(A.20g)}
\end{aligned}$$

where $\underset{\sim}{\vec{p}}$ is the (relative) momentum operator, $\underset{\sim}{\vec{L}}$ the (relative) orbital angular momentum operator, $\underset{\sim}{\vec{S}}$ the total spin operator, $\underset{\sim}{\vec{J}}$ the total angular momentum operator and $\underset{\sim}{\vec{T}}$ the total isospin operator for the two-nucleon system.

Since the nuclear interaction is invariant under rotations and approximately invariant under rotations in isospin space†, the matrix element $\left\langle k(LS)JM;TM_T \middle| \underset{\sim}{V} \middle| k'(L'S)JM;TM_T \right\rangle$ shows no dependence on the quantum numbers M and M_T. For simplification these quantum numbers are often omitted and the matrix element is written as $\left\langle k(LS)J;T \middle| \underset{\sim}{V} \middle| k'(L'S)J;T \right\rangle$ ignoring M and M_T. Note that these quantum numbers still exist and are just not written out.

---

[*] This basis describes the relative motion in the two-nucleon space. The full two body state is supplemented by the center-of-mass motion.

[†] This reflects the approximate charge symmetry of the nucleon-nucleon interaction.

The overlaps with the momentum basis states $\left|\vec{p}\,\right\rangle$ and the position basis states $\left|\vec{r}\,\right\rangle$ are given by

$$\left\langle \vec{p}\,\middle|\,k(LS)JM;TM_T\right\rangle = \sum_{M_L,M_S}\frac{1}{k^2}\delta(|\vec{p}|-k)\,C\left(\begin{array}{cc|c} L & S & J \\ M_L & M_S & M\end{array}\right)Y^L_M(\widehat{\vec{p}})\left|SM_S;TM_T\right\rangle \quad \text{(A.21a)}$$

$$\left\langle \vec{r}\,\middle|\,k(LS)JM;TM_T\right\rangle = \sum_{M_L,M_S}\sqrt{\frac{2}{\pi}}i^L j_L(kr)\,C\left(\begin{array}{cc|c} L & S & J \\ M_L & M_S & M\end{array}\right)Y^L_M(\widehat{\vec{r}})\left|SM_S;TM_T\right\rangle. \quad \text{(A.21b)}$$

Instead of working in momentum space, one can define the partial wave basis in position space $\left|r(LS)JM;TM_T\right\rangle$ which is the eigenbasis of the operators in Eqs. (A.20b) - (A.20g) and of the squared relative distance operator $\underset{\sim}{\vec{r}}^{\,2}$:

$$\underset{\sim}{\vec{r}}^{\,2}\left|r(LS)JM;TM_T\right\rangle = r^2\left|r(LS)JM;TM_T\right\rangle. \quad \text{(A.22)}$$

Similarly, one can use eigenstates of the relative harmonic oscillator Hamiltonian $\underset{\sim}{H}_\omega = \frac{\underset{\sim}{\vec{p}}^{\,2}}{2\mu}+\frac{1}{2}\mu\omega^2\underset{\sim}{\vec{r}}^{\,2}$ to define the radial part of the partial wave state. The harmonic oscillator partial wave basis $\left|n(LS)JM;TM_T\right\rangle$ with the radial oscillator quantum number* n is the eigenbasis of the operators in Eqs. (A.20b) - (A.20g) and of $\underset{\sim}{H}_\omega$

$$\underset{\sim}{H}_\omega\left|n(LS)JM;TM_T\right\rangle = \left(2n+L+\frac{3}{2}\right)\omega\left|n(LS)JM;TM_T\right\rangle. \quad \text{(A.23)}$$

A.2.4 Spectroscopic notation

A set of the quantum numbers $\{L,S,J,T\}$ describing a basis state of the partial wave basis $\left|k(LS)JM;TM_T\right\rangle$ introduced in Sec. A.2.3 is called a “channel”. Instead of writing down those quantum numbers explicitly, one often uses the spectroscopic notation

$${}^{2S+1}\text{“L”}_J$$

The angular momentum quantum number L is encoded by a letter. Tab. A.1 shows the corresponding letters for the lowest angular momenta L. For example, the channel with $L=0$, $S=1$, $J=1$ and $T=0$ is called the ${}^3S_1$-channel. It is not necessary to explicitly mention the isospin quantum number T in that notation, because it follows automatically from the fact that the total two-nucleon state has to be antisymmetric and only the two quantum numbers $T=0$ and 1 (where $T=0$ yields an antisymmetric isospin part and $T=1$ a symmetric isospin part) are possible.

L	0	1	2	3	4	5
“name”	S	P	D	F	G	H

Table A.1: Spectroscopic notation.

---

* In this case the radial oscillator quantum number takes the values $n=0,1,2,\cdots$. Often the oscillator quantum number is defined slightly differently by $\underset{\sim}{H}_\omega\left|\tilde{n}(LS)JM;TM_T\right\rangle = \left(2(\tilde{n}-1)+L+\frac{3}{2}\right)\omega\left|\tilde{n}(LS)JM;TM_T\right\rangle$, where $\tilde{n}=n+1$ and $\tilde{n}=1,2,3,\cdots$.

B Tools to probe nucleon-nucleon interactions

In this section, technical details of the methods used to calculate the two-nucleon properties discussed in Sec. 2.2.1 are presented.

B.1 Solving the Rarita-Schwinger equations

The deuteron properties are obtained by solving the Rarita-Schwinger equations

$$\begin{aligned} \frac{k^2}{2\mu}\tilde{\phi}_0(k) \quad &+ \int_0^\infty \mathrm{d}k'\, k'^2 \langle\, k(01)1;00 \,|\, \underset{\sim}{V} \,|\, k'(01)1;00 \,\rangle\, \tilde{\phi}_0(k') \\ &+ \int_0^\infty \mathrm{d}k'\, k'^2 \langle\, k(01)1;00 \,|\, \underset{\sim}{V} \,|\, k'(21)1;00 \,\rangle\, \tilde{\phi}_2(k') = E_B\, \tilde{\phi}_0(k) \end{aligned} \tag{B.1a}$$

$$\begin{aligned} \frac{k^2}{2\mu}\tilde{\phi}_2(k) \quad &+ \int_0^\infty \mathrm{d}k'\, k'^2 \langle\, k(21)1;00 \,|\, \underset{\sim}{V} \,|\, k'(01)1;00 \,\rangle\, \tilde{\phi}_0(k') \\ &+ \int_0^\infty \mathrm{d}k'\, k'^2 \langle\, k(21)1;00 \,|\, \underset{\sim}{V} \,|\, k'(21)1;00 \,\rangle\, \tilde{\phi}_2(k') = E_B\, \tilde{\phi}_2(k). \end{aligned} \tag{B.1b}$$

For that purpose, an equidistant momentum grid is introduced. It is characterized by the grid points ranging from k_0 to k_N with the spacing step size Δ_k. The nth grid point k_n is given by:

$$k_n = k_0 + n\Delta_k. \tag{B.2}$$

In this calculation, k_0 is set to zero. k_N and Δ_k have to be chosen such that neither increasing the cutoff k_N nor decreasing the step size Δ_k will affect the result of the calculation. Typically $\Delta_k = 0.1\,\mathrm{fm}^{-1}$ is a sufficiently small step size. The required value of k_N depends on the interaction. The bare Argonne potential needs momenta up to $15\,\mathrm{fm}^{-1}$, while for UCOM- or SRG transformed potentials [*] results become stable at around $10\,\mathrm{fm}^{-1}$.

The Rarita-Schwinger equations read in the discretized form:

$$\begin{aligned} \frac{k_i^2}{2\mu}\tilde{\phi}_0(k_i) \quad &+ \sum_{j=0}^{N} \Delta_k\, k_j^2 \langle\, k_i(01)1;00 \,|\, \underset{\sim}{V} \,|\, k_j(01)1;00 \,\rangle\, \tilde{\phi}_0(k_j) \\ &+ \sum_{j=0}^{N} \Delta_k\, k_j^2 \langle\, k_i(01)1;00 \,|\, \underset{\sim}{V} \,|\, k_j(21)1;00 \,\rangle\, \tilde{\phi}_2(k_j) = E_B\, \tilde{\phi}_0(k_i) \end{aligned} \tag{B.3a}$$

$$\begin{aligned} \frac{k_i^2}{2\mu}\tilde{\phi}_2(k_i) \quad &+ \sum_{j=0}^{N} \Delta_k\, k_j^2 \langle\, k_i(21)1;00 \,|\, \underset{\sim}{V} \,|\, kj(01)1;00 \,\rangle\, \tilde{\phi}_0(k_j) \\ &+ \sum_{j=0}^{N} \Delta_k\, k_j^2 \langle\, k_i(21)1;00 \,|\, \underset{\sim}{V} \,|\, k_j(21)1;00 \,\rangle\, \tilde{\phi}_2(k_j) = E_B\, \tilde{\phi}_2(k_i). \end{aligned} \tag{B.3b}$$

---

[*] These potentials show a clear decoupling of high and low momentum components.

One can define the matrices

$$\begin{aligned} (T^{00})_{ij} &= (T^{22})_{ij} = \frac{k_i^2}{2\mu}\delta_{ij} \qquad \text{(B.4a)} \\ (T^{02})_{ij} &= (T^{20})_{ij} = 0 \qquad \text{(B.4b)} \end{aligned}$$

$$\begin{aligned} (V^{00})_{ij} &= \Delta_k\, k_j^2 \big\langle\, k_i(01)1;00 \,\big|\, \underset{\sim}{V} \,\big|\, k_j(01)1;00 \,\big\rangle \qquad \text{(B.4c)} \\ (V^{02})_{ij} &= \Delta_k\, k_j^2 \big\langle\, k_i(01)1;00 \,\big|\, \underset{\sim}{V} \,\big|\, k_j(21)1;00 \,\big\rangle \qquad \text{(B.4d)} \\ (V^{20})_{ij} &= \Delta_k\, k_j^2 \big\langle\, k_i(21)1;00 \,\big|\, \underset{\sim}{V} \,\big|\, k_j(01)1;00 \,\big\rangle \qquad \text{(B.4e)} \\ (V^{22})_{ij} &= \Delta_k\, k_j^2 \big\langle\, k_i(21)1;00 \,\big|\, \underset{\sim}{V} \,\big|\, k_j(21)1;00 \,\big\rangle \qquad \text{(B.4f)} \end{aligned}$$

and

$$H := \left(\begin{array}{c|c} H^{00} & H^{02} \\ \hline H^{20} & H^{22} \end{array}\right) = \left(\begin{array}{c|c} T^{00} & T^{02} \\ \hline T^{20} & T^{22} \end{array}\right) + \left(\begin{array}{c|c} V^{00} & V^{02} \\ \hline V^{20} & V^{22} \end{array}\right). \qquad \text{(B.4g)}$$

Solving the discretized Rarita-Schwinger Eqs. (B.3) is equivalent to solving the (non-hermitian) matrix eigenvalue problem

$$H\vec{\Phi} = E_B\vec{\Phi}. \qquad \text{(B.5)}$$

The lowest eigenvalue and the corresponding eigenvector are related to the deuteron ground state. The eigenvalue gives the binding energy. The eigenvector $\vec{\Phi}$ obtained from the numerical solution of this problem contains the solution for $\tilde{\phi}_0(k)$ and $\tilde{\phi}_2(k)$ on the momentum grid from Eq. (B.2):

$$\vec{\Phi} = \left(\begin{array}{c} \tilde{\phi}_0(k_0) \\ \tilde{\phi}_0(k_1) \\ \vdots \\ \tilde{\phi}_0(k_N) \\ \hline \tilde{\phi}_2(k_0) \\ \tilde{\phi}_2(k_1) \\ \vdots \\ \tilde{\phi}_2(k_N) \end{array}\right). \qquad \text{(B.6)}$$

The solution in position space is derived by a Fourier-Bessel transformation

$$\begin{aligned} \phi_0(r) &= \sqrt{\frac{2}{\pi}}\int_0^\infty \mathrm{d}k\, k^2 j_0(kr)\tilde{\phi}_0(k) \\ \phi_2(r) &= -\sqrt{\frac{2}{\pi}}\int_0^\infty \mathrm{d}k\, k^2 j_2(kr)\tilde{\phi}_2(k) \qquad \text{(B.7)} \end{aligned}$$

which is again performed on the discretized momentum grid Eq. (B.2).

Once calculated, the radial solutions can be used to calculate the properties described in Sec. 2.1. The radius is obtained by calculating

$$\langle R^2 \rangle = \langle \phi_D | \underset{\sim}{R}^2 | \phi_D \rangle = \frac{1}{2}\Big(\int_0^\infty \mathrm{d}r\, r^4 |\phi_0(r)|^2 + \int_0^\infty \mathrm{d}r\, r^4 |\phi_2(r)|^2 \Big), \tag{B.8}$$

with $| \phi_D \rangle$ from Eq. (2.4). The magnetic dipole moment (without meson exchange currents) is given by

$$\mu = \langle \phi_D | \underset{\sim}{\mu} | \phi_D \rangle = \left(\frac{1}{2}(g_p + g_n) + \frac{3}{4}|c_2|^2 (1 - (g_p + g_n)) \right) \mu_N, \tag{B.9}$$

and depends only on the D-wave admixture

$$|c_2|^2 = \int_0^\infty \mathrm{d}k\, k^2 |\tilde{\phi}_2(k)|^2 = \int_0^\infty \mathrm{d}r\, r^2 |\phi_2(r)|^2. \tag{B.10}$$

For the electric quadrupole moment one finds

$$Q = \langle \phi_D | \underset{\sim}{Q} | \phi_D \rangle = e \left(\frac{1}{\sqrt{50}} \int_0^\infty \mathrm{d}r\, r^4 \phi_0(r) \phi_2(r) - \frac{1}{20} \int_0^\infty \mathrm{d}r\, r^4 |\phi_2(r)|^2 \right). \tag{B.11}$$

B.2 Calculating phase shifts

The phase shifts at the energy $E_{\mathrm{lab}} = \frac{\mathfrak{K}^2}{2\mu}$ for a potential $\underset{\sim}{V}$ are obtained from the on-shell matrix elements of the operator $\underset{\sim}{R}(\mathfrak{K})$, defined by Eq. (2.42)[*]

$$\begin{aligned} \langle k(LS)J;T | \underset{\sim}{R}(\mathfrak{K}) | k'(L'S)J;T \rangle &= \langle k(LS)J;T | \underset{\sim}{V} | k'(L'S)J;T \rangle \\ &+ \sum_{L''=0}^{\infty} \mathscr{P} \int_0^\infty \mathrm{d}q\, q^2 \frac{\langle k(LS)J;T | \underset{\sim}{V} | q(L''S)J;T \rangle \langle q(L''S)J;T | \underset{\sim}{R}(\mathfrak{K}) | k'(L'S)J;T \rangle}{\frac{1}{2\mu}(\mathfrak{K}^2 - q^2)}. \end{aligned} \tag{B.12}$$

Since the numerical treatment of the Cauchy principal value integral is difficult, one can use the following trick [71]: Using the fact that for $\mathfrak{K}^2 \neq 0$

$$\mathscr{P} \int_0^\infty \frac{\mathrm{d}k}{k^2 - \mathfrak{K}^2} = 0, \tag{B.13}$$

one can write the following principal value integral as

$$\mathscr{P} \int_0^\infty \frac{\mathrm{d}k\, f(k)}{k^2 - \mathfrak{K}^2} = \int_0^\infty \frac{\mathrm{d}k\, (f(k) - f(\mathfrak{K}))}{k^2 - \mathfrak{K}^2}. \tag{B.14}$$

---

[*] Eq. (2.42) contains only the half-on-shell matrix elements $\langle k(LS)JT | \underset{\sim}{R}(k') | k'(L'S)JT \rangle$ of $\underset{\sim}{R}$. In the following, this equation is generalized to the matrix elements $\langle k(LS)JT | \underset{\sim}{R}(\mathfrak{K}) | k'(L'S)JT \rangle$, where $\mathfrak{K}$ (corresponding to the scattering energy) and k' in the ket do not have to be identical.

The right-hand side of Eq. (B.14) shows no pole at $k = \mathfrak{K}$ (if f(k) is smooth around $k = \mathfrak{K}$) and can be evaluated numerically. Using Eq. (B.14) and the fact that the interaction only connects different L with $L{=}J{-}1$ and $L'{=}J{+}1$, Eq. (B.12) can be written on the equidistant momentum grid Eq. (B.2) as [71, 72]

$$\begin{aligned}\left\langle k_i(LS)J;T\left|\underset{\sim}{R}(\mathfrak{K})\right|k_j(L'S)J;T\right\rangle &= \left\langle k_i(LS)JT\left|\underset{\sim}{V}\right|k_j(L'S)J;T\right\rangle \\ &+\sum_{L''=|J-S|}^{J+S}\sum_{n=0}^{N}\Delta_k k_n^2\frac{\left\langle k_i(LS)J;T\left|\underset{\sim}{V}\right|k_n(L''S)J;T\right\rangle\left\langle k_n(L''S)J;T\left|\underset{\sim}{R}(\mathfrak{K})\right|k_j(L'S)J;T\right\rangle}{\frac{1}{2\mu}\left(\mathfrak{K}^2-k_n^2\right)} \\ &-\sum_{L''=|J-S|}^{J+S}\sum_{n=0}^{N}\Delta_k \mathfrak{K}^2\frac{\left\langle k_i(LS)J;T\left|\underset{\sim}{V}\right|\mathfrak{K}(L''S)J;T\right\rangle\left\langle \mathfrak{K}(L''S)J;T\left|\underset{\sim}{R}(\mathfrak{K})\right|k_j(L'S)J;T\right\rangle}{\frac{1}{2\mu}\left(\mathfrak{K}^2-k_n^2\right)}. \qquad \text{(B.15)}\end{aligned}$$

Note that $\mathfrak{K}$ is chosen such, that it is not a point of the momentum grid. By introducing a new momentum grid, containing the grid points k_0 to k_N from Eq. (B.15) plus $k_{N+1} := \mathfrak{K}$, one can define for $i = 0, \cdots, N+1$ the matrices

$$A_{ij}^{LL'SJT} = \delta_{ij}\cdot\delta_{LL'} - \frac{\Delta_k k_j^2}{\frac{1}{2\mu}\left(\mathfrak{K}^2-k_j^2\right)}\left\langle k_i(LS)J;T\left|\underset{\sim}{V}\right|k_j(L'S)J;T\right\rangle; \quad j = 0,\cdots,N \qquad \text{(B.16a)}$$

$$A_{iN+1}^{LL'SJT} = -\sum_{n=0}^{N}\frac{\Delta_k \mathfrak{K}^2}{\frac{1}{2\mu}\left(\mathfrak{K}^2-k_n^2\right)}\left\langle k_i(LS)J;T\left|\underset{\sim}{V}\right|k_{N+1}(L'S)J;T\right\rangle \qquad \text{(B.16b)}$$

$$V_{ij}^{LL'SJT} = \left\langle k_i(LS)J;T\left|\underset{\sim}{V}\right|k_j(L'S)J;T\right\rangle; \qquad \text{(B.16c)}$$

$$R_{ij}^{LL'SJT}(\mathfrak{K}) = \left\langle k_i(LS)J;T\left|\underset{\sim}{R}(\mathfrak{K})\right|k_j(L'S)J;T\right\rangle; \qquad \text{(B.16d)}$$

For the channels with $L = J$ (which do not mix with other channels) Eq. (B.15) can be written as the matrix equation

$$\sum_{n=0}^{N+1} A_{in}^{JJSJT} R_{nj}^{JJSJT}(\mathfrak{K}) = V_{ij}^{JJSJT}, \qquad \text{(B.17)}$$

so that $R_{ij}^{JJSJT}(\mathfrak{K})$ can be obtained numerically by inverting the Matrix A^{JJSJT}:

$$R_{ij}^{JJSJT}(\mathfrak{K}) = \sum_{n=0}^{N+1}\left(A^{JJSJT}\right)_{in}^{-1} V_{nj}^{JJSJT}. \qquad \text{(B.18)}$$

The phase shifts can be extracted from $R_{ij}^{JJSJT}(\mathfrak{K})$ by the relation

$$-\frac{\pi}{2}\frac{1}{2\mu\mathfrak{K}}\tan\delta_{JSJT}(\mathfrak{K}) = \left\langle \mathfrak{K}(JS)JT\left|\underset{\sim}{R}(\mathfrak{K})\right|\mathfrak{K}(JS)JT\right\rangle = R_{N+1N+1}^{JJSJT}(\mathfrak{K}). \qquad \text{(B.19)}$$

For $S = 1$ and $L = J \pm 1$ the situation becomes more complicated, due to the coupling between the $L = J \pm 1$ and $L = J \mp 1$ channels. Written in terms of the matrices defined in Eqs. (B.16), Eq. (B.15) reads

$$\left(\begin{array}{c|c} A^{J-1\,J-1\,1JT} & A^{J-1\,J+1\,1JT} \\ \hline A^{J+1\,J-1\,1JT} & A^{J+1\,J+1\,1JT}\end{array}\right)\left(\begin{array}{c|c} R^{J-1\,J-1\,1JT}(\mathfrak{K}) & R^{J-1\,J+1\,1JT}(\mathfrak{K}) \\ \hline R^{J+1\,J-1\,1JT}(\mathfrak{K}) & R^{J+1\,J+1\,1JT}(\mathfrak{K})\end{array}\right) = \left(\begin{array}{c|c} V^{J-1\,J-1\,1JT} & V^{J-1\,J+1\,1JT} \\ \hline V^{J+1\,J-1\,1JT} & V^{J+1\,J+1\,1JT}\end{array}\right), \qquad \text{(B.20)}$$

where $A^{J-1\,J-1\,1\,J\,T}, \cdots$ are $(N+2)\times(N+2)$ matrices on the momentum grid defined above. By multiplying with the inverted matrix on the left side one obtains

$$\left(\begin{array}{c|c} R^{J-1\,J-1\,1\,J\,T}(\mathfrak{K}) & R^{J-1\,J+1\,1\,J\,T}(\mathfrak{K}) \\ \hline R^{J+1\,J-1\,1\,J\,T}(\mathfrak{K}) & R^{J+1\,J+1\,1\,J\,T}(\mathfrak{K}) \end{array}\right) = \left(\begin{array}{c|c} A^{J-1\,J-1\,1\,J\,T} & A^{J-1\,J+1\,1\,J\,T} \\ \hline A^{J+1\,J-1\,1\,J\,T} & A^{J+1\,J+1\,1\,J\,T} \end{array}\right)^{-1} \left(\begin{array}{c|c} V^{J-1\,J-1\,1\,J\,T} & V^{J-1\,J+1\,1\,J\,T} \\ \hline V^{J+1\,J-1\,1\,J\,T} & V^{J+1\,J+1\,1\,J\,T} \end{array}\right). \tag{B.21}$$

To calculate the phase shifts one has to consider the on-shell R-Matrix elements $\left\langle \mathfrak{K}(LS)JT \left| \underset{\sim}{R}(\mathfrak{K}) \right| \mathfrak{K}(L'S)JT \right\rangle = R^{LL'SJT}_{N+1\,N+1}(\mathfrak{K})$. One can diagonalize the matrix in analogy to the procedure for the S-Matrix in Eq. (2.28):

$$\begin{pmatrix} R^{J-1\,J-1\,1\,J\,T}_{N+1\,N+1}(\mathfrak{K}) & R^{J-1\,J+1\,1\,J\,T}_{N+1\,N+1}(\mathfrak{K}) \\ R^{J+1\,J-1\,1\,J\,T}_{N+1\,N+1}(\mathfrak{K}) & R^{J+1\,J+1\,1\,J\,T}_{N+1\,N+1}(\mathfrak{K}) \end{pmatrix} = U_J^{-1}\, D_{JT}\, U_J, \tag{B.22}$$

with U_J containing the mixing angle $\epsilon_J(\mathfrak{K})$

$$U_J = \begin{pmatrix} \cos\epsilon_J(\mathfrak{K}) & \sin\epsilon_J(\mathfrak{K}) \\ -\sin\epsilon_J(\mathfrak{K}) & \cos\epsilon_J(\mathfrak{K}) \end{pmatrix} \tag{B.23}$$

and D_{1JT} containing the eigen phase shifts $\tilde{\delta}_{1,1JT}(\mathfrak{K})$ and $\tilde{\delta}_{3,1JT}(\mathfrak{K})$

$$D_{JT} = -\frac{\pi}{2}\frac{1}{2\mu\mathfrak{K}} \begin{pmatrix} \tan\tilde{\delta}_{1,1JT}(\mathfrak{K}) & 0 \\ 0 & \tan\tilde{\delta}_{3,JT;2}(\mathfrak{K}) \end{pmatrix}. \tag{B.24}$$

As discussed in Sec. 2.1, one usually labels the first phase shift with the quantum numbers $L = J-1$, J and T and the second $L = J+1$, J and T , which is strictly speaking not correct since the phase shifts show contributions from both angular momenta. To compare these phase shifts with experimental data, the eigen phase shifts are converted into bar phase shifts. Using the relations between eigen- and bar phase shifts given in Ref. [46], the bar phase shifts are calculated by

$$\begin{aligned} \bar{\epsilon}_J(\mathfrak{K}) &= \frac{1}{2}\arcsin\left(\sin\left(\tilde{\delta}_{1,1JT}(\mathfrak{K}) - \tilde{\delta}_{3,1JT}(\mathfrak{K})\right)\sin 2\epsilon_J(\mathfrak{K})\right) && \text{(B.25)} \\ \bar{\delta}_{1,1JT}(\mathfrak{K}) &= \frac{1}{2}\left(\tilde{\delta}_{1,1JT}(\mathfrak{K}) + \tilde{\delta}_{3,1JT}(\mathfrak{K}) + \arcsin\left(\frac{\cos 2\epsilon_J(\mathfrak{K})}{\cos 2\bar{\epsilon}_J(\mathfrak{K})}\sin\left(\tilde{\delta}_{1,1JT}(\mathfrak{K}) - \tilde{\delta}_{3,1JT}(\mathfrak{K})\right)\right)\right) \\ \bar{\delta}_{3,1JT}(\mathfrak{K}) &= \frac{1}{2}\left(\tilde{\delta}_{1,1JT}(\mathfrak{K}) + \tilde{\delta}_{3,1JT}(\mathfrak{K}) - \arcsin\left(\frac{\cos 2\epsilon_J(\mathfrak{K})}{\cos 2\bar{\epsilon}_J(\mathfrak{K})}\sin\left(\tilde{\delta}_{1,1JT}(\mathfrak{K}) - \tilde{\delta}_{3,1JT}(\mathfrak{K})\right)\right)\right). \end{aligned}$$

C Operator representation

C.1 Separation of central, spin-orbit and tensor components

The operator representation of the potentials discussed in Sec. 4 is obtained by fitting an ansatz for the operator representation to the partial wave matrix elements of the considered potential. One can classify the operators occurring in the ansatz by their spin dependence. The central part $\underset{\sim}{V}_{\text{central}}$ of the interaction consists of terms with operators which do not depend on the spin operator, such as $\underset{\sim}{1}$, $\underset{\sim}{\vec{L}}^2$ and $\underset{\sim}{\vec{p}}^2$. The spin-orbit part contains operators with tensor rank one in spin space like $\underset{\sim}{\vec{L}}\cdot\underset{\sim}{\vec{S}}$ and $\underset{\sim}{\vec{L}}^2(\underset{\sim}{\vec{L}}\cdot\underset{\sim}{\vec{S}})$. The operators of the tensor part are of rank two, such as $\underset{\sim}{S}_{12}$, $S_{12}(\underset{\sim}{\vec{L}},\underset{\sim}{\vec{L}})$, $\bar{S}_{12}(\underset{\sim}{\vec{p}}_{\Omega},\underset{\sim}{\vec{p}}_{\Omega})$ and $S_{12}(\underset{\sim}{\vec{r}},\underset{\sim}{\vec{p}}_{\Omega})$.

In the partial waves matrix elements with $S=0$, only the central part contributes. The $S=1$ matrix elements connecting different angular momenta contain only tensor contributions. In the other cases, all three components are present. In that case one can separate the central, spin-orbit and tensor components for a given angular momentum L by calculating linear combinations of the partial wave matrix elements with $J=L-1$, $J=L$ and $J=L+1$ [54].

The central part of the potential $\underset{\sim}{V}$ can be isolated via the linear combination

$$\Big(\sum_{J=L-1}^{L+1}(2J+1)\Big)^{-1}\sum_{J=L-1}^{L+1}(2J+1)\big\langle\, k(L1)J;T\,\big|\underset{\sim}{V}\big|\,k'(L1)J;T\,\big\rangle = \\ \big\langle\, k(L1)J;T\,\Big|\underbrace{V_{1T}^{C}(\underset{\sim}{\vec{r}},\underset{\sim}{\vec{p}})+V_{1T}^{L2}(\underset{\sim}{\vec{r}},\underset{\sim}{\vec{p}})\underset{\sim}{\vec{L}}^2+\cdots}_{\text{only central terms}}\Big|\,k'(L1)J;T\,\big\rangle. \quad \text{(C.1)}$$

Using the parameters

$$\alpha_J^L=\begin{cases} -\frac{2L^2+L-1}{4L^3+6L^2+2L}, & J=L-1\\ -\frac{2L+1}{4L^3+6L^2+2L}, & J=L\\ \frac{2L^2+3L}{4L^3+6L^2+2L}, & J=L+1 \end{cases} \quad \text{(C.2)}$$

one obtains the spin-orbit contributions

$$\sum_{J=L-1}^{L+1}\alpha_J^L\,\big\langle\, k(L1)J;T\,\big|\underset{\sim}{V}\big|\,k'(L1)J;T\,\big\rangle \;=\; \\ \big\langle\, k(L1)J;T\,\Big|\underbrace{V_{1T}^{LS}(\underset{\sim}{\vec{r}},\underset{\sim}{\vec{p}})+V_{1T}^{L2LS}(\underset{\sim}{\vec{r}},\underset{\sim}{\vec{p}})\underset{\sim}{\vec{L}}^2+\cdots}_{\text{only spin}-\text{orbit terms}}\Big|\,k'(L1)J;T\,\big\rangle. \quad \text{(C.3)}$$

For the tensor part one can use for example

$$\beta_J^L=\begin{cases} \frac{L+1}{12L^3+18L^2+6L}, & J=L-1\\ -\frac{2L+1}{12L^3+18L^2+6L}, & J=L\\ \frac{L}{12L^3+18L^2+6L}, & J=L+1 \end{cases} \quad \text{(C.4)}$$

and one obtains

$$\sum_{J=L-1}^{L+1} \beta_J^L \left\langle k(L1)J;T \right| \underset{\sim}{V} \left| k'(L1)J;T \right\rangle =$$

$$\left\langle k(L1)J;T \right| \underbrace{-\frac{2}{(2L+3)(2L-1)} V_{1T}^{T}(\underset{\sim}{\vec{r}},\underset{\sim}{\vec{p}}) + V_{1T}^{Tll}(\underset{\sim}{\vec{r}},\underset{\sim}{\vec{p}}) + \cdots}_{\text{only tensor terms}} \left| k'(L1)J;T \right\rangle . \tag{C.5}$$

By using this technique, it is possible to fit individually the central, spin-orbit and tensor component in the ansatz of the operator representation to the linear combined matrix elements containing only the desired component of the interaction. This method is used for the derivation of the operator representations presented in Sec. 4.

C.2 Weights

As discussed in Sec. 4.1, the fitting method to derive the operator representation allows the partial waves included in the fit to be weighted differently. The weight factors are chosen such that the lowest angular momentum partial wave matrix elements are reproduced in an optimal way and the deviations in the partial waves with higher L remain as small as possible. Tab. C.1 to C.3 show the weight factors that were used in the fits to obtain the operator representations presented in Sec. 4. For $S = 1$ central, spin-orbit and tensor part were fitted separately (see Appendix C.1), so the weight factors for each of these fits are given separately as well.

pw's with	$S=0$	$S=0$	$S=1,\ T=0$			$S=1,\ T=1$		
L	$T=0$	$T=1$	central	spin-orbit	tensor	central	spin-orbit	tensor
0	-	1	1	-	-	-	-	-
0-2	-	-	-	-	0.1	-	-	-
1	1	-	-	-	-	1	1	1
1-3	-	-	-	-	-	-	-	0.01
2	-	1	1	1	1	-	-	-
2-4	-	-	-	-	0.01	-	-	-
3	1	-	-	-	-	1	0.1	0.01
3-5	-	-	-	-	-	-	-	0.01
4	-	0.1	0.1	0.2	0.2	-	-	-

Table C.1: Weight factors for partial wave channels with angular momentum L used in the fit for the operator representation of the reduced UCOM potential.

pw's with	$S=0$	$S=0$		$S=1$, $T=0$			$S=1$, $T=1$	
L	$T=0$	$T=1$	central	spin-orbit	tensor	central	spin-orbit	tensor
0	-	1	1	-	-	-	-	-
0-2	-	-	-	-	0.5	-	-	-
1	1	-	-	-	-	1	1	1
1-3	-	-	-	-	-	-	-	0.5
2	-	0.1	1	1	1	-	-	-
3	0.1	-	-	-	-	0.1	0.5	0.5
4	-	0.1	1	0.1	0.5	-	-	-
5	0.1	-	-	-	-	0.1	0	0

Table C.2: Same as Tab. C.1, but for the operator representation of SRG transformed Argonne potential.

pw's with	$S=0$	$S=0$		$S=1$, $T=0$			$S=1$, $T=1$	
L	$T=0$	$T=1$	central	spin-orbit	tensor	central	spin-orbit	tensor
0	-	1	1	-	-	-	-	-
0-2	-	-	-	-	1	-	-	-
1	1	-	-	-	-	1	1	1
1-3	-	-	-	-	-	-	-	0.01
2	-	1	1	1	1	-	-	-
3	0.1	-	-	-	-	0.1	0.1	0.5
4	-	0.1	0.1	0.1	0.1	-	-	-
5	0	-	-	-	-	0.1	0	0

Table C.3: Same as Tab. C.1, but for the operator representation of the JISP16 interaction.

C.3 Local radial functions

C.3.1 Parameterization

The local radial functions $\mathcal{V}^{P}_{ST}(r)$ of the reduced UCOM potential Eq. (4.6) described in Sec. 4.2 are parameterized by a sum of gaussians

$$\mathcal{V}^{P}_{ST}(r)=\sum_{\mu}\gamma^{P}_{ST,\mu}\exp\left\{-\frac{\vec{r}^{2}}{2\kappa_{\mu}}\right\} \tag{C.6a}$$

with $P\in\{C,\,L2,\,p2,\,LS,\,Tll\}$ and

$$\begin{aligned}
\mathcal{V}^{T}_{1T}(r) &= \sum_{\mu}\gamma^{T}_{1T,\mu}r^{2}\exp\left\{-\frac{\vec{r}^{2}}{2\kappa_{\mu}}\right\} && \text{(C.6b)}\\
\mathcal{V}^{Trp}_{1T}(r) &= \sum_{\mu}\gamma^{Trp}_{1T,\mu}r^{3}\exp\left\{-\frac{\vec{r}^{2}}{2\kappa_{\mu}}\right\}. && \text{(C.6c)}
\end{aligned}$$

The parameters κ are chosen by the relation

$$\kappa_{\mu}=\kappa_{1}\cdot b^{\mu-1},$$

with $\kappa_1=0.05\,\mathrm{fm}^2$, $b=\sqrt{2}$ and $\mu_{\max}=15$, which corresponds to a maximum width parameter $\kappa_{15}=6.4\,\mathrm{fm}^2$. With these parameters one is able to cover the whole range of the interaction, which is a few fm. The parameters $\gamma^{P}_{ST,\mu}$ are obtained by the fitting procedure described in Sec. 4.1. The results for the UCOM(SRG) transformed Argonne potential with a flow parameter of $0.04\,\mathrm{fm}^4$ (see Ref. [55]) are presented in Tab. C.4 - C.6 and Fig. C.1 - C.5. The results for the UCOM(SRG) transformed Argonne potential with $s_{max}=0.2\,\mathrm{fm}^4$ are presented in Tabs. C.7 - C.9 and Figs. C.6 - C.10.

#	κ_μ [fm^2]	$\gamma^{C}_{00,\mu}$ [MeV]	$\gamma^{L2}_{00,\mu}$ [MeV]	$\gamma^{p2}_{00,\mu}$ [MeV]	$\gamma^{C}_{01,\mu}$ [MeV]	$\gamma^{L2}_{01,\mu}$ [MeV]	$\gamma^{p2}_{01,\mu}$ [MeV]
1	0.05	712.7	89.334	-19.297	325.85	2066.251	-191.431
2	$0.05\sqrt{2}$	-566.115	-118.034	37.784	3920.257	-7247.099	633.246
3	0.1	1202.491	138.141	-78.767	-6535.051	11037.876	-1206.669
4	$0.1\sqrt{2}$	-785.972	-71.723	70.121	9233.681	-11720.318	1456.091
5	0.2	736.188	0.582	-103.047	-10346.387	9457.131	-1551.054
6	$0.2\sqrt{2}$	-786.101	10.397	113.632	9969.869	-6700.145	1460.481
7	0.4	1029.47	-33.876	-141.824	-10069.815	4085.687	-1394.709
8	$0.4\sqrt{2}$	-1111.071	13.918	144.677	8531.19	-2307.417	1610.493
9	0.8	1033.029	-22.059	-122.934	-5531.215	1176.7	-1906.482
10	$0.8\sqrt{2}$	-821.186	7.22	94.52	2154.132	-574.324	2034.386
11	1.6	541.21	-5.755	-24.584	-92.004	270.662	-1468.740
12	$1.6\sqrt{2}$	-266.744	3.342	4.565	-349.164	-103.687	665.806
13	3.2	111.482	-1.435	-1.795	171.554	29.656	-201.356
14	$3.2\sqrt{2}$	-33.191	0.37	1.059	-39.144	-5.712	39.651
15	6.4	6.908	-0.054	-0.037	3.232	0.560	-4.047

Table C.4: The parameters $\gamma^{P}_{ST,\mu}$ of the reduced UCOM potential ($s_{max}=0.04\,\mathrm{fm}^4$) for $S=0$ and $T=0$ and 1.

#	κ_μ [fm^2]	$\gamma^{C}_{10,\mu}$ [MeV]	$\gamma^{L2}_{10,\mu}$ [MeV]	$\gamma^{p2}_{10,\mu}$ [MeV]	$\gamma^{LS}_{10,\mu}$ [MeV]	$\gamma^{T}_{10,\mu}$ [MeV]	$\gamma^{Tll}_{10,\mu}$ [MeV]	$\gamma^{Trp}_{10,\mu}$ [MeV]
1	0.05	-5944.741	2266.207	-32.988	0	5990.291	0	-2029.546
2	$0.05\sqrt{2}$	29899.458	-6999.674	35.982	0	-10472.515	0	2629.173
3	0.1	-60064.289	10174.344	-128.501	1471.196	9904.005	57.42	-1976.164
4	$0.1\sqrt{2}$	82524.391	-10469.741	266.354	-3688.953	-6848.02	-153.516	1122.077
5	0.2	-88045.154	8312.709	-747.413	5348.818	3887.859	200.713	-548.224
6	$0.2\sqrt{2}$	79081.711	-5842.228	1507.655	-5486.396	-1932.068	-220.462	287.188
7	0.4	-62479.648	3599.194	-2657.765	4749.055	842.375	188.062	-153.243
8	$0.4\sqrt{2}$	41961.019	-2048.747	4095.671	-3437.413	-365.751	-127.536	107.621
9	0.8	-22695.659	1112.090	-5178.730	2143.28	133.188	76.099	-70.151
10	$0.8\sqrt{2}$	8425.599	-617.96	5107.083	-1179.267	-48.288	-31.217	42.708
11	1.6	-1320.619	329.811	-3415.07	550.869	10.41	9.846	-17.326
12	$1.6\sqrt{2}$	-414.638	-132.624	1482.266	-205.972	-2.329	-2.932	4.674
13	3.2	283.754	37.964	-431.429	59.555	0.043	0.797	-0.922
14	$3.2\sqrt{2}$	-69.694	-7.116	80.694	-11.89	0.031	-0.159	0.129
15	6.4	6.544	0.672	-7.751	1.222	-0.032	0.016	-0.01

Table C.5: The parameters $\gamma^{P}_{10,\mu}$ of the reduced UCOM potential ($s_{max} = 0.04\,\mathrm{fm}^4$) for $S = 1$ and $T = 0$.

#	κ_μ [fm^2]	$\gamma^{C}_{11,\mu}$ [MeV]	$\gamma^{L2}_{11,\mu}$ [MeV]	$\gamma^{p2}_{11,\mu}$ [MeV]	$\gamma^{LS}_{11,\mu}$ [MeV]	$\gamma^{T}_{11,\mu}$ [MeV]	$\gamma^{Tll}_{11,\mu}$ [MeV]	$\gamma^{Trp}_{11,\mu}$ [MeV]
1	0.05	-2184.286	991.170	-16.791	0	0	0	-2566.818
2	$0.05\sqrt{2}$	6654.921	-2060.26	32.743	0	0	0	5515.851
3	0.1	-6516.51	2223.6	-95.598	364.856	3309.983	0	-3372.048
4	$0.1\sqrt{2}$	5681.024	-1708.747	75.58	-1375.069	-4999.741	0	1081.74
5	0.2	-4682.467	1313.167	-95.541	1514.84	4903.535	0	-151.485
6	$0.2\sqrt{2}$	2489.505	-712.372	108.81	-2017.832	-3390.781	0	-63.646
7	0.4	-1239.577	396.662	-98.226	1641.851	1932.656	0	62.365
8	$0.4\sqrt{2}$	582.376	-236.769	96.441	-1178.877	-941.118	0	-34.508
9	0.8	-195.045	109.104	-82.059	730.254	411.656	0	15.347
10	$0.8\sqrt{2}$	-26.386	-53.971	78.186	-392.868	-157.068	0	-6.372
11	1.6	84.292	23.755	-27.317	180.36	53.85	0	2.173
12	$1.6\sqrt{2}$	-47.534	-8.111	-0.944	-68.807	-15.404	0	-0.647
13	3.2	15.696	2.196	2.787	20.355	3.647	0	0.158
14	$3.2\sqrt{2}$	-3.779	-0.418	-0.754	-4.14	-0.596	0	-0.028
15	6.4	0.717	0.041	0.068	0.429	0.06	0	0.003

Table C.6: The parameters $\gamma^{P}_{11,\mu}$ of the reduced UCOM potential ($s_{max} = 0.04\,\mathrm{fm}^4$) for $S = 1$ and $T = 1$.

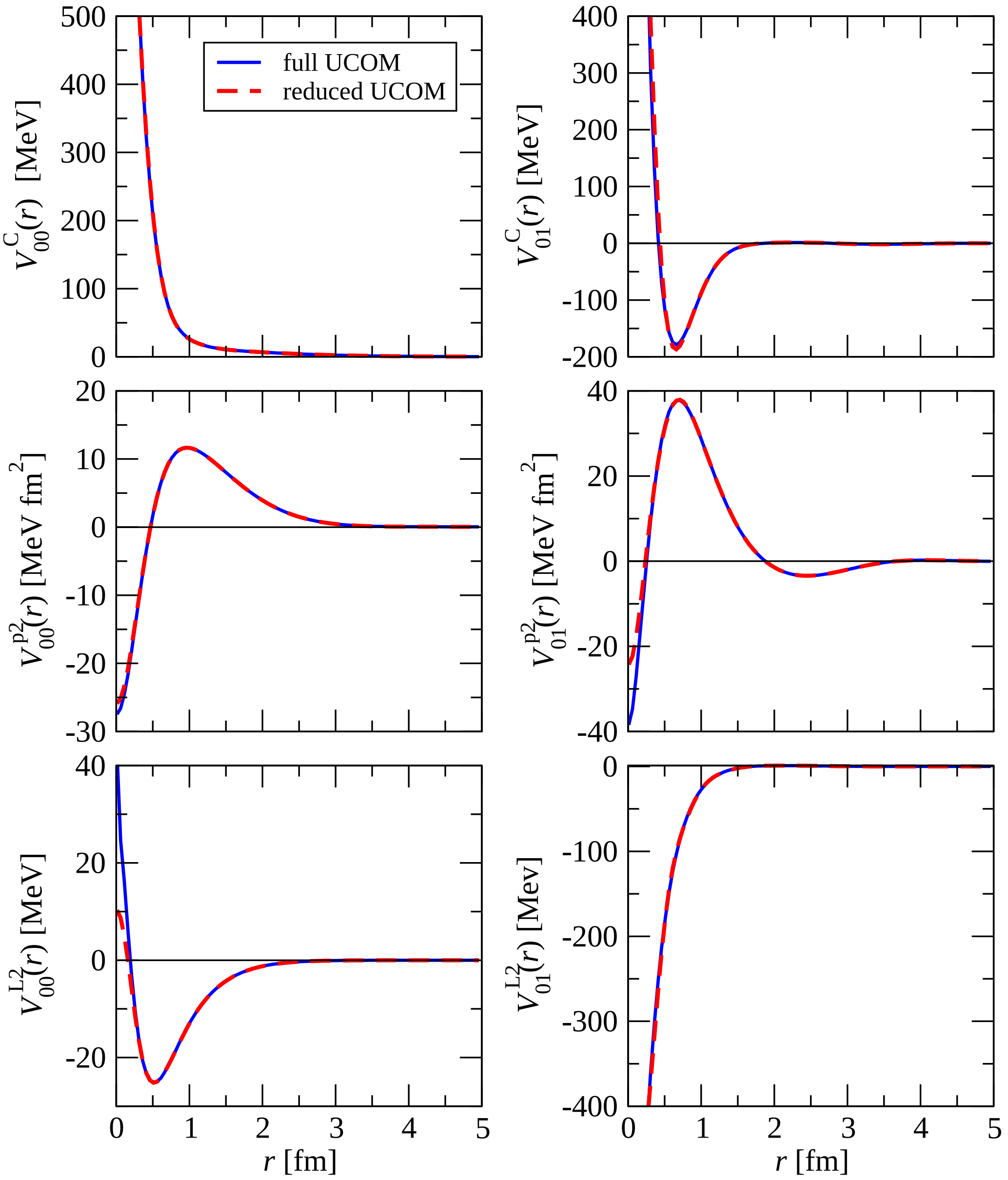

Figure C.1: The radial functions of the reduced UCOM potential (red dashed line) for $S = 0$ and $T = 0$ or 1. The radial functions are given by the parameterization Eq. (C.6a) and the parameters in Tab. C.4. The blue lines indicate the radial functions of the full UCOM potential.

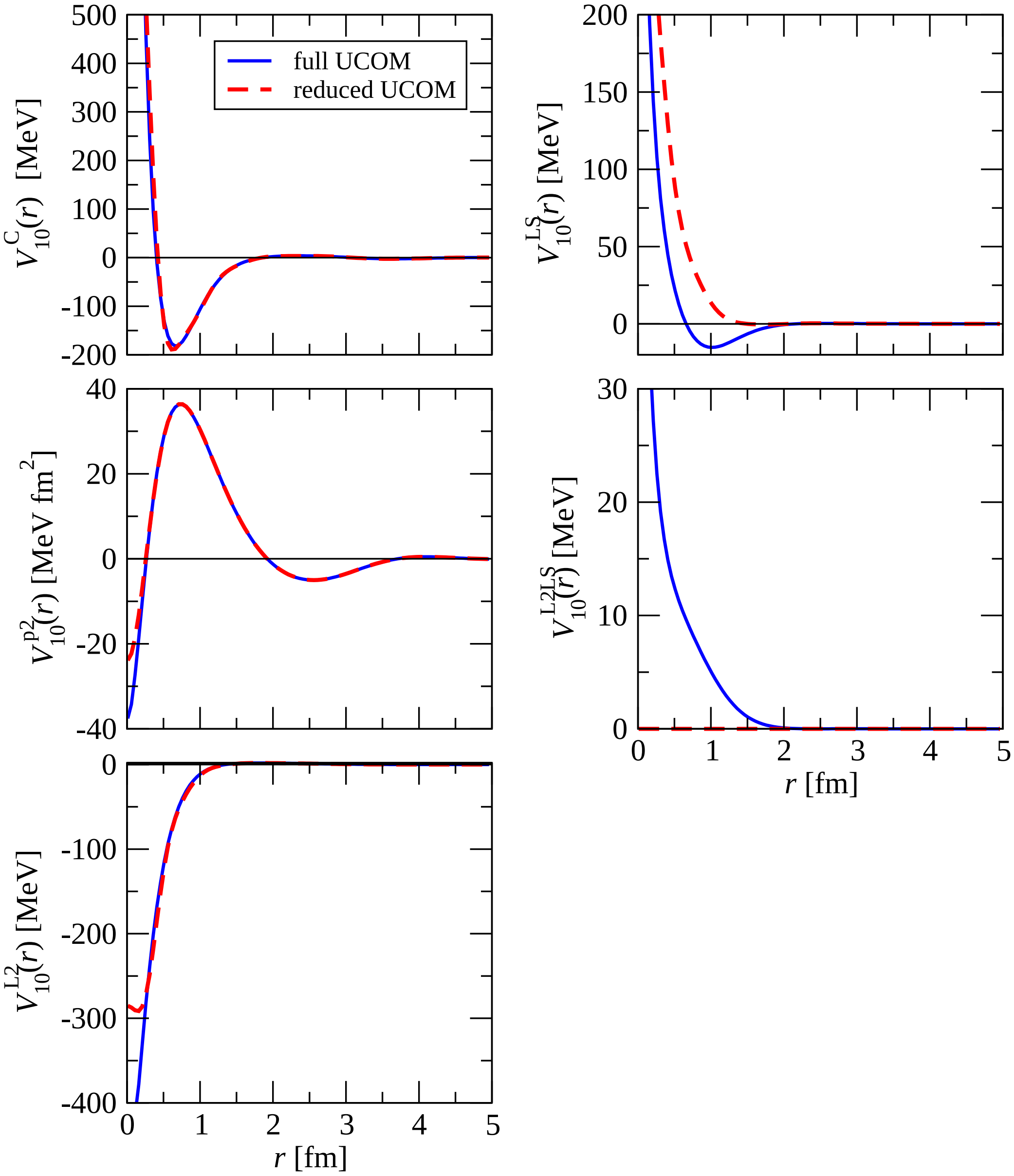

Figure C.2: The radial functions of the central and spin-orbit part of the reduced UCOM potential (red dashed line) for $S = 1$ and $T = 0$. The radial functions are given by the parameterization Eq. (C.6a) and the parameters in Tab. C.5. The blue lines indicate the radial functions of the full UCOM potential.

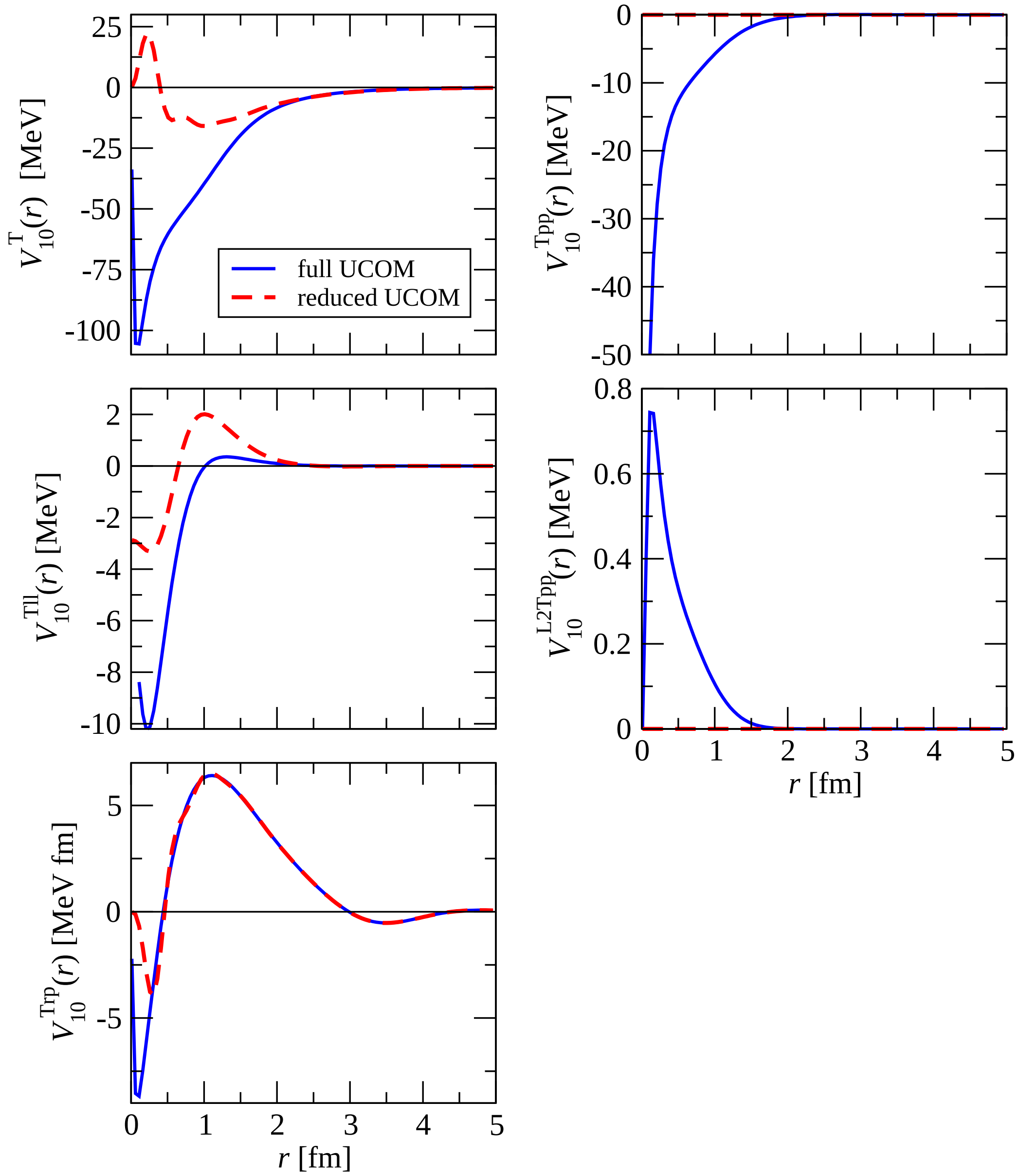

Figure C.3: The radial functions of the tensor part of the reduced UCOM potential (red dashed line) for $S = 1$ and $T = 0$. The radial functions are given by the parameterization Eqs. (C.6) and the parameters in Tab. C.5. The blue lines indicate the radial functions of the full UCOM potential.

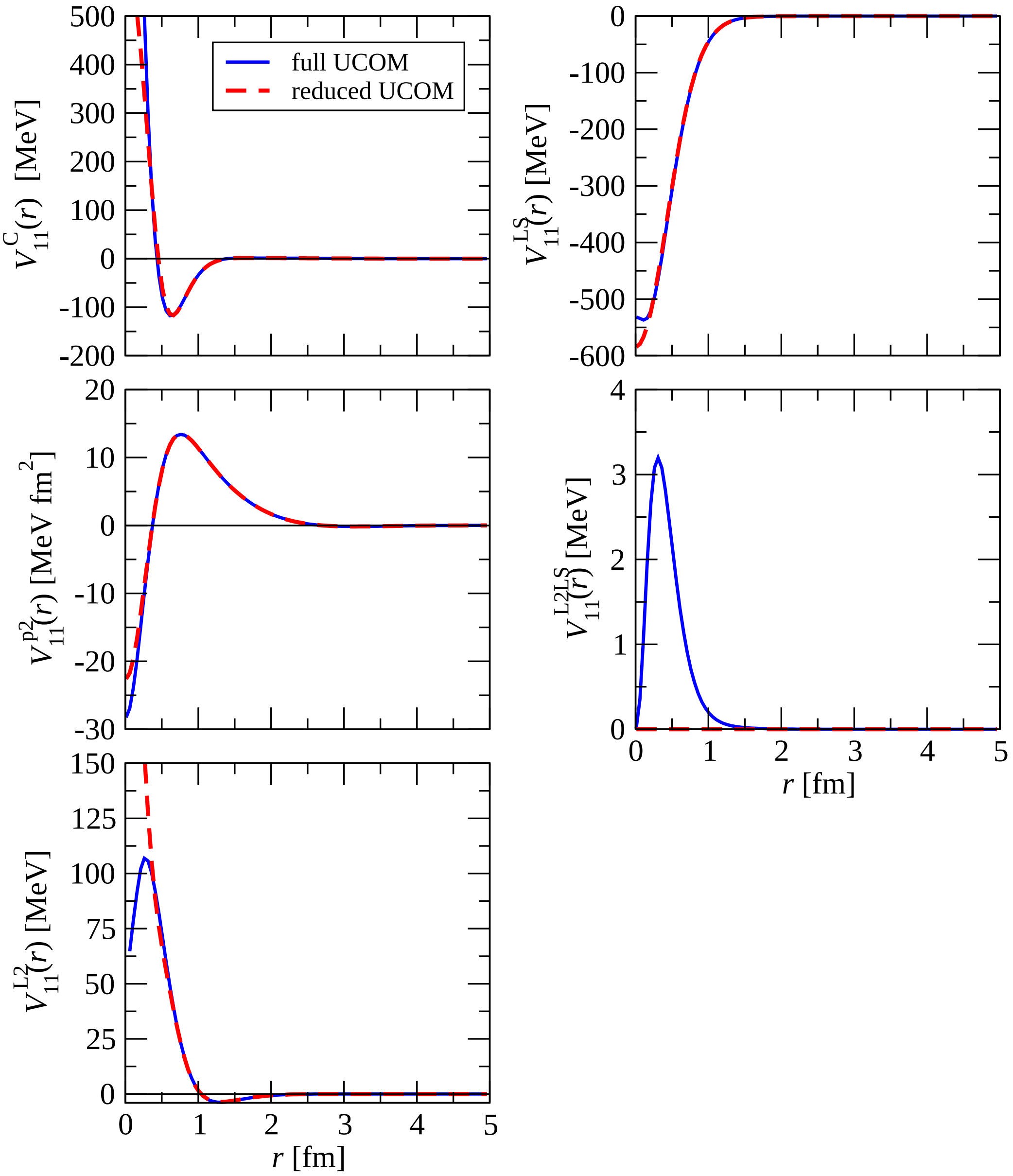

Figure C.4: Same as Fig. C.2, but for $S = 1$ and $T = 1$. The parameters from Tab. C.6 are used.

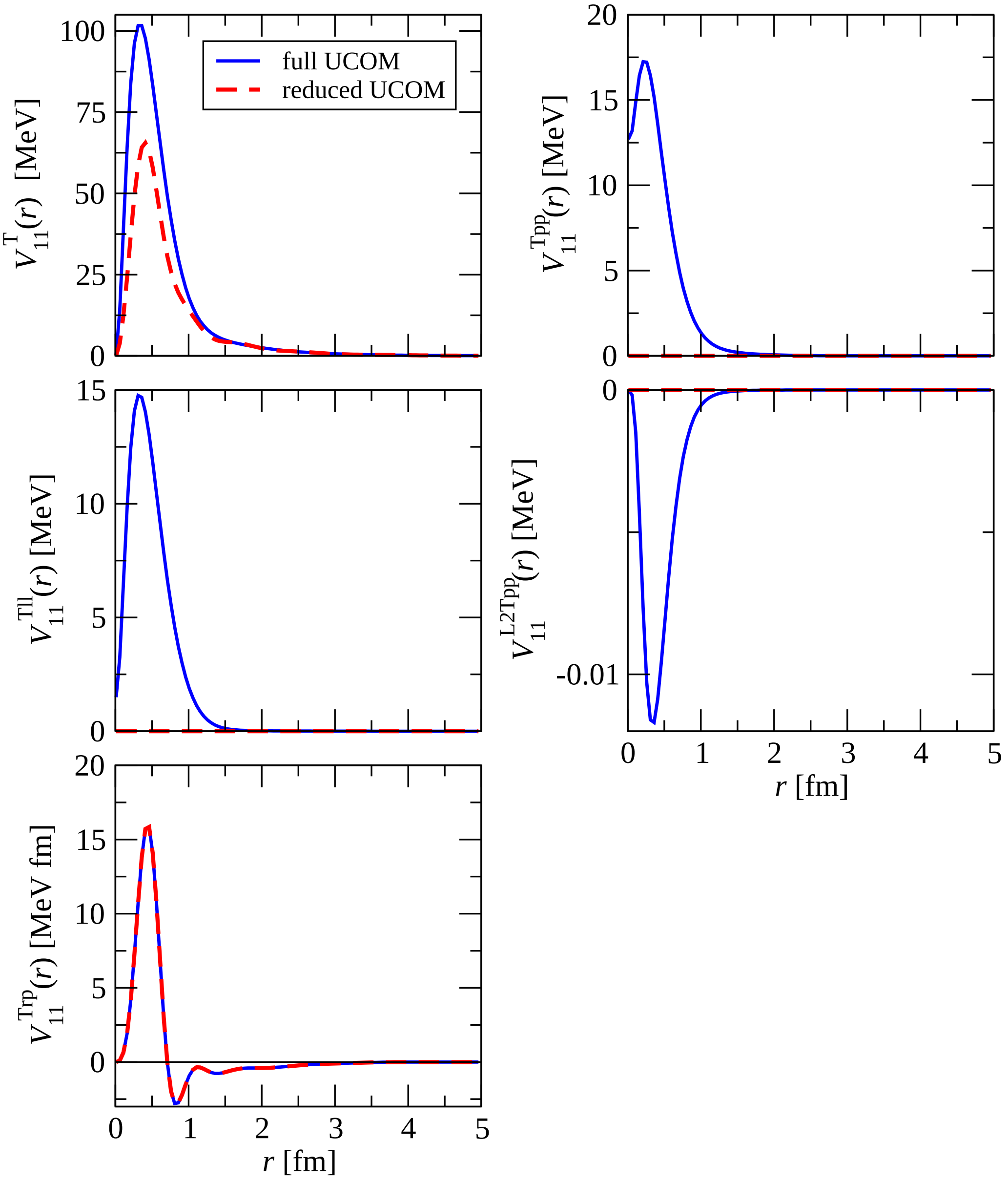

Figure C.5: Same as Fig. C.3, but for $S = 1$ and $T = 1$. The parameters from Tab. C.6 are used.

#	κ_μ [fm^2]	$\gamma^{C}_{00,\mu}$ [MeV]	$\gamma^{L2}_{00,\mu}$ [MeV]	$\gamma^{p2}_{00,\mu}$ [MeV]	$\gamma^{C}_{01,\mu}$ [MeV]	$\gamma^{L2}_{01,\mu}$ [MeV]	$\gamma^{p2}_{01,\mu}$ [MeV]
1	0.05	-0.909	0.388	0.185	11.083	21.174	-2.392
2	$0.05\sqrt{2}$	22.714	0.083	-0.802	-81.902	-69.023	9.291
3	0.1	-47.121	-0.602	1.238	256.400	104.886	-18.237
4	$0.1\sqrt{2}$	63.776	1.051	-1.422	-421.484	-110.714	22.996
5	0.2	-62.340	-1.230	0.992	493.588	90.929	-22.439
6	$0.2\sqrt{2}$	50.358	1.000	-0.439	-459.704	-65.201	16.761
7	0.4	-34.638	-0.841	-0.209	354.320	41.121	-8.890
8	$0.4\sqrt{2}$	21.081	0.523	0.661	-236.799	-23.986	1.625
9	0.8	-11.204	-0.391	-0.899	136.257	12.594	4.268
10	$0.8\sqrt{2}$	4.989	0.198	0.957	-65.127	-5.921	-6.895
11	1.6	-1.593	-0.113	-0.748	23.528	2.356	6.136
12	$1.6\sqrt{2}$	0.216	0.041	0.450	-5.536	-0.736	-2.376
13	3.2	0.138	-0.016	-0.124	0.832	0.209	-0.285
14	$3.2\sqrt{2}$	-0.079	0.004	0.018	-0.167	-0.047	0.408
15	6.4	0.026	-0.001	0.006	0.027	0.005	-0.080

Table C.7: The parameters $\gamma^{P}_{ST,\mu}$ of the reduced UCOM potential ($s_{max} = 0.2\,\mathrm{fm}^4$) for $S = 0$ and $T = 0$ and 1.

#	κ_μ [fm^2]	$\gamma^{C}_{10,\mu}$ [MeV]	$\gamma^{L2}_{10,\mu}$ [MeV]	$\gamma^{p2}_{10,\mu}$ [MeV]	$\gamma^{LS}_{10,\mu}$ [MeV]	$\gamma^{T}_{10,\mu}$ [MeV]	$\gamma^{Tll}_{10,\mu}$ [MeV]	$\gamma^{Trp}_{10,\mu}$ [MeV]
1	0.05	103.679	27.635	-4.654	0	44.679	0	-8.016
2	$0.05\sqrt{2}$	-501.081	-85.972	18.460	0	-80.133	0	8.412
3	0.1	1150.974	129.503	-35.688	9.547	78.278	0.208	-4.924
4	$0.1\sqrt{2}$	-1676.691	-135.634	43.930	-24.374	-55.914	-0.484	1.599
5	0.2	1825.727	112.036	-38.756	35.523	32.912	0.585	-0.033
6	$0.2\sqrt{2}$	-1612.292	-80.927	21.936	-36.897	-17.136	-0.684	-0.368
7	0.4	1203.276	51.848	-0.677	32.065	8.130	0.588	0.354
8	$0.4\sqrt{2}$	-774.039	-30.455	-18.224	-24.144	-3.707	-0.502	-0.180
9	0.8	421.746	16.077	29.500	16.368	1.566	0.456	0.060
10	$0.8\sqrt{2}$	-186.660	-7.255	-28.433	-9.641	-0.633	-0.306	0.036
11	1.6	61.876	2.671	16.563	4.940	0.223	0.174	-0.065
12	$1.6\sqrt{2}$	-14.485	-0.791	-1.914	-2.102	-0.067	-0.0558	0.052
13	3.2	3.162	0.272	-4.060	0.685	0.011	0.007	-0.020
14	$3.2\sqrt{2}$	-0.961	-0.078	2.308	-0.142	-0.001	0.000	0.004
15	6.4	0.174	0.010	-0.407	0.015	0.000	0.000	0.000

Table C.8: The parameters $\gamma^{P}_{10,\mu}$ of the reduced UCOM potential ($s_{max} = 0.2\,\mathrm{fm}^4$) for $S = 1$ and $T = 0$.

#	κ_μ [fm^2]	$\gamma^{C}_{11,\mu}$ [MeV]	$\gamma^{L2}_{11,\mu}$ [MeV]	$\gamma^{p2}_{11,\mu}$ [MeV]	$\gamma^{LS}_{11,\mu}$ [MeV]	$\gamma^{T}_{11,\mu}$ [MeV]	$\gamma^{Tll}_{11,\mu}$ [MeV]	$\gamma^{Trp}_{11,\mu}$ [MeV]
1	0.05	-9.239	4.900	-0.051	0	0	0	-8.016
2	$0.05\sqrt{2}$	31.638	-10.248	0.021	0	0	0	8.412
3	0.1	-33.245	11.154	-0.218	1.647	16.895	0	-4.924
4	$0.1\sqrt{2}$	30.674	-8.426	0.061	-6.608	-25.606	0	1.599
5	0.2	-26.789	6.462	-0.143	7.204	25.075	0	-0.033
6	$0.2\sqrt{2}$	16.079	-3.514	0.230	-9.627	-17.357	0	-0.368
7	0.4	-9.365	1.941	-0.210	7.863	9.896	0	0.354
8	$0.4\sqrt{2}$	5.503	-1.147	0.224	-5.656	-4.821	0	-0.180
9	0.8	-3.061	0.515	-0.188	3.511	2.108	0	0.060
10	$0.8\sqrt{2}$	1.500	-0.247	0.248	-1.894	-0.804	0	0.036
11	1.6	-0.638	0.100	-0.197	0.870	0.276	0	-0.065
12	$1.6\sqrt{2}$	0.212	-0.036	0.178	-0.332	-0.079	0	0.052
13	3.2	-0.028	0.0114	-0.096	0.098	0.019	0	-0.020
14	$3.2\sqrt{2}$	-0.006	-0.002	0.024	-0.020	-0.003	0	0.004
15	6.4	0.003	0.0002	-0.002	0.002	0.000	0	0.000

Table C.9: The parameters $\gamma^{P}_{11,\mu}$ of the reduced UCOM potential ($s_{max} = 0.2\,\mathrm{fm}^4$) for $S = 1$ and $T = 1$.

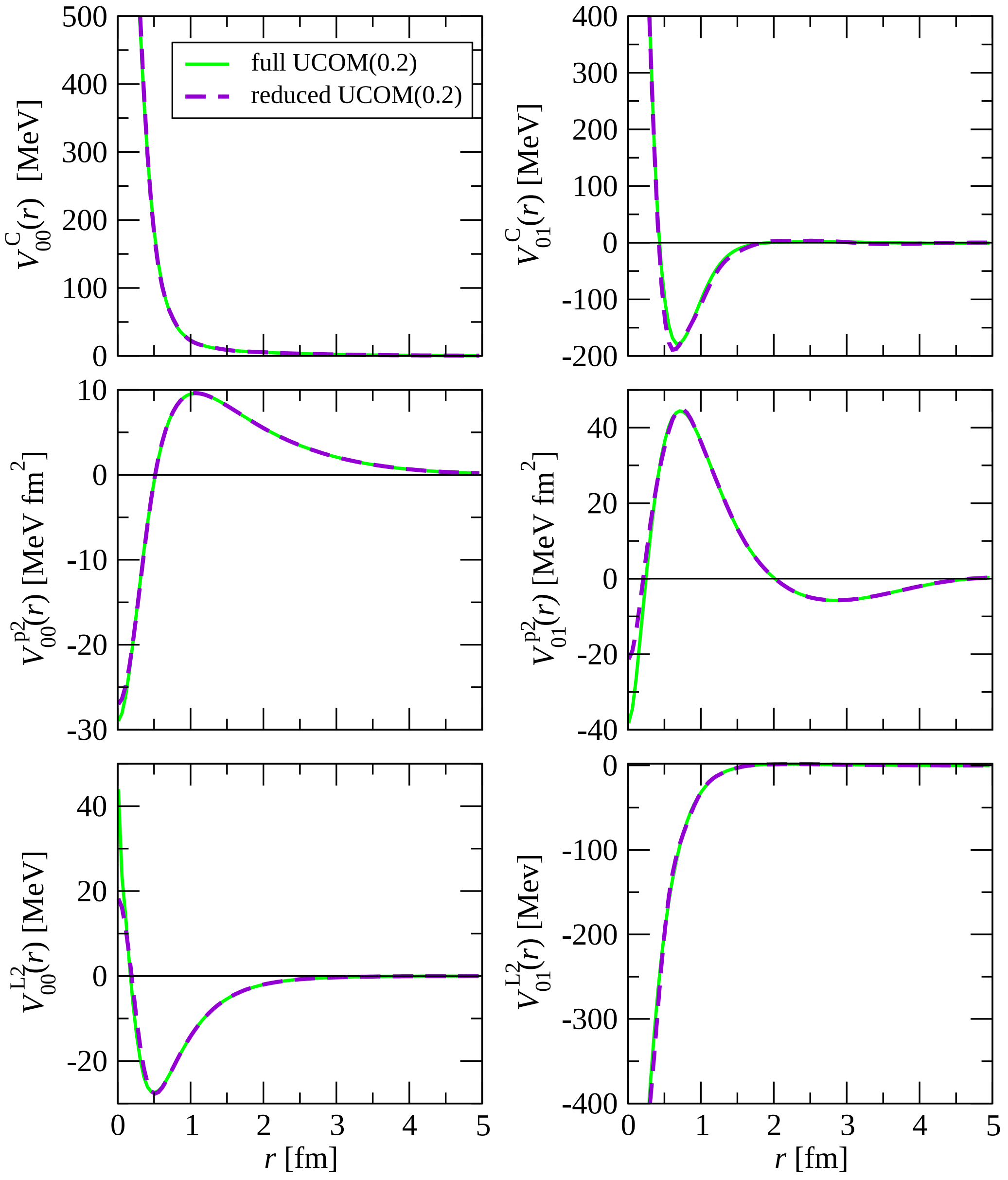

Figure C.6: The radial functions of the reduced UCOM(0.2) potential (violet dashed line) for $S = 0$ and $T = 0$ or 1. The radial functions are given by the parameterization Eq. (C.6a) and the parameters in Tab. C.7. The green lines indicate the radial functions of the full UCOM(0.2) potential.

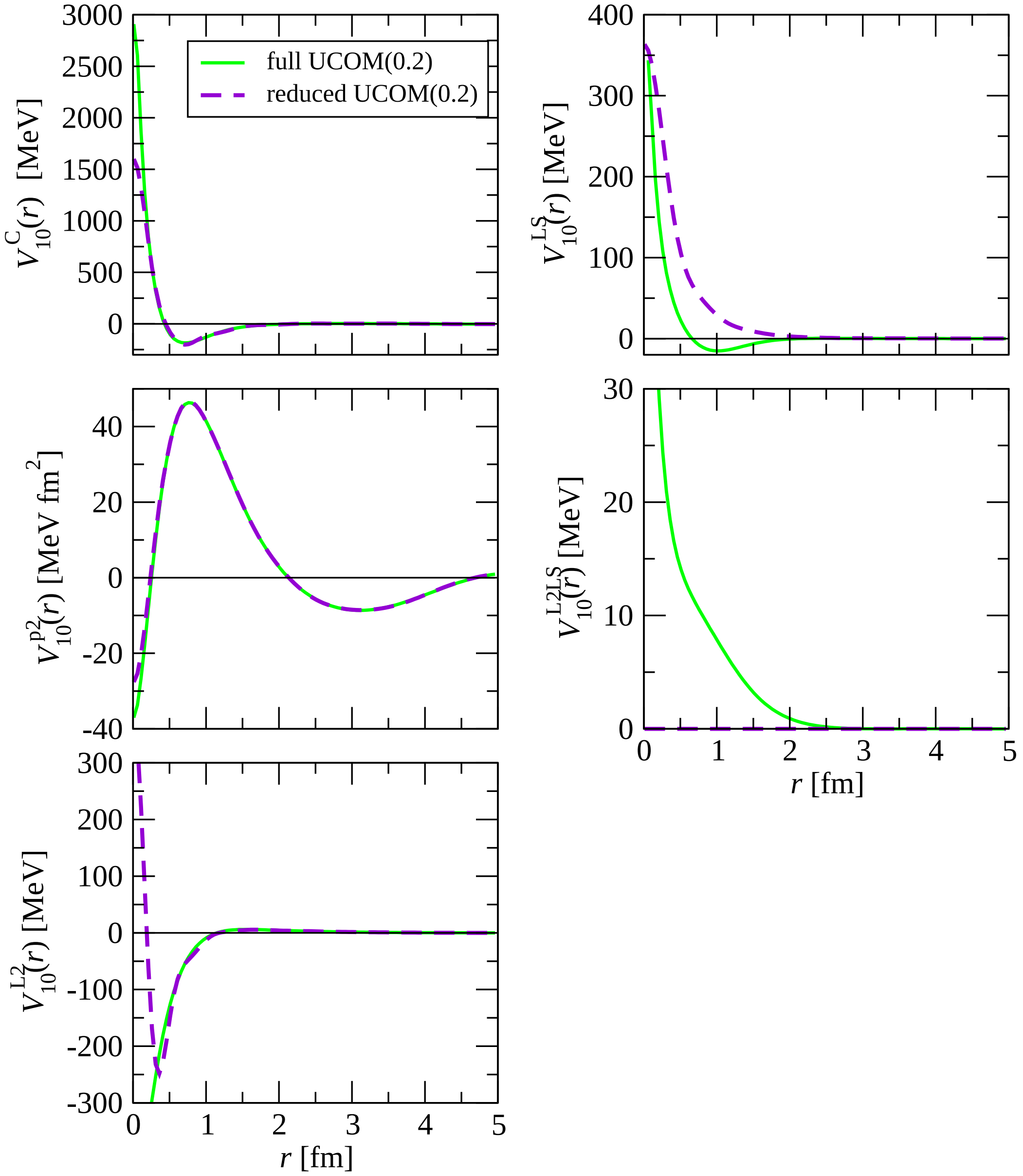

Figure C.7: The radial functions of the central and spin-orbit part of the reduced UCOM(0.2) potential (violet dashed line) for $S = 1$ and $T = 0$. The radial functions are given by the parameterization Eq. (C.6a) and the parameters in Tab. C.8. The green lines indicate the radial functions of the full UCOM(0.2) potential.

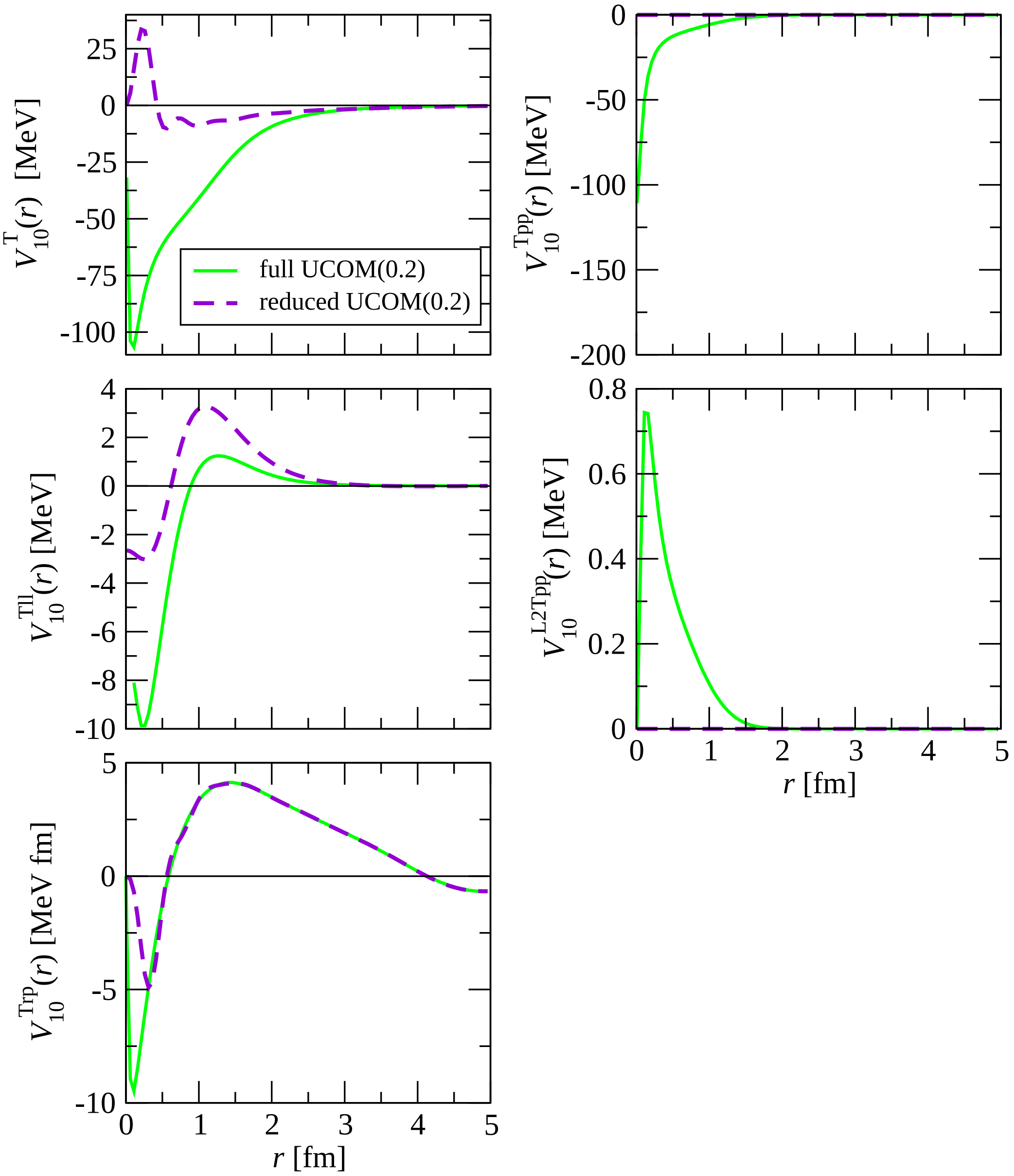

Figure C.8: The radial functions of the tensor part of the reduced UCOM potential (violet dashed line) for $S = 1$ and $T = 0$. The radial functions are given by the parameterization Eqs. (C.6) and the parameters in Tab. C.8. The green lines indicate the radial functions of the full UCOM(0.2) potential.

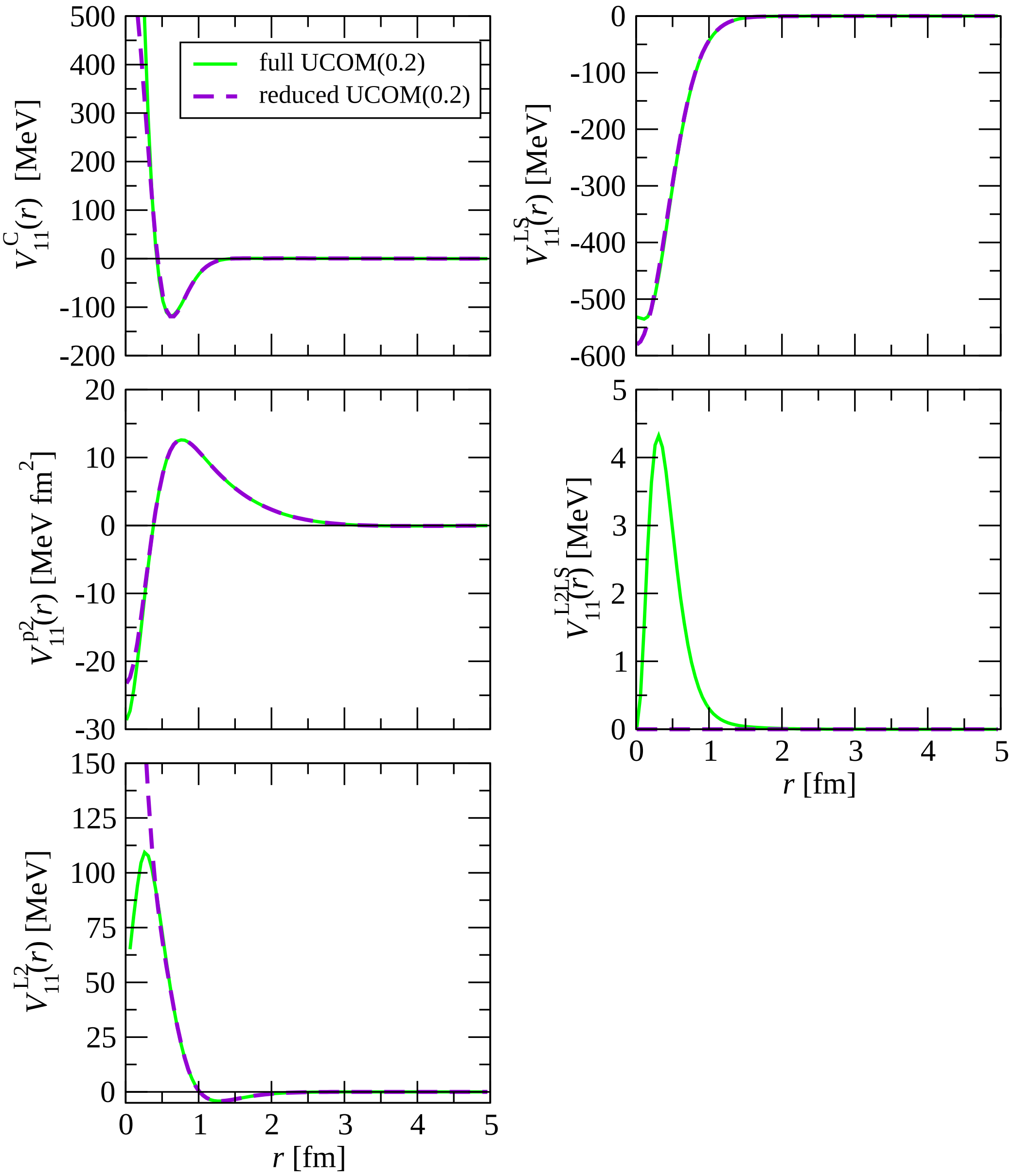

Figure C.9: Same as Fig. C.7, but for $S = 1$ and $T = 1$. The parameters from Tab. C.9 are used.

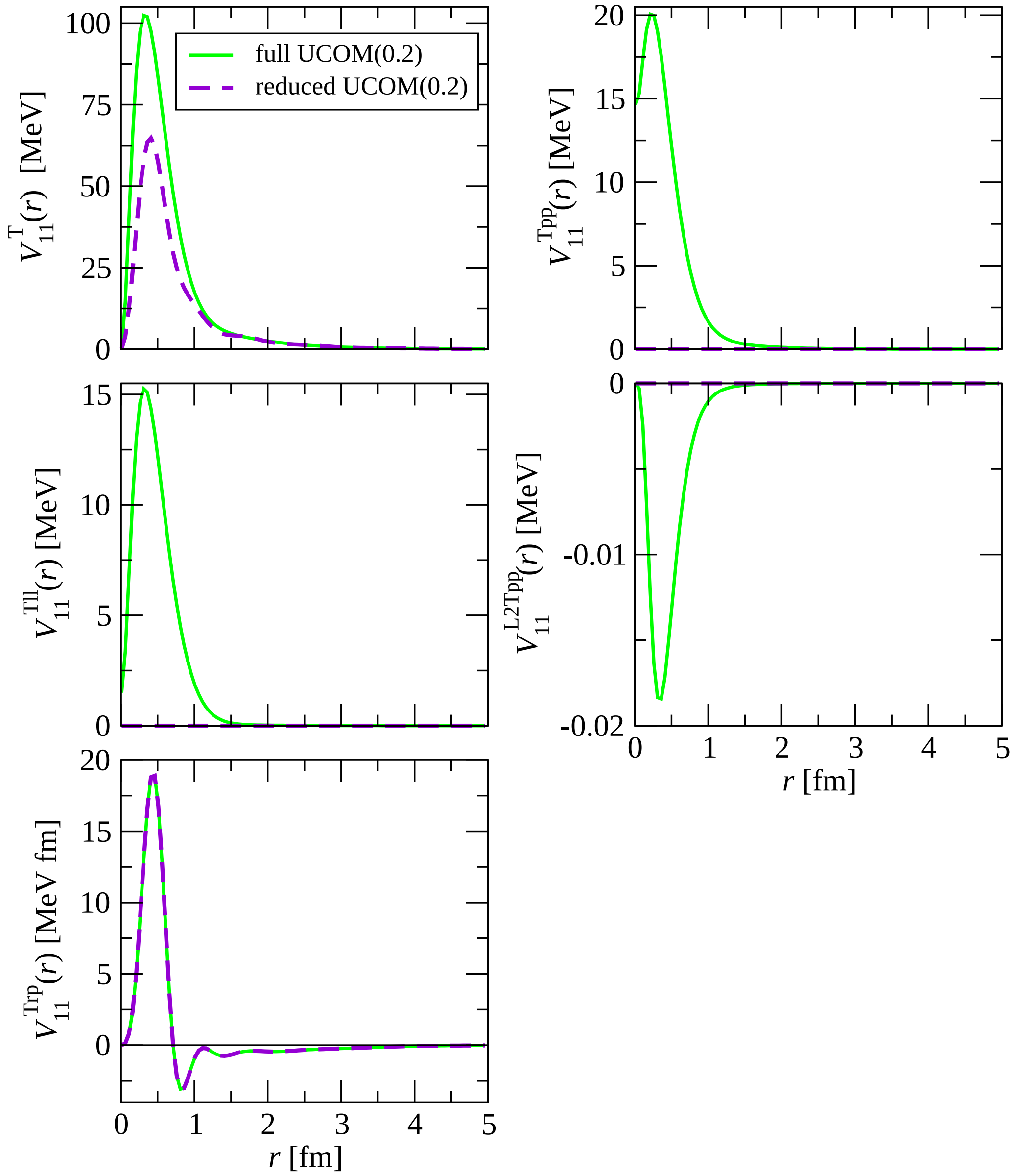

Figure C.10: Same as Fig. C.8, but for $S = 1$ and $T = 1$. The parameters from Tab. C.9 are used.

C.3.2 Partial wave matrix elements

To calculate the partial wave matrix elements Eq. (4.4) of the ansatz for the operator representation with local radial functions, it is necessary to find an analytical expression for the integrals in Eq. (4.5a) - (4.5c). In this work recursion formulas to calculate the matrix elements for a angular momentum quantum number $L+1$ by means of the matrix elements with L have been derived.

The integral

$$I^{r2\alpha}_{LL}(k,k') := \int_0^\infty dr\, r^2 j_L(kr)\exp\left[-\alpha r^2\right] j_L(k'r) \tag{C.7}$$

in Eqs. (4.5a) and (4.5b)[*] can be calculated as follows: For $L=0$ one finds

$$I^{r2\alpha}_{00}(k,k') = \int_0^\infty dr\, r^2 j_0(kr)\exp\left\{-\alpha r^2\right\} j_0(k'r) = \frac{\sqrt{\pi}}{4}\frac{1}{kk'\alpha^{1/2}}\left[e^{-\frac{(k-k')^2}{4\alpha}} - e^{-\frac{(k+k')^2}{4\alpha}}\right]. \tag{C.8}$$

Using the recursion relations for spherical Bessel functions [70]

$$j_{L+1}(kr) = \left(\frac{L}{kr} - \frac{1}{r}\frac{\partial}{\partial k}\right) j_L(kr) \tag{C.9}$$

and the fact that

$$\int_\alpha^\infty d\alpha' \exp\left\{-\alpha' r^2\right\} = \frac{1}{r^2}\exp\left\{-\alpha r^2\right\}, \tag{C.10}$$

one finds the recursion formula

$$I^{r2\alpha}_{L+1L+1}(k,k') = \int_\alpha^\infty d\alpha' \left(\frac{L^2}{kk'} - \frac{L}{k}\frac{\partial}{\partial k'} - \frac{L}{k'}\frac{\partial}{\partial k} + \frac{\partial}{\partial k}\frac{\partial}{\partial k'}\right) I^{r2\alpha'}_{LL}(k,k'). \tag{C.11}$$

This relation can be used to calculate successively the integrals $I^{r2\alpha}_{LL}(k,k')$ for all L.

The analytical solution of the integral

$$I^{r4\alpha}_{LL'}(k,k') := \int_0^\infty dr\, r^4 j_L(kr)\exp\left\{-\alpha r^2\right\} j_{L'}(k'r) \tag{C.12}$$

in Eq. (4.5a) can be calculated for $L = L'$ from the solution of integral $I^{r2\alpha}_{LL}(k,k')$ Eq. (C.7) by the derivative

$$I^{r4\alpha}_{LL}(k,k') = -\frac{\partial}{\partial\alpha} I^{r2\alpha}_{LL}(k,k'). \tag{C.13}$$

---

[*] α has to be replaced by $\frac{1}{2\kappa_\mu}$.

For for $L \neq L'$ one needs

$$\begin{aligned} I_{02}^{r4\,\alpha}(k,k') &= \int_0^\infty dr r^4 j_0(kr) \exp\left\{-\alpha r^2\right\} j_2(k'r) \\ &= \frac{\sqrt{\pi}}{16} \frac{1}{kk'^3 \alpha^{5/2}} \Big[\left(12\alpha^2 + 4k'^2\alpha - 6kk'\alpha - k'^4 - 2kk'^3 + (kk')^2\right) e^{-\frac{(k-k')^2}{4\alpha}} \\ &\qquad + \left(-12\alpha^2 - 4k'^2\alpha - 6kk'\alpha - k'^4 - 2kk'^3 - (kk')^2\right) e^{-\frac{(k+k')^2}{4\alpha}} \Big]. \end{aligned} \tag{C.14}$$

The other integrals can be derived by a recursion relation similar to Eq. (C.11):

$$I_{L+1L'+1}^{r4\,\alpha}(k,k') = \int_\alpha^\infty \mathrm{d}\alpha' \left(\frac{LL'}{kk'} - \frac{L}{k}\frac{\partial}{\partial k'} - \frac{L'}{k'}\frac{\partial}{\partial k} + \frac{\partial}{\partial k}\frac{\partial}{\partial k'} \right) I_{LL'}^{r4\,\alpha'}(k,k'). \tag{C.15}$$

The explicit analytical expressions for the lowest L of the integrals above can be found in Ref. [54].

For the matrix elements Eq. (4.5c) the solution of the integral

$$I_{LL'}^{r5d\,\alpha}(k,k') := \int_0^\infty dr r^5 \left(\frac{1}{r}\frac{\partial}{\partial r}(r j_L(kr)) j_{L'}(k'r) - \frac{1}{r} j_L(kr) \frac{\partial}{\partial r}(r j_{L'}(k'r)) \right) \exp\left\{-\alpha r^2\right\} \tag{C.16}$$

is required. For the integral $I_{02}^{r5d\,\alpha}(k,k')$ one finds

$$\begin{aligned} I_{02}^{r5d\,\alpha}(k,k') &= \int_0^\infty dr r^5 \left(\frac{1}{r}\frac{\partial}{\partial r}(r j_0(kr)) j_2(k'r) - \frac{1}{r} j_0(kr) \frac{\partial}{\partial r}(r j_2(k'r)) \right) \exp\left\{-\alpha r^2\right\} \\ &= \frac{\sqrt{\pi}}{4} \frac{1}{kk'^3\alpha^{7/2}} \Bigg[\Bigg(-6\alpha^3 + \frac{3}{2}\left(-k'^2 + 2kk' + k^2\right)\alpha^2 + \frac{3}{4}kk'\left(k'^2 - k^2\right)\alpha \\ &\qquad + \frac{1}{8}k'^2\left(-k'^4 + 2kk'^3 - 2k^3k' + k^4\right) \Bigg) e^{-\frac{(k-k')^2}{4\alpha}} \\ &\qquad + \Bigg(6\alpha^3 + \frac{3}{2}\left(k'^2 + 2kk' - k^2\right)\alpha^2 + \frac{3}{4}kk'\left(k'^2 - k^2\right)\alpha \\ &\qquad + \frac{1}{8}k'^2\left(k'^4 + 2kk'^3 - 2k^3k' - k^4\right) \Bigg) e^{-\frac{(k+k')^2}{4\alpha}} \Bigg]. \end{aligned} \tag{C.17}$$

The integrals for other L and L' can be obtained by a recursion relation analogous to Eq. (C.15):

$$I_{L+1L'+1}^{r5d\,\alpha}(k,k') = \int_\alpha^\infty \mathrm{d}\alpha' \left(\frac{LL'}{kk'} - \frac{L}{k}\frac{\partial}{\partial k'} - \frac{L'}{k'}\frac{\partial}{\partial k} + \frac{\partial}{\partial k}\frac{\partial}{\partial k'} \right) I_{LL'}^{r5d\,\alpha'}(k,k'). \tag{C.18}$$

C.3.3 FMD matrix elements

The FMD basis matrix elements Eq. (2.49) for the operators in the operator representation of the reduced UCOM potential Eq. (4.6) have been worked out previously [13, 67]. For the operators

$$\left\{ \underset{\sim}{1},\ \underset{\sim}{\vec{L}}^2,\ \underset{\sim}{\vec{L}} \cdot \underset{\sim}{\vec{S}},\ \underset{\sim}{S}_{12},\ S_{12}(\underset{\sim}{\vec{L}},\underset{\sim}{\vec{L}}) \right\}$$

the FMD matrix elements can be found in Appendix C.4.2, in which the FMD matrix elements for the nonlocal radial functions Eq. (4.9) are presented. The expressions for local radial functions can be obtained easily from these expressions by setting the parameter λ to zero. For calculations with the reduced set of operators the matrix elements of the momentum dependent operators in Eq. (4.6) are needed in addition. They are presented in the following:

The definitions

$$\begin{aligned}
\lambda_{kl} &= \frac{1}{a_k^\star + a_l} \\
\alpha_{kl} &= \frac{a_k^\star a_l}{a_k^\star + a_l} \\
\vec{\pi}_{kl} &= i\frac{\vec{b}_k^\star - \vec{b}_l}{a_k^\star + a_l} \\
\vec{\rho}_{kl} &= \frac{a_l \vec{b}_k^\star + a_k^\star \vec{b}_l}{a_k^\star + a_l} \\
R_{kl} &= \langle\, a_k \vec{b}_k \,|\, a_l \vec{b}_l \,\rangle = (2\pi\alpha_{kl})^{3/2} \exp\left\{ \frac{\vec{\pi}_{kl}^2}{2\lambda_{kl}} \right\}
\end{aligned}$$

and

$$\begin{aligned}
\lambda_{klmn} &= \lambda_{km} + \lambda_{ln} \\
\alpha_{klmn} &= \alpha_{km} + \alpha_{ln} \\
\vec{\pi}_{klmn} &= i\frac{1}{2}(\vec{\pi}_{km} - \vec{\pi}_{ln}) \\
\vec{\rho}_{klmn} &= \vec{\rho}_{km} - \vec{\rho}_{ln} \\
\beta_{klmn} &= i[(a_k^\star - a_m)\lambda_{km} + (a_l^\star - a_n)\lambda_{ln}] \\
\theta_{klmn} &= (a_k^\star \lambda_{km} + a_l^\star \lambda_{ln})(a_m \lambda_{km} + a_n \lambda_{ln})
\end{aligned}$$

are used, where a and $\vec{b}$ describe the spatial part of the FMD state (Eq. (2.50)). To calculate the matrix elements of the local radial function parameterized by a sum of gaussians (as in Eq. (C.6a)), one needs the FMD basis matrix element of the gaussian operator

$$\underset{\sim}{G}{}_\kappa^{\mathrm{loc}} = \exp\left\{ -\frac{\underset{\sim}{\vec{r}}{}^2}{2\kappa} \right\}, \tag{C.19}$$

which is given by

$$G_{klmn,\kappa}^{\mathrm{loc}} := \langle\, a_k \vec{b}_k, a_l \vec{b}_l \,|\, \underset{\sim}{G}{}_\kappa^{\mathrm{loc}} \,|\, a_m \vec{b}_m, a_n \vec{b}_n \,\rangle = R_{km} R_{ln} \left(\frac{\kappa}{\alpha_{klmn} + \kappa} \right)^{3/2} \exp\left\{ \frac{-\vec{\rho}_{\mathrm{klmn}}^{\,2}}{2(\alpha_{\mathrm{klmn}} + \kappa)} \right\}. \tag{C.20}$$

For the quadratic momentum dependent part of the interaction, one finds

$$\begin{aligned}
&\langle\, a_k \vec{b}_k, a_l \vec{b}_l \,|\, \frac{1}{2} \left[\underset{\sim}{\vec{p}}{}^2 \underset{\sim}{G}{}_\kappa^{\mathrm{loc}} + \underset{\sim}{G}{}_\kappa^{\mathrm{loc}} \underset{\sim}{\vec{p}}{}^2 \right] \,|\, a_m \vec{b}_m, a_n \vec{b}_n \,\rangle = \\
&\qquad \left\{ \vec{\pi}_{klmn}^2 - \frac{1}{2} \frac{\beta_{klmn}}{\alpha_{klmn} + \kappa} \vec{\rho}_{klmn} \cdot \vec{\pi}_{klmn} + \frac{1}{4} \frac{\theta_{klmn} - 1}{(\alpha_{klmn} + \kappa)^2} \vec{\rho}_{klmn}^{\,2} + \frac{3}{4} (\lambda_{klmn} - \frac{\theta_{klmn} - 1}{\alpha_{klmn} + \kappa}) \right\} G_{klmn,\kappa}^{\mathrm{loc}}
\end{aligned} \tag{C.21}$$

and for the momentum dependent tensor operator:

$$
\begin{aligned}
&\Big\langle\, a_k\vec{b}_k\chi_k, a_l\vec{b}_l\chi_l \Big| \frac{1}{2}\left[\underset{\sim}{p}_r\underset{\sim}{r}^3\underset{\sim}{G}^{\mathrm{loc}}_{\kappa} + \underset{\sim}{r}^3\underset{\sim}{G}^{\mathrm{loc}}_{\kappa}\underset{\sim}{p}_r\right] S_{12}(\underset{\sim}{\vec{r}},\underset{\sim}{\vec{p}}_{\Omega})\Big| a_m\vec{b}_m\chi_m, a_n\vec{b}_n\chi_n \,\Big\rangle = \frac{1}{2}\left(\frac{\kappa}{\alpha_{klmn}+\kappa}\right)^2 \cdot \\
&\quad\Bigg\{ S_{12}(\vec{\rho}_{klmn},\vec{\rho}_{klmn})\Bigg(\frac{1}{2}\frac{\kappa^2\beta_{klmn}\vec{\rho}^{\,2}_{klmn}\vec{\rho}_{klmn}\cdot\vec{\pi}_{klmn}}{(\alpha_{klmn}+\kappa)^3} - 2\left(\frac{\kappa\,\vec{\rho}_{klmn}\cdot\vec{\pi}_{klmn}}{\alpha_{klmn}+\kappa}\right)^2 \\
&\qquad + \frac{3}{8}\frac{\kappa\beta^2_{klmn}\vec{\rho}^{\,2}_{klmn}}{(\alpha_{klmn}+\kappa)^2} - \frac{1}{2}\left(1+9\frac{\kappa}{\alpha_{klmn}+\kappa}\right)\frac{\kappa\beta_{klmn}\vec{\rho}_{klmn}\cdot\vec{\pi}_{klmn}}{\alpha_{klmn}+\kappa} \\
&\qquad - 2\frac{\alpha_{klmn}\kappa\,\vec{\pi}^{2}_{klmn}}{\alpha_{klmn}+\kappa} + \frac{3}{2}\theta_{klmn} - \frac{21}{8}\frac{\kappa\beta^2_{klmn}}{\alpha_{klmn}+\kappa} - 3\Bigg) \\
&\qquad + S_{12}(\vec{\rho}_{klmn},\vec{\pi}_{klmn})\Bigg(- \frac{1}{2}\frac{\kappa^2\beta_{klmn}\left(\vec{\rho}^{\,2}_{klmn}\right)^2}{(\alpha_{klmn}+\kappa)^3} + 2\frac{\kappa^2\vec{\rho}^{\,2}_{klmn}(\vec{\rho}_{klmn}\cdot\vec{\pi}_{klmn})}{(\alpha_{klmn}+\kappa)^2} \\
&\qquad - \left(\frac{5}{2} - \frac{6\kappa}{\alpha_{klmn}+\kappa}\right)\frac{\kappa\beta_{klmn}\vec{\rho}^{\,2}_{klmn}}{\alpha_{klmn}+\kappa} + 6\frac{\alpha_{klmn}\kappa\,\vec{\rho}_{klmn}\cdot\vec{\pi}_{klmn}}{\alpha_{klmn}+\kappa} \\
&\qquad - \frac{3}{2}\left(2-7\frac{\kappa}{\alpha_{klmn}+\kappa}\right)\alpha_{klmn}\beta_{klmn}\Bigg) \\
&\qquad + 2\alpha_{klmn}S_{12}(\vec{\pi}_{klmn},\vec{\pi}_{klmn})\left(\frac{\kappa\vec{\rho}^{\,2}_{klmn}}{\alpha_{klmn}+\kappa} + 3\alpha_{klmn}\right)\Bigg\}\, G^{\mathrm{loc}}_{klmn,\kappa}.
\end{aligned}
\tag{C.22}
$$

C.4 Nonlocal radial functions

C.4.1 Parameterization

The nonlocal radial functions $\mathcal{V}^{P}_{ST}(\underset{\sim}{\vec{r}},\underset{\sim}{\vec{p}})$ used for the operator representation of the SRG transformed Argonne potential Eq.(4.16) have the gaussian form

$$
\mathcal{V}^{P}_{ST}(\underset{\sim}{\vec{r}},\underset{\sim}{\vec{p}}) = \sum_{\nu}\sum_{\mu}\gamma^{P}_{ST,\mu\nu}\left(\frac{\kappa_\mu}{\kappa_\mu-\lambda_\nu/4}\right)^{3/2} e^{-\frac{\lambda_\nu}{4}\underset{\sim}{\vec{p}}^{2}}\, e^{-\frac{\underset{\sim}{\vec{r}}^{2}}{2(\kappa_\mu-\lambda_\nu/4)}}\, e^{-\frac{\lambda_\nu}{4}\underset{\sim}{\vec{p}}^{2}},
\tag{C.23a}
$$

with $P \in \{C,\, L2,\, p2,\, LS,\, Tll\}$. The tensor part is parameterized by

$$
\underset{\sim}{\mathcal{V}}^{T}_{1T}(\underset{\sim}{\vec{r}},\underset{\sim}{\vec{p}},\underset{\sim}{S}_{12}) = \sum_{\nu}\sum_{\mu}\gamma^{T}_{1T,\mu\nu}\left(\frac{\kappa_\mu}{\kappa_\mu-\lambda_\nu/4}\right)^{3/2} e^{-\frac{\lambda_\nu}{4}\underset{\sim}{\vec{p}}^{2}}\,\underset{\sim}{\vec{r}}^{2}\, e^{-\frac{\underset{\sim}{\vec{r}}^{2}}{2(\kappa_\mu-\lambda_\nu/4)}}\,\underset{\sim}{S}_{12}\, e^{-\frac{\lambda_\nu}{4}\underset{\sim}{\vec{p}}^{2}}.
\tag{C.23b}
$$

The parameters κ and λ in the nonlocal functions $\mathcal{V}^{P}_{ST}(r,p)$ are chosen on a grid:

$$
\begin{aligned}
\kappa &= \{0.1, 0.2, 0.4, \cdots, 6.4\}\mathrm{fm}^2. \\
\lambda &= \left\{0, \frac{1}{16}, \frac{\sqrt{2}}{16}, \frac{1}{8}, \frac{\sqrt{2}}{8}, \frac{1}{4}\right\}\mathrm{fm}^2.
\end{aligned}
$$

For the tensor part, additional parameters λ are used:

$$
\lambda = \left\{0, \frac{1}{16}, \frac{\sqrt{2}}{16}, \frac{1}{8}, \frac{\sqrt{2}}{8}, \frac{1}{4}, \frac{1}{2}, 1\right\}\mathrm{fm}^2.
$$

The parameters $\gamma^{P}_{ST,\mu\nu}$ are obtained from the fit to the partial wave matrix elements of the SRG transformed Argonne potential (Sec. 4.3.2). They are listed in Tab. C.10 - C.12. The local part (see Eq. (4.20a) in Sec. 4.3.4) of the nonlocal radial functions defined by these parameters is shown in Fig. C.11 - C.13.

#	κ_μ [fm^2]	λ_ν [fm^2]	$\gamma^{C}_{00,\mu\nu}$ [MeV]	$\gamma^{L2}_{00,\mu\nu}$ [MeV]	$\gamma^{C}_{01,\mu\nu}$ [MeV]	$\gamma^{L2}_{01,\mu\nu}$ [MeV]
1	0.1	0	-0.354	0.175	1.274	0.085
2	0.1	0.0625	199.400	34.907	80.712	-79.083
3	0.1	$0.0625\sqrt{2}$	-589.220	-106.788	-253.511	274.948
4	0.1	0.125	687.656	97.828	295.114	-386.430
5	0.1	$0.125\sqrt{2}$	-447.496	14.244	-163.472	233.540
6	0.1	0.25	100.751	-10.690	43.289	43.898
7	0.2	0	0.519	-0.079	-1.071	0.006
8	0.2	0.0625	-669.182	-33.185	-333.431	78.324
9	0.2	$0.0625\sqrt{2}$	2054.904	101.836	966.856	-270.257
10	0.2	0.125	-2413.258	-103.219	-1021.111	385.037
11	0.2	$0.125\sqrt{2}$	1331.807	14.249	463.092	-283.396
12	0.2	0.25	-330.245	33.579	-76.043	91.575
13	0.4	0	-0.097	0.051	1.000	-0.023
14	0.4	0.0625	960.789	19.863	763.082	-55.461
15	0.4	$0.0625\sqrt{2}$	-2982.643	-67.028	-2320.760	177.281
16	0.4	0.125	3524.406	88.009	2655.761	-225.071
17	0.4	$0.125\sqrt{2}$	-1901.786	-54.009	-1372.166	142.468
18	0.4	0.25	400.827	12.340	273.420	-40.654
19	0.8	0	0.462	-0.018	-0.351	0.010
20	0.8	0.0625	-1021.460	-6.223	-1219.679	55.415
21	0.8	$0.0625\sqrt{2}$	3157.773	19.559	3807.582	-172.193
22	0.8	0.125	-3720.389	-23.598	-4533.528	205.876
23	0.8	$0.125\sqrt{2}$	2005.920	13.696	2477.248	-115.429
24	0.8	0.25	-422.197	-3.498	-531.635	26.581
25	1.6	0	-0.026	0.006	-0.212	0.016
26	1.6	0.0625	816.051	3.338	1260.061	-52.945
27	1.6	$0.0625\sqrt{2}$	-2477.968	-10.865	-3908.796	162.250
28	1.6	0.125	2840.704	13.627	4613.829	-188.753
29	1.6	$0.125\sqrt{2}$	-1472.506	-8.107	-2486.533	100.056
30	1.6	0.25	293.827	2.015	521.671	-20.631
31	3.2	0	0.008	0.000	0.053	-0.005
32	3.2	0.0625	-480.674	-4.070	-794.536	32.084
33	3.2	$0.0625\sqrt{2}$	1392.349	14.322	2368.543	-93.946
34	3.2	0.125	-1491.812	-19.482	-2642.675	102.207
35	3.2	$0.125\sqrt{2}$	704.899	12.175	1320.552	-49.320
36	3.2	0.25	-124.771	-2.948	-251.959	8.98
37	6.4	0	0.009	0.000	-0.009	0.001
38	6.4	0.0625	170.732	2.648	284.023	-10.435
39	6.4	$0.0625\sqrt{2}$	-461.899	-9.368	-790.007	27.648
40	6.4	0.125	456.658	12.448	810.900	-26.436
41	6.4	$0.125\sqrt{2}$	-197.352	-7.397	-368.299	10.815
42	6.4	0.25	31.861	1.670	63.392	-1.592

Table C.10: The parameters $\gamma^{P}_{ST,\mu}$ used in the operator representation of the SRG transformed Argonne potential; for $S = 0$ and $T = 0$ and 1.

#	κ_μ [fm^2]	λ_ν [fm^2]	$\gamma^{C}_{10,\mu\nu}$ [MeV]	$\gamma^{L2}_{10,\mu\nu}$ [MeV]	$\gamma^{LS}_{10,\mu\nu}$ [MeV]	$\gamma^{T}_{10,\mu\nu}$ [MeV]	$\gamma^{Tll}_{10,\mu\nu}$ [MeV]
1	0.1	0	1.163	0.188	0.084	0.028	0.010
2	0.1	0.0625	60.477	-18.761	14.477	-2224.907	5.417
3	0.1	$0.0625\sqrt{2}$	-202.647	48.938	-57.286	9118.312	-30.511
4	0.1	0.125	253.816	-29.021	121.552	-16270.781	51.544
5	0.1	$0.125\sqrt{2}$	-156.223	-67.322	-206.426	16635.170	28.518
6	0.1	0.25	47.838	166.718	279.788	-10429.143	-260.694
7	0.2	0	-0.983	-0.066	0.018	-0.187	-0.029
8	0.2	0.0625	-198.067	16.689	-19.471	2588.538	16.985
9	0.2	$0.0625\sqrt{2}$	576.382	-58.149	39.180	-10251.972	-39.741
1.	0.2	0.125	-596.010	88.375	-5.311	17157.919	1.764
11	0.2	$0.125\sqrt{2}$	250.970	-72.261	-35.153	-15366.001	73.516
12	0.2	0.25	-34.736	24.079	19.027	6934.151	-57.186
13	0.2	0.5	0	0	0	-1814.246	0
14	0.4	0	0.984	0.012	0.078	0.111	0.002
15	0.4	0.0625	470.916	-9.705	23.742	-1255.732	-27.186
16	0.4	$0.0625\sqrt{2}$	-1441.411	31.441	-57.032	4909.887	96.789
17	0.4	0.125	1655.919	-43.426	37.133	-8050.106	-135.080
18	0.4	$0.125\sqrt{2}$	-853.757	32.743	4.654	6967.804	85.532
19	0.4	0.25	167.796	-11.632	-8.532	-2963.242	-19.938
20	0.4	0.5	0	0	0	519.993	0
21	0.4	1	0	0	0	-224.632	0
22	0.8	0	-0.532	0.028	-0.096	-0.099	0.019
23	0.8	0.0625	-808.456	15.884	-27.825	302.814	6.946
24	0.8	$0.0625\sqrt{2}$	2535.787	-50.869	72.488	-1145.432	-25.089
25	0.8	0.125	-3037.245	64.035	-60.410	1800.875	36.151
26	0.8	$0.125\sqrt{2}$	1673.714	-39.179	12.474	-1477.978	-24.251
27	0.8	0.25	-363.726	10.282	3.496	587.673	6.292
28	0.8	0.5	0	0	0	-83.488	0
29	0.8	1	0	0	0	17.739	0
30	1.6	0	-0.143	0.013	0.014	-0.015	-0.011
31	1.6	0.0625	877.669	-20.798	41.202	-54.674	-1.741
32	1.6	$0.0625\sqrt{2}$	-2725.908	63.920	-122.639	203.938	6.254
33	1.6	0.125	3225.736	-75.039	136.543	-314.061	-9.375
34	1.6	$0.125\sqrt{2}$	-1747.030	40.500	-68.018	251.531	6.810
35	1.6	0.25	369.710	-8.597	12.881	-97.649	-1.954
36	1.6	0.5	0	0	0	13.088	0
37	1.6	1	0	0	0	-2.274	0
38	3.2	0	0.040	-0.004	-0.002	0	0.002
39	3.2	0.0625	-566.136	12.637	-34.116	7.275	2.169
40	3.2	$0.0625\sqrt{2}$	1690.518	-36.299	103.741	-25.815	-7.193
41	3.2	0.125	-1892.06	38.500	-119.353	37.644	9.587
42	3.2	$0.125\sqrt{2}$	950.464	-17.970	62.313	-28.490	-6.136
43	3.2	0.25	-182.847	3.135	-12.583	10.472	1.575
44	3.2	0.5	0	0	0	-1.293	0
45	3.2	1	0	0	0	0.212	0
46	6.4	0	-0.008	0.001	0.000	0.000	0.000
47	6.4	0.0625	208.295	-3.655	14.161	-0.737	-1.279
48	6.4	$0.0625\sqrt{2}$	-583.277	8.834	-41.809	2.523	4.004
49	6.4	0.125	604.139	-7.193	46.312	-3.431	-4.797
50	6.4	$0.125\sqrt{2}$	-277.674	2.122	-23.091	2.288	2.641
51	6.4	0.25	48.523	-0.109	4.427	-0.690	-0.570
52	6.4	0.5	0	0	0	0.055	0
53	6.4	1	0	0	0	-0.009	0

Table C.11: The same as in Tab. C.10, but for $S = 1$ and $T = 0$.

#	κ_μ [fm^2]	λ_ν [fm^2]	$\gamma^{C}_{11,\mu\nu}$ [MeV]	$\gamma^{L2}_{11,\mu\nu}$ [MeV]	$\gamma^{LS}_{11,\mu\nu}$ [MeV]	$\gamma^{T}_{11,\mu\nu}$ [MeV]	$\gamma^{Tll}_{11,\mu\nu}$ [MeV]
1	0.1	0	-0.207	0.456	-0.022	-0.259	0.016
2	0.1	0.0625	34.208	81.616	-336.034	-830.067	-53.768
3	0.1	$0.0625\sqrt{2}$	-69.979	-262.861	1046.585	3371.103	183.861
4	0.1	0.125	118.678	281.046	-1231.377	-6024.385	-259.474
5	0.1	$0.125\sqrt{2}$	-318.820	-39.282	639.868	6386.518	208.572
6	0.1	0.25	219.159	-23.659	-108.319	-4706.115	-128.558
7	0.2	0	0.332	-0.187	-0.058	0.083	-0.034
8	0.2	0.0625	-406.095	-91.353	705.883	470.03	88.657
9	0.2	$0.0625\sqrt{2}$	1167.766	290.831	-2233.956	-1771.800	-290.185
10	0.2	0.125	-1255.071	-330.581	2706.786	2778.446	361.344
11	0.2	$0.125\sqrt{2}$	653.419	121.150	-1505.823	-2280.277	-197.919
12	0.2	0.25	-209.574	33.744	325.693	912.818	36.670
13	0.2	0.5	0	0	0	-136.085	0
14	0.4	0	0.016	0.123	-0.028	-0.024	0.021
15	0.4	0.0625	724.467	66.162	-766.867	-175.497	-89.209
16	0.4	$0.0625\sqrt{2}$	-2173.118	-219.406	2432.767	663.823	304.73
17	0.4	0.125	2438.11	281.615	-2961.339	-1041.650	-407.058
18	0.4	$0.125\sqrt{2}$	-1214.983	-168.730	1664.601	848.679	253.282
19	0.4	0.25	227.059	39.480	-369.343	-331.000	-61.014
20	0.4	0.5	0	0	0	42.360	0
21	0.4	1	0	0	0	0.690	0
22	0.8	0	0.065	-0.021	-0.340	0.013	-0.042
23	0.8	0.0625	-848.893	-39.660	641.894	47.389	42.210
24	0.8	$0.0625\sqrt{2}$	2573.589	125.511	-2003.879	-180.168	-143.783
25	0.8	0.125	-2944.568	-151.849	2396.111	284.569	195.526
26	0.8	$0.125\sqrt{2}$	1522.445	84.745	-1320.940	-233.603	-128.435
27	0.8	0.25	-302.655	-18.713	287.291	91.812	34.828
28	0.8	0.5	0	0	0	-12.165	0
29	0.8	1	0	0	0	2.565	0
30	1.6	0	-0.049	0.008	0.053	0.005	0.005
31	1.6	0.0625	779.701	25.603	-428.411	-5.911	-4.934
32	1.6	$0.0625\sqrt{2}$	-2356.153	-80.317	1298.854	22.422	11.901
33	1.6	0.125	2683.879	96.029	-1486.738	-35.303	-9.761
34	1.6	$0.125\sqrt{2}$	-1380.197	-52.757	770.148	28.650	3.124
35	1.6	0.25	272.791	11.452	-153.959	-10.939	-0.363
36	1.6	0.5	0	0	0	1.267	0
37	1.6	1	0	0	0	-0.204	0
38	3.2	0	0.005	-0.001	-0.003	0	0
39	3.2	0.0625	-513.535	-16.399	234.161	0.068	0.884
40	3.2	$0.0625\sqrt{2}$	1509.810	51.753	-676.956	-0.383	0.556
41	3.2	0.125	-1652.980	-62.328	722.784	0.92	-5.507
42	3.2	$0.125\sqrt{2}$	804.990	34.385	-339.415	-1.079	5.986
43	3.2	0.25	-148.285	-7.415	59.435	0.555	-1.917
44	3.2	0.5	0	0	0	-0.098	0
45	3.2	1	0	0	0	0.018	0
46	6.4	0	0	0	0	0	0
47	6.4	0.0625	194.403	7.429	-84.722	0.515	-0.167
48	6.4	$0.0625\sqrt{2}$	-540.511	-23.652	232.459	-1.702	-1.058
49	6.4	0.125	553.949	28.561	-234.059	2.247	3.220
50	6.4	$0.125\sqrt{2}$	-250.573	-15.656	103.483	-1.476	-2.756
51	6.4	0.25	42.729	3.320	-17.162	0.442	0.760
52	6.4	0.5	0	0	0	-0.028	0
53	6.4	1	0	0	0	0.002	0

Table C.12: The same as in Tab. C.10, but for $S = 1$ and $T = 1$.

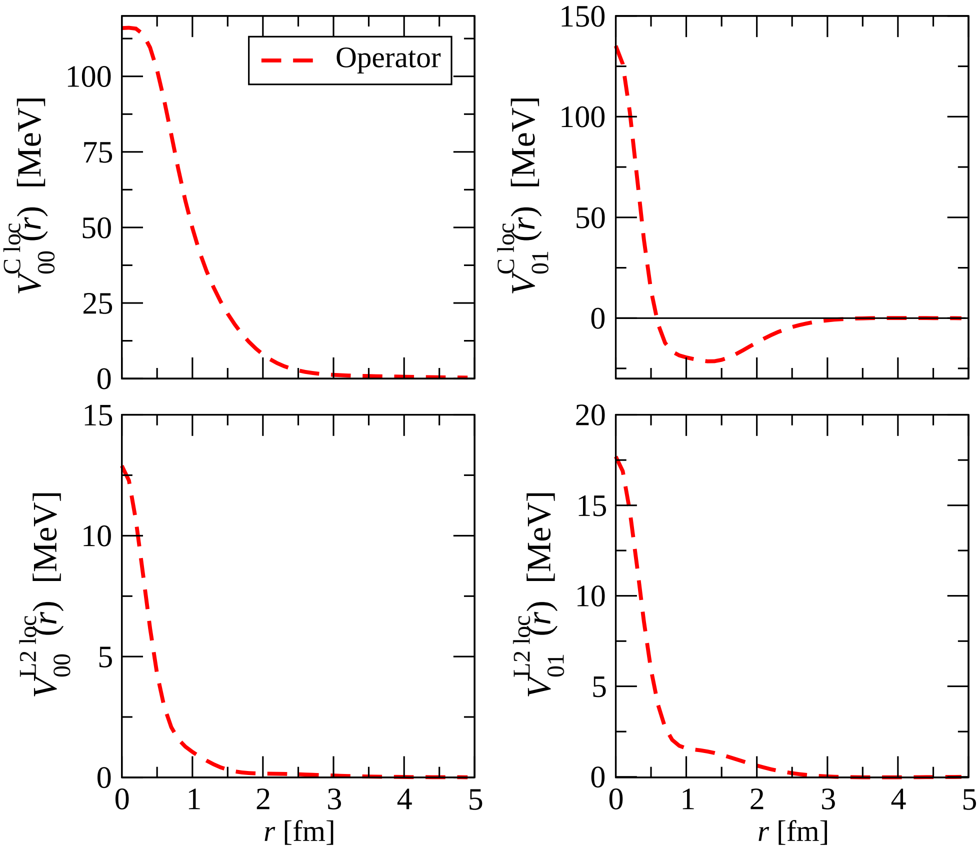

Figure C.11: The local part of the radial functions of the SRG transformed Argonne potential for $S = 0$ and $T = 0$ and 1. The parameterization Eq. $(\mathrm{C.23a})$ and the parameters from Tab. C.10 with $\lambda = 0$ are used.

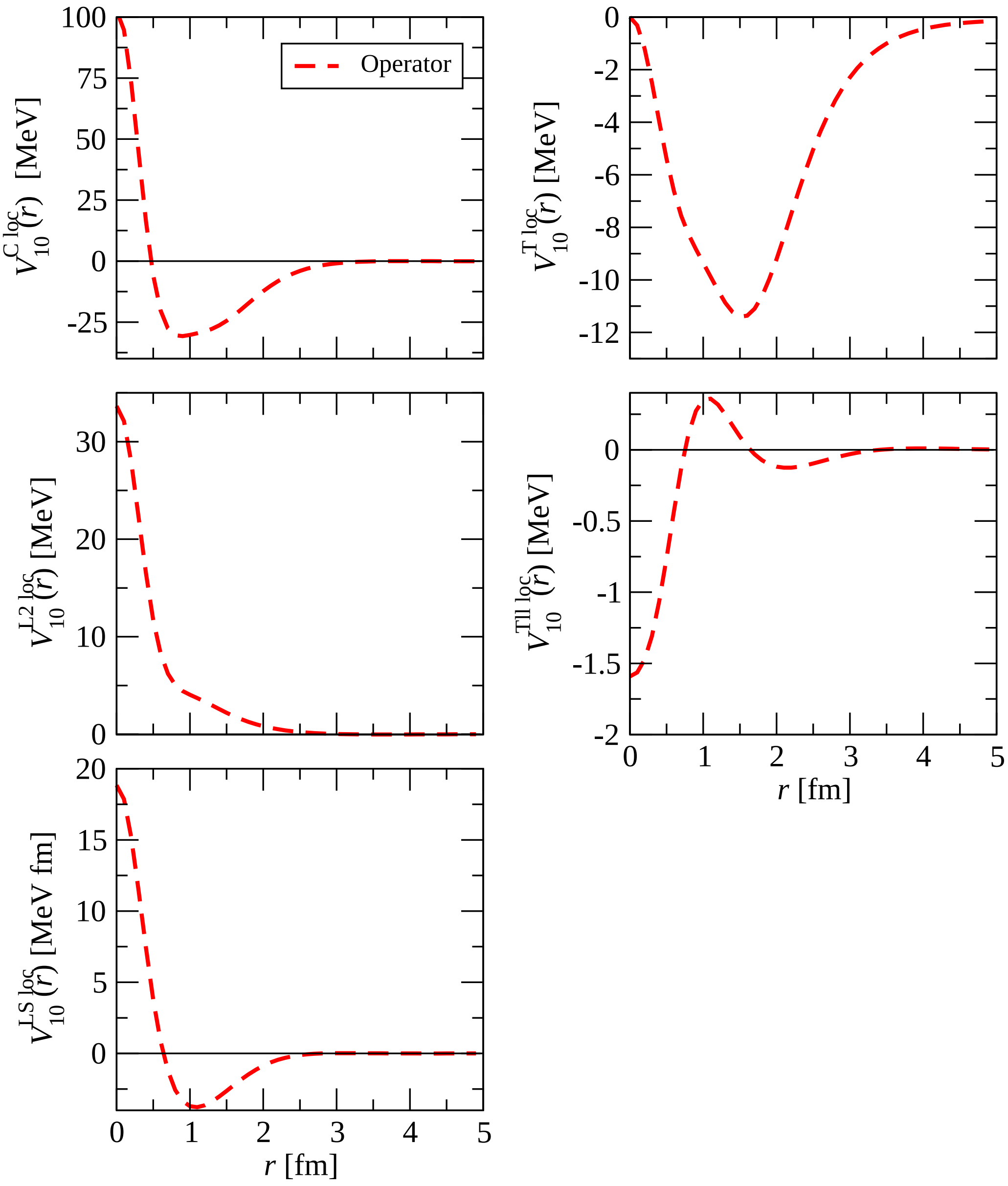

Figure C.12: Same as Fig. C.11, but for $S = 1$ and $T = 0$. The parameters from Tab. C.11 with $\lambda = 0$ are used.

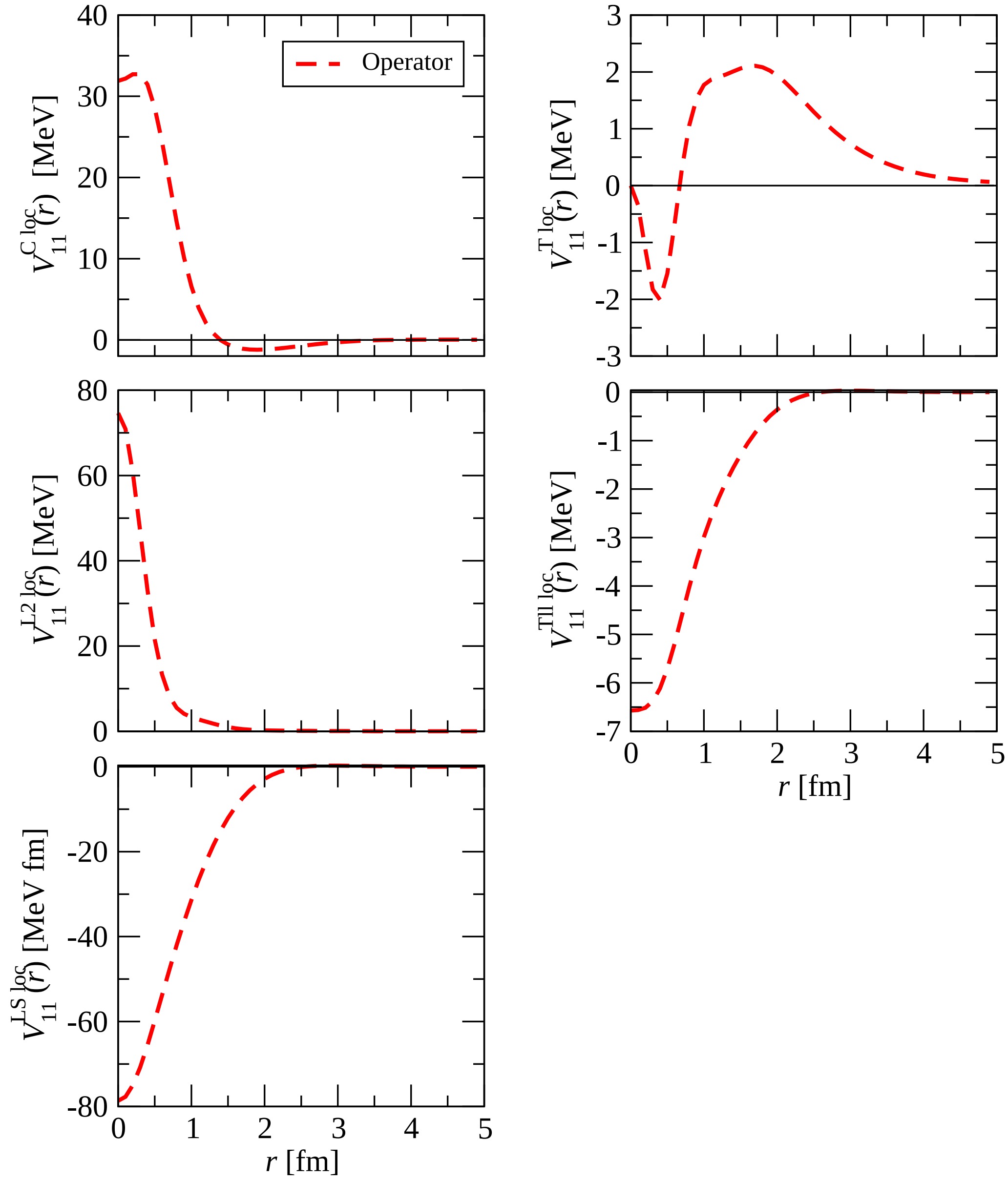

Figure C.13: Same as Fig. C.11, but for $S = 1$ and $T = 1$. The parameters from Tab. C.12 with $\lambda = 0$ are used.

C.4.2 FMD matrix elements

The FMD single-particle basis is given by

$$\left| a_k \, \vec{b}_k, \chi_k; \xi \right\rangle, \tag{C.24}$$

where

$$\left\langle \vec{r} \,\middle|\, a_k \, \vec{b}_k \right\rangle = \exp\left\{ -\frac{1}{2a_k} (\vec{r} - \vec{b}_k)^2 \right\} \tag{C.25}$$

and χ_k and ξ describe the spin and isospin orientation of the nucleon.

In this section the FMD matrix elements for the operator representation with nonlocal radial functions (see Eq. (4.16)) are derived.

The nonlocal radial function $\mathscr{V}(\utilde{\vec{r}}, \utilde{\vec{p}})$ is parameterized by a sum of gaussians of the position and momentum operator:

$$\mathscr{V}(\utilde{\vec{r}}, \utilde{\vec{p}}) = \sum_{\nu} \sum_{\mu} \gamma_{\mu\nu} \left(\frac{\kappa_\mu}{\kappa_\mu - \lambda_\nu / 4} \right)^{3/2} e^{-\frac{\lambda_\nu}{4} \utilde{\vec{p}}^2} \, e^{-\frac{\utilde{\vec{r}}^2}{2(\kappa_\mu - \lambda_\nu/4)}} \, e^{-\frac{\lambda_\nu}{4} \utilde{\vec{p}}^2} . \tag{C.26}$$

To calculate the matrix elements of this nonlocal function in the FMD basis, it is sufficient to calculate the matrix element of the operator

$$\utilde{G}^{\text{nonloc}}_{\kappa\lambda} = \left(\frac{\kappa}{\kappa - \lambda/4} \right)^{3/2} e^{-\frac{\lambda}{4} \utilde{\vec{p}}^2} \, e^{-\frac{\utilde{\vec{r}}^2}{2(\kappa - \lambda/4)}} \, e^{-\frac{\lambda}{4} \utilde{\vec{p}}^2} . \tag{C.27}$$

The FMD matrix element of the radial function Eq. (C.26) is then given by a linear combination of the FMD matrix elements of the gaussian operator Eq. (C.27) with the parameters κ_μ and λ_ν and the factors $\gamma_{\mu\nu}$ from Eq. (C.26).

Central potential

In the following, the definitions

$$\begin{aligned}
\lambda_{kl} &= \frac{1}{a_k^\star + a_l} \\
\alpha_{kl} &= \frac{a_k^\star a_l}{a_k^\star + a_l} \\
\vec{\pi}_{kl} &= i \frac{\vec{b}_k^\star - \vec{b}_l}{a_k^\star + a_l} \\
\vec{\rho}_{kl} &= \frac{a_l \vec{b}_k^\star + a_k^\star \vec{b}_l}{a_k^\star + a_l} \\
R_{kl} &= \left\langle a_k \vec{b}_k \,\middle|\, a_l \vec{b}_l \right\rangle = (2\pi\alpha_{kl})^{3/2} \exp\left\{ \frac{\vec{\pi}_{kl}^2}{2\lambda_{kl}} \right\}
\end{aligned}$$

and

$$
\begin{aligned}
\lambda_{klmn} &= \lambda_{km} + \lambda_{ln} \\
\alpha_{klmn} &= \alpha_{km} + \alpha_{ln} \\
\vec{\pi}_{klmn} &= i\frac{1}{2}(\vec{\pi}_{km} - \vec{\pi}_{ln}) \\
\vec{\rho}_{klmn} &= \vec{\rho}_{km} - \vec{\rho}_{ln} \\
\beta_{klmn} &= i[(a_k^\star - a_m)\lambda_{km} + (a_l^\star - a_n)\lambda_{ln}] \\
\theta_{klmn} &= (a_k^\star\lambda_{km} + a_l^\star\lambda_{ln})(a_m\lambda_{km} + a_n\lambda_{ln}) \\
A^{(rr)}_{klmn} &= \frac{1}{2}\left(\frac{1}{a_k^\star + a_n} + \frac{1}{a_l^\star + a_m}\right) = \frac{1}{2}\lambda_{klnm} \\
A^{(rp)}_{klmn} &= (a_k^\star - a_n)\lambda_{kn} + (a_l^\star - a_m)\lambda_{lm} = -i\beta_{klnm} \\
A^{(pp)}_{klmn} &= 2\left(\frac{a_k^\star a_n}{a_k^\star + a_n} + \frac{a_l^\star a_m}{a_l^\star + a_m}\right) = 2\alpha_{klnm}
\end{aligned}
$$

are used.

The matrix element $G^{\text{nonloc}}_{klmn,\kappa\lambda} := \left\langle\, a_k\vec{b}_k, a_l\vec{b}_l \,\middle|\, \underset{\sim}{G}{}^{\text{nonloc}}_{\kappa\lambda} \,\middle|\, a_m\vec{b}_m, a_n\vec{b}_n \,\right\rangle$ is calculated by using the Wigner representation [68] of the FMD basis states and the operator $\underset{\sim}{G}{}^{\text{nonloc}}_{\kappa\lambda}$:

$$
\begin{aligned}
\mathscr{P}_{klmn}(\vec{r},\vec{p}) &= \int d^3y \left\langle\, a_k\vec{b}_k, a_l\vec{b}_l \,\middle|\, \vec{r} + \vec{y}/2 \,\right\rangle \left\langle\, \vec{r} - \vec{y}/2 \,\middle|\, a_m\vec{b}_m, a_n\vec{b}_n \,\right\rangle e^{i\vec{p}\vec{y}} \\
&= \exp\Big\{ -A^{(rr)}_{klmn}\left(\vec{r} - \vec{\rho}_{klmn}\right)^2 + iA^{(rp)}_{klmn}\left(\vec{r} - \vec{\rho}_{klmn}\right)\left(\vec{p} - \vec{\pi}_{klmn}\right) - A^{(pp)}_{klmn}\left(\vec{p} - \vec{\pi}_{klmn}\right)^2 \Big\}
\end{aligned}
\tag{C.28a}
$$

$$
\begin{aligned}
\mathscr{G}_{\kappa\lambda}(\vec{r},\vec{p}) &= \int d^3y \left\langle\, \vec{r} - \vec{y}/2 \,\middle|\, \underset{\sim}{G}{}^{\text{nonloc}}_{\kappa\lambda} \,\middle|\, \vec{r} + \vec{y}/2 \,\right\rangle e^{i\vec{p}\vec{y}} \\
&= e^{-\frac{1}{2\kappa}\vec{r}^2}\, e^{-\frac{\lambda}{2}\vec{p}^2}.
\end{aligned}
\tag{C.28b}
$$

The matrix element is then given by

$$
\begin{aligned}
G^{\text{nonloc}}_{klmn,\kappa\lambda} &= \int d^3r\, d^3p\, \mathscr{P}_{klmn}(\vec{r},\vec{p})\, \mathscr{G}_{\kappa\lambda}(\vec{r},\vec{p}) \\
&= R_{km}R_{ln}\left(\frac{2A^{(pp)}_{klmn}\kappa}{\alpha_{klmn}(2A^{(pp)}_{klmn} + \lambda) + 2(A^{(pp)}_{klmn} + \alpha_{klmn}A^{(rr)}_{klmn}\lambda)\kappa}\right)^{3/2} \cdot \\
&\quad \exp\left\{\frac{-(A^{(pp)}_{klmn} + \alpha_{klmn}A^{(rr)}_{klmn}\lambda)\vec{\rho}^{\,2}_{klmn} + i\alpha_{klmn}A^{(rp)}_{klmn}\lambda\vec{\rho}_{klmn}\cdot\vec{\pi}_{klmn} - (\alpha_{klmn} + \kappa)A^{(pp)}_{klmn}\lambda\vec{\pi}^{\,2}_{klmn}}{\alpha_{klmn}(2A^{(pp)}_{klmn} + \lambda) + 2(A^{(pp)}_{klmn} + \alpha_{klmn}A^{(rr)}_{klmn}\lambda)\kappa}\right\}.
\end{aligned}
\tag{C.29}
$$

For $\lambda = 0$, the expressions for the nonlocal parameterization reduce to the expressions for the FMD matrix elements for local radial functions [13, 67]. Eq. (C.29) then leads to:

$$
G^{\text{loc}}_{klmn,\kappa\lambda} = R_{km}R_{ln}\left(\frac{\kappa}{\alpha_{klmn} + \kappa}\right)^{3/2} \exp\Big\{\frac{-\vec{\rho}^{\,2}_{\text{klmn}}}{2(\alpha_{\text{klmn}} + \kappa)}\Big\}. \tag{C.30}
$$

Spin-Orbit potential

The result for the matrix element $G^{\text{nonloc}}_{klmn,\kappa\lambda}$ (Eq. (C.29)) are used to calculate the matrix elements for other terms of the operator representation. For this, the operators have to be rewritten in terms of the parameters a and $\vec{b}$ of the FMD basis states Eq. (C.24). In case of the spin orbit operator this can be done as follows:

$$\begin{aligned}
&\langle\, a_k\vec{b}_k\chi_k, a_l\vec{b}_l\chi_l \,\big|\underset{\sim}{G}^{\text{nonloc}}_{\kappa\lambda}(\underset{\sim}{\vec{L}}\cdot\underset{\sim}{\vec{S}})\big|\, a_m\vec{b}_m\chi_m, a_n\vec{b}_n\chi_n \,\rangle = \\
&= \int d^3r\, d^3r'\; e^{-\frac{1}{2a_k^*}(\vec{r}-\vec{b}_k^*)^2}\, e^{-\frac{1}{2a_l^*}(\vec{r}-\vec{b}_l^*)^2}\, \langle\, \vec{r}\,\big|\underset{\sim}{G}^{\text{nonloc}}_{\kappa\lambda}\big|\,\vec{r}'\,\rangle\,(\vec{r}'\times\vec{\nabla}_{\vec{r}'})\cdot\vec{S}_{klmn}\, e^{-\frac{1}{2a_m}(\vec{r}'-\vec{b}_m)^2}\, e^{-\frac{1}{2a_n}(\vec{r}'-\vec{b}_n)^2} \\
&= \int d^3r\, d^3r'\; e^{-\frac{1}{2a_k^*}(\vec{r}-\vec{b}_k^*)^2}\, e^{-\frac{1}{2a_l^*}(\vec{r}-\vec{b}_l^*)^2}\, \langle\, \vec{r}\,\big|\underset{\sim}{G}^{\text{nonloc}}_{\kappa\lambda}\big|\,\vec{r}'\,\rangle \\
&\qquad \frac{i}{2}\Big(a_m\frac{\partial}{\partial\vec{b}_m} - a_n\frac{\partial}{\partial\vec{b}_n} + \vec{b}_m - \vec{b}_n\Big)\times\Big(\frac{\partial}{\partial\vec{b}_n} - \frac{\partial}{\partial\vec{b}_m}\Big)\cdot\vec{S}_{klmn}\, e^{-\frac{1}{2a_m}(\vec{r}'-\vec{b}_m)^2}\, e^{-\frac{1}{2a_n}(\vec{r}'-\vec{b}_n)^2} \\
&= \frac{i}{2}\Big(a_m\frac{\partial}{\partial\vec{b}_m} - a_n\frac{\partial}{\partial\vec{b}_n} + \vec{b}_m - \vec{b}_n\Big)\times\Big(\frac{\partial}{\partial\vec{b}_n} - \frac{\partial}{\partial\vec{b}_m}\Big)\cdot\vec{S}_{klmn} \\
&\qquad \int d^3r\, d^3r'\;\langle\, a_k\vec{b}_k, a_l\vec{b}_l\,\big|\,\vec{r}\,\rangle\langle\,\vec{r}\,\big|\underset{\sim}{G}^{\text{nonloc}}_{\kappa\lambda}\big|\,\vec{r}'\,\rangle\langle\,\vec{r}'\,\big|\, a_m\vec{b}_m, a_n\vec{b}_n\,\rangle \\
&= \frac{i}{2}\Big(a_m\frac{\partial}{\partial\vec{b}_m} - a_n\frac{\partial}{\partial\vec{b}_n} + \vec{b}_m - \vec{b}_n\Big)\times\Big(\frac{\partial}{\partial\vec{b}_n} - \frac{\partial}{\partial\vec{b}_m}\Big)\cdot\vec{S}_{klmn}\, G^{\text{nonloc}}_{klmn,\kappa\lambda}
\end{aligned} \tag{C.31}$$

with

$$\vec{S}_{klmn} = \langle\, \chi_k, \chi_l \,\Big|\frac{1}{2}\Big(\underset{\sim}{\vec{\sigma}}(1)+\underset{\sim}{\vec{\sigma}}(2)\Big)\Big|\, \chi_m, \chi_n \,\rangle. \tag{C.32}$$

In the third step, one uses that

$$\begin{aligned}
&\frac{i}{2}\Big(a_m\frac{\partial}{\partial\vec{b}_m} - a_n\frac{\partial}{\partial\vec{b}_n} + \vec{b}_m - \vec{b}_n\Big)\times\Big(\frac{\partial}{\partial\vec{b}_n} - \frac{\partial}{\partial\vec{b}_m}\Big)\cdot\vec{S}_{klmn}\, e^{-\frac{1}{2a_m}(\vec{r}'-\vec{b}_m)^2}\, e^{-\frac{1}{2a_n}(\vec{r}'-\vec{b}_n)^2} = \\
&\qquad (\vec{r}'\times\vec{\nabla}_{\vec{r}'})\cdot\vec{S}_{klmn}\, e^{-\frac{1}{2a_m}(\vec{r}'-\vec{b}_m)^2}\, e^{-\frac{1}{2a_n}(\vec{r}'-\vec{b}_n)^2},
\end{aligned} \tag{C.33}$$

so that the integration can be carried out first and leads to G^{nonloc}_{klmn} from Eq. (C.29). Afterwards, the derivative of G^{nonloc}_{klmn} has to be calculated. A similar method is applied for the other operators presented in this section.

With the definitions

$$A_1 = \frac{2A^{(pp)}_{klmn}\kappa + 2\alpha_{klmn}A^{(rr)}_{klmn}\kappa\lambda + 1/2\alpha_{klmn}A^{(rp)}_{klmn}\lambda}{\alpha_{klmn}(2A^{(pp)}_{klmn}+\lambda) + 2(A^{(pp)}_{klmn}+\alpha_{klmn}A^{(rr)}_{klmn}\lambda)\kappa} \tag{C.34a}$$

$$B_1 = i\frac{2\alpha_{klmn}A^{(pp)}_{klmn}\lambda + (1+\frac{i}{2}\beta_{klmn})A^{(pp)}_{klmn}\kappa\lambda}{\alpha_{klmn}(2A^{(pp)}_{klmn}+\lambda) + 2(A^{(pp)}_{klmn}+\alpha_{klmn}A^{(rr)}_{klmn}\lambda)\kappa} \tag{C.34b}$$

$$A_2 = \frac{2(1-\frac{i}{2}\beta_{klmn})A^{(pp)}_{klmn} + 2\alpha_{klmn}A^{(rr)}_{klmn}\lambda}{\alpha_{klmn}(2A^{(pp)}_{klmn}+\lambda) + 2(A^{(pp)}_{klmn}+\alpha_{klmn}A^{(rr)}_{klmn}\lambda)\kappa} \tag{C.34c}$$

$$B_2 = i\frac{4(\alpha_{klmn}+\kappa)A^{(pp)}_{klmn} - \alpha_{klmn}A^{(rp)}_{klmn}\lambda}{\alpha_{klmn}(2A^{(pp)}_{klmn}+\lambda)+2(A^{(pp)}_{klmn}+\alpha_{klmn}A^{(rr)}_{klmn}\lambda)\kappa}, \tag{C.34d}$$

the spin-orbit interaction matrix element reads:

$$\begin{aligned}
\langle\, a_k\vec{b}_k\chi_k, a_l\vec{b}_l\chi_l \,\Big|\underset{\sim}{G}{}^{\text{nonloc}}_{\kappa\lambda}(\underset{\sim}{\vec{L}}\cdot\underset{\sim}{\vec{S}})\Big|\, a_m\vec{b}_m\chi_m, a_n\vec{b}_n\chi_n \,\rangle = \\
&= -\frac{1}{2i}\Big(a_m\frac{\partial}{\partial\vec{b}_m} - a_n\frac{\partial}{\partial\vec{b}_n} + \vec{b}_m - \vec{b}_n\Big)\times\Big(\frac{\partial}{\partial\vec{b}_n} - \frac{\partial}{\partial\vec{b}_m}\Big)\cdot\vec{S}_{klmn}G^{\text{nonloc}}_{klmn,\kappa\lambda} \\
&= \frac{1}{2i}(A_1B_2-A_2B_1)(\vec{\rho}_{klmn}\times\vec{\pi}_{klmn})\cdot\vec{S}_{klmn}\,G^{\text{nonloc}}_{klmn,\kappa\lambda} \\
&= \frac{2(\kappa-\lambda/4)A^{(pp)}_{klmn}}{\alpha_{klmn}(2A^{(pp)}_{klmn}+\lambda)+2(A^{(pp)}_{klmn}+\alpha_{klmn}A^{(rr)}_{klmn}\lambda)\kappa}(\vec{\rho}_{klmn}\times\vec{\pi}_{klmn})\cdot\vec{S}_{klmn}\,G^{\text{nonloc}}_{klmn,\kappa\lambda}.
\end{aligned} \tag{C.35}$$

In the local case ($\lambda\to 0$, $A_1\to\frac{\kappa}{\alpha_{klmn}+\kappa}$, $A_2\to\frac{(1-\frac{i}{2}\beta)}{\alpha_{klmn}+\kappa}$, $B_1\to 0$, $B_2\to 2i$) the expression for the matrix elements simplifies to

$$\langle\, a_k\vec{b}_k\chi_k, a_l\vec{b}_l,\chi_l \,\Big|\underset{\sim}{G}{}^{\text{loc}}_{\kappa}(\underset{\sim}{\vec{L}}\cdot\underset{\sim}{\vec{S}})\Big|\, a_m\vec{b}_m\chi_m, a_n\vec{b}_n\chi_n \,\rangle = \frac{\kappa}{\alpha_{klmn}+\kappa}(\vec{\rho}_{klmn}\times\vec{\pi}_{klmn})\cdot\vec{S}_{klmn}\,G^{\text{loc}}_{klmn,\kappa}. \tag{C.36}$$

Tensor potential

Using the definitions Eqs. (C.34) and

$$S_{12}(\vec{a},\vec{b}) = 3/2\Big((\vec{\sigma}(1)\cdot\vec{a})(\vec{\sigma}(2)\cdot\vec{b})+(\vec{\sigma}(1)\cdot\vec{b})(\vec{\sigma}(2)\cdot\vec{a})\Big)-(\vec{\sigma}(1)\cdot\vec{\sigma}(2))(\vec{a}\cdot\vec{b}), \tag{C.37}$$

one finds

$$\begin{aligned}
\langle\, a_k\vec{b}_k\chi_k, a_l\vec{b}_l\chi_l \,\Big|\Big(\frac{\kappa}{\kappa-\lambda/4}\Big)^{3/2}\mathrm{e}^{-\frac{\lambda}{4}\underset{\sim}{\vec{p}}^2}\,\mathrm{e}^{-\frac{\underset{\sim}{\vec{r}}^2}{2(\kappa-\lambda/4)}}\,\underset{\sim}{\vec{r}}^2\underset{\sim}{S}_{12}\mathrm{e}^{-\frac{\lambda}{4}\underset{\sim}{\vec{p}}^2}\Big|\, a_m\vec{b}_m\chi_m, a_n\vec{b}_n\chi_n \,\rangle = \\
= \langle\, a_k\vec{b}_k\chi_k, a_l\vec{b}_l\chi_l \,\Big|\underset{\sim}{G}{}^{\text{nonloc}}_{\kappa\lambda}\cdot\Big(\underset{\sim}{S}_{12}-\frac{i}{2}\lambda S_{12}(\underset{\sim}{\vec{r}},\underset{\sim}{\vec{p}})-\frac{\lambda^2}{4}S_{12}(\underset{\sim}{\vec{p}},\underset{\sim}{\vec{p}})\Big)\Big|\, a_m\vec{b}_m\chi_m, a_n\vec{b}_n\chi_n \,\rangle \\
= \frac{1}{(\alpha_{klmn}(2A^{(pp)}_{klmn}+\lambda)+2(A^{(pp)}_{klmn}+\alpha_{klmn}A^{(rr)}_{klmn}\lambda)\kappa)^2} \\
\Big\{(A_1^2-\frac{\lambda}{2}A_1A_2+\frac{\lambda^2}{16}A_2^2)S_{12}(\vec{\rho}_{klmn},\vec{\rho}_{klmn}) \\
+(A_1B_1-\frac{\lambda}{2}(A_1B_2+A_2B_1)+\frac{\lambda^2}{16}A_2B_2)S_{12}(\vec{\rho}_{klmn},\vec{\pi}_{klmn}) \\
+(B_1^2-\frac{\lambda}{2}B_1B_2+\frac{\lambda^2}{16}B_2^2)S_{12}(\vec{\pi}_{klmn},\vec{\pi}_{klmn})\Big\}\,G^{\text{nonloc}}_{klmn,\kappa\lambda}.
\end{aligned} \tag{C.38}$$

In the local case ($\lambda\to 0$, $A_1\to\frac{\kappa}{\alpha_{klmn}+\kappa}$, $A_2\to\frac{(1-\frac{i}{2}\beta)}{\alpha_{klmn}+\kappa}$, $B_1\to 0$, $B_2\to 2i$), this expression simplifies to

$$\langle\, a_k\vec{b}_k\chi_k, a_l\vec{b}_l,\chi_l \,\Big|\mathrm{e}^{-\frac{\underset{\sim}{\vec{r}}^2}{2\kappa}}\,\underset{\sim}{\vec{r}}^2\underset{\sim}{S}_{12}\Big|\, a_m\vec{b}_m\chi_m, a_n\vec{b}_n\chi_n \,\rangle = \Big(\frac{\kappa}{\alpha_{klmn}+\kappa}\Big)^2 S_{12}(\vec{\rho}_{klmn},\vec{\rho}_{klmn})\,G^{\text{loc}}_{klmn,\kappa}. \tag{C.39}$$

Quadratic angular momentum potential

Introducing

$$\begin{aligned}
C_1 &= \frac{2A^{(pp)}_{klmn}\kappa + 2\alpha_{klmn}A^{(rr)}_{klmn}\kappa\lambda - 1/2\alpha_{klmn}A^{(rp)}_{klmn}\lambda}{\alpha_{klmn}(2A^{(pp)}_{klmn} + \lambda) + 2(A^{(pp)}_{klmn} + \alpha_{klmn}A^{(rr)}_{klmn}\lambda)\kappa} && \text{(C.40a)}\\
D_1 &= i\frac{-2\alpha_{klmn}A^{(pp)}_{klmn}\lambda - (1 - \frac{i}{2}\beta_{klmn})A^{(pp)}_{klmn}\kappa\lambda}{\alpha_{klmn}(2A^{(pp)}_{klmn} + \lambda) + 2(A^{(pp)}_{klmn} + \alpha_{klmn}A^{(rr)}_{klmn}\lambda)\kappa} && \text{(C.40b)}\\
C_2 &= \frac{2(1 + \frac{i}{2}\beta_{klmn})A^{(pp)}_{klmn} + 2\alpha_{klmn}A^{(rr)}_{klmn}\lambda}{\alpha_{klmn}(2A^{(pp)}_{klmn} + \lambda) + 2(A^{(pp)}_{klmn} + \alpha_{klmn}A^{(rr)}_{klmn}\lambda)\kappa} && \text{(C.40c)}\\
D_2 &= i\frac{-4(\alpha_{klmn} + \kappa)A^{(pp)}_{klmn} - \alpha_{klmn}A^{(rp)}_{klmn}\lambda}{\alpha_{klmn}(2A^{(pp)}_{klmn} + \lambda) + 2(A^{(pp)}_{klmn} + \alpha_{klmn}A^{(rr)}_{klmn}\lambda)\kappa}, && \text{(C.40d)}
\end{aligned}$$

one finds

$$\begin{aligned}
&\left\langle\, a_k\vec{b}_k, a_l\vec{b}_l \,\middle|\underset{\sim}{G}^{\text{nonloc}}_{\kappa\lambda}\underset{\sim}{\vec{L}}^{\,2}\middle|\, a_m\vec{b}_m, a_n\vec{b}_n \,\right\rangle = -\frac{1}{4}\left(\left(a_k\frac{\partial}{\partial\vec{b}_k} - a_l\frac{\partial}{\partial\vec{b}_l} + \vec{b}_k - \vec{b}_l\right) \times (\left(\frac{\partial}{\partial\vec{b}_l} - \frac{\partial}{\partial\vec{b}_k}\right)\right)\\
&\qquad\qquad \cdot\left(\left(a_m\frac{\partial}{\partial\vec{b}_m} - a_n\frac{\partial}{\partial\vec{b}_n} + \vec{b}_m - \vec{b}_n\right) \times \left(\frac{\partial}{\partial\vec{b}_n} - \frac{\partial}{\partial\vec{b}_m}\right)\right)G^{\text{nonloc}}_{klmn,\kappa\lambda}\\
&= \frac{1}{2i}(A_1B_2 - A_2B_1)\cdot\\
&\quad \Big\{\frac{1}{2i}(A_1B_2 - A_2B_1)(\vec{\rho}_{klmn} \times \vec{\pi}_{klmn})^2 + \frac{1}{2}(\lambda_{klmn}C_1 + (1 - \frac{i}{2}\beta_{klmn})C_2)\vec{\rho}^{\,2}_{klmn}\\
&\quad +i\left((1 + \frac{i}{2}\beta_{klmn})C_1 - \frac{i}{2}\lambda_{klmn}D_1 + \alpha_{klmn}C_2 - \frac{i}{2}(1 - \frac{i}{2}\beta_{klmn})D_2\right)\vec{\rho}_{klmn}\cdot\vec{\pi}_{klmn}\\
&\quad +i\left((1 + \frac{i}{2}\beta_{klmn})D_1 + \alpha_{klmn}D_2\right)\vec{\pi}^{\,2}_{klmn} - \frac{3}{2}(\theta_{klmn} - \alpha_{klmn}\lambda_{klmn})\Big\}\, G^{\text{nonloc}}_{klmn,\kappa\lambda} \qquad \text{(C.41)}
\end{aligned}$$

or

$$\begin{aligned}
&\left\langle\, a_k\vec{b}_k, a_l\vec{b}_l \,\middle|\; \underset{\sim}{G}^{\text{nonloc}}_{\kappa\lambda}\underset{\sim}{\vec{L}}^{\,2}\middle|\, a_m\vec{b}_m, a_n\vec{b}_n \,\right\rangle = \frac{2(\kappa - \lambda/4)A^{(pp)}_{klmn}}{\alpha_{klmn}(2A^{(pp)}_{klmn} + \lambda) + 2(A^{(pp)}_{klmn} + \alpha_{klmn}A^{(rr)}_{klmn}\lambda)\kappa}\cdot\\
&\quad\cdot\Big\{\frac{2(\kappa - \lambda/4)A^{(pp)}_{klmn}}{\alpha_{klmn}(2A^{(pp)}_{klmn} + \lambda) + 2(A^{(pp)}_{klmn} + \alpha_{klmn}A^{(rr)}_{klmn}\lambda)\kappa}(\vec{\rho}_{klmn} \times \vec{\pi}_{klmn})^2\\
&\quad + \frac{\lambda_{klmn}A^{(pp)}_{klmn}\kappa + \theta_{klmn}A^{(pp)}_{klmn} + \alpha_{klmn}A^{(rr)}_{klmn}\lambda + \alpha_{klmn}\lambda_{klmn}A^{(rr)}_{klmn}\kappa\lambda}{\alpha_{klmn}(2A^{(pp)}_{klmn} + \lambda) + 2(A^{(pp)}_{klmn} + \alpha_{klmn}A^{(rr)}_{klmn}\lambda)\kappa}\vec{\rho}^{\,2}_{klmn}\\
&\quad - \frac{2\beta_{klmn}(\alpha_{klmn} + \kappa)A^{(pp)}_{klmn} + i\alpha_{klmn}A^{(rp)}_{klmn}\lambda + 2\alpha_{klmn}\beta_{klmn}A^{(rr)}_{klmn}\kappa\lambda}{\alpha_{klmn}(2A^{(pp)}_{klmn} + \lambda) + 2(A^{(pp)}_{klmn} + \alpha_{klmn}A^{(rr)}_{klmn}\lambda)\kappa}\vec{\rho}_{klmn}\cdot\vec{\pi}_{klmn}\\
&\quad + \frac{4\alpha_{klmn}A^{(pp)}_{klmn}(\alpha_{klmn} + \kappa) + \alpha_{klmn}A^{(pp)}_{klmn}\lambda + \theta_{klmn}A^{(pp)}_{klmn}\kappa\lambda}{\alpha_{klmn}(2A^{(pp)}_{klmn} + \lambda) + 2(A^{(pp)}_{klmn} + \alpha_{klmn}A^{(rr)}_{klmn}\lambda)\kappa}\vec{\pi}^{\,2}_{klmn}\\
&\quad - \frac{3}{2}(\theta_{klmn} - \alpha_{klmn}\lambda_{klmn})\Big\}\, G^{\text{nonloc}}_{klmn,\kappa\lambda}. \qquad \text{(C.42)}
\end{aligned}$$

For the local case ($\lambda \to 0$, $A_1 \to \frac{\kappa}{\alpha_{klmn}+\kappa}$, $A_2 \to \frac{(1-\frac{i}{2}\beta)}{\alpha_{klmn}+\kappa}$, $B_1 \to 0$, $B_2 \to 2i$, $C_1 \to \frac{\kappa}{\alpha_{klmn}+\kappa}$, $C_2 \to \frac{(1+\frac{i}{2}\beta)}{\alpha_{klmn}+\kappa}$, $D_1 \to 0$, $D_2 \to -2i$) one obtains

$$\begin{aligned}
&\left\langle\, a_k\vec{b}_k a_l\vec{b}_l \left| \underset{\sim}{G}{}^{\mathrm{loc}}_{\kappa} \underset{\sim}{\vec{L}}{}^{2} \right| a_m\vec{b}_m, a_n\vec{b}_n \,\right\rangle = \\
&= \quad \frac{\kappa}{\alpha_{klmn}+\kappa}\Big\{ \frac{\kappa}{\alpha_{klmn}+\kappa}(\vec{\rho}_{klmn}\times\vec{\pi}_{klmn})^2 + \frac{1}{2}\left(\frac{\lambda_{klmn}\kappa}{\alpha_{klmn}+\kappa} + \frac{\theta_{klmn}}{\alpha_{klmn}+\kappa}\right)\vec{\rho}^{\,2}_{klmn} \\
&\qquad +2\alpha\vec{\pi}^{\,2}_{klmn} - \beta_{klmn}\vec{\rho}_{klmn}\cdot\vec{\pi}_{klmn} - \frac{3}{2}(\theta_{klmn}-\alpha_{klmn}\lambda_{klmn})\Big\}\, G^{\mathrm{loc}}_{klmn,\kappa}. \qquad \text{(C.43)}
\end{aligned}$$

$S_{12}(L,L)$ **potential**

The Tensor operator $S_{12}(\underset{\sim}{\vec{L}},\underset{\sim}{\vec{L}})$ is defined as

$$S_{12}(\underset{\sim}{\vec{L}},\underset{\sim}{\vec{L}}) = 3(\underset{\sim}{\vec{\sigma}}(1)\cdot\underset{\sim}{\vec{L}})(\underset{\sim}{\vec{\sigma}}(2)\cdot\underset{\sim}{\vec{L}}) - (\underset{\sim}{\vec{\sigma}}(1)\cdot\underset{\sim}{\vec{\sigma}}(2))\underset{\sim}{\vec{L}}{}^{2}. \qquad \text{(C.44)}$$

The matrix element can be separated into two parts

$$\begin{aligned}
&\left\langle\, a_k\vec{b}_k\chi_k, a_l\vec{b}_l\chi_l \left| \underset{\sim}{G}{}^{\mathrm{nonloc}}_{\kappa\lambda} S_{12}(\underset{\sim}{\vec{L}},\underset{\sim}{\vec{L}}) \right| a_m\vec{b}_m\chi_m, a_n\vec{b}_n\chi_n \,\right\rangle = \\
&\quad = \quad 3\left\langle\, a_k\vec{b}_k\chi_k, a_l\vec{b}_l\chi_l \left| \underset{\sim}{G}{}^{\mathrm{nonloc}}_{\kappa\lambda} \left(\underset{\sim}{\vec{\sigma}}(1)\cdot\underset{\sim}{\vec{L}}\right)\left(\underset{\sim}{\vec{\sigma}}(2)\cdot\underset{\sim}{\vec{L}}\right) \right| a_m\vec{b}_m\chi_m, a_n\vec{b}_n\chi_n \,\right\rangle \\
&\qquad -\left\langle\, a_k\vec{b}_k\chi_k, a_l\vec{b}_l\chi_l \left| \underset{\sim}{G}{}^{\mathrm{nonloc}}_{\kappa\lambda} (\underset{\sim}{\vec{\sigma}}(1)\cdot\underset{\sim}{\vec{\sigma}}(2))\underset{\sim}{\vec{L}}{}^{2} \right| a_m\vec{b}_m\chi_m, a_n\vec{b}_n\chi_n \,\right\rangle. \qquad \text{(C.45)}
\end{aligned}$$

In the first step, the the quadratic spin-orbit matrix element is calculated:

$$\begin{aligned}
&\left\langle\, a_k\vec{b}_k\chi_k, a_l\vec{b}_l\chi_l \left| \underset{\sim}{G}{}^{\mathrm{nonloc}}_{\kappa\lambda} \left(\underset{\sim}{\vec{\sigma}}(1)\cdot\underset{\sim}{\vec{L}}\right)\left(\underset{\sim}{\vec{\sigma}}(2)\cdot\underset{\sim}{\vec{L}}\right) \right| a_m\vec{b}_m\chi_m, a_n\vec{b}_n\chi_n \,\right\rangle = \\
&= \frac{1}{2}\Bigg[-\frac{1}{4}\Bigg(\left(\vec{\sigma}_{km}\cdot\left(a_k\frac{\partial}{\partial\vec{b}_k} - a_l\frac{\partial}{\partial\vec{b}_l} + \vec{b}_k - \vec{b}_l\right)\times\left(\frac{\partial}{\partial\vec{b}_l} - \frac{\partial}{\partial\vec{b}_k}\right)\right)\cdot \\
&\qquad \left(\vec{\sigma}_{ln}\cdot\left(a_m\frac{\partial}{\partial\vec{b}_m} - a_n\frac{\partial}{\partial\vec{b}_n} + \vec{b}_m - \vec{b}_n\right)\times\left(\frac{\partial}{\partial\vec{b}_n} - \frac{\partial}{\partial\vec{b}_m}\right)\right)\Bigg) + \vec{\sigma}_{km}\longleftrightarrow\vec{\sigma}_{ln}\Bigg] G^{\mathrm{nonloc}}_{klmn,\kappa\lambda} \\
&= \frac{1}{2i}(A_1B_2 - A_2B_1)\cdot \\
&\quad \Big\{\frac{1}{2i}(A_1B_2 - A_2B_1)(\vec{\sigma}_{km}\cdot\vec{\rho}_{klmn}\times\vec{\pi}_{klmn})(\vec{\sigma}_{ln}\cdot\vec{\rho}_{klmn}\times\vec{\pi}_{klmn}) \\
&\quad -\frac{1}{4}(\lambda_{klmn}C_1 + (1-\frac{i}{2}\beta_{klmn})C_2)\left((\vec{\sigma}_{km}\cdot\vec{\rho}_{klmn})(\vec{\sigma}_{ln}\cdot\vec{\rho}_{klmn}) - (\vec{\sigma}_{km}\cdot\vec{\sigma}_{ln})\vec{\rho}^{\,2}_{klmn}\right) \\
&\quad -\frac{i}{2}((1+\frac{i}{2}\beta_{klmn})D_1 + \alpha_{klmn}D_2)\left((\vec{\sigma}_{km}\cdot\vec{\pi}_{klmn})(\vec{\sigma}_{ln}\cdot\vec{\pi}_{klmn}) - (\vec{\sigma}_{km}\cdot\vec{\sigma}_{ln})\vec{\pi}^{\,2}_{klmn}\right) \\
&\quad -\frac{i}{2}\left((1+\frac{i}{2}\beta_{klmn})C_1 - \frac{i}{2}\lambda_{klmn}D_1 + \alpha_{klmn}C_2 - \frac{i}{2}(1-\frac{i}{2}\beta_{klmn})D_2\right)\cdot \\
&\qquad \left(\frac{1}{2}(\vec{\sigma}_{km}\cdot\vec{\rho}_{klmn})(\vec{\sigma}_{ln}\cdot\vec{\pi}_{klmn}) + \frac{1}{2}(\vec{\sigma}_{km}\cdot\vec{\pi}_{klmn})(\vec{\sigma}_{ln}\cdot\vec{\rho}_{klmn}) - (\vec{\sigma}_{km}\cdot\vec{\sigma}_{ln})(\vec{\rho}_{klmn}\cdot\vec{\pi}_{klmn})\right) \\
&\quad -\frac{1}{2}(\theta_{klmn} - \alpha_{klmn}\lambda_{klmn})\Big\}\, G^{\mathrm{nonloc}}_{klmn,\kappa\lambda}. \qquad \text{(C.46)}
\end{aligned}$$

With Eqs. (C.37), (C.41), (C.45) and (C.46) one finds

$$
\begin{aligned}
&\langle\, a_k \vec{b}_k \chi_k, a_l \vec{b}_l \chi_l \,\big|\underset{\sim}{G}^{\text{nonloc}}_{\kappa\lambda} S_{12}(\underset{\sim}{\vec{L}}, \underset{\sim}{\vec{L}})\big|\, a_m \vec{b}_m \chi_m, a_n \vec{b}_n \chi_n \,\rangle = \\
&\quad = \frac{1}{2i}(A_1 B_2 - A_2 B_1)\cdot \\
&\qquad \Big\{ \frac{1}{2i}(A_1 B_2 - A_2 B_1)\, S_{12}(\vec{\rho}_{klmn} \times \vec{\pi}_{klmn}, \vec{\rho}_{klmn} \times \vec{\pi}_{klmn}) \\
&\qquad -\frac{1}{4}(\lambda_{klmn} C_1 + (1 - \frac{i}{2}\beta_{klmn}) C_2)\, S_{12}(\vec{\rho}_{klmn}, \vec{\rho}_{klmn})) \\
&\qquad -\frac{i}{2}((1 + \frac{i}{2}\beta_{klmn}) D_1 + \alpha_{klmn} D_2)\, S_{12}(\vec{\pi}_{klmn}, \vec{\pi}_{klmn}) \\
&\qquad -\frac{i}{2}((1 + \frac{i}{2}\beta_{klmn}) C_1 - \frac{i}{2}\lambda_{klmn} D_1 + \alpha_{klmn} C_2 - \frac{i}{2}(1 - \frac{i}{2}\beta_{klmn}) D_2)\cdot \\
&\qquad S_{12}(\vec{\rho}_{klmn}, \vec{\pi}_{klmn}) \Big\}\, G^{\text{nonloc}}_{klmn,\kappa\lambda}, \qquad\qquad (\text{C.47})
\end{aligned}
$$

or, written out explicitly:

$$
\begin{aligned}
&\langle\, a_k \vec{b}_k \chi_k, a_l \vec{b}_l \chi_l \,\big|\underset{\sim}{G}^{\text{nonloc}}_{\kappa\lambda} S_{12}(\underset{\sim}{\vec{L}}, \underset{\sim}{\vec{L}})\big|\, a_m \vec{b}_m \chi_m, a_n \vec{b}_n \chi_n \,\rangle = \\
&\quad = \frac{2(\kappa - \lambda/4) A^{(pp)}_{klmn}}{\alpha_{klmn}(2A^{(pp)}_{klmn} + \lambda) + 2(A^{(pp)}_{klmn} + \alpha_{klmn} A^{(rr)}_{klmn}\lambda)\kappa} \times \\
&\quad \Bigg\{ \frac{2(\kappa - \lambda/4) A^{(pp)}_{klmn}}{\alpha_{klmn}(2A^{(pp)}_{klmn} + \lambda) + 2(A^{(pp)}_{klmn} + \alpha_{klmn} A^{(rr)}_{klmn}\lambda)\kappa}\, S_{12}(\vec{\rho}_{klmn} \times \vec{\pi}_{klmn}, \vec{\rho}_{klmn} \times \vec{\pi}_{klmn}) \\
&\quad -\frac{1}{2}\frac{\lambda_{klmn} A^{(pp)}_{klmn}\kappa + \theta_{klmn} A^{(pp)}_{klmn} + \alpha_{klmn} A^{(rr)}_{klmn}\lambda + \alpha_{klmn}\lambda_{klmn} A^{(rr)}_{klmn}\kappa\lambda}{\alpha_{klmn}(2A^{(pp)}_{klmn} + \lambda) + 2(A^{(pp)}_{klmn} + \alpha_{klmn} A^{(rr)}_{klmn}\lambda)\kappa}\, S_{12}(\vec{\rho}_{klmn}, \vec{\rho}_{klmn}) \\
&\quad -\frac{1}{2}\frac{4\alpha_{klmn} A^{(pp)}_{klmn}(\alpha_{klmn} + \kappa) + \alpha_{klmn} A^{(pp)}_{klmn}\lambda + \theta_{klmn} A^{(pp)}_{klmn}\kappa\lambda}{\alpha_{klmn}(2A^{(pp)}_{klmn} + \lambda) + 2(A^{(pp)}_{klmn} + \alpha_{klmn} A^{(rr)}_{klmn}\lambda)\kappa}\, S_{12}(\vec{\pi}_{klmn}, \vec{\pi}_{klmn}) \\
&\quad +\frac{1}{2}\frac{2\beta_{klmn}(\alpha_{klmn} + \kappa) A^{(pp)}_{klmn} + i\alpha_{klmn} A^{(rp)}_{klmn}\lambda + 2\alpha_{klmn}\beta_{klmn} A^{(rr)}_{klmn}\kappa\lambda}{\alpha_{klmn}(2A^{(pp)}_{klmn} + \lambda) + 2(A^{(pp)}_{klmn} + \alpha_{klmn} A^{(rr)}_{klmn}\lambda)\kappa}\cdot \\
&\quad S_{12}(\vec{\rho}_{klmn}, \vec{\pi}_{klmn}) \Bigg\}\, G^{\text{nonloc}}_{klmn,\kappa\lambda}. \qquad\qquad (\text{C.48})
\end{aligned}
$$

In the local case, the matrix element is given by

$$
\begin{aligned}
&\langle\, a_k \vec{b}_k \chi_k, a_l \vec{b}_l \chi_l \,\big|\underset{\sim}{G}^{\text{loc}}_{\kappa} S_{12}(\underset{\sim}{\vec{L}}, \underset{\sim}{\vec{L}})\big|\, a_m \vec{b}_m \chi_m, a_n \vec{b}_n \chi_n \,\rangle = \\
&\quad = \frac{\kappa}{\alpha_{klmn} + \kappa} \Bigg\{ \frac{\kappa}{\alpha_{klmn} + \kappa}\, S_{12}(\vec{\rho}_{klmn} \times \vec{\pi}_{klmn}, \vec{\rho}_{klmn} \times \vec{\pi}_{klmn}) \\
&\qquad -\frac{1}{4}\left(\frac{\lambda_{klmn}\kappa}{\alpha_{klmn} + \kappa} + \frac{\theta_{klmn}}{\alpha_{klmn} + \kappa} \right) S_{12}(\vec{\rho}_{klmn}, \vec{\rho}_{klmn}) \\
&\qquad -\alpha_{klmn}\, S_{12}(\vec{\pi}_{klmn}, \vec{\pi}_{klmn}) + \frac{1}{2}\beta_{klmn}\, S_{12}(\vec{\rho}_{klmn}, \vec{\pi}_{klmn}) \Bigg\}\, G^{\text{loc}}_{klmn,\kappa}. \qquad (\text{C.49})
\end{aligned}
$$

References

[1] W. Heisenberg. Über den Bau der Atomkerne. *Zeitschrift für Physik*, (77):1, 1932.

[2] W. Glöckle. *The Quantum Mechanical Few-Body Problem*. Springer, 1983.

[3] N.Barnea, W. Leidemann, and G. Orlandini. Ground state wave functions in the hyperspherical formalism for nuclei with A>4. *Nucl. Phys.*, A650:427, 1999.

[4] S.C. Pieper and R.B. Wiringa. Quantum Monte Carlo calculations of light nuclei. *Annu. Rev. Nucl. Part. S.*, 51:53, 2001.

[5] P. Navrátil, G. P. Kamuntavičius, and B. R. Barrett. Few-nucleon systems in a translationally invariant harmonic oscillator basis. *Phys. Rev. C*, 61:044001, 2000.

[6] E. Caurier and F. Nowacki. Present status of shell model techniques. *Acta Phys. Pol.*, B30:705, 1999.

[7] E. Caurier, P. Navrátil, W. E. Ormand, and J. P. Vary. Intruder states in ^{8}Be. *Phys. Rev. C*, 64:051301, 2001.

[8] R. Roth. Importance truncation for large-scale configuration interaction approaches. *Phys. Rev. C*, 79:064324, 2009.

[9] R. Roth, J. Langhammer, A. Calci, S. Binder, and P. Navrátil. Similarity-transformed chiral $nn + 3n$ interactions for the *Ab Initio* description of ^{12}**C** and ^{16}**O**. *Phys. Rev. Lett.*, 107:072501, 2011.

[10] R. Roth, J. R. Gour, and P. Piecuch. *Ab initio* coupled-cluster and configuration interaction calculations for ^{16}O using the V_{UCOM} interaction. *Phys. Rev. C*, 79:054325, 2009.

[11] H. Feldmeier. Fermionic Molecular Dynamics. *Nucl. Phys.*, A515:147, 1990.

[12] H. Feldmeier and J. Schnack. Molecular dynamics for fermions. *Rev. Mod. Phys.*, 72:655, 2000.

[13] T. Neff. Fermionische Molekulardynamik mit Konfigurationsmischungen und realistischen Wechselwirkungen. Diplomarbeit, TH Darmstadt, Darmstadt, 1998.

[14] A. Ono, H. Horiuchi, T. Maruyama, and A. Ohnishi. Antisymmetrized Version of Molecular Dynamics with Two-Nucleon Collisions and Its Application to Heavy Ion Reactions. *Prog. Theo. Phys.*, 87:1185, 1992.

[15] N. Ishii, S. Aoki, and T. Hatsuda. Nuclear Force from Lattice QCD. *Phys. Rev. Lett.*, 99:022001, 2007.

[16] A. Günther, R. Roth, H. Hergert, and S. Reinhardt. Systematics of binding energies and radii based on realistic two-nucleon plus phenomenological three-nucleon interactions. *Phys. Rev. C*, 82:024319, 2010.

[17] P. Ring and P. Schuck. *The Nuclear Many-Body-Problem*. Springer, 1980.

[18] R. B. Wiringa, V. G. J. Stoks, and R. Schiavilla. Accurate nucleon-nucleon potential with charge-independence breaking. *Phys. Rev. C*, 51(1):38, 1995.

[19] A.M. Shirokov, J.P. Vary, A.I. Mazur, and T.A. Weber. Realistic nuclear Hamiltonian: Ab exitu approach. *Phys. Lett.*, B644:33, 2007.

[20] R. Machleidt. High-precision, charge-dependent Bonn nucleon-nucleon potential. *Phys. Rev. C*, 63:024001, 2001.

[21] D. R. Entem and R. Machleidt. Accurate charge-dependent nucleon-nucleon potential at fourth order of chiral perturbation theory. *Phys. Rev. C*, 68:041001, 2003.

[22] E. Epelbaum, A. Nogga, W. Glöckle, H. Kamada, Ulf-G. Meißner, and H. Witała. Three-nucleon forces from chiral effective field theory. *Phys. Rev. C*, 66:064001, 2002.

[23] E. Epelbaum. Few-nucleon forces and systems in chiral effective field theory. *Prog. Part. Nucl. Phys.*, 57(2):654, 2006.

[24] J.-I. Fujita and H. Miyazawa. Pion Theory of Three-Body Forces. *Prog. Theo. Phys.*, 17(3):360–365, 1957.

[25] A. Deltuva and A. C. Fonseca. Four-nucleon scattering: *Ab initio* calculations in momentum space. *Phys. Rev. C*, 75:014005, 2007.

[26] A. Nogga, H. Kamada, and W. Glöckle. Modern Nuclear Force Predictions for the α Particle. *Phys. Rev. Lett.*, 85:944, 2000.

[27] W. N. Polyzou and W. Glöckle. Three-body interactions and on-shell equivalent two-body interactions. *Few-Body Syst.*, 9:97, 1990.

[28] H. Feldmeier, T. Neff, R. Roth, and J. Schnack. A unitary correlation operator method. *Nucl. Phys.*, A632:61, 1998.

[29] T. Neff and H. Feldmeier. Tensor correlations in the unitary correlation operator method. *Nucl. Phys.*, A713:311, 2003.

[30] R. Roth, T. Neff, H. Hergert, and H. Feldmeier. Nuclear structure based on correlated realistic nucleon-nucleon potentials. *Nucl. Phys.*, A745:3, 2004.

[31] R. Roth, H. Hergert, P. Papakonstantinou, T. Neff, and H. Feldmeier. Matrix elements and few-body calculations within the unitary correlation operator method. *Phys. Rev. C*, 72:034002, 2005.

[32] R. Roth, T. Neff, and H. Feldmeier. Nuclear structure in the framework of the Unitary Correlation Operator Method. *Prog. Part. Nucl. Phys.*, 65:50, 2010.

[33] R. Roth. *Effektive Wechselwirkungen für Quantenflüssigkeiten und Quantengase:Kernmaterie, flüssiges Helium und ultrakalte atomare Fermigase*. PhD thesis, TH Darmstadt, Darmstadt, 2000.

[34] T. Neff. *Short-Ranged Central and Tensor Correlations in Nuclear Many-Body Systems*. PhD thesis, TU Darmstadt, Darmstadt, 2002.

[35] S.K. Bogner, T.T.S. Kuo, and A. Schwenk. Model-independent low momentum nucleon interaction from phase shift equivalence. *Phys. Rep.*, 386:1, 2003.

[36] S.K. Bogner, T.T.S. Kuo, A. Schwenk, D.R. Entem, and R. Machleidt. Towards a model-independent low momentum nucleon-nucleon interaction. *Phys. Lett.*, B576:265, 2003.

[37] S. K. Bogner, R. J. Furnstahl, and R. J. Perry. Similarity renormalization group for nucleon-nucleon interactions. *Phys. Rev. C*, 75:061001, 2007.

[38] K. Suzuki and S.Y. Lee. Convergent Theory for Effective Interaction in Nuclei. *Prog. Theo. Phys.*, 64:2091, 1980.

[39] L.-B. Wang et al. Laser Spectroscopic Determination of the ^{6}He Nuclear Charge Radius. *Phys. Rev. Lett.*, 93:142501, 2004.

[40] I. Sick. On the rms-radius of the proton. *Phys. Lett.*, B576:62, 2003.

[41] S. Kopecky, P. Riehs, J. A. Harvey, and N. W. Hill. New Measurement of the Charge Radius of the Neutron. *Phys. Rev. Lett.*, 74:2427, 1995.

[42] O. Dumbrajs, R. Koch, H. Pilkuhn, G.C. Oades, H. Behrens, J.J. de Swart, and P. Kroll. Compilation of coupling constants and low-energy parameters. *Nucl. Phys.*, B216:277, 1983.

[43] W. Rarita and J. Schwinger. On the Neutron-Proton Interaction. *Phys. Rev.*, 59:436, 1941.

[44] J. J. Sakurai. *Modern Quantum Mechanics*. Benjamin/Cummings, 1985.

[45] W. Heisenberg. Die "beobachtbaren Größen" in der Theorie der Elementarteilchen. *Zeitschrift für Physik*, A120:513, 1943.

[46] H. P. Stapp, T. J. Ypsilantis, and N. Metropolis. Phase-Shift Analysis of 310-Mev Proton-Proton Scattering Experiments. *Phys. Rev.*, 105:302, 1957.

[47] V. G. J. Stoks, R. A. M. Klomp, M. C. M. Rentmeester, and J. J. de Swart. Partial-wave analysis of all nucleon-nucleon scattering data below 350 MeV. *Phys. Rev. C*, 48:792, 1993.

[48] G.E. Brown and A.D. Jackson. *The nucleon-nucleon interaction*. North-Holland, 1976.

[49] D.J. Kouri and F.S. Levin. A new method for determining K-matrix elements. *Phys. Lett.*, B48:203, 1974.

[50] J.B. McGrory and B.H. Wildenthal. Further comment on spurious center-of-mass motion. *Phys. Lett.*, B60:5, 1975.

[51] D. R. Tilley, C. M. Cheves, J. L. Godwin, et al. Energy levels of light nuclei A=5, 6, 7. *Nucl. Phys.*, A708:3, 2002.

[52] R. Sánchez, W. Nörtershäuser, G. Ewald, et al. Nuclear Charge Radii of Li9, 11: The Influence of Halo Neutrons. *Phys. Rev. Lett.*, 96:033002, 2006.

[53] K. Vantournhout, T. Neff, H. Feldmeier, N. Jachowicz, and J. Ryckebusch. Towards a quantal dynamical simulation of the neutron star's crust. *Prog. Part. Nucl. Phys.*, 66:271, 2011.

[54] D. Weber. Transformation nuklearer Potentiale von Partialwellendarstellung im Impulsraum auf Operatordarstellung. Master's thesis, TU Darmstadt, Darmstadt, 2009.

[55] R. Roth, S. Reinhardt, and H. Hergert. Unitary correlation operator method and similarity renormalization group: Connections and differences. *Phys. Rev. C*, 77:064003, Jun 2008.

[56] F. Wegener. Flow equations for Hamiltonians. *Ann. Phys.*, 3:77, 1994.

[57] F. Wegener. Flow Equations for Hamiltonians. *Nucl. Phys. B Proc. Suppl.*, 90:141, 2000.

[58] S. D. Głazek and K. G. Wilson. Renormalization of Hamiltonians. *Phys. Rev. D*, 48:5863, 1993.

[59] E. Anderson, S. K. Bogner, R. J. Furnstahl, E. D. Jurgenson, R. J. Perry, and A. Schwenk. Block diagonalization using similarity renormalization group flow equations. *Phys. Rev. C*, 77:037001, 2008.

[60] W. Li, E. R. Anderson, and R. J. Furnstahl. Similarity renormalization group with novel generators. *Phys. Rev. C*, 84:054002, 2011.

[61] H. Hergert and R. Roth. Unitary correlation operator method from a similarity renormalization group perspective. *Phys. Rev. C*, 75:051001, 2007.

[62] E. D. Jurgenson, P. Navrátil, and R. J. Furnstahl. Evolution of Nuclear Many-Body Forces with the Similarity Renormalization Group. *Phys. Rev. Lett.*, 103:082501, 2009.

[63] A. M. Shirokov, A. I. Mazur, S. A. Zaytsev, J. P. Vary, and T. A. Weber. Nucleon-nucleon interaction in the J-matrix inverse scattering approach and few-nucleon systems. *Phys. Rev. C*, 70:044005, 2004.

[64] A.M. Shirokov, J.P. Vary, A.I. Mazur, S.A. Zaytsev, and T.A. Weber. Novel NN interaction and the spectroscopy of light nuclei. *Phys. Lett.*, B621:96, 2005.

[65] J.P. Vary. *private communication*.

[66] R. Roth, P. Papakonstantinou, N. Paar, H. Hergert, T. Neff, and H. Feldmeier. Hartree-fock and many body perturbation theory with correlated realistic *NN* interactions. *Phys. Rev. C*, 73:044312, 2006.

[67] H. Hergert. *private communication*.

[68] E. Wigner. On the Quantum Correction For Thermodynamic Equilibrium. *Phys. Rev.*, 40:749, 1932.

[69] K. A. Wendt, R. J. Furnstahl, and S. Ramanan. Local Projections of Low-Momentum Potentials. http://arxiv.org/abs/1203.5993v2, 2012.

[70] M. Abramowitz and I. A. Stegun. *Handbook of Mathematical Functions with Formulas, Graphs, and Mathematical Tables*. Courier Dover Publications, 1964.

[71] M. Hjorth-Jensen. Nuclear structure from nuclei to neutron stars. Lecture notes, Twelfth Summer School in Nuclear Physics, University of California, Santa Cruz, 2000.

[72] M. Hjorth-Jensen, T.T.S. Kuo, and E. Osnes. Realistic effective interactions for nuclear systems. *Phys. Rep.*, 261:125, 1995.

Danksagung

Zu aller Erst möchte ich mich bei Prof. Hans Feldmeier und Dr. Thomas Neff für die Betreuung dieser Arbeit bedanken. Beide haben es verstanden, mir während dieser Arbeit einerseits ein großes Maß an Freiraum und eigenverantwortlichem Arbeiten zu ermöglichen und andererseits bei konkreten Problemen jederzeit ansprechbar zu sein und mit Rat zur Seite zu stehen. Ohne ihre Unterstützung wäre die Arbeit in dieser Form nicht möglich gewesen. Besonders möchte ich mich dafür bedanken, dass man es mir ermöglicht hat, an internationalen Programmen wie dem “ECT* Doctoral Training Programme 2010” in Trento teilzunehmen und meine physikalischen Kenntnisse so entscheidend weiterzuentwickeln.

Weiterhin danke ich besonders Dr. Klaas Vantournhout für die interessanten Diskussionen über Physik und viele andere Dinge. Insbesondere bedanke ich mich für seine hilfreichen Kommentare und das Korrekturlesen dieser Arbeit.

Mein Dank gilt außerdem der Theorie-Abteilung der GSI. Diese hat nicht nur die notwendige Infrastruktur für diese Arbeit bereitgestellt, sondern ihre Mitglieder haben es auch verstanden, eine angenehme und produktive Atmosphäre zu schaffen. Besonders möchte ich mich hier bei Prof. Karlheinz Langanke, Ilka Petermann, Markus Leykauf, Hans-Peter Loens, Lutz Huther, Andreas Lohs, Tomislav Marketin, Katharine Henninger und Almudena Arcones für zahlreiche gute Gespräche bedanken. Mein besonderer Dank gilt auch Marina Varentsova für ihre schnelle, unkomplizierte Hilfe bei allen möglichen administrativen und organisatorischen Problemchen.

Darüber hinaus danke ich Prof. Robert Roth für die Übernahme des Zweitgutachtens dieser Arbeit.

Der TU Darmstadt danke ich für die Gewährung meines Promotionsstipendiums und dem Extreme Matter Institute “Emmi” für die Unterstützung dieser Arbeit. Der Helmholtz Graduate School for Hadron and Ion Research “HGS-HIRe for FAIR” möchte ich für die promotionsbegleitenden Veranstaltungen wie Lecture-Weeks und Softskill-Seminare danken.

Zu guter Letzt, aber nicht weniger herzlich, danke ich meinen Eltern, meiner Schwester und ganz besonders Lydia für die Unterstützung während dieser Arbeit und dafür, dass sie all die kleineren und größeren Verschrobenheiten, die ich mir während meiner Arbeit als theoretischer Physiker angeeignet habe, so tapfer weggesteckt haben.

Zur Person

Name:	Dennis Weber
Geburtsdatum:	14.07.1983
Geburtsort:	Darmstadt
Eltern:	Wolfgang und Helga Weber geb. Dölitzsch
Familienstand:	ledig

Bildungsweg

08/1990–07/1993	Besuch der Gutenbergschule (Grundschule) in Eschollbrücken
08/1993–07/1994	Besuch der Friedrich-Ebert-Schule (Grundschule) in Griesheim
08/1994–06/2003	Besuch der Justus-Liebig-Schule (Gymnasium) in Darmstadt
06/2003	Abitur
10/2003–03/2009	Studium der Physik an der Technischen Universität Darmstadt
02/2007	Abschluss: Bachelor of Science in Physics Titel der Bachelorarbeit: *„Simulation der Refraktion im Konversionsvolumen des CERN Axion Solar Telescope (CAST)“*
03/2009	Abschluss: Master of Science in Physics Titel der Masterarbeit am GSI Helmholtzzentrum für Schwerionenforschung: *„Transformation nuklearer Potentiale von Partialwellendarstellung im Impulsraum auf Operatordarstellung“*
seit 04/2009	Promotionsstudium an der Technischen Universität Darmstadt Doktorand in der Theorie-Abteilung des GSI Helmholtzzentrums für Schwerionenforschung und Anfertigung der Dissertation